$^{40}Ar/^{39}Ar$ Study of the Northwestern Reindeer Zone, Trans-Hudson Orogen: Reindeer Lake, Saskatchewan

Joyia Chakungal

Submitted in partial fulfillment of the requirements
for the degree of Master of Science

Dalhousie University
Department of Earth Sciences
Halifax, Nova Scotia
December 2001

DALHOUSIE UNIVERSITY

DEPARTMENT OF EARTH SCIENCES

The undersigned hereby certify that they have read and recommend to the Faculty of Graduate Studies for acceptance a thesis entitled " $^{40}Ar/^{39}Ar$ study of the Northwestern Reindeer Zone, Trans-Hudson Orogen: Reindeer Lake, Saskatchewan" by Joyia Chakungal in partial fulfillment of the requirements for the degree of Master of Science.

Dated: 2001/12/14

Supervisor(s):

Readers:

DALHOUSIE UNIVERSITY

DATE: 2001/12/14

AUTHOR: Joyia Chakungal

TITLE: $^{40}Ar/^{39}Ar$ study of the Northwestern Reindeer Zone, Trans-Hudson Orogen: Reindeer Lake, Saskatchewan

DEPARTMENT OR SCHOOL: Earth Sciences

DEGREE: M.Sc. CONVOCATION: May YEAR: 2002

Permission is herewith granted to Dalhousie University to circulate and to have copied for non-commercial purposes, at its discretion, the above title upon the request of individuals or institutions.

To my fellow grad students on the second and fourth floors of Oceanography, who are going through what I went through. You know who you are, and I wish you all the very best of luck!

TABLE of CONTENTS

LIST of FIGURES

LIST of MAPS

LIST of PLATES

LIST of TABLES

LIST of APPENDICES

Abstract

An important task is to determine the processes that led to exhumation of rocks in ancient orogens like the Trans-Hudson Orogen (THO). Processes that exhume deeply buried rocks rapidly are syn-orogenic erosion and normal faulting, whereas ductile thinning of the crust and post-orogenic erosion are characterized by slow exhumation rates. In the absence of direct evidence for exhumation processes, the most effective approach is to use thermochronological techniques in which radiometric ages are obtained from a number of minerals characterized by different closure temperatures (T_c). Ages are used to constrain the time at which the rock passed through a particular mineral's T_c. With this information, cooling rates are calculated and compared with those estimated from known settings.

Along the shores and islands of Reindeer Lake, Saskatchewan, the Paleoproterozoic Trans-Hudson Orogen comprises a collage of deformed and metamorphosed sedimentary, and mantle-derived arc volcanics and plutonic terranes collectively termed the Reindeer Zone (RZ). From south to north, the RZ includes the Glennie, Kisseynew and La Ronge domains, and Wathaman Batholith, which were trapped between the Archean Rae-Hearne and Superior cratons during continent-continent collision at ca 1850 – 1800 Ma. Peak metamorphism throughout the orogen occurred during the interval ca. 1820 – 1790 Ma. Metamorphic grade throughout the zone varies from transitional granulite facies in the Kisseynew Domain, to upper greenschist - lower amphibolite facies at the northern margin of the Wathaman Batholith and in the Archean Peter Lake Domain, but does not display marked variations across domain boundaries. Similarly, U-Pb monazite and titanite ages obtained by previous workers display little variation across domain boundaries.

In the current study, 28 samples collected from a geologically well-constrained, 200 km south - north transect across the RZ and into the Archean Peter Lake domain along Reindeer Lake, were analyzed using the $^{40}Ar/^{39}Ar$ method of thermochronology. Analyses were conducted on hornblende (T_c = 500 ^{0}C), muscovite (T_c = 350 ^{0}C) and K-feldspar (T_c ~ 260 ^{0}C) grains to constrain the time at which the RZ cooled through the T_c of each mineral. Preservation of comparatively uniform hornblende ages across most of the Reindeer Lake transect suggests the RZ cooled to 500 ^{0}C by ~ 1770 Ma. Preservation of the youngest hornblende ages in the southern La Ronge Domain, above the Duck Lake shear zone (DLSZ), suggests that following thermal equilibration fluid flow within the DLSZ may have affected the thermal structure such that rocks immediately north of it remained at temperatures ≥ 500 ^{0}C until ~ 1740 Ma. Preservation of the oldest hornblende ages in the Archean Peter Lake Domain, where metamorphic grade is lowest, suggests that it was metamorphosed at low temperatures, possibly because it was not buried to depths that rocks in the south were buried to, and thus cooled through 500 ^{0}C earlier than rocks to the south. Calculated cooling rates for the RZ (Kisseynew and La Ronge domains, and Wathaman Batholith) average ~ 5.0 ^{0}C/My suggesting exhumation of the Reindeer Zone to its present structural level was dominated by the process of post-orogenic erosion.

Acknowledgments

First and foremost, I extend my utmost gratitude to Dr. R.A. Jamieson for all of her time, patience and guidance. Many thanks also to Dr. P.H. Reynolds for his assistance with the interpretation of the data. For providing me with the opportunity to work in the Trans-Hudson Orogen, extra special thanks goes to Dr. D. Corrigan. And last but not least, to my father, Dr. T. Chakungal, who never faltered from his place beside me and provided me with the encouragement needed to see this through to the end.

Chapter I – Introduction

1.1 Introduction

The Trans-Hudson Orogen (THO; Hoffman, 1981) is perhaps the largest well preserved and best exposed Paleoproterozoic orogenic belt in the world (Hoffman, 1988). Extending in subsurface from South Dakota through the Canadian Shield, across Hudson Bay to Greenland (Figure 1.1; Bickford et al., 1990), the THO is a dominant component of the North American Craton (Lewry et al., 1987). Its development coincides with a critical period of continental accretionary tectonics during the late Paleoproterozoic, which contributed to the growth of the North American continent (Van Schmus et al., 1987; Hoffman, 1988; Lewry et al., 1994). The orogen comprises a collage of deformed and metamorphosed juvenile terranes (Lewry & Collerson, 1990; Lewry et al., 1994) that were trapped between the Archean Superior and Rae-Hearne cratons during continent – continent collision at ca. 1850 – 1800 Ma (Gordon et al., 1990; Machado, 1990).

The northwestern component of the THO, exposed in northern Saskatchewan and Manitoba, can be divided into external and internal zones. Deformed Archean basement (Hearne Province) and its cover sequence, the Wollaston Group, comprise the external zone (Figure 1.2), whereas the internal zone comprises a complex collage of mantle-derived, arc-related volcanic and plutonic rocks, volcanogenic clastic rocks and younger arkosic molasse assemblages, collectively termed the "Reindeer Zone" (figure 1.2; Stauffer, 1984; Hoffman, 1988). The Reindeer Zone is bounded to the southeast by the Churchill-Superior Boundary zone, and to the north – northwest by the Wathaman – Chipewyan Batholith (Hoffman, 1988). U-Pb zircon crystallization ages from felsic arc volcanics range from ca. 1910 – 1875 Ma, whereas ages of plutonic rocks range from ca. 1910 – 1830 Ma (Baldwin et al., 1985; Lewry et al., 1987; Van Schmus et al., 1987). Major and trace element data from volcanic and plutonic rocks, and Nd, Pb and Sr isotopic data from a variety of rock types suggest that much of the Reindeer Zone is allochthonous, having formed in an oceanic, subduction-related arc setting prior to the collision of the Superior, Saskatchewan (Sask) and Rae-Hearne cratons (Lewry et al., 1981; Hoffman, 1988).

Several studies have been conducted across the THO in an attempt to understand the crustal structure and tectonic history of the Reindeer Zone, with particular interest in

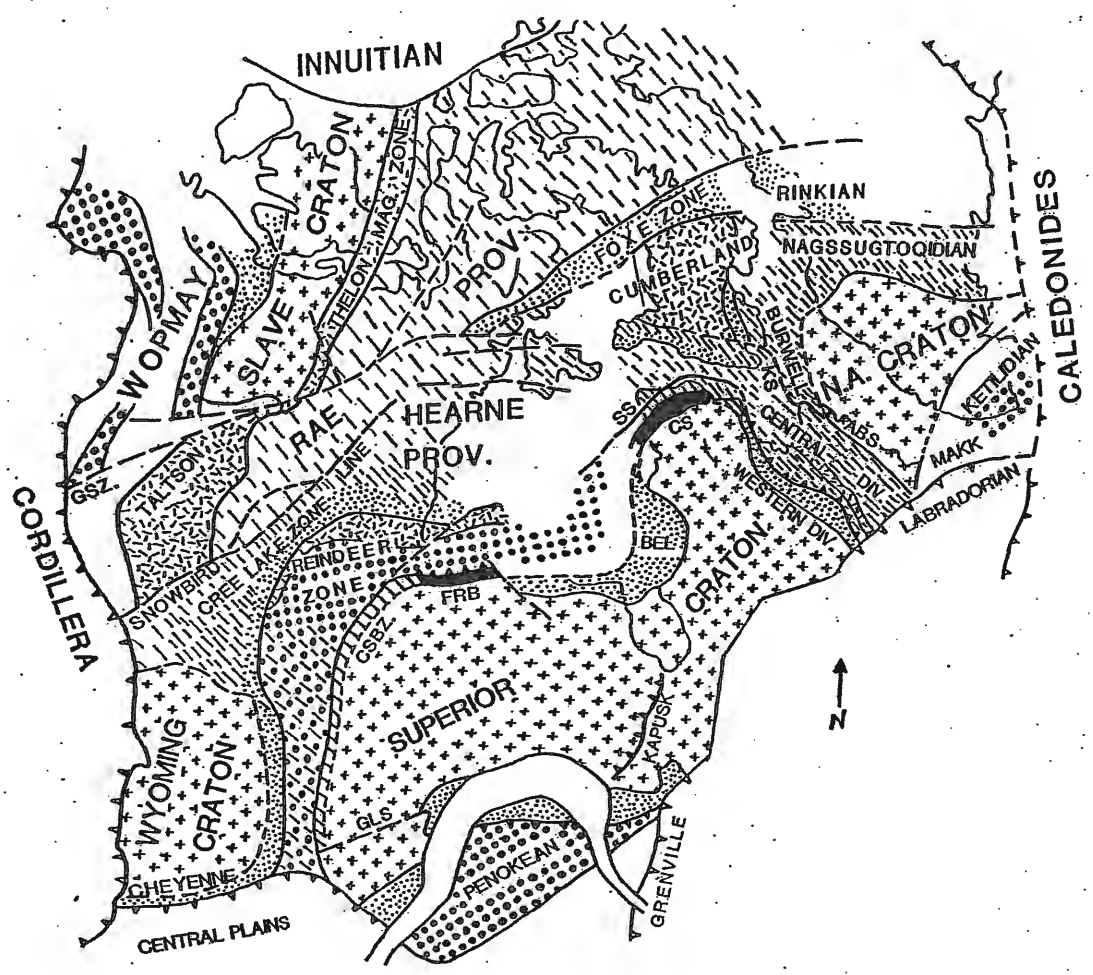

Figure 1.1: Major elements of the Trans-Hudson Orogen, other early Proterozoic orogenic belts, and Archean cratons in North America. **Legend**: *crosses*, slightly reworked cratons; *oblique dash*, Archean continental crust variably reworked during early Proterozoic orogeny and with scattered remnants of early Proterozoic inboard (relative to Archean cratons) supracrustals (*closer dashes* indicate generally high grade reworking); *stipple*, early Proterozoic foreland fold/thrust belts and other areas preserving abundant early Proterozoic supracrustal rocks; *random ticks*, major continental magmatic arc batholiths; *heavy dots*, mostly accreted juvenile (mantle-derived) early Proterozoic arc terranes; *mixture of heavy dots and oblique dash*, southern Reindeer Zone, likely occurrence of both allochthonous juvenile elements and highly reworked (Archean) continental crust; *solid black*, predominantly mafic – ultramafic allochthons thrust over the margins of the Superior craton (mainly ophiolitic in the Cape Smith Belt, possibly representing foredeep volcanics and intrusions in the Fox River belt). (Lewry & Collerson, 1990)

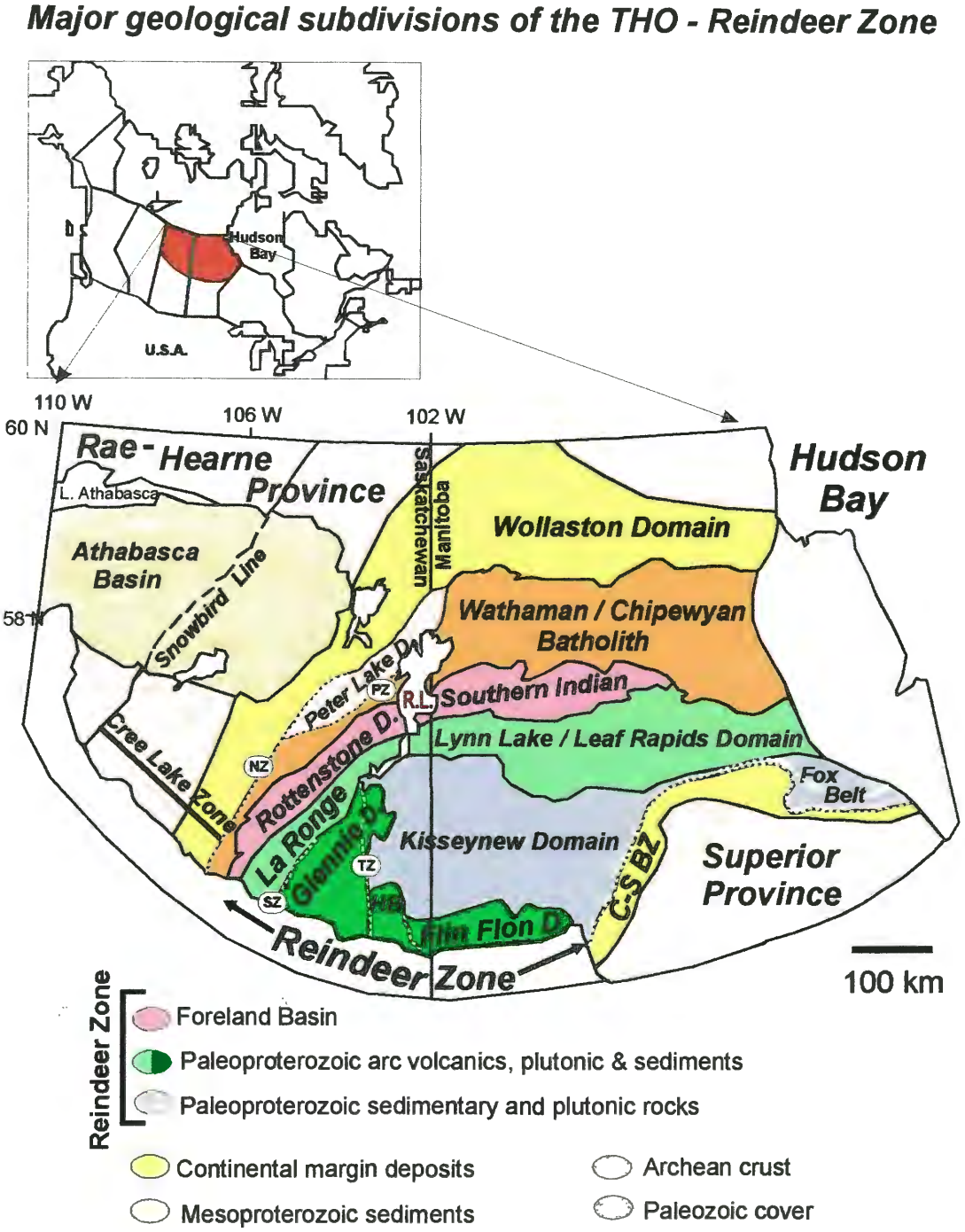

Figure 1.2: Generalized map of the Trans-Hudson Orogen along the Reindeer Zone showing the distribution of the major lithotectonic domains. Heavy dashed lines indicate major ductile shear zones or brittle-ductile faults. *C-S BZ*, Churchill-Superior Boundary Zone; *HB*, Hanson Lake Block; *TZ*, Tabbernor Fault Zone; *SZ*, Stanley Fault Zone; *NZ, PZ*, Needle Falls and Parker Lake Shear Zones. Reindeer Lake (*RL*) is outlined. (Lewry et al., 1990)

the accretionary history prior to terminal collision. Only a limited amount of work has been done with respect to unravelling the collisional history and related tectono-thermal evolution. Across the orogen, metamorphic grade varies from predominantly granulite facies in the Cree Lake and Churchill-Superior Boundary zones, upper greenschist facies in the Flin Flon domain, transitional granulite facies in the Kisseynew domain (orogen core) to mid-amphibolite facies in the northern La Ronge domain (orogen margin). Despite their complex structural relationships, however, field observations made in the current study suggest that domain boundaries lack abrupt variations in metamorphic grade. Similarly, in the Flin Flon, Kisseynew and Wollaston domains, U/Pb data obtained from monazite and titanite grains are consistent, displaying little variation in metamorphic ages (1830 - 1800 Ma) across domain boundaries (Figure 1.3). The exception to this trend is the preservation of consistently young U-Pb ages in the Churchill-Superior Boundary Zone and older ages in the Archean Cree Lake Zone (Figure 1.3).

Recent $^{40}Ar/^{39}Ar$ analyses obtained by Heizler et al. (1999, 2000) from hornblende, muscovite and biotite also suggest little variation from orogen core to margin. Data were obtained from over 100 samples collected along a 700 km transect from the northern margin of the La Ronge domain to the Churchill-Superior Boundary Zone (Figure 1.3). Hornblende plateau ages across the orogen range from 1770 – 1750 Ma, implying that most of the THO was either metamorphosed at, or cooled through ~ 500 °C by 1750 Ma. Muscovite and biotite ages from the Rottenstone, La Ronge, Glennie, and Flin Flon domains vary from 1740 – 1700 Ma. Biotite and muscovite ages from the Kisseynew, Snow Lake and Flin Flon Domains cluster around 1760 Ma. The lowest metamorphic grade rocks from the southern Flin Flon Domain gave older (> 1800 Ma) amphibole and mica dates that were interpreted by Heizler et al. (1999, 2000) to represent crystallization ages. In the east, mica and amphibole ages are younger and show more scatter (1680 – 1760 Ma). Heizler et al. (1999) concluded that west - east variations in mica ages may indicate differential cooling through 500 – 300 °C, possibly due to differential erosion and/or tilting. Since domain boundaries do not define age boundaries, Heizler et al. (2000) suggested that the Reindeer Zone likely cooled as a single block that was subjected to differential cooling along its margins.

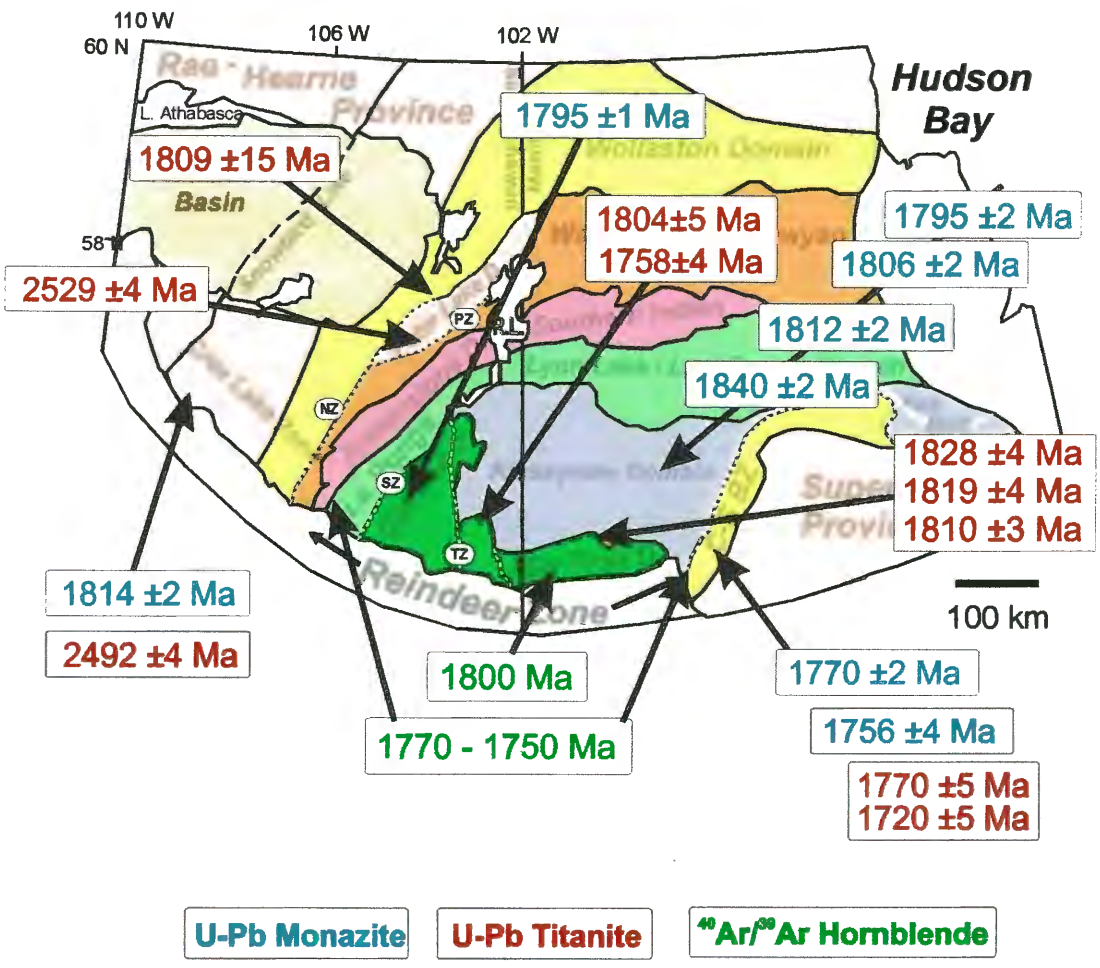

Figure 1.3: Distribution of U-Pb monazite and titanite, and $^{40}Ar/^{39}Ar$ hornblende ages obtained from across the Trans-Hudson Orogen - Reindeer Zone, prior to this study. Sources include Gordon et al. (1990); Machado et al. (1987, 1990); Zwanzig (1990); Stauffer (1990); Annesley et al. (1992); Ansdell et al. (1995); Heizler et al. (1999).

1.2 Thermal Model of Thickened Crust

To understand the thermal history of a point within the crust, ideally all data pertaining to the temperature-time path (T-t) followed by the point should be obtained from one sample or from several samples taken from a single horizon that was likely to have experienced a similar thermal history. In an orogenic belt comprising several domains, an understanding of the timing and rates of cooling of each domain may be used to identify the processes that have resulted in the present-day configuration of the orogen. Ring et al. (1999) have noted that in addition to T-t histories for single samples or sample sets, the pattern of cooling ages across a transect can be used to differentiate between the different exhumation processes.

1D Model

As discussed by England and Thompson (1984), major sources of heat during regional metamorphism are radiogenic heat produced by the decay of radioactive elements in the continental crust, and heat transferred to the base of the crust from the upper mantle. In steady state, crust of normal thickness (i.e. ~ 35 km from surface to Moho) should be in equilibrium with its internal heat production and the heat supplied to its base such that isotherms (i.e. a surface within the lithosphere of equal temperature at a particular point in time; Allaby & Allaby, 1990) are distributed parallel to the surface. The geothermal gradient is highest at the Earth's surface as a consequence of high radiogenic heat input (Figure 1.4a). In thermally equilibrated crust, the T-t path followed by a point (A) within the crust is representative of thermal equilibrium (Figure 1.4a). If the crust is thickened to twice its original thickness by thrusting, point A will be buried and will undergo an instantaneous increase in pressure (P), and a slower increase in temperature where maximum temperatures will be reached at the maximum burial depth (Figure 1.4b). Upon termination of tectonic activity, and assuming the continental lithosphere is always close to isostatic equilibrium, the geothermal gradient within the crustal pile will ultimately return to a steady state temperature regime that is governed by the new internal heat production distribution and the heat supply from below (England & Thompson, 1984; Dunlap, 2000). If, however, thrusting is accompanied by erosion, the crust isostatically rebounds as material is removed from the surface, and the T-t path of point A is characterized by an increase in temperature followed by a gradual decrease in

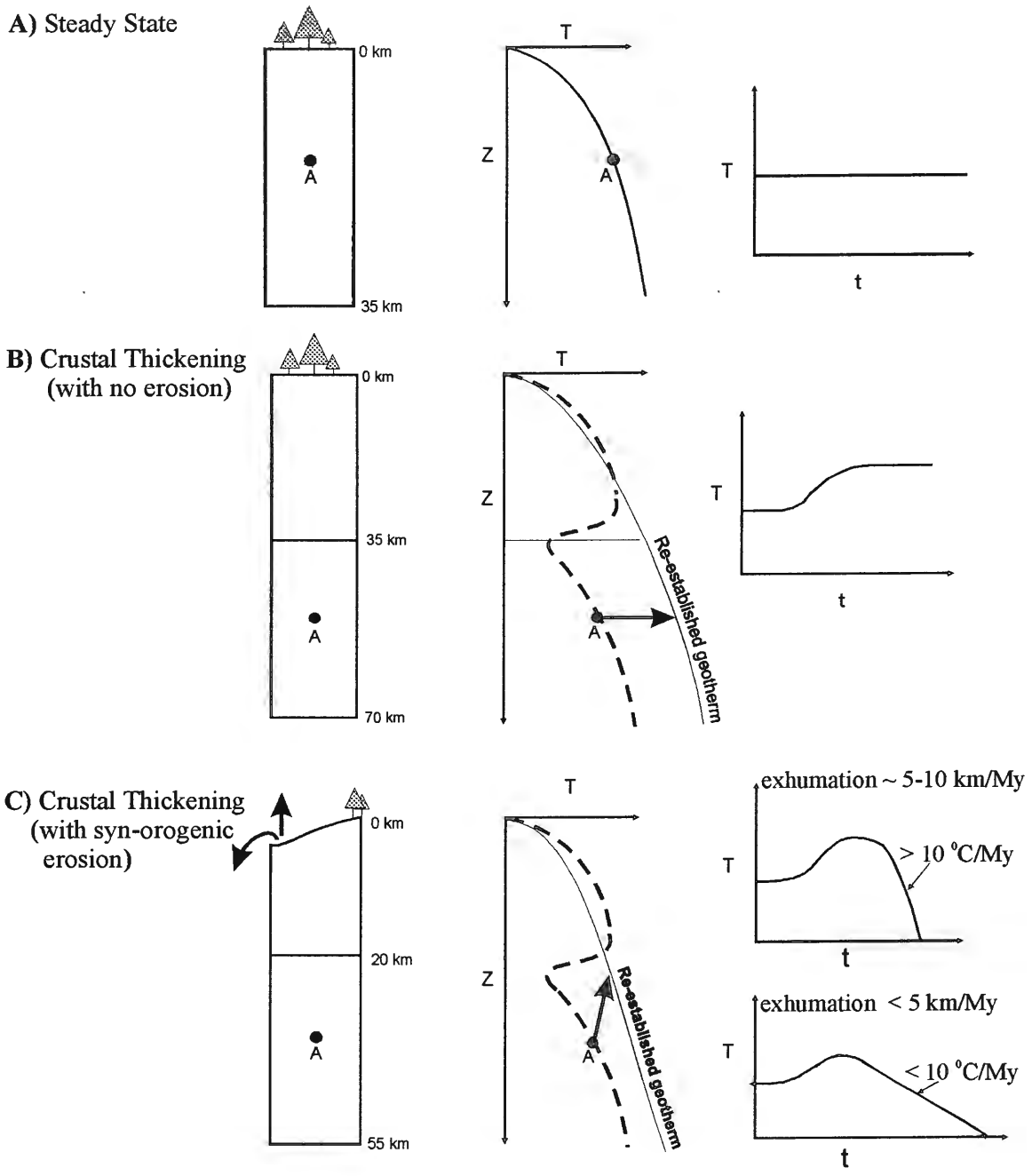

Figure 1.4: A one dimensional thermal model of an orogen. a) The geothermal gradient of the Earth's crust in steady state, and the Temperature - time path (T-t) for point A within crust that is in thermal equilibrium; b) The geothermal gradient of doubly thickened crust (stippled line represents the original geotherm and the solid line represents the re-established geotherm), and the T-t path followed by point A during crustal thickening; c) The geothermal gradient of doubly thickened crust accompanied by syn-orogenic erosion (stippled line represents the original geotherm and the solid line represents the re-established geotherm), and the T-t path followed by point A. Based on Jamieson et al. (1998).

temperature as the point is exhumed (Figure 1.4c). The rate of cooling is dependent on the rate of exhumation.

2D Model (based on Jamieson et al., 2002)

In real orogens, lateral variations in crustal structure should lead to lateral variations in thermal structure. Figure 1.5a illustrates a transect in which the crust is in thermal equilibrium and thus, the T of points A and B does not change with time. Crustal thickening driven by subduction below point A disturbs the geothermal gradient of the crust, and produces laterally variable isotherms. Point A, situated near the margin of the orogen, will undergo rapid exhumation by thrusting, whereas point B, in the orogenic core, will likely heat up and cool more slowly. Thus, the T-t path followed by point A will be characterized by an increase in temperature followed by a rapid decrease in temperature as it is exhumed (Figure 1.5b). In the event that subduction ceases and erosion rates decline, the T-t time path of A is similar to that depicted in Figure 1.5b until orogenesis ceases, after which the T-t path is characterized by a slow decrease in temperature approaching thermal equilibrium over timel, depending on the rate of exhumation (Figure 1.5c). Following orogenesis, the T-t path followed by point B will be characterized by a slow decrease in temperature as the crust relaxes to a steady state thermal regime (Figure 1.5c).

Thus, the thermal history of a rock offers clues to process(es) that were responsible for its exhumation. Based on a comparison of the T-t paths of several spatially related rocks, the process(es) that resulted in the present day 2D configuration of the may be estimated. Ring et al. (1999) noted that normal faulting and syn-orogenic erosion are characterized by rapid exhumation rates (i.e. 5-10 km/My), where as the processes of ductile thinning and post-orogenic erosion are characterized by slow exhumation rates (i.e. $\leq$ 5 km/My). The T-t paths characteristic of rocks exhumed at different rates are illustrated in Figure 1.6. Further constraint on the process responsible for exhumation must come from structures and other geological evidence observed in the field.

1.3 Method of Study – Thermochronology

Radiometric dates obtained from metamorphic minerals may represent the age of crystallization, cooling, or partial thermal overprinting (Zeitler, 1989). For any particular

A) Steady State (pre-orogenesis)

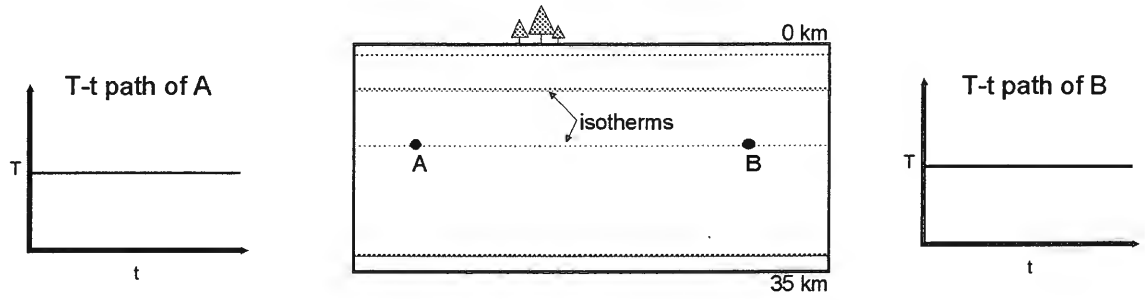

B) Syn-orogenic (with erosion focused along flanks)

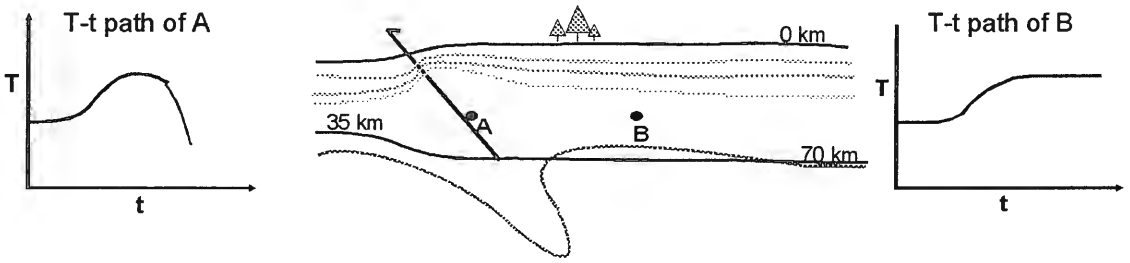

C) Post-orogenic (with slow erosion across entire orogen)

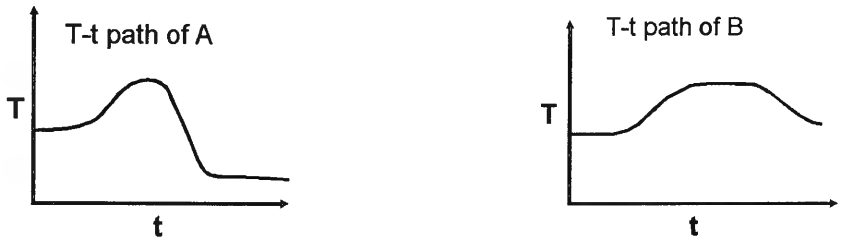

Figure 1.5: A two dimensional thermal model of an orogen. a) The T-t paths followed by two points, A and B, situated within crust that is in steady state, or thermal equilibrium; b) The T-t paths followed by points A and B during orogenesis accompanied by erosion focused along the flanks; c) The T-t paths of points A and B following orogenesis, when the crust returns to a steady state thermal regime. Based on Jamieson et al. (2002).

Using cooling rates to estimate the process(s) that may have lead to exhumation

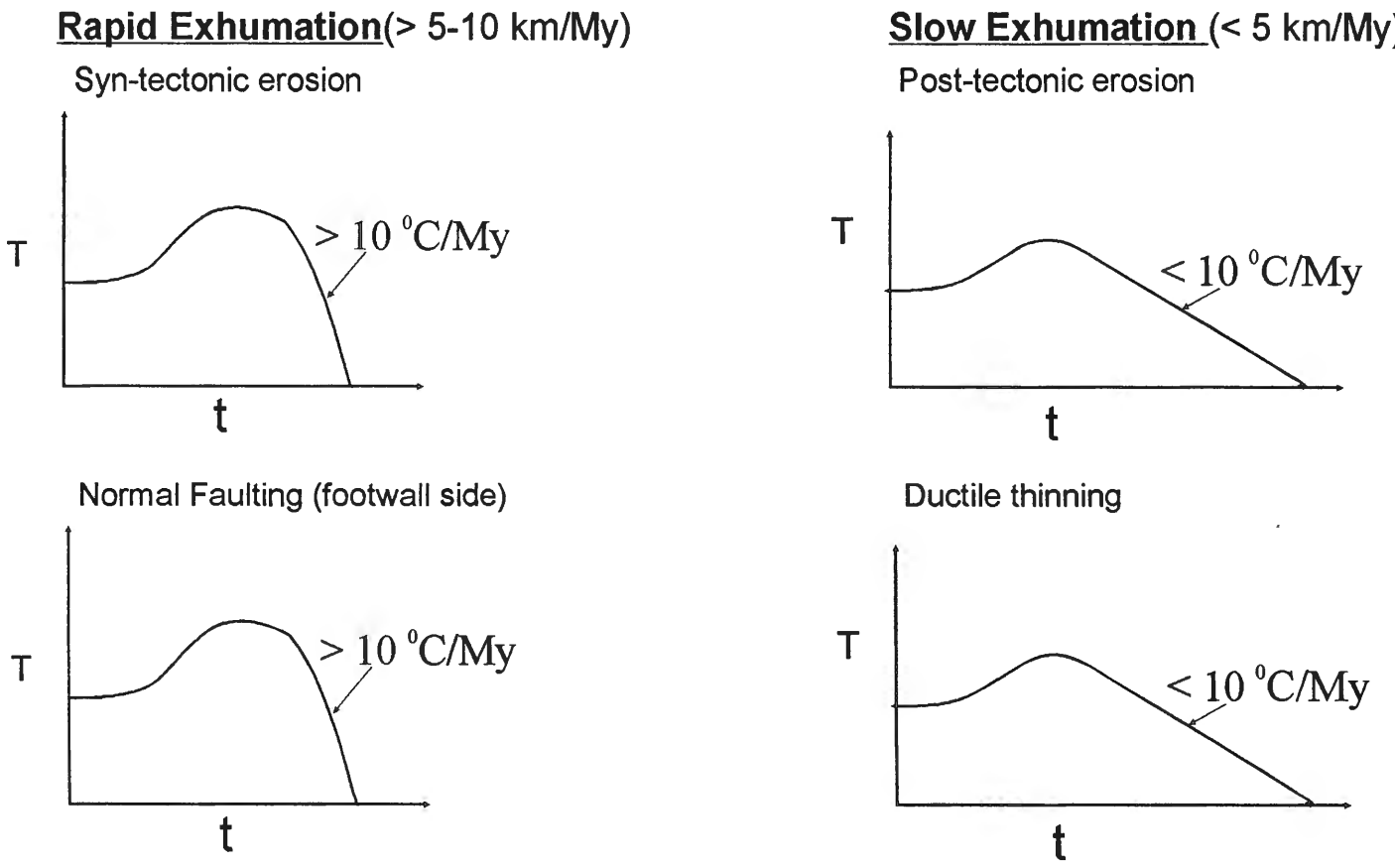

Figure 1.6: Temperature-time paths that are typical of rapid and slow exhumation processes. Further constraint on the process responsible for exhumation (i.e. distiguishing between syn-tectonic erosion versus normal faulting) must be made based on structures and kinematic indicators observed in the field. Based on Ring et al. (1999).

decay scheme, cooling ages represent the time at which the radiogenic daughter product ceased to diffuse out of the mineral. The temperature at which this occurs is the closure temperature (T_c; Dodson, 1973). If a mineral grows at or below T_c, the age is interpreted to represent the growth or crystallization age. Any subsequent increase in temperature above T_c may cause complete or partial resetting of the Ar isotopes within the mineral. The degree of resetting depends not only on temperature, but is also influenced by the duration of heating, deformation, and the chemical environment, especially when fluids are present.

Several mineral thermochronometers of varying T_c are currently used to determine cooling histories. In this study, the U-Pb isotopic system in monazite and titanite, and the K-Ar isotopic system in hornblende, muscovite, and K-feldspar are of particular interest. The T_c of the minerals have been experimentally well constrained (Purdy & Jager, 1976; Berger & York, 1981; Harrison, 1981; Parrish, 1990; Heaman & Parrish, 1991), or may be calculated. Since different minerals have different closure temperatures (> 800°C for U-Pb in zircon; Heaman & Parrish, 1991; ~ 530 ^{0}C for $^{40}Ar/^{39}Ar$ in hornblende; Harrison, 1981; and 60 - 125 ^{0}C for U-Pb for annealing of fission tracks in apatite; Gleadow et al., 1983), analysis of various minerals from the same locality provides a series of spatially related temperature-time (T-t) points.

Willigers et al. (2000) suggested that the thermal evolution of Precambrian orogens is distinct from Phanerozoic orogens. Geochronometers in young (Phanerozoic) orogens tend to record short-lived tectonic processes. They typically preserve diverse T-t paths within different terranes that reflect fast cooling rates (i.e. > 10 ^{0}C/My). Variations in mineral ages are often interpreted in terms of different local tectonic events and/or processes such as plutonism, fault displacement, rapid exhumation, or large-scale folding that may or may not occur synchronously at different locations within the orogen. Dynamic recrystallization in high strain zones may rest isotopic systems without necessarily perturbing the thermal regime. Juxtaposition of terranes with varying thermal histories may also occur during tectonic movements (Grasemann & Mancktelow, 1993). Local contrasts in thermal history may be preserved in the isotopic record as long as rocks remain at crustal levels where the ambient temperature is below the closure temperature of the affected geochronometer. Short-lived processes that are recorded at

near-surface levels, however, will not affect isotopic systems in the deeper levels of an orogen where ambient temperatures are above the closure temperature of an isotopic system. Therefore, in an orogen that has experienced crustal thickening, evidence for rapid, syn-orogenic exhumation may be limited to rocks that are carried to the upper crust, where thermochronometers can close as the geothermal gradient quickly relaxes to its equilibrium position. Rocks at lower levels, on the other hand, will reflect post-tectonic cooling and exhumation of the orogen as a whole, and may lack significant age variations (Willigers et al., 2000). Currently available data from the Paleoproterozoic Trans-Hudson Orogen suggest slow post-orogenic cooling at mid-deep crustal levels.

1.4 Statement of Problem & Purpose of Study

With the exception of the Churchill-Superior Boundary Zone, the current thermochronological data set shows apparent uniformity in metamorphic and cooling ages across the orogen. Most of the ages have been obtained from the Flin Flon, Kisseynew and Wollaston domains, where few of the ages have been linked to specific deformational and metamorphic events. Even fewer samples come from boundary shear zones.

In order to provide constraints on the post-orogenic cooling history of the THO, the main objectives of this study were to:

i) Acquire $^{40}Ar/^{39}Ar$ ages from 22 amphibole, 6 muscovite and 6 K-feldspar separates, which will represent the time at which the Reindeer Lake transect passed through 500 ^{0}C, 350 ^{0}C and ~ $\leq$ 350 ^{0}C respectively.

ii) Use these data with U-Pb ages from monazite and titanite (Corrigan et al., in prep.) to establish cooling history of the Reindeer Zone across the Reindeer Lake transect (Map 1).

iii) If possible, reconstruct the post-collisional thermal state of the THO – Reindeer Zone.

In the current study, analyzed samples have been geologically well constrained based on mapping carried out by myself under the field supervision of D. Corrigan of the Geological Survey of Canada (GSC), during a three year (1997-1999) collaborative mapping project with R. Maxiener of the Saskatchewan Geological Survey (SGS). Following the 1997 mapping season, two contiguous 1:20,000 scale maps were published

by the provincial and federal surveys (Maxeiner, 1997; Corrigan et al., 1997) and regional coverage was initiated by the GSC, extending from the northern flanks of the Glennie and Kisseynew Domains, across the Wathaman Batholith and into the Archean Peter Lake Domain. Logistical support for the three year mapping project was provided by the GSC.

Of the 28 samples analysed in this study, 25 were collected specifically for $^{40}Ar/^{39}Ar$ analyses during fieldwork conducted in 1999. The remaining 3 were obtained from the GSC collection in Ottawa, Ontario. Concordant U-Pb crystallization and metamorphic ages were obtained by D. Corrigan from the GSC geochronology laboratory for 10 of the 28 samples.

The purpose of this study is to determine whether the uniformity observed in monazite and titanite U-Pb ages is present in minerals (e.g. hornblende, muscovite and K-feldspar) with lower closure temperatures. Also, using the cooling pattern observed along the entire transect, and cooling histories determined for individual samples and domains, it is the aim of this project to constrain the post-orogenic history of the THO – Reindeer Zone.

Chapter II - Geology of the Reindeer Lake Transect

The Geological Survey of Canada (GSC) conducted the first reconnaissance mapping (1:380,160) of the islands and shoreline of Reindeer Lake, Saskatchewan (Stockwell, 1929). Subsequently, Alcock (1938), also of the GSC, mapped the southern portion of Reindeer Lake at 1:253,400 scale. Since then, detailed 1:20,000 scale mapping of the area has continued, much of the work having been carried out by the Saskatchewan Geological Survey (SGS).

In 1997, the GSC and SGS combined efforts in a new mapping initiative aimed at establishing the lithotectonic framework of the northwestern Reindeer Zone of the Trans-Hudson Orogen (Corrigan et al., 1999). The area mapped covered an area approximately 200 km x 40 km, spanning from the north flank of the Levesque Bay supracrustal assemblage to the Archean Peter Lake Domain. A detailed account of the field relations is found in Corrigan et al. (1998, 1999, 2000); a summary is presented below.

2.1 The Reindeer Zone

As was discussed in the previous chapter, development of the Trans – Hudson Orogen (THO) coincided with a critical period of continental accretionary tectonics during the late Paleoproterozoic, which contributed to the growth of the North American continent by the accretion of smaller cratons (Van Schmus et al., 1987; Hoffman, 1988; Lewry et al., 1994). Comprising reworked margins of three or more bounding Archean continental platforms, the THO was amalgamated ca. 1900 – 1800 Ma. Trapped between the continental paleoplatforms is a belt of juvenile early Proterozoic crust known as the Reindeer Zone (Lewry, 1990).

Along the shores and islands of Reindeer Lake, Saskatchewan, the Reindeer Zone comprises a stack of west-southwest striking, north-dipping, juvenile magmatic arc terranes and sedimentary basins that were accreted to the Archean Hearne Province during the Paleoproterozoic collision, as well as a younger molasse basin (McLennan Group) that was deformed with the other components during post-collisional convergence (Figure 1.3; Corrigan et al.; 1999). From south to north, in order of increasing structural level, the imbricated stack consists of the Glennie, Kisseynew and La Ronge Domains. North of the collage lie the Wathaman Batholith and the Archean Peter Lake Domain (see Map1).

2.1.1 Glennie Domain

The Glennie Domain comprises granodioritic orthogneisses and subordinate metavolcanic rocks and pelitic paragneisses. At the northern limit of the domain, progressive decrease in granodioritic orthogneiss and increasing abundance of migmatitic turbidites of the Burntwood Group (Kisseynew Domain) suggests that the Glennie-Kisseynew boundary is a transition zone between granitoid-dominated versus sedimentary-dominated domains. Granodioritic sheets of the Glennie Domain are, therefore, interpreted to be intrusive bodies in the Burntwood Group turbidites.

2.1.2 Kisseynew Domain

The Kisseynew Domain is an area of complex tectonostratigraphy. From south to north, towards higher structural level, it comprises migmatitic turbidite rocks of the Burntwood Group, and mafic volcanic and sedimentary rocks of the Levesque Bay supracrustal assemblage, as well as younger arkoses of the McLennan Group. Relative to each other, all three units are in fold-thrust relationship.

Burntwood Group (>1880 Ma?)

The Burntwood Group is the most voluminous component of the Kisseynew Domain, comprising stromatic migmatite, metatexite and diatexite derived from psammitic to pelitic turbidites with rare calc-silicate layers. Biotite – plagioclase – K-feldspar – quartz ± garnet ± cordierite ± sillimanite ± graphite is the characteristic assemblage. Diatexite is observed along the shores of Deep Bay, in the southern part of Reindeer Lake (Map 1). Forming a minor component of the northern Burntwood Group is an orthopyroxene - bearing gneiss of mafic to intermediate composition, possibly derived from gabbroic to tonalitic intrusions.

The exact age of the Burntwood Group is unclear. The most popular interpretation is that it was deposited in a back-arc basin to the La Ronge arc that formed at ca. 1850 – 1840 Ma (Ansdell et al., 1995) during continued convergence following continent-continent collision between the Superior, Sask and Hearne cratons. Recent data from the northern flank of the Kisseynew Domain, however, indicate that the northern portion of the domain contains turbidites that were coeval with the 1900 – 1880 Ma volcanic arc (Corrigan et al. 2001), in agreement with the interpretation of Lewry (1981).

Levesque Bay Supracrustal Assemblage (> 1870 Ma)

Structurally interleaved with the McLennan Group to the north, and separated from the latter by narrow high strain zones, is a heterogeneous rock package referred to as the Levesque Bay supracrustal assemblage. This heterogeneous package consists of garnet amphibolite, garnet – biotite ± sillimanite pelite and psammite, calc-silicate gneiss, impure quartzite, minor diopside marble, and minor sillimanite - anthophyllite ± cordierite gneiss. The supracrustal rocks are also intruded by ca. 1870 Ma tonalitic and leucotonalite dykes, one of which yielded a U-Pb zircon age of ca. 1897 Ma. The leucotonalite dyke also contained accessory monazite and titanite which yielded concordant $^{206}Pb/^{207}Pb$ ages of 1813 ± 2 Ma, 1817 ± 2 Ma and 1776 ± 4 Ma respectively (D. Corrigan pers. comm.).

McLennan Group (< 1840 Ma)

The McLennan Group, the Saskatchewan equivalent to the Sickle Group in Manitoba (Gilbert et al., 1980), consists primarily of magnetite-bearing, pink to grey, metamorphosed conglomerate, arkosic arenite and calcic psammites. In low strain domains, primary sedimentary textures are commonly preserved. Faserkiesel (sillimanite nodules) are characteristic of the unit and occur as deformed flattened ellipsoids up to 30 cm long. Minor polymictic conglomerate, restricted to the base of the sedimentary succession, contains clasts of granitic, fine-grained volcanic and sedimentary rocks that are interpreted to have been predominantly derived from the neighbouring La Ronge Domain (Maxeiner, 1998). The conglomerate is interpreted to represent a molasse type sedimentary basin (Stauffer, 1990).

2.1.3 La Ronge Domain

In the Reindeer Lake area, the La Ronge Domain comprises three main units. From south to north, these include the Central Metavolcanic Belt, the Milton Island metasedimentary assemblage, and the Park Island metasedimentary assemblage. Prior to mapping done by Corrigan et al. (1999, 2000) migmatitic orthogneisses in the northern reaches of the La Ronge Domain were assigned to the Rottenstone Domain. Previous workers (Lewry et al., 1981; Lewry et al., 1994; Stauffer, 1984) believed the intrusive Rottenstone tonalite-migmatite complex was emplaced contemporaneously with the Wathaman Batholith, as a result of north-directed subduction. Mapping conducted by

Corrigan et al. (1999, 2000) in the Reindeer Lake area, however, suggested the Rottenstone Domain comprises orthogneisses that are coeval with magmatism in the La Ronge arc and migmatitic rocks of the La Ronge Domain. Hence, in the Reindeer Lake area, what was previously known as the Rottenstone Domain has been included with the La Ronge Domain.

Central Metavolcanic Belt (CMB: 1892 –1878 Ma)

Within the CMB, volcanic rocks and their reworked and/or altered equivalents form numerous, highly recrystallized and moderately to highly strained layers intercalated with metasediment. These supracrustal rocks are well preserved in the Laxdal and Clements Island areas (Map 1), and the Lawrence Point and Reed Lake belts where vocaniclastic rocks predominate, with smaller amounts of mafic volcanic rocks with relict pillows, and amphibolites. Silicate- and oxide-facies banded iron formations also occur and are associated with gossan zones. Titanite obtained from Reed Lake belt yield U-Pb ages of 1781 ± 2 Ma and 1779 ± 2 Ma.

The northern reaches of the La Ronge Domain, formally interpreted as the Rottenstone Domain, comprise a package of banded orthogneiss of mixed dioritic, tonalitic, granodioritic and granitic composition. The unit intruded, and is spatially associated with the volcanogenic rocks of the CMB, where it is characterized by mafic to intermediate volcanic rocks injected by multiple felsic dykes. Preliminary U-Pb zircon ages of 1892 ± 2 Ma and 1878 ± 2 Ma from a tonalite and granite suggest the southernmost portion of the orthogneiss unit may be the plutonic root of the La Ronge arc, which includes volcanic rocks of similar age (Corrigan et al., 1999).

Milton Island Metasedimentary Assemblage

A remarkably homogeneous unit over a wide area, the Milton Island metasedimentary assemblage sits structurally above the CMB. It lies conformably over volcanic and volcaniclastic rocks of the CMB and is interpreted to have evolved penecontemporaneously with the latter. The assemblage consists of variably migmatitic, finely graded and thinly layered psammite and semipelite containing leucosomes of granitic composition that are separated from the mesosome by thin biotite-rich selvages. Metasediments have the assemblage biotite - muscovite ± fibrolite (sillimanite) ± graphite with rare garnet and apatite. Three single grain monazite analyses from this

assemblage yielded U-Pb ages of 1822 ± 1 Ma, 1804 ± 1 Ma and 1794 ± 3 Ma (Corrigan et al., in prep). The assemblage is interpreted to represent a forearc basin deposited on the northern flank of the La Ronge-Lynn Lake arc (Corrigan et al., 1999).

Park Island Metasedimentary Assemblage (1878 – 1865 Ma)

Situated structurally and unconformably above both the CMB and Milton Island assemblage is the Park Island metasedimentary assemblage. Lewry et al. (1981) recognized this unit and correlated it with the McLennan (Sickle) Group. Corrigan et al. (1999), however, recognized that the assemblage, though similar to the McLennan Group in some respects, must be older as it is intruded by the ca. 1865 – 1850 Ma Wathaman Batholith. They have interpreted it as the remnant of a foreland basin that formed during tectonic loading of the La Ronge arc onto the Hearne continental margin. It is a distinct package of siliciclastic rocks that comprises a basal conglomerate with clasts of metavolcanic and metasedimentary rocks that are interpreted to have originated from the CMB and Milton Island assemblage, pink to grey K-feldspar - dominated arkose, calcareous arkose, and psammite. Locally, faserkiesel nodules are present and within arkosic units, well-preserved trough crossbeds and laminar beds are also observed. Biotite, magnetite and hornblende locally form the main mafic minerals observed within the assemblage.

The Park Island metasediments display variable degrees of partial melting, with the proportion of leucosome increasing towards the Wathaman Batholith. Large enclaves of this unit are present in the batholith, constraining the depositional age of the Park Island assemblage to between 1878 Ma (age of youngest volcanics in the CMB) and 1865 Ma (earliest phases of the Wathaman Batholith).

Plutonic Rocks (1865 – 1850 Ma)

Within the La Ronge Domain, several large (tens of kilometres) plutons are observed. They range from ultramafic and gabbroic plugs and/or dykes, to voluminous quartz diorite and diorite (Cowie, Walter Island, Milton Island and Butler Island plutons), monzodiorite and granodiorite (Jackpine Bay pluton), monzogranite (McMillan Lake pluton), to granite. Generally, they preserve relict igneous minerals and textures and, in contrast to the orthogneisses of the CMB, individual plutons are compositionally

homogeneous. All plutons crosscut structures and fabrics observed in the enclosing gneiss, and were locally affected by regional deformation at high metamorphic grade.

U-Pb analysis on a zircon from the Butler Island Diorite, located in the southern portion of the La Ronge Domain, yielded an age of 1858 ± 2 Ma (Corrigan et al., in prep.). Plutons within the La Ronge Domain are similar in age and share many geochemical characteristics with the Wathaman Batholith, suggesting their emplacement was contemporaneous and that they may represent satellites to the latter (MacHattie, 2001).

2.2 Wathaman Batholith

The Wathaman Batholith is a stitching pluton that was emplaced ca. 1865 – 1850 Ma (Ray & Wanless, 1980) at the boundary between the margin of the Archean Hearne craton and accreted volcano-sedimentary rocks of the La Ronge Domain (Map 1 & Figure 2.1). In the Reindeer Lake area the batholith is bounded by the Reilly Lake and Parker Lake shear zones in the south and north respectively, with both shear zones merely reworking intrusive margins. Along its southern margin, megacrystic granitoid rocks of the Wathaman suite intruded metasediments of the Park Island assemblage and were subsequently reworked by south-directed thrusting along the Reilly Lake Shear Zone. Along the northern shore of Reindeer Lake, the batholith intruded gneisses of the Archean Peter Lake Domain and was subsequently reworked along the Parker Lake shear zone (Corrigan et al., 2000; Lafrance and Varga, 1996). These observations contrast with those of previous workers who interpreted the Wathaman batholith as a magmatic arc that was emplaced between the reworked margin of the Hearne craton and arc-related domains of the Reindeer Zone along the Parker Lake and Reilly Lake shear zones respectively (Lewry & Collerson, 1990, and references therein).

Within the Wathaman Batholith, five different compositional types of potassium feldspar megacrystic granitoid bodies have been identified (Figure 2.1). In order of decreasing abundance, the bodies are granodiorite, granite, monzogranite (± quartz), syenite, and monzodiorite. Biotite is common to all phases and occurs in varying proportions. In addition to biotite, and common to all but the granitic phases, are hornblende, titanite and epidote. Microcline megacrysts may be anywhere from 1 cm to 8 cm in size, with rapakivi textures locally preserved. Generally, the central portion of

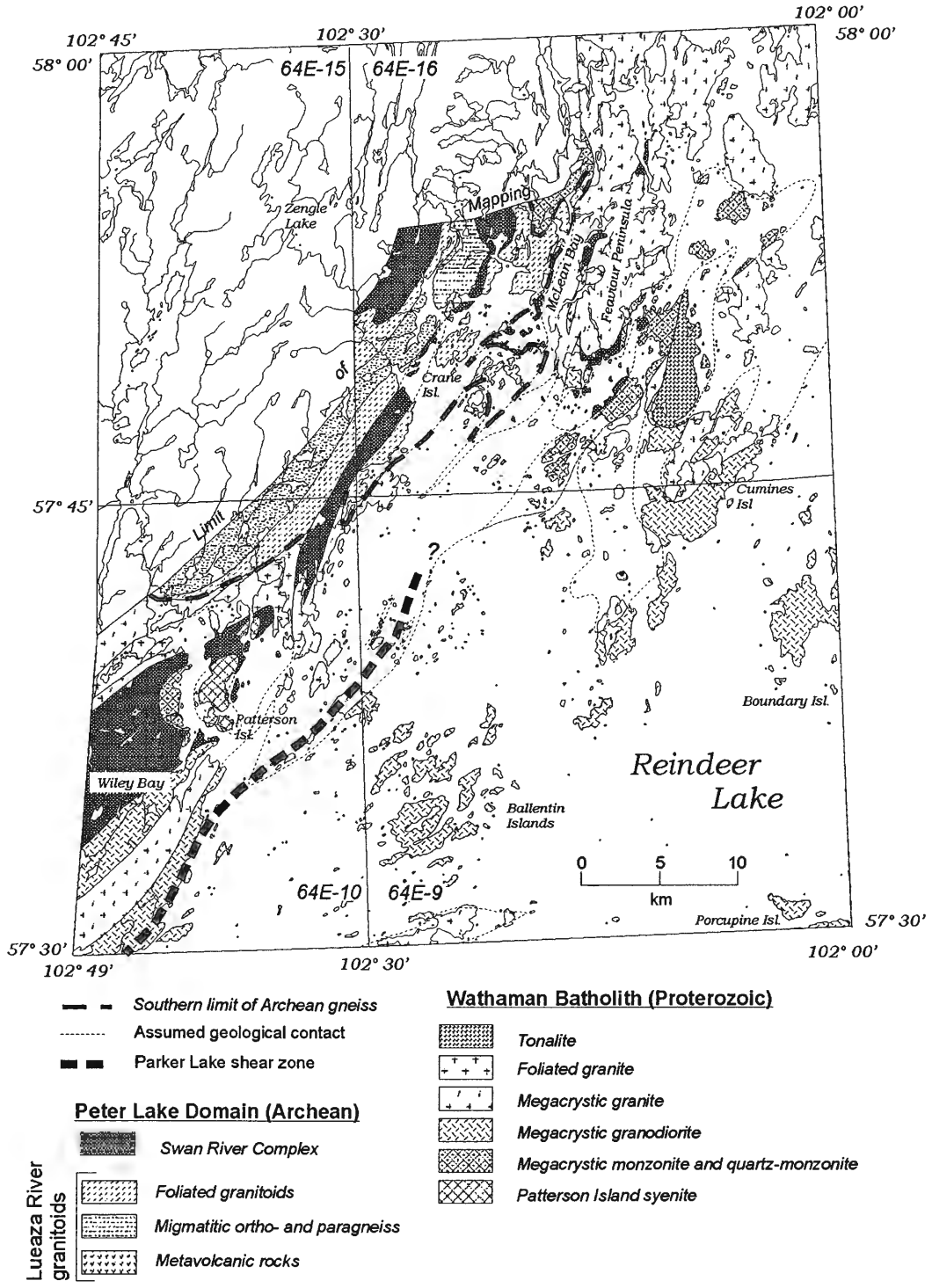

Figure 2.1: Geological map of the northern shore and islands of Reindeer Lake, Saskatchewan. After Corrigan et al. (2000).

the batholith is only mildly re-crystallized, preserving igneous minerals and crystal zoning. Primary igneous textures such as magmatic flow alignment and accumulated megacrysts indicate that the crystals are igneous in origin.

A U-Pb zircon age from a pluton located southwest of the study area yielded a crystallization age of 1865 Ma (Ray & Wanless, 1980). Titanite from a sample collected from Reindeer Lake yielded a U-Pb cooling age of 1790 ± 8 Ma (Corrigan et al., in prep).

2.3 Peter Lake Domain

Mapping in the Peter Lake Domain concentrated on an 8 – 10 km strip along its southeastern margin, corresponding mainly to the Lueaza River granitoids of Stauffer et al. (1981). The region comprises a belt of migmatitic ortho- and paragneisses flanked by abundant, non-migmatitic, recrystallized, strongly foliated granitoid rocks, and screens of minor supracrustal material, all of which have been intruded by recrystallized and highly deformed amphibolite dykes, younger plagioclase-phyric mafic dykes, and granitoid plutons related to the Wathaman suite (Figure 2.1). The northwestern belt of granitoid rocks includes granite and granodiorite with numerous transposed diorite enclaves. The southeastern belt comprises sugary-textured leucogranite and associated granodiorite. Minor pink biotite granite commonly forms narrow dykes intruding the leucogranites and granodiorites. The most distinctive phases of this complex are a salmon-pink quartz syenite and syenite which contain biotite and abundant accessory allanite. U-Pb zircon analysis of two granitoid samples just south of Crane Island (Figure 2.1) yielded ages of 2582 ± 19 Ma and 2556 ± 22 Ma (Bickford et al., 1986).

Locally, a few outcrops of heterogeneous amphibolite with calc-silicate alteration bands and pods were found intercalated with the Lueaza River granitoids. Rarely exceeding a few tens of metres in thickness, these units are generally discontinuous along strike, and due to their compositionally heterogeneous and fine-grained nature, have been interpreted as metavolcanic rocks of uncertain affinity.

Swan River Complex

The "Swan River Pluton" (Lewry et al., 1981; Stauffer et al., 1981), is a compositionally heterogeneous intrusive complex involving small plutons as well as sills and/or dykes. As the composition of bodies within the unit ranges from ultramafic to mafic, Corrigan et al. (2000) have modified the name to the "Swan River Complex".

Sills and/or dykes of the complex are commonly layered; crosscutting sets of rhythmic layers are locally observed suggesting emplacement in a tectonically active environment. Sills and dykes are ultramafic with alternating layers of dunite and harzburgite that grade into orthopyroxene-bearing gabbro with well developed subophitic textures and layered gabbro with rhythmic layering. Locally, layers of leucogabbro and anorthosite are also observed. The Swan River Complex locally contains coronitic gabbro with garnet + pargasite rims surrounding olivine, suggesting metamorphism was upper greenschist - lower amphibolite facies.

A preliminary U-Pb zircon age of 1865 ± 10 Ma from the Swan River Complex (Bickford et al., 1986) was later revised to 1908 ± 27 Ma (Bickford et al. 1987). Recent U-Pb zircon data (D. Corrigan pers comm.) from a gabbro yielded a discordant array with an upper intercept of 2562 ± 4 Ma which is interpreted as the time of emplacement, and a lower intercept of 1830 ± 12 Ma indicating the approximate time of Trans-Hudson age tectonothermal overprinting (Corrigan et al., in prep.). U-Pb data from both studies support the interpretation of Lewry et al. (1981) who suggested members of the Swan River complex are late Archean – early Paleoproterozoic intrusive rocks that were emplaced prior to the Hudsonian orogeny.

2.4 Structural and Metamorphic Framework

Based on geochronological data (Corrigan et al., in prep.), and tectonostratigraphic relationships (Corrigan et al., 1998, 1999), four structural levels have been identified within the Reindeer Lake area. The Levesque Bay supracrustal assemblage, the CMB and associated orthogneisses of the Crowe Island complex, and the Peter Lake Domain are the oldest recognizable protoliths, forming "level 1". Stratigraphically overlying the CMB and its associated orthogneisses lies the Milton Island metasedimentary assemblage which forms "level 2". The third structural level comprises the Park Island metasediments, which were deposited unconformably over the first two levels and later infolded with the latter. Finally, structural "level 4" consists of the younger McLennan Group arkoses and Burntwood Group turbidites.

In the Reindeer Lake area, three major generations of ductile structures are observed (Corrigan et al., 1999). D_1 structures consist of large-scale recumbent folds involving the CMB and the Milton Island metasedimentary assemblage, which are

interpreted to have formed during the accretion of the La Ronge arc to the Archean Hearne margin between ca. 1880 – 1865 Ma. Based on SHRIMP zircon data, and structural and tectonostratigraphic relationships, deposition of the Park Island assemblage in a foredeep basin setting is interpreted to have resulted from the accretion of the La Ronge arc to the Rae-Hearne craton.

Prior to D_2 deformation, the Wathaman Batholith began forming above the subduction zone. During the interval ca. 1865 - 1850 Ma (Bickford et al., 1980; Ray & Wanless, 1980, Meyer et al., 1992), the batholith was emplaced along the accreted margin of the La Ronge-Lynn Lake arc. Peak regional metamorphism to maximum temperatures of ~ 750 ^{0}C within the Kisseynew Domain at ca. 1820 – 1790 Ma followed emplacement of the Wathaman Batholith during D_2. At this time, the Reilly Lake and Duck Lake shear zones developed along the structural base of the Wathaman Batholith and La Ronge Domain respectively. Contemporaneous with movement along these shear zones, the Levesque Bay thrust zone formed an imbricated stack of thrust slices involving supracrustal basement rocks (Levesque Bay assemblage), and the younger McLennan Group molasse deposit.

D_3 structures comprising north-south trending upright open folds are observed between the Duck Lake and Reilly Lake shear zones within the La Ronge Domain. D_3 axial planar foliations are steep and locally defined by chlorite and muscovite, suggesting that D_3 was a late-orogenic event that occurred at relatively low metamorphic grade. U-Pb titanite ages of ca. 1780 Ma are interpreted by Corrigan et al. (1999) to represent post peak-metamorphic cooling through 600 ^{0}C, and thus provide a maximum age for D_3.

Despite the structural complexity of the Reindeer Zone, metamorphic grade from orogen core to margin does not vary greatly across major shear zones. Chakungal (1999) documented a south-to-north gradational decrease in both temperature and pressure, with P-T conditions in the core of the orogen (Kisseynew Domain) averaging 5.5 kb-700 ^{0}C (transitional granulite facies), decreasing to an average of 4.2 kb-600 ^{0}C (mid-amphibolite facies) at the northern most edge of the La Ronge Domain (Figure 2.2). Field observations north of the Wathaman Batholith suggest that within the Peter Lake Domain, P-T conditions did not exceed upper greenschist – lower amphibolite facies.

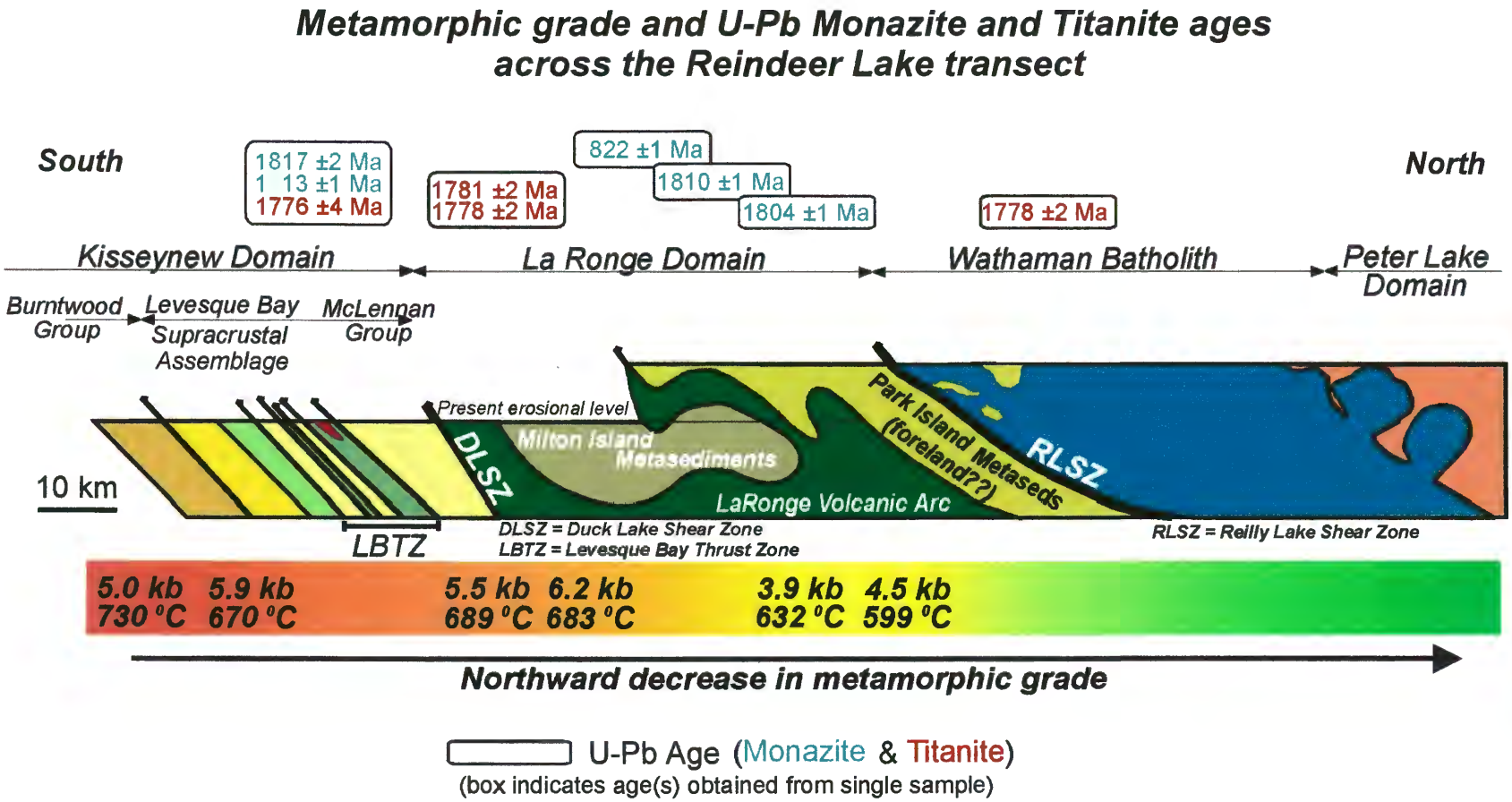

Figure 2.2: Metamorphic and U-Pb geochronologic constraints on the tectonothermal evolution of the Reindeer Lake transect. (P-T data from Chakungal, 1999 unpublished B.Sc. thesis; U-Pb ages from Corrigan et al., 1999 and Corrigan et al. in prep.)

U-Pb data obtained from monazite and titanite grains display little variation in metamorphic ages (Figure 2.2). From orogen margin to core, U-Pb monazite ages range from 1822 ± 1 Ma to 1817 ± 2 Ma. These dates are interpreted to represent the time of peak metamorphism and/or cooling through ca. 750 - 700 °C. U-Pb titanite ages range from 1790 ± 8 Ma to 1776 ± 4 Ma, and are interpreted as the time of cooling through ca. 600 - 550 °C. (Ansdell et al., 1995; Corrigan et al., 1999; Corrigan et al., in prep.)

2.5 Tectonic History

Based on U-Pb zircon data and the structural and metamorphic framework of the Reindeer Lake transect, the La Ronge arc was volcanically active during the interval between ca. ~ 1920 – 1880 Ma. Volcanism was contemporaneous with south-southeast directed subduction and possibly deposition of the Milton Island sediments to the north. Between the interval 1880 – 1865 Ma the La Ronge arc was accreted to the Hearne margin. This event resulted in the deposition of the Park Island sediments. Between ca. 1865 – 1850 Ma, the Wathaman Batholith was emplaced along the accreted margin of the La Ronge Domain. Terminal continent-continent collision at ca. 1830 – 1800 Ma resulted in penetrative regional deformation and the development of the Reilly Lake and Duck Lake shear zones at the structural base of the Wathaman Batholith and La Ronge Domain, respectively. Contemporaneous with regional deformation was also the formation of a molasse basin into which the McLennan Group arkoses were deposited. As post-collisional convergence continued, rocks of the Reindeer Zone were buried to increasing depths, reaching peak metamorphic conditions of ~ 5.5 kb and 700 ^{0}C in the orogen core at ca. 1820 – 1810 Ma. Following peak metamorphism, Ma tectonic activity throughout the Reindeer Zone may have ceased permitting the zone to reach thermal equilibrium as is suggested by the widespread preservation of U-Pb monazites of that age across the orogen. Post-tectonic thermal equilibration of the orogen may also explain the lack of variation in the metamorphic grade across domain boundaries.

The present study was designed to test this interpretation by using the $^{40}Ar/^{39}Ar$ geochronological method on hornblende, muscovite, and K-feldspar grains to constrain the time at which the zone cooled through their respective closure temperatures (500 ^{0}C, 350 ^{0}C and ~250 ^{0}C). If the rocks of the Reindeer Zone exposed along Reindeer Lake reached thermal equilibrium following convergence, prior to exhumation, then

hornblende, muscovite and K-feldspar could be expected to preserve similar $^{40}Ar/^{39}Ar$ ages and similar, slow cooling rates across the transect, from margin to core.

CHAPTER III – $^{40}Ar/^{39}Ar$ Thermochronology

3.1 Introduction – Basis of the $^{40}Ar/^{39}Ar$ Method

Developed by Merrihue and Turner (1966), the $^{40}Ar/^{39}Ar$ method of thermochronology has its foundations in the potassium-argon (K-Ar) isotopic dating method. The following summary is based on a more detailed discussion of the method found in McDougall and Harrison (1988).

The K-Ar method of thermochronology is based on the natural occurrence of ^{40}K, which has a half-life of 1.25×10^9 years and decays to both ^{40}Ca and ^{40}Ar. In a closed system, the total number of radiogenic ^{40}Ca and ^{40}Ar atoms formed during time (t) can be expressed as:

$$^{40}Ar + ^{40}Ca = ^{40}K\left(e^{\lambda t} - 1\right) \qquad (1)$$

where ^{40}K, ^{40}Ar, and ^{40}Ca are the present-day atomic abundances of the isotopes, and λ is the total decay constant for ^{40}K. However, since it is the branch yielding ^{40}Ar as the daughter product that provides the basis for the conventional K-Ar dating technique, and thus the $^{40}Ar/^{39}Ar$ method, equation 1 can be modified as follows:

$$^{40}Ar = ^{40}K \frac{\lambda_e + \lambda_e'}{\lambda}\left(e^{\lambda t} - 1\right) \qquad (2)$$

where $\lambda_e + \lambda_e'$ are the relevant decay constants for the decay of ^{40}K to ^{40}Ar. The $^{40}Ar/^{39}Ar$ dating method differs from the K-Ar method in that the sample to be analyzed is first irradiated in a nuclear reactor where a proportion of the ^{39}K atoms is transformed to ^{39}Ar by the bombardment of fast neutrons, thus permitting measurement of the $^{40}Ar/^{40}K$ ratio (i.e. $^{40}Ar^*/^{39}Ar_K$) in a single isotopic analysis. The number of ^{39}Ar atoms formed by the irradiation process may be expressed as:

$$^{39}Ar_K = ^{39}K\Delta\int \phi_E \sigma_E dE \qquad (3)$$

where the limits of the integration are determined by the range of neutron energies (E), $^{39}Ar_K$ is the number of ^{39}Ar atoms produced from ^{39}K in the sample, Δ is the radiation time in seconds, ϕ_E is the neutron flux at energy E, and σ_E is the capture cross section of ^{39}K nuclei for neutrons of energy E. By dividing equation 2 by equation 3, one is able to obtain the ratio of ^{40}Ar to ^{39}Ar:

$$\frac{^{40}Ar}{^{39}Ar_K} = \frac{^{40}K\left(\lambda_e + \lambda_e'\right)\left[e^{\lambda t} - 1\right]}{^{39}K\lambda\Delta\int \phi_E \sigma_E dE} \qquad (4)$$

To avoid the complications involved in evaluating all variables in equation 4, Mitchell (1968) introduced a dimensionless irradiation parameter, J, that is defined as follows:

$$J = \frac{^{39}K}{^{40}K}\frac{\lambda}{\lambda_e + \lambda_e'}\Delta\int \phi_E \sigma_E dE \qquad (5)$$

Due to the difficulty in accurately determining the integrated fast neutron dose a sample has received, the J parameter is evaluated by irradiation of a standard sample of known age, termed a flux monitor (Merrihue and Turner, 1966). In this study, the flux monitor used was MMhb-1 (McClure Mountain hornblende; Roddick, 1983) with a known age of 520 ± 2 Ma (Samson & Alexander, 1987). Thus, from equations 4 and 5, the J parameter is:

$$J = \frac{e^{(\lambda t_m)} - 1}{\left(\frac{^{40}Ar}{^{39}Ar_K}\right)_m} \qquad (6)$$

where t_m is the known age and $(^{40}Ar/^{39}Ar)_m$ is the measured argon isotopic ratio of the monitored mineral. Once the J parameter has been evaluated, the substitution of equation 5 into equation 4 permits calculation of age, t, of the unknown sample:

$$t = \frac{1}{\lambda}\ln\left(1 + J\frac{^{40}Ar}{^{39}Ar_K}\right) \qquad (7)$$

The $^{40}Ar/^{39}Ar$ dating technique rests upon several assumptions (McDougall Harrison, 1988). Firstly it is assumed that the rate at which the parent nuclide (^{40}K) decays is independent of its physical state and is not affected by pressure or temperature. Secondly, it is assumed that all radiogenic argon measured in the sample is a product of in situ decay of ^{40}K since cooling to Ar retention temperatures following crystallization or recrystallization of the rock. In other words, the sample must have remained a closed system since the event being dated. Thirdly, the $^{40}K/K$ ratio is assumed to be constant in nature, and finally, it is normally assumed that all nonradiogenic ^{40}Ar present in the sample being dated is atmospheric in origin.

3.1.1 Basis of the $^{40}Ar/^{39}Ar$ Step Heating Method

Once a sample has been irradiated, the $^{40}Ar/^{39}Ar_K$ ratio is determined by isotopic analysis in a mass spectrometer. The sample is first placed in a vacuum furnace and then Ar is extracted as it is heated in increments beginning at temperatures well below that of

fusion (Merrihue and Turner, 1966). The gas extracted at each step is purified before being admitted to the mass spectrometer where the relative abundances of ^{40}Ar, ^{39}Ar, ^{37}Ar and ^{36}Ar are measured. The $^{40}Ar/^{39}Ar_K$ ratio is then determined and the age calculated for each temperature increment. Upon complete analysis, a series of apparent ages is obtained for the sample, and plotted against the percentage of total ^{39}Ar released, to produce an age spectrum. The latter provides information on the distribution of ^{40}Ar within the sample, relative to ^{39}K and thus ^{40}K. A "total gas age" is determined by calculating the weighted mean of the ages from all steps, where the weight factor is the percentage of ^{39}Ar gas released in each step. The larger the step (i.e. steps for which large volumes of gas were released), the more its apparent age contributes to the age of the sample as a whole (Turner, 1968).

3.1.2 Introduction to interpretation of $^{40}Ar/^{39}Ar$ Age Spectra:

Interpretation of age spectra is commonly based on the single-site diffusion model of Turner (1968). In this model, the T-dependence of thermally activated solid diffusion is described by an Arrhenius relationship (McDougall and Harrison, 1988):

$$\frac{D}{a^2} = \frac{D_o}{a^2} e^{(-E_a/RT)} \qquad (8)$$

in which D is the diffusion coefficient that is determined by combining the molecular permeability of the system and the solubility of the diffusant, a is the effective diffusion radius, D_o is the frequency factor (diffusivity when $T = \infty$), E_a is the activation energy in kcal/mol, T is the absolute temperature in K, and R is the ideal gas constant (kPa/mol K).

At sufficiently high temperatures, D may be high enough that Ar produced by radioactive decay almost immediately diffuses out of the crystal structure, and the system behaves as an open system (Reynolds, 1992). However, as the change in the value of D with temperature is exponential, decreasing temperature gives rise to the transition from open-system behaviour to one in which daughter products become effectively immobile and the system becomes closed to diffusion (Dodson, 1973). The temperature at which a system becomes closed to diffusion of daughter elements is known as the closure temperature (T_c). This has been defined by Dodson (1973) as follows:

$$T_c = \frac{E_a / R}{\ln\left[\frac{ART_c^2(D_o/a^2)}{E_a(dT/dt)}\right]} \qquad (9)$$

where A is a geometrical constant and dT/dt is the cooling rate.

As is mathematically stated above, the closure temperature of a system is highly dependent on the activation energy, frequency factor, and effective diffusion radius, all of which depend on the structural state of the grains being analyzed. Thus, before T_c can be calculated the diffusion parameters must be evaluated. Several numerical solutions that describe diffusion out of simple geometric shapes have been developed based on Fick's second law, which has the form:

$$\frac{\partial C}{\partial t} = D\left(\frac{\partial^2 C}{\partial x^2} + \frac{\partial^2 C}{\partial y^2} + \frac{\partial^2 C}{\partial z^2}\right) \qquad (10)$$

The numerical solutions include geometric shapes such as spheres, cylinders, plane-sheets and cubes, and express the fraction of gas lost by diffusion (f) in terms of D_o/a^2 and the diffusion time (t), where both f and t may be measured in laboratory step-heating experiments in order to calculate D_o/a^2. However, due to the complexity of natural systems, a number of restrictions must be applied (see McDougall and Harrison, 1988). One such restriction is that the phase being analyzed must remain stable. Hydrous phases such as amphibole and biotite decompose during vacuum extraction heating and therefore, diffusion experiments are not applicable unless conducted under hydrothermal, oxygen buffered conditions. For this reason, closure temperatures for conventional $^{40}Ar/^{39}Ar_K$ dates on micas and amphiboles are assumed based on temperatures calculated in previous studies (i.e. Hanes, 1991; Purdy and Jager, 1976), and not calculated. In the case of K-feldspars, Berger and York (1981) determined a means of obtaining values for D_o/a^2 and E_a directly from the $^{40}Ar/^{39}Ar_K$ step-heating data using Arrhenius plots, a method that is discussed further in section 3.5.1.

The single-site diffusion model requires that a geologically meaningful age should be characterized by a perfectly flat spectrum (plateau) obtained from samples that cooled rapidly through their closure temperature (T_c), and subsequently remain thermally undisturbed (Turner, 1968). In such a sample both ^{39}Ar and radiogenic ^{40}Ar ideally occur in the same proportions within the same site, and during a step heating experiment, the two isotopes should be released in the same proportions as a consequence of their similar diffusion coefficients. Thus, a constant $^{40}Ar/^{39}Ar_K$ ratio would be observed for each step, yielding a flat age spectrum interpreted to indicate the sample had remained thermally

undisturbed (a closed system) since the time at which it passed through its T_c. This model predicts that thermally disturbed samples produce age gradients in which the initial age is lowered as a consequence of Ar loss, depending on the intensity of the overprinting thermal event (Berger and York, 1981). Berger and York (1981) also noted that in disturbed samples the initial closure age is often recorded in the high temperature extraction steps, thus permitting the method to be used in thermally complex areas.

In practice, age spectra produced by real samples display considerable deviations from the theoretical model. These observations have led to the establishment of criteria for the interpretation of age spectra in order to determine a geologically meaningful age for samples that produce irregular spectra. Generally, a plateau is defined on the basis of several contiguous steps making up a significant proportion ($\geq$ 50%) of the total gas released that have the same age within analytical error (Fleck et al., 1977). Although the tradition of describing a sample as having or lacking a plateau still persists, absence of a plateau is no longer a basis for the rejection of an analysis. Likewise, the presence of a plateau is not necessarily indicative of a geologically meaningful age.

Age spectra commonly yield disturbed plateaus, or may even fail to yield a plateau at all, due to violation of one or both of the basic assumptions, or to experimental and/or geological effects. Common geological effects include excess Ar, and the presence of impurities in the separate that may release components of radiogenic argon that differ in age from the bulk of the separate. For relatively low-K phases, such as amphibole, the presence of impurities is especially problematic since the total radiogenic Ar produced is low and thus easily outweighed by high-K impurities (eg. biotite) that may also release gas during the same analysis. To confirm that the gas analyzed for each sample is derived from amphibole, Ca^{2+}/K^{+} ratios are calculated from amphibole microprobe analyses and converted to $^{37}Ar/^{39}Ar$ ratios using the relationship:

$$\frac{\left(Ca^{2+}/K^{+}\right)_M \left(Ca^{2+}/K^{+}\right)}{1.9} = {}^{37}Ar/{}_{39}Ar \qquad (11)$$

where, $(Ca^{2+}/K^{+})_M$ is the ratio of the atomic percentages calculated from microprobe data and (Ca^{2+}/K^{+}) is the ratio of the atomic weights. The range of calculated ratios is then used to determine which steps during the experiment released gas that was derived from amphibole.

The most difficult problem in $^{40}Ar/^{39}Ar$ spectrum interpretation is that of "excess Ar". This is ^{40}Ar that has not been produced by the in situ decay of ^{40}K, and is distinct from inherited Ar, which is old in situ radiogenic ^{40}Ar that has been retained during a thermal event. The excess Ar effect is often recognized by "U-shaped" spectra, where both low and high temperature steps are characterized by anomalously high ages with lower ages in between (Figure 3.1). These "U-shaped" spectra may be observed in various minerals from different geological environments and are believed to be the result of local Ar overpressure during mineral crystallization (or recrystallization) which forces Ar of non-atmospheric composition with an excess ^{40}Ar component to enter the structure at temperatures where diffusion is too slow to expel it (Harrison and McDougall, 1981). In such cases the low age(s) between the low and high temperature steps may be geologically reasonable, possibly defining (at best) a maximum age for the sample.

In some cases even more irregular age spectra may result from excess Ar. Based on the observation that different non-radiogenic components are released in different temperature ranges, an irregular age spectrum can be analyzed using an inverse isochron plot in which the $^{36}Ar/^{40}Ar$ ratio is plotted against the $^{39}Ar/^{40}Ar$ ratio for each step (Figure 3.2). If several contiguous steps define a line, one or several components of non-atmospheric Ar may be distinguished, in which case the $^{36}Ar/^{40}Ar$ ratio defined by the y-intercept of the line, not the atmospheric ratio (295.5; Attendorn & Bowen, 1997), is used to correct for non-radiogenic ^{40}Ar for these steps (Heizler and Harrison, 1988). The $^{39}Ar/^{40}Ar$ ratio defined by the x-intercept of this line, corrected for the sample line blank, may then be used to calculate the age of these steps. In the case of a single non-radiogenic component, steps making up a plateau will always plot in a straight line, intersecting the $^{36}Ar/^{40}Ar$ axis at the atmospheric value and the $^{39}Ar/^{40}Ar$ axis at the plateau value.

Common experimental effects that give rise to irregular argon age spectra include differential movement of ^{39}Ar from near-surface sites and/or redistribution of ^{39}Ar within the grain during irradiation, due to the recoil energy of the reaction of ^{39}K to ^{39}Ar. With the exception of fine-grained samples, however, loss due to recoil generally affects only the first few percent of gas released and is easily recognized as it causes anomalously high ages due to the loss of ^{39}Ar relative to ^{40}Ar.

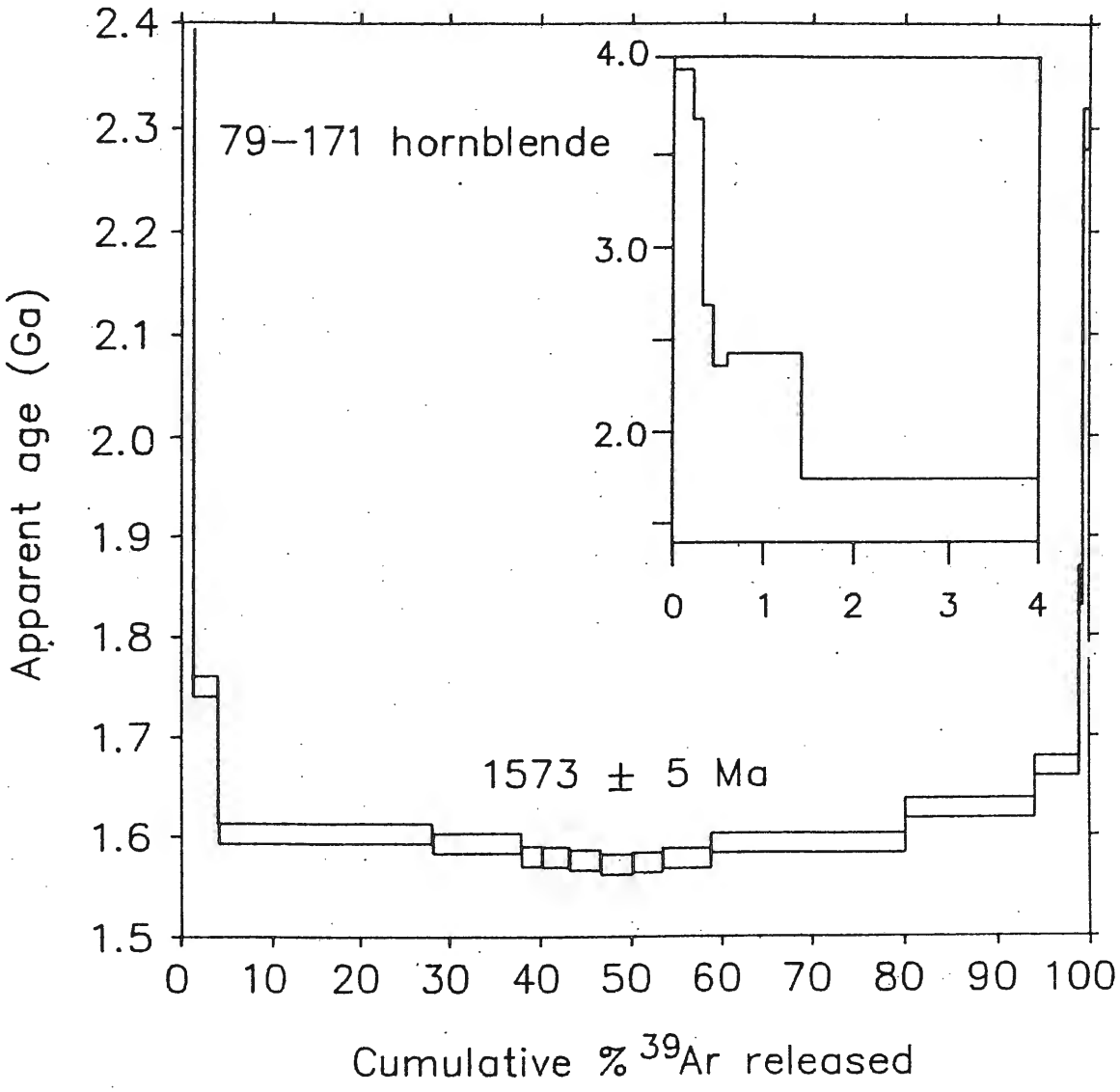

Figure 3.1: An example of an age spectrum yielded from hornblende containing excess ^{40}Ar (after Harrison and McDougall, 1981). The inset is an expanded scale of the age spectrum over the first 4% of cumulative ^{39}Ar released. Note, excess ^{40}Ar is released in both the initial and final stages of gas release, whereas the intermediate region is not contaminated and yields a maximum age for the sample. (McDougall & Harrison, 1988)

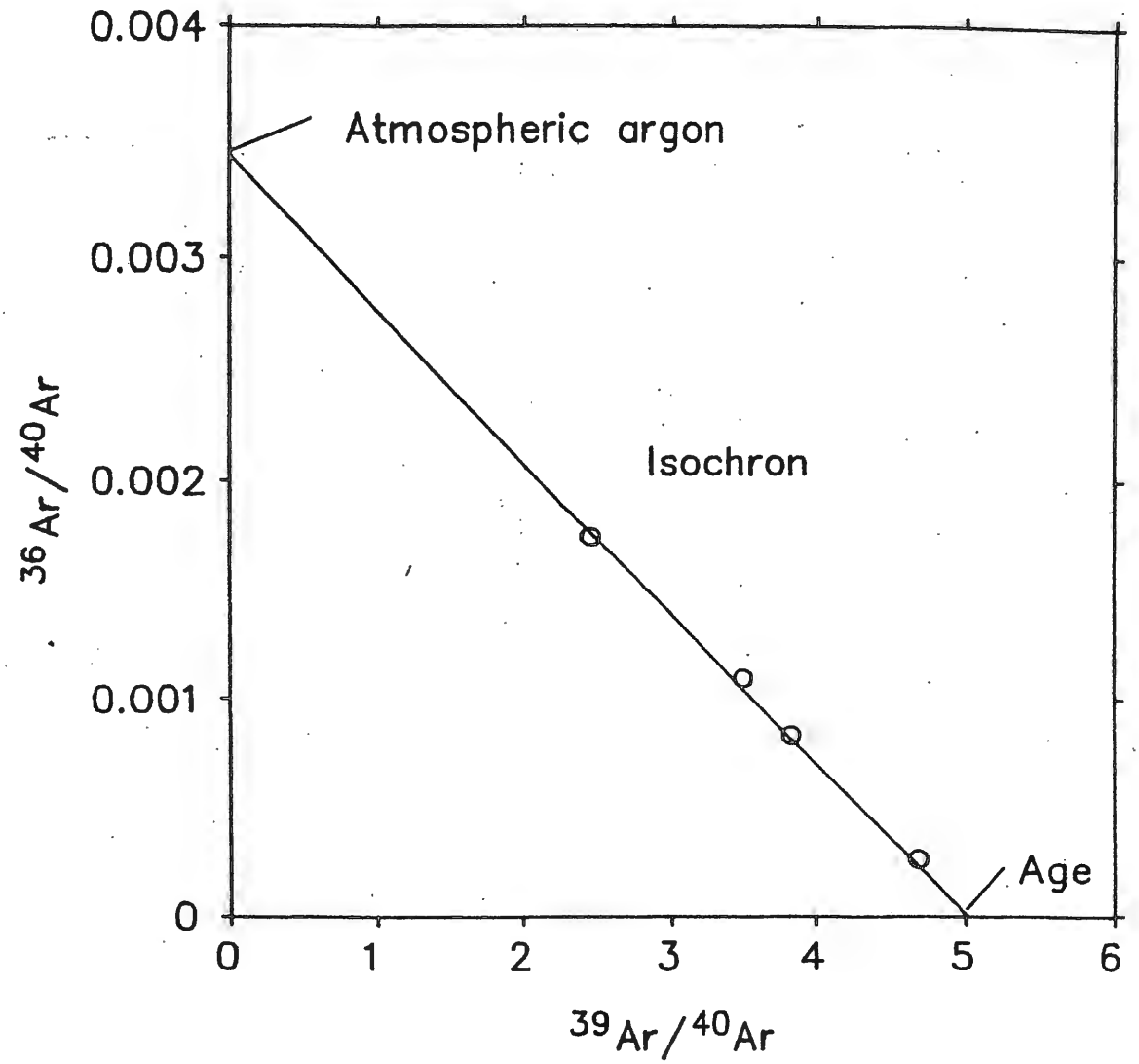

Figure 3.2: Schematic illustration of the inverse isochron plot. If several contiguous steps define a line, one or more non-atmospheric components of Ar may be distinguished, in which case the $^{36}Ar/^{40}Ar$ ratio defined by the line is used to correct for non-radiogenic ^{40}Ar for the steps. The x-intercept, on the other hand, when corrected for the sample line blank, corresponds with the radiogenic component of trapped argon and is used to calculate the age of the sample (the inverse $^{40}Ar/^{39}Ar$ ratio). (McDougall & Harrison, 1988)

A more serious experimental artifact is the problem of sample breakdown during dry *in vacuo* heating. In this environment hydrous minerals become unstable during heating. For example, it has been shown that unless diffusion experiments are conducted under hydrothermal, isothermal, oxygen-buffered conditions, delamination and alteration of the crystal structure of biotite occurs at or even below the temperatures at which argon release usually occurs in step-heating experiments (Gaber et al.1988). As this mechanism of argon release differs greatly from the way in which it is released in nature, the significance of gradients and/or a plateau must be questioned. In contrast, during heating muscovite grains are generally well behaved relative to biotite. It has been observed that muscovite is less likely to incorporate excess Ar during a thermal event compared with coexisting biotite (Roddick, 1986). It seems also that white micas yield ideal, essentially flat age spectra when undisturbed, and sensible diffusion loss profiles when partially overprinted (Harrison and McDougall, 1981; Wijbrans and McDougall, 1986). Though Harrison (1983) suggested muscovite remains metastable during in vacuo heating to higher temperatures than biotite because of more sluggish dehydration kinetics, why exactly muscovite behaves more systematically than biotite still remains poorly understood. Empirical observations suggest that the instability of biotite in nature and during in vacuo heating may be a function of the incipient alteration of biotite to chlorite.

Amphiboles are also stable under dry heating conditions. The age spectra are therefore often interpreted with confidence (Gaber et al. 1988). However, care must still be taken, as Maboko et al. (1991) showed that in some cases amphiboles known to have been partially reset or contain excess ^{40}Ar, also yielded a plateau (e.g Haggart et al., 1993).

All in all, the interpretation of $^{40}Ar/^{39}Ar$ age spectra is highly subjective. This can be overcome, to some degree, by dating the same mineral from closely associated samples, and by dating suites of minerals with different closure temperatures. In such cases, the reproduction of ages within one phase provides some assurance that the interpreted ages are valid, where as data from different minerals provides information regarding the time at which the rock passed through their respective closure temperatures.

3.2 Methodology

The following is a brief outline of the methods that were used in this study. For a full and more detailed description of the technical aspects, please refer to McDougall & Harrison (1988).

3.2.1 Sample Selection

Samples considered for $^{40}Ar/^{39}Ar$ thermochronology were selected in the field based on the presence of the K-bearing minerals hornblende, muscovite, and K-feldspar. At least one sample was collected from each lithotectonic terrane within the study area and, where possible, several closely spaced ($\leq$ 1 km) samples containing the same phase(s) were collected from the same horizon within each terrane. In the lab, samples selected for $^{40}Ar/^{39}Ar$ step-heating analysis were initially chosen on the basis of whether or not U-Pb data from monazite and/or titanite grains were available from the same sample. Further selection of samples was based on the appearance of the K-bearing phases in thin section. Brief field and thin section descriptions of samples selected for this study are found in Appendix A.

Hornblende, muscovite, and K-feldspar grains deemed appropriate for $^{40}Ar/^{39}Ar$ analysis were examined with the following criteria in mind. First, samples should be unaltered to avoid grains that may have experienced gain or loss of K or Ar during weathering or retrogression. Secondly, if possible, intergrown phases were avoided, especially in the case of hornblende, for reasons noted above. Ideally, individual generations of particular phases should be segregated during separation; however, since their identification was virtually impossible in the crushed sample, samples with multiple generations of the same mineral were noted to assist in the interpretation of the spectra. Finally, the range in grain size of each phase to be dated was noted so that during sample preparation the appropriate grain size fraction could be selected.

3.2.2 Sample Preparation

All samples analyzed in this study are fairly coarse grained and so were crushed using a rock hammer. Bulk samples were then sieved using 2mm – 85μ sieves, where fractions to be dated were $\leq$ 1mm. Mineral fractions were extracted using Frantz magnetic, heavy liquid, and paper-panning techniques. Mineral separates were then hand-picked under a binocular microscope to sample purity. Each amphibole separate

consisted of 15 - 25 mg of picked material. For muscovite and K-feldspar phases ~ 5 mg of separates were picked.

3.3 Hornblende Results

Data obtained from hornblende have been grouped according to the domain from which they were collected, and are presented in order of their position along the study transect, from south (Glennie Domain) to north (Peter Lake Domain). Both age spectra and corresponding $^{37}Ar/^{39}Ar$ spectra are presented here. Initial and final steps contributing less than 3% of the total ^{39}Ar gas released, which are likely due to minor irregularities and/or recoil effects, were not included in the calculation of mean ages, and are not discussed in detail. Complete microprobe data and $^{40}Ar/^{39}Ar$ data summary sheets may be found in Appendices B-1 and C-1.

3.3.1 Glennie Domain

Sample 98-D42, a medium- to coarse-grained diorite from the south end of Reindeer Lake (Map 1), contains 0.15 – 3 mm hornblende intergrown with biotite along grain margins and containing biotite inclusions (photo A.1 in Appendix A). The spectrum is discordant, with low temperature steps comprising 4% of the total ^{39}Ar released recording anomalously low ages. The main part of the spectrum (950 – 1450 ^{0}C), contributing 93% of the total ^{39}Ar released, is U-shaped with maximum ages at low to moderate and high temperatures (Figure 3.3a). The middle part of the spectrum, contributing ~ 40% of the total gas released (1025 – 1100 ^{0}C), yields a minimum age of ~ 1781 ± 11 Ma. $^{37}Ar/^{39}Ar$ ratios measured during the experiment correspond to Ca/K ratios calculated from microprobe data for hornblendes except for the initial low-temperature steps (Figure 3.3a), which may reflect the presence of biotite impurities in the sample. For this sample, the corresponding inverse isochron plot produced an age of 1800 ± 21 Ma (Figure 3.3b), and is considered to be the more reliable of the two ages.

3.3.2 Kisseynew Domain

Sample 98-L48, a hornblende-bearing granodiorite that intruded turbiditic rocks of the Burntwood Group (Map 1), yielded a spectrum with a well-defined plateau (Figure 3.3c). Amphiboles in this sample vary in size (0.15 – 3 mm), and are moderately intergrown with biotite along grain margins (photo A.2 - Appendix A). The range of Ca/K values calculated from microprobe data corresponds well with $^{37}Ar/^{39}Ar$ measured

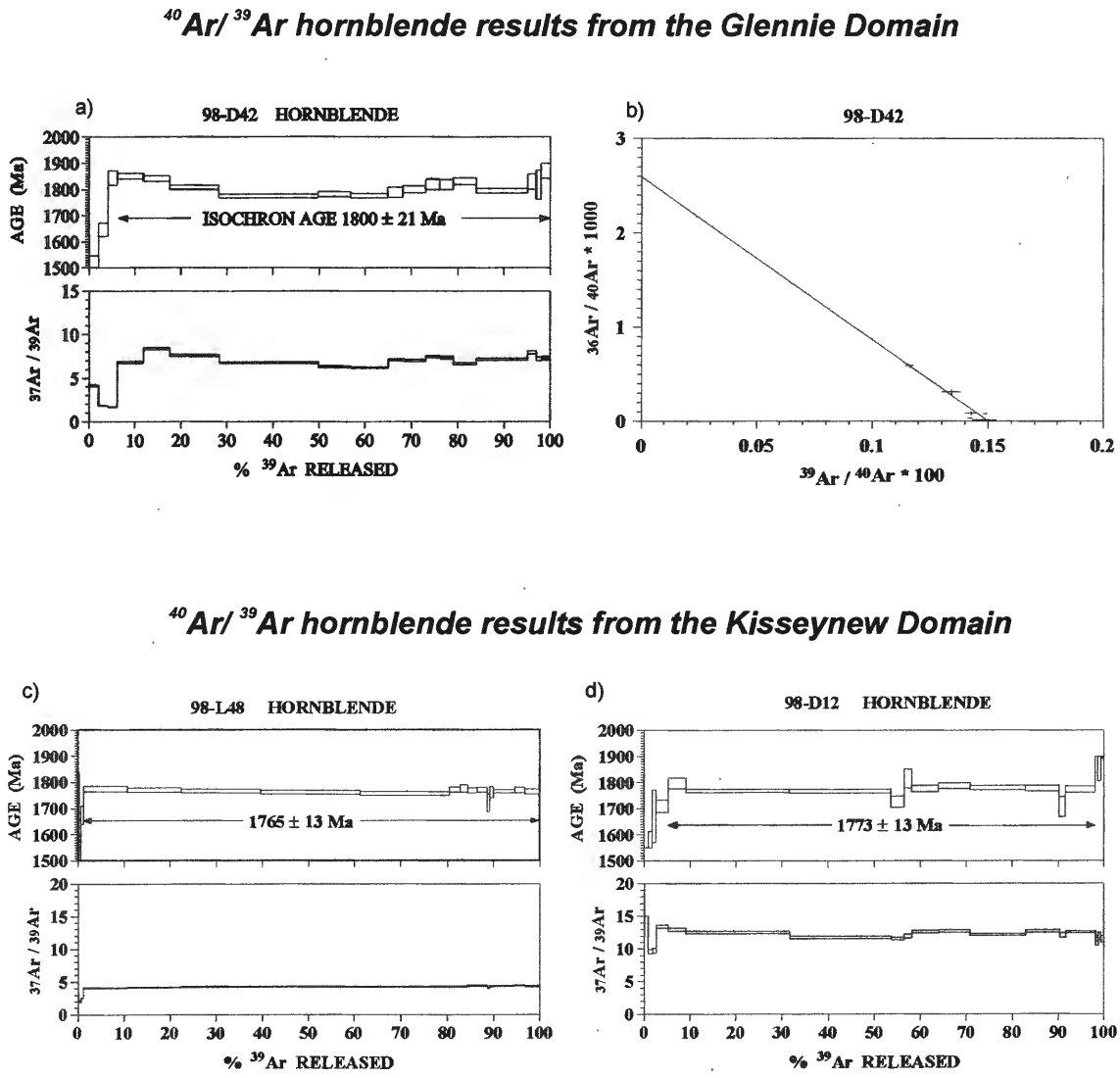

Figure 3.3: a) Hornblende $^{40}Ar/^{39}Ar$ age and corresponding $^{37}Ar/^{39}Ar$ spectra for sample 98-D42 from the northern Glennie domain. b) Corresponding inverse isochron plot for sample 98-D42. c) Hornblende $^{40}Ar/^{39}Ar$ age and corresponding $^{37}Ar/^{39}Ar$ spectra for sample 98-L48 from the Burntwood group, Kisseynew domain. d) Hornblende $^{40}Ar/^{39}Ar$ age and corresponding $^{37}Ar/^{39}Ar$ spectra for sample 98-D12 from the Levesque Bay supracrustal assemblage, Kisseynew domain. Shaded areas in $^{37}Ar/^{39}Ar$ spectra indicate range of Ca/K ratios calculated from microprobe data.

during the experiment, with the exception of the initial low-temperature steps, which may reflect the presence of biotite impurities in the sample. Fourteen increments (950 – 1350^{0}C), comprising 98% of the total ^{39}Ar released, define a mean age of 1765 ± 13 Ma.

Amphiboles from sample 98-D12, a metavolcanic rock from the Levesque Bay supracrustal assemblage (Map 1), are 0.2 - 1 mm in size and extensively intergrown along grain margins with biotite that has been retrograded to chlorite (photo A.3 - Appendix A). The spectrum is concordant (Figure 3.3d), and Ca/K values calculated from microprobe data correspond with ^{37}Ar/^{39}Ar ratios measured over eleven increments of the experiment (975 – 1250 ^{0}C; Figure 3.3d). These increments, comprising ~92 % of the total ^{39}Ar released, define a mean age of 1773 ± 13 Ma (Figure 3.3d).

3.3.3 La Ronge Domain

Sample 97-A404a, a metavolcanic rock of intermediate composition from the Central Metavolcanic Belt (CMB) immediately above the Duck Lake Shear zone (Map 1), yielded a disturbed spectrum in which increments record gradually increasing apparent ages (Figure 3.4a). Amphiboles in this sample are fine (200 μm to 1 mm), pale green and only moderately intergrown with biotite (photo A.8 - Appendix A). Ca/K values calculated from microprobe data correspond to ^{37}Ar/^{39}Ar values measured during the 1110 – 1300 ^{0}C increments that define a mean age of 1804 ± 41 Ma. However, these increments yielded less than 30% of the total ^{39}Ar gas, therefore, no significance has been attributed to the mean age calculated for this sample.

Sample 97-D004, a metavolcanic rock of intermediate composition from within the CMB approximately 300 m above the Duck Lake Shear Zone (Map 1), yielded a concordant spectrum with a relatively well-defined plateau (Figure 3.4b). Amphiboles are 200 – 300 μm and pale green in colour (see photo A.9 - Appendix A). Ca/K ratios calculated from microprobe data plot well above ^{37}Ar/^{39}Ar ratios measured during the experiment. Based on the microprobe analysis and according to the classification scheme of Leake et al. (1997), amphiboles in this sample are magnesiohornblende with a high percentage of Ca^{2+} relative to K^+. Thus, the discrepancy observed between experimental ^{37}Ar/^{39}Ar ratios and those measured from microprobe data may be attributed to an actinolitic component within the amphiboles. For this sample, fifteen increments (950 –

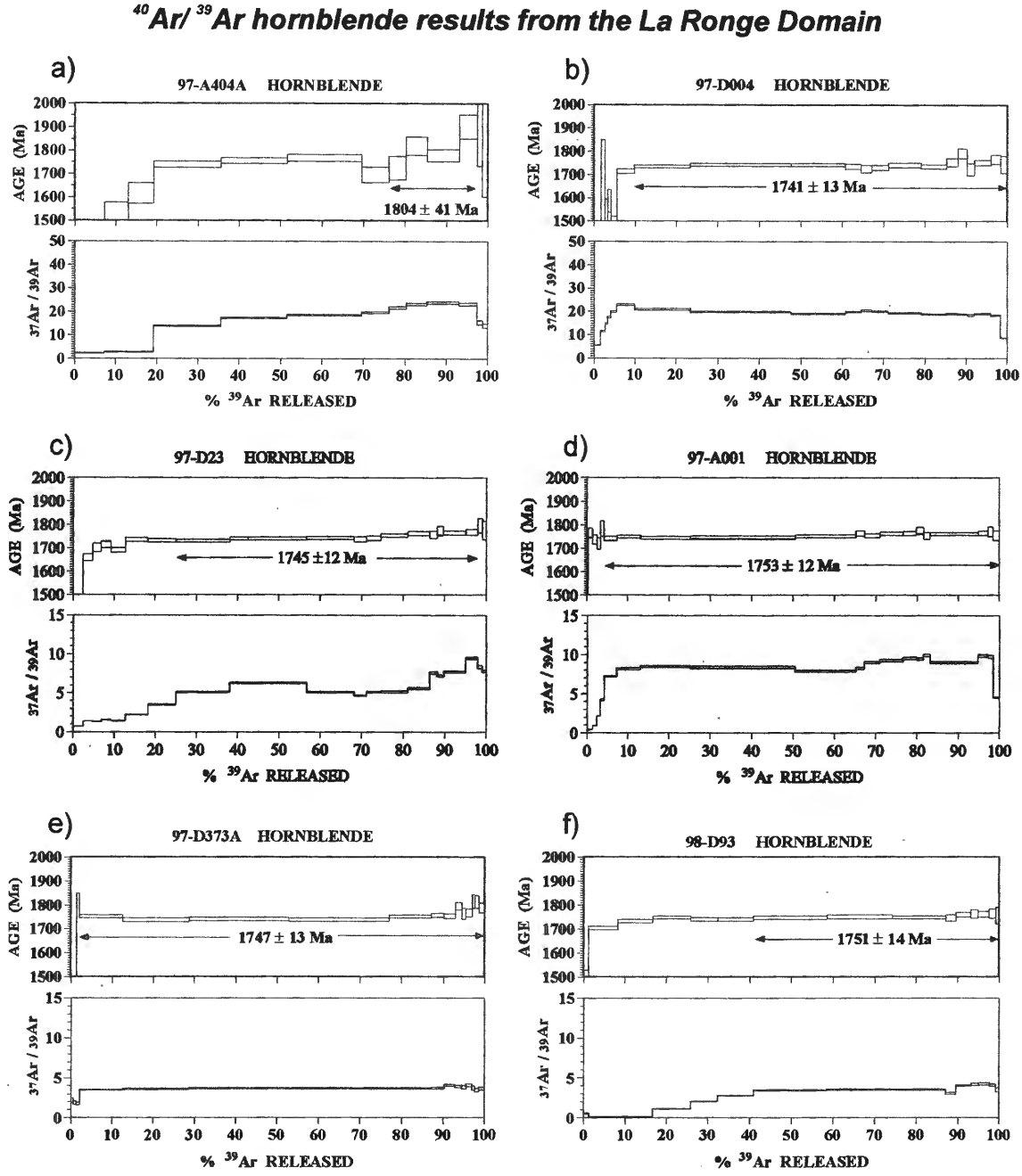

Figure 3.4: a) & b) Hornblende $^{40}Ar/^{39}Ar$ age and corresponding $^{37}Ar/^{39}Ar$ spectra for samples from the Central Metavolcanic Belt, La Ronge domain. c) & d) Hornblende $^{40}Ar/^{39}Ar$ age and corresponding $^{37}Ar/^{39}Ar$ spectra for samples from the Butler Island diorite, La Ronge domain. e) Hornblende $^{40}Ar/^{39}Ar$ age and corresponding $^{37}Ar/^{39}Ar$ spectra for sample 97-D373A from a tonalite that intruded Milton Island sediments of the La Ronge domain. f) Hornblende $^{40}Ar/^{39}Ar$ age and corresponding $^{37}Ar/^{39}Ar$ spectra for sample 98-D93 from the McMillian Lake monzogranite, La Ronge domain. Shaded areas in $^{37}Ar/^{39}Ar$ spectra indicate range of Ca/K ratios calculated from microprobe data.

^{40}Ar/ ^{39}Ar hornblende results from the La Ronge Domain

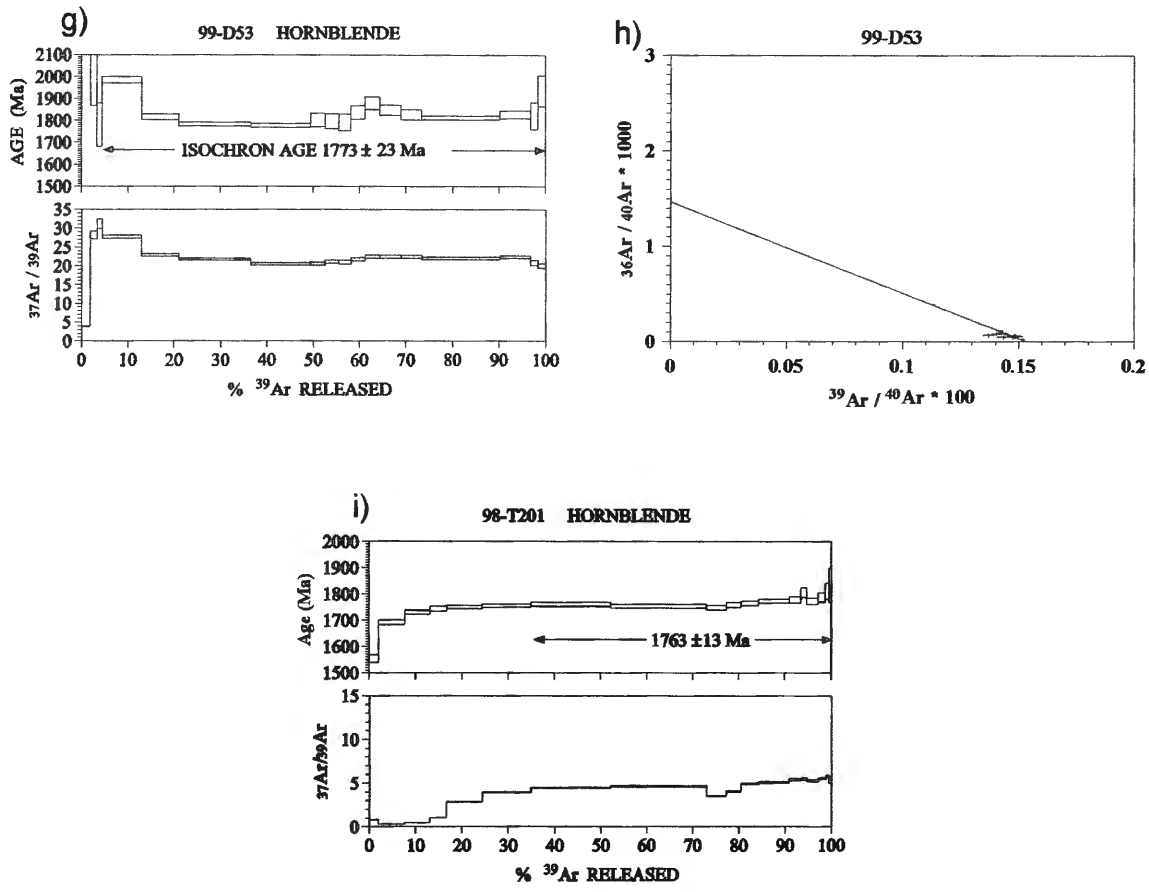

Figure 3.4 (cont'd): g) Hornblende ^{40}Ar/ ^{39}Ar age and corresponding ^{37}Ar/ ^{39}Ar spectra for sample 98-T201 from the Crowe Island complex, La Ronge domain. h) Hornblende ^{40}Ar/ ^{39}Ar age and corresponding ^{37}Ar/ ^{39}Ar spectra for sample 98-D53 from a pegmatitic gabbro intruding the McMillian Lake monzogranite, La Ronge domain. i) Corresponding inverse isochron plot for sample 98-D53. Shaded areas in ^{37}Ar/ ^{39}Ar spectra indicate range of Ca/K ratios calculated from microprobe data.

1450 ^{0}C) contributing to 94% of the total ^{39}Ar gas released define a mean age of 1741 ± 13 Ma.

Sample 97-D23, a medium – coarse-grained diorite intruded into the La Ronge Domain at ca. 1858 ± 2 Ma (Map 1), contains 0.3 – 4 mm amphibole grains (see A.10 - Appendix A). The sample was collected from the sheared margin. In hand sample two generations of amphibole may be distinguished – randomly oriented clots and elongate clots that define the stretching lineation. In thin-section and based on microprobe data, however, the two phases are indistinguishable. The spectrum is stepped with ten increments (1000 – 1250 ^{0}C) recording increasing apparent ages (1730 – 1760 Ma) with increasing temperature (Figure 3.4c). The steep, stepped nature of the first part of the spectrum and its extremely low ages are matched by irregularities in the ^{37}Ar/^{39}Ar ratios obtained during the experiment, and may be due to contamination of the sample by a high K phase or ^{39}Ar recoil effects. Ten increments (1000 – 1250 ^{0}C), comprising 70% of the total ^{39}Ar gas released, define a mean age of 1745 ± 12 Ma.

Sample 97-A001 was collected from an undeformed part of the same pluton as 97-D23 (Map 1). It contains 0.5 – 4 mm hornblende grains that are associated with biotite along grain margins, and contain inclusions of quartz, plagioclase, K-feldspar and titanite (see photo A.11 - Appendix A). Despite the presence of impurities, however, the spectrum is concordant (Figure 3.4d). Ca/K ratios calculated from microprobe data correspond to measured ^{37}Ar/^{39}Ar values obtained over the major portion of gas released. Measured ^{37}Ar/^{39}Ar values that fall above the calculated range may be attributed to contamination by a Ca-rich phase such as plagioclase. Fifteen increments (950 – 1450 ^{0}C), contributing 95% of the total ^{39}Ar released, define a mean apparent age of 1753 ± 12 Ma.

Amphiboles in sample 97-D373A, a medium grained tonalite from the Crowe Island complex of the La Ronge Domain (Map 1), are 0.2 – 1 mm in size, and most grains are intergrown with biotite along grain margins. There are, however, a few grains that are extensively intergrown with biotite (photo A.14 - Appendix A). With the exception of a few small first and last steps that yield high ages, the spectrum is concordant (Figure 3.4e). ^{37}Ar/^{39}Ar ratios measured throughout the experiment correspond well with Ca/K calculated from microprobe data. Seven increments (950 –

1130 ^{0}C), contributing to 95% of the total ^{39}Ar released, define a mean age of 1747 ± 13 Ma.

In sample 98-D93, a monzogranite from the east and central part of the La Ronge Domain, amphiboles are 0.1 – 1 mm in size (Map 1), extensively intergrown with biotite, and contain inclusions of allanite, quartz and/or plagioclase and K-feldspar (photo A.15 - Appendix A). The spectrum from this sample is stepped at low to moderate temperatures and flattens out at moderate to high temperatures (Figure 3.4f). The stepped nature of the first part of the age spectrum corresponds to low ^{37}Ar/^{39}Ar ratios that plot below the range of Ca/K ratios calculated from microprobe data, which may be attributed to contamination by a high K phase such as biotite. Nine increments (1025 – 1450 ^{0}C), contributing 59% of the total ^{39}Ar gas released define a mean age of 1751 ± 14 Ma.

Amphiboles in sample 99-D53, from a pegmatitic gabbro that intruded the pluton from which sample 98-D93 was collected (Map 1), range in size from 0.1 - 4 mm. Small grains occur as inclusions within intensely altered plagioclase grains, and large grains are fractured, altered to a black, fine-grained aggregate along grain margins, and contain inclusions of titanite and quartz (photo A.16 - Appendix A). The spectrum is highly discordant and the main part is U-shaped (Figure 3.4g), where the oldest ages are recorded at low (950 ^{0}C; 1985 ± 15 Ma) and high temperatures (1450 ^{0}C; 1935 ± 80 Ma), and the youngest age is recorded at low-moderate temperatures (1025 ^{0}C; 1777 ± 10 Ma). This type of spectrum is characteristic of samples that have retained excess ^{40}Ar. ^{37}Ar/^{39}Ar ratios measured during the experiment correspond to the range of Ca/K ratios calculated from microprobe data across fifteen increments contributing to 95% of the total ^{39}Ar gas released. The fifteen increments (950 – 1450 ^{0}C) define a mean apparent age of 1827 ± 15 Ma. The corresponding inverse isochron plot, although the sums are quite high and give a less than ideal fit, produced an age of 1773 ± 23 Ma (Figure 3.4h).

Sample 98-T201, a granodiorite from the Cowie pluton (Map 1), contains 0.5 - 2 mm amphibole grains that are intergrown with biotite and titanite (see photo A.17 - Appendix A). The spectrum looks very much like that from sample 98-D93, where low temperature increments are stepped and flatten out at moderate to high temperatures (Figure 3.4i). Low ^{37}Ar/^{39}Ar ratios that plot well below the Ca/K range calculated from microprobe data correspond to the stepped portion of the age spectrum, and may indicate

contamination by a high K phase such as biotite. For this sample, twelve increments (1000 – 1450 ^{0}C) contributing to 65% of the total ^{39}Ar gas released range from 1750 – 1775 Ma and define a mean age of 1763 ± 13 Ma.

3.3.4 Wathaman Batholith

Sample 98-T300A, a diorite from the southern margin of the Wathaman Batholith (Map 1), contains amphiboles that range in size from 0.5 - 4 mm. Small grains are generally inclusion-free whereas larger grains contain inclusions of titanite ± apatite ± quartz and are intergrown with biotite that has been retrograded to chlorite along grain margins (see A.18 - Appendix A). The spectrum is moderately U-shaped (Figure 3.5a) with maximum ages recorded at low (950 ^{0}C; 1770 ± 9 Ma) and high temperatures (1250 ^{0}C; 1787 ± 30 Ma). The lowest age is recorded in the main part of the spectrum at moderate temperature (1075 ^{0}C; 1760 ± 7 Ma). The range of Ca/K values calculated from microprobe data corresponds to ^{37}Ar/^{39}Ar values measured during seven steps of the experiment. Low values at low temperatures may be attributed to the presence of biotite. High values at high temperatures may be due to contamination by a high-Ca phase. For this sample, seven increments (950 – 1100 ^{0}C) contributing ~ 85% of the total ^{39}Ar gas released define a mean age of 1765 ± 13 Ma.

Amphiboles in sample 98-T300B, a granodiorite that is interpreted to have intruded the diorite from which 98-T300A was collected (Map 1), are 0.7 - 1 mm in size and contain inclusions of titanite ± quartz. Grain margins appear to have been retrograded to chlorite and are also associated with biotite (see A.19 - Appendix A). The spectrum is mildly discordant and slightly U-shaped (Figure 3.5b). Ages range from 1750 – 1785 Ma, where the minimum age is observed over two increments (1025 – 1050 ^{0}C). Ca/K ratios calculated from microprobe data correspond to ^{37}Ar/^{39}Ar values measured during nine steps of the experiment. Low values at low temperatures may be attributed to the presence of biotite. High values at high temperatures may be due to contamination by a high Ca phase. For this sample, fourteen increments (950 – 1450 ^{0}C) contributing to ~ 96% of the total ^{39}Ar gas released define a mean age of 1764 ± 15 Ma.

Sample 99-D76, a granodiorite from the marginal zone of the Wathaman Batholith (Map 1), contains amphiboles of variable size (250 μm - 2 mm) that are intergrown with biotite. Grains larger than 0.3 mm generally contain inclusions of quartz

$^{40}Ar/^{39}Ar$ hornblende results from the Wathaman Batholith

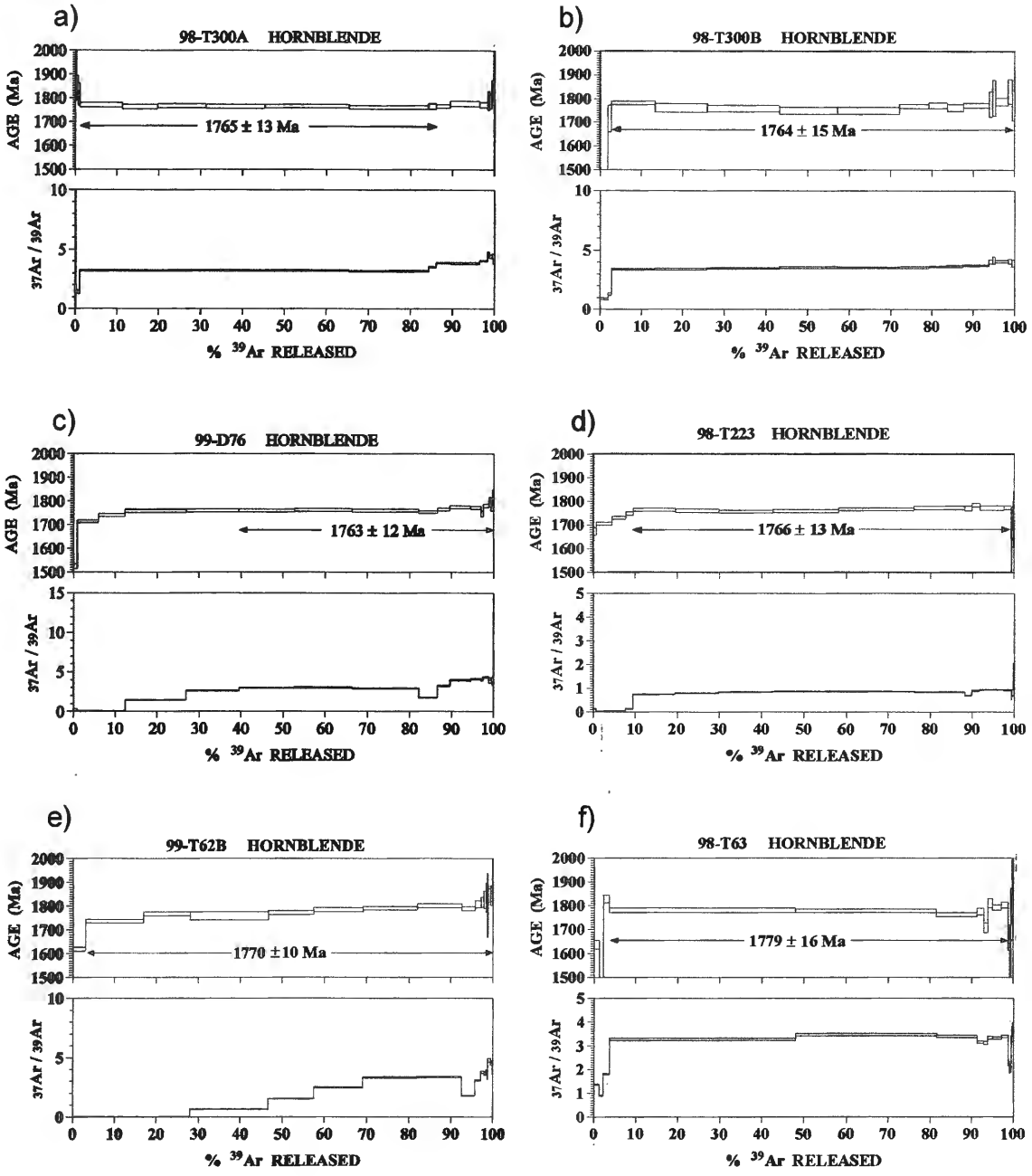

Figure 3.5: a), b) & c) Hornblende $^{40}Ar/^{39}Ar$ age and corresponding $^{37}Ar/^{39}Ar$ spectra for samples from the marginal zone of the Wathaman Batholith. d), e) & f) Hornblende $^{40}Ar/^{39}Ar$ age and corresponding $^{37}Ar/^{39}Ar$ spectra for samples from the main body of the batholith. Shaded areas in $^{37}Ar/^{39}Ar$ spectra indicate range of Ca/K ratios calculated from microprobe data.

$^{40}Ar/^{39}Ar$ hornblende results from the Wathaman Batholith

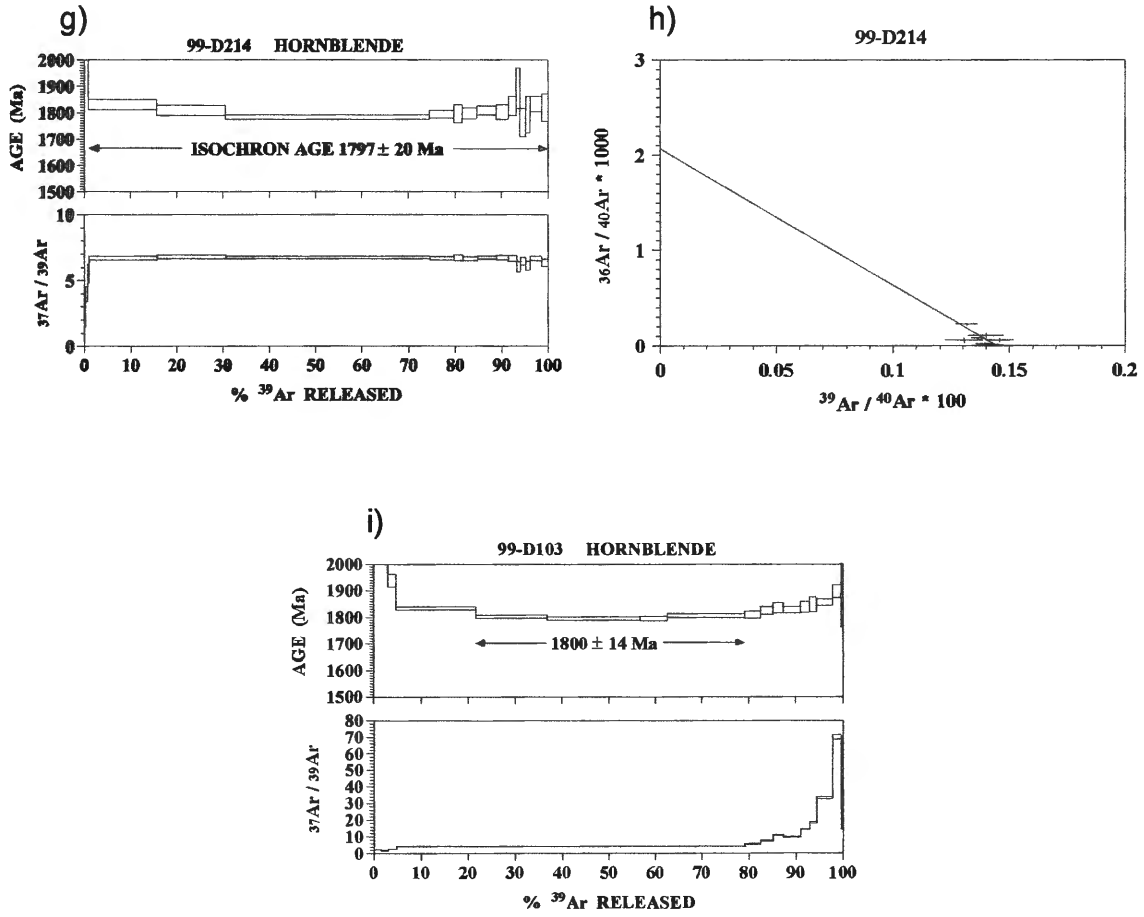

Figure 3.5 (cont'd): g) Hornblende $^{40}Ar/^{39}Ar$ age and corresponding $^{37}Ar/^{39}Ar$ spectra for sample 99-D214 from a metavolcanic enclave in the Wathaman Batholith. h) Corresponding inverse isochron plot for sample 99-D214. i) Hornblende $^{40}Ar/^{39}Ar$ age and corresponding $^{37}Ar/^{39}Ar$ spectra for sample 99-D103 from the Patterson Island megacrystic syenite. Shaded areas in $^{37}Ar/^{39}Ar$ spectra indicate range of Ca/K ratios calculated from microprobe data.

+ titanite ± allanite ± plagioclase ± K-feldspar (see A.20 - Appendix A). The spectrum for this sample is stepped at low to moderate temperatures and flattens out at moderate to high temperatures (Figure 3.5c), where apparent ages range from 1755 – 1775 Ma.. $^{37}Ar/^{39}Ar$ values measured during the experiment correspond to Ca/K ratios calculated from microprobe data, with the exception of low temperature increments, which fall below the calculated range and may be attributed to contamination by biotite. Twelve increments (1025 – 1450 ^{0}C) contributing to ~ 60% of the total ^{39}Ar gas released define a mean age of 1763 ± 12 Ma.

Sample 98-T223, a quartz-monzodiorite phase of the Wathaman Batholith (Map 1), contains 0.5 - 2 mm amphibole grains that are present in clots with epidote, titanite and biotite that has locally been retrograded to chlorite (see photo A.21 - Appendix A). The age spectrum looks very similar to that obtained from sample 99-D76, where low temperature increments are stepped and flatten out at moderate to high temperatures (Figure 3.5d). $^{37}Ar/^{39}Ar$ values measured during the experiment, however, do not correspond to Ca/K values calculated from microprobe data but rather plot well below the range, suggesting the sample used in the experiment may have been contaminated by a high K phase such as biotite. Ten increments (950 – 1175 ^{0}C) contributing to ~ 90% of the total ^{39}Ar gas released define a mean apparent age of 1766 ± 13 Ma.

Amphiboles in sample 99-T62B, from a monzodioritic phase of the Wathaman Batholith (Map 1), are small (≤ 1 mm), intergrown with epidote, titanite and biotite, and may also have inclusions of quartz (see A.22 - Appendix A). The spectrum records progressively increasing apparent ages with increasing temperature (Figure 3.5e). A similar pattern is observed in the corresponding $^{37}Ar/^{39}Ar$ spectrum, suggesting contamination of the sample by a high K, low Ca phase. $^{37}Ar/^{39}Ar$ values calculated from microprobe Ca/K data also indicate that most of the gas released (except at 1250 ^{0}C and 1350 ^{0}C, the second and third last steps of the spectrum) was not derived from the out-gassing of hornblende, but may be from biotite. For this reason, no significance is attributed to the age (1770 ± 10 Ma) of this sample.

In sample 98-T63, from a well-foliated recrystallized granite that appears to have intruded into a dioritic phase of the Wathaman Batholith (Map 1), amphibole grains are 0.4 - 1 mm in size and form clots with titanite, allanite and biotite (see A.23 - Appendix

A). Two large concordant steps dominate the spectrum (Figure 3.5f). $^{37}Ar/^{39}Ar$ ratios correspond well to those calculated from microprobe Ca/K data except for the initial low temperature steps, which may reflect the presence of biotite impurities. For this sample, eight increments (950 – 1125 ^{0}C) contributing ~ 95% of the total ^{39}Ar gas released, define a mean age of 1779 ± 16 Ma.

Sample 99-D214, from a mafic metavolcanic rock that is likely Archean in age and forms an enclave within the Swan River complex (Map 1), contains amphiboles of variable size (0.1 - 2 mm) that are locally intergrown with biotite (see A.24 - Appendix A). The spectrum is discordant, with low temperature steps comprising ~ 1% of the total ^{39}Ar gas released yielding anomalously high ages. The main part of the spectrum is U-shaped (Figure 3.5g), with maximum apparent ages at low (950 ^{0}C; 1832 ± 20 Ma) and high temperatures (1450 ^{0}C; 1821 ± 52 Ma) and a minimum age of 1785 ± 8 Ma at moderate temperature (1000 ^{0}C). $^{37}Ar/^{39}Ar$ ratios correspond well to those calculated from microprobe Ca/K data, suggesting the U-shaped spectrum may be the result of excess ^{40}Ar. The corresponding isotope correlation plot produced an age of 1797 ± 20 Ma (Figure 3.5h).

99-D103, a sample from a megacrystic syenitic phase of the Wathaman Batholith (Map 1), contains aggregates of 0.25 – 1 mm amphiboles that are cored by and intergrown with green clinopyroxene (see A.25 - Appendix A). The spectrum is discordant, similar to the spectrum from 99-D214, with initial low temperature steps comprising ~ 5% of the total ^{39}Ar gas released yielding anomalously high ages (Figure 3.5i). The main part of the spectrum is U-shaped (Figure 3.5i), which may be attributed to excess ^{40}Ar, with maximum apparent ages at low (950 ^{0}C; 1835 ± 6 Ma) and high temperatures (1350 ^{0}C; 1898 ± 25 Ma) and a minimum age of 1796 ± 9 Ma at moderate temperature (1025 ^{0}C; 1796 ± 9 Ma). Ca/K ratios calculated from microprobe data correspond to $^{37}Ar/^{39}Ar$ values measured during seven steps of the experiment. Low values at low temperatures may be attributed to the presence of biotite. High values at high temperatures may be due to contamination by a high Ca phase such as clinopyroxene. For this sample, four increments (975 – 1050 ^{0}C) contributing to ~ 64% of the total ^{39}Ar gas released define a mean age of 1800 ± 14 Ma.

3.3.5 Peter Lake Domain

Sample 99-D162, collected from a granitic to dioritic, highly migmatitic orthogneiss (Map 1), contains 0.1 – 4 mm amphiboles that are intergrown with and bearded by biotite grains along grain boundaries (see photo A.26 - Appendix A). Most grains contain inclusions of biotite, titanite, and quartz and have been retrograded to chlorite along grain margins. The spectrum has a stepped nature (Figure 3.6a) that is matched by irregularities in the apparent $^{37}Ar/^{39}Ar$ ratios measured during the experiment. Low experimental values, which plot well below the range calculated from microprobe Ca/K data, may reflect contamination by biotite. The remaining $^{37}Ar/^{39}Ar$ values, which also roughly match the irregularities in the age spectrum and plot within the calculated range, may be due to contamination by a high Ca phase. For this reason a mean apparent age was not calculated for this sample, but rather from increments 1025 - 1450 ^{0}C, which correspond to $^{37}Ar/^{39}Ar$ ratios that fall within the calculated range, a range of apparent ages was calculated. The minimum apparent age of ca. 1997 Ma corresponds to the 1025 ^{0}C increment and the maximum apparent age of ca. 2200 Ma corresponds to the 1450 ^{0}C step.

Sample 99-D87B, from a pristine gabbro belonging to the Swan River Complex (Map 1), contains aggregates of 0.1 – 0.7 mm amphibole grains cored by and intergrown with primary clinopyroxene (see A.27 - Appendix A). Amphiboles are zoned with rims characterized by slightly higher Ca/K ratios and thus higher $^{37}Ar/^{39}Ar$ ratios (13 – 29) than the cores (10 – 24; see Appendix B-1). The age spectrum is irregular and is matched by an equally irregular $^{37}Ar/^{39}Ar$ spectrum (Figure 3.6b). Low $^{37}Ar/^{39}Ar$ ratios and apparent ages that characterize the first 8% of the total gas released are likely due to contamination by a high K phase. Fourteen increments (950 – 1450 ^{0}C) contributing 91% of the total ^{39}Ar gas released define a mean apparent age of 1818 ± 15 Ma.

Amphiboles in sample 99-D89A, from a gabbro belonging to the Swan River Complex (Map 1), are 0.5 – 1 mm in size and locally contain sericite patches or inclusions of sericitized plagioclase. As in sample 99-D87B, amphiboles in this sample are zoned with rims characterized by slightly higher Ca/K ratios and thus higher $^{37}Ar/^{39}Ar$ ratios (34 - 12) than the cores (9 – 21; see Appendix B-1). The irregular age spectrum is matched by an equally irregular $^{37}Ar/^{39}Ar$ spectrum (Figure 3.6c). Low ratios

$^{40}Ar/^{39}Ar$ hornblende results from the Peter Lake Domain

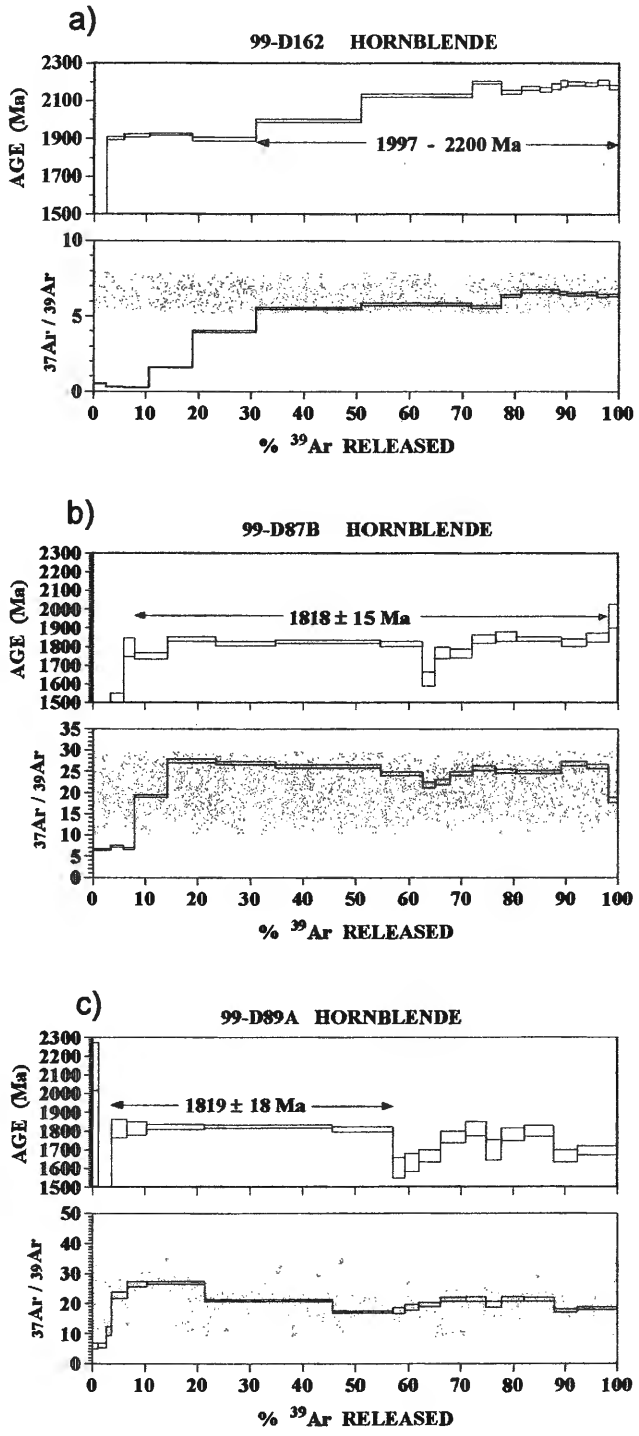

Figure 3.6: a) Hornblende $^{40}Ar/^{39}Ar$ age and corresponding $^{37}Ar/^{39}Ar$ spectra for sample 99-D162 from an orthogneiss, Peter Lake domain. b) & c) Hornblende $^{40}Ar/^{39}Ar$ age and corresponding $^{37}Ar/^{39}Ar$ spectra for samples from the Swan River complex, Peter Lake domain. Shaded areas in $^{37}Ar/^{39}Ar$ spectra indicate range of Ca/K ratios calculated from microprobe data.

associated with the initial low temperature steps contributing 2.5% of the total ^{39}Ar gas released may reflect contamination by a high K phase such as sericite. The total gas age for this sample is 1771 ± 14 Ma. Five steps (950 – 1050 ^{0}C) contributing 53% of the total ^{39}Ar gas released define a mean apparent age of 1819 ± 18 Ma.

3.4 Muscovite Results

Data obtained from muscovites have been grouped according to the domain from which they were collected, and are presented in order of their position along the study transect, from south (Kisseynew Domain) to north (La Ronge Domain). Only the age spectra are presented here. Microprobe data and $^{40}Ar/^{39}Ar$ data summary sheets are found in Appendices B-2 and C-2. Initial and final steps contributing less than 3% of the total ^{39}Ar gas released, which are likely due to minor irregularities and/or recoil effects, were not included in the calculation of mean ages, and thus are not discussed in detail.

3.4.1 Kisseynew Domain

Four muscovite-bearing samples collected from the McLennan Group arkoses of the Kisseynew Domain yielded concordant spectra (location map reference & Figure 3.7). For sample 97-D222, which contains 0.5 – 4 mm muscovite grains, the gap in the age spectrum is the result of a step lost due to a leak in the extraction system. For this sample, twenty-one increments (600– 825 ^{0}C and 863 - 1300 ^{0}C), comprising 91% of the total ^{39}Ar gas released, define a mean age of 1733 ± 13 Ma (Figure 3.7a). For sample 97-D31, containing 0.25 – 2 mm muscovite grains, twenty-one increments (600 – 1250 ^{0}C), contributing to 99% of the total ^{39}Ar gas released, define a mean age of 1731 ± 13 Ma (Figure 3.7b). In the case of 97-D26A, with muscovite grains between 0.25 - 1 mm, twenty-one increments (650 – 1300 ^{0}C), comprising 98% of the total gas released, define a mean age of 1736 ± 13 Ma (Figure 3.7c). Finally, for sample 97-D26B, from a granitic pegmatite that intruded the McLennan Group arkoses and contains 1 – 3 mm sized muscovites, eighteen increments (680 – 1200 ^{0}C) contributing to 98% of the total gas released define a mean age of 1726 ± 13 Ma (Figure 3.7d).

3.4.2 La Ronge Domain

Two muscovite-bearing samples were collected from the same horizon within the Milton Island metasedimentary assemblage. They yielded almost concordant spectra with similar ages to those obtained from muscovites south of the Duck Lake Shear Zone

$^{40}Ar/^{39}Ar$ muscovite results from the Kisseynew Domain

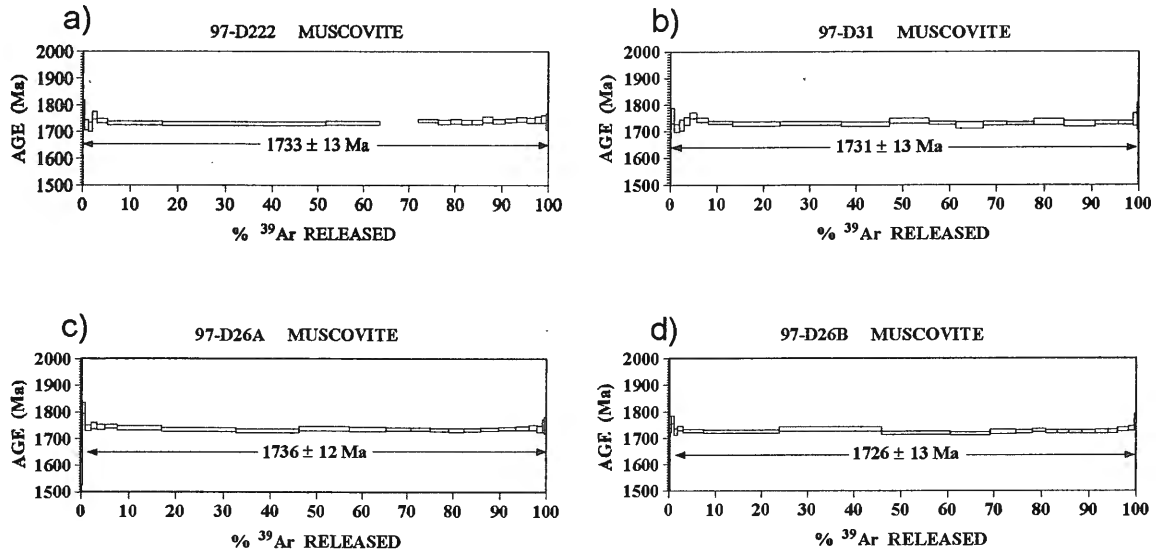

$^{40}Ar/^{39}Ar$ muscovite results from the La Ronge Domain

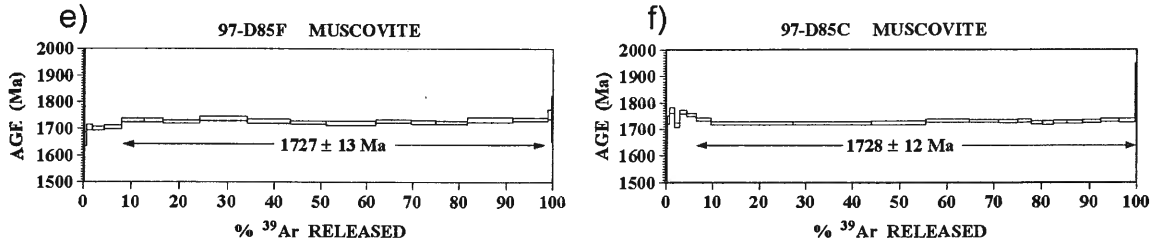

Figure 3.7: a) $^{40}Ar/^{39}Ar$ muscovite age spectra for sample 97-D222 from the McLennan Group metasediments, Kisseynew Domain. b) $^{40}Ar/^{39}Ar$ muscovite age spectra for sample 97-D31 from a muscovite granite intruding sample 97-D222, Kissyenew Domain. c) $^{40}Ar/^{39}Ar$ muscovite age spectra for sample 97-D26A from the McLennan Group metasediments, proximal to the Duck Lake shear zone, Kisseynew Domain. d) $^{40}Ar/^{39}Ar$ muscovite age spectra for sample 97-D26B from a muscovite pegmatite intruding sample 97-D26A, Kisseynew Domain. e) $^{40}Ar/^{39}Ar$ muscovite age spectra for fine grained sample 97-D85 from the Milton Island metasediments, La Ronge Domain. f) $^{40}Ar/^{39}Ar$ muscovite age spectra for coarse grained sample 97-D85 from the Milton Island metasediments, La Ronge Domain.

in the McLennan Group (Map 1 & Figure 3.7). For fine-grained sample 97-D85, from a well foliated, migmatitic biotite + muscovite psammite in which muscovite grains are 0.4 – 1 mm in size, fifteen increments (770 – 1200 ^{0}C) comprising 93% of the total ^{39}Ar gas released define a mean age of 1727 ± 13 Ma (Figure 3.7e). Similarly, sample 97-D85, from a moderately migmatitic, coarse-grained layer of biotite + muscovite psammite located in the same outcrop as the fine-grained sample, eleven steps (750 – 1100 ^{0}C) comprising 90% of the total gas released define a mean age of 1728 ± 12 Ma (Figure 3.7f).

3.5 K-Feldspar Results

3.5.1 Introduction to the Multiple Diffusion Domain Model

Unlike amphiboles and micas, K-feldspars are anhydrous and do not seem to change their crystal structure or break down during in vacuo heating below 1100 ^{0}C (Harrison et al., 1991). Diffusion of Ar in K-feldspars during step-heating experiments, therefore, may occur by volume diffusion following Fick's second law which is mathematically represented by the diffusion equation with the form (Harrison, 1990; see section 3.1.1):

$$\frac{\partial C}{\partial t} = D\left(\frac{\partial^2 C}{\partial x^2} + \frac{\partial^2 C}{\partial y^2} + \frac{\partial^2 C}{\partial z^2}\right)$$

Several numerical solutions that describe diffusion out of simple geometric shapes (e.g. spheres, cylinders, plane-sheets and cubes) have been developed (McDougall & Harrison, 1988). For example, the numerical solution that describes diffusion (f) out of a sphere with radius, a, for $0 < f < 0.85$ is:

$$f \approx \left(\frac{6}{\sqrt{\pi}}\right)\left(\frac{3Dt}{a^2}\right)^{\frac{1}{2}} - \left(\frac{3Dt}{a^2}\right) \qquad (12)$$

where the fraction of gas lost by diffusion (f) is expressed in terms of D/a^2 and the diffusion time (t). To explicitly solve for Dt/a^2, the quadratic equation must be rearranged such that:

$$\frac{Dt}{a^2} = \frac{2}{\pi} - \frac{f}{3} - \frac{2}{\pi}\sqrt{1 - \frac{\pi f}{3}}$$

This equation may then be applied to an experiment. For example (Figure 3.8), at temperature T(1), for ^{39}Ar gas released in the first step of duration t(1), $D(1)/a^2$ is defined by:

$$\frac{D(1)t(1)}{a^2} = \frac{2}{\pi} - \frac{f(1)}{3} - \frac{2}{\pi}\sqrt{1 - \frac{\pi f(1)}{3}}$$

If at time, t(1), the sample had been at a higher temperature, T(2), diffusion would be faster such that:

$$\frac{D(2)t(2)}{a^2} = \frac{2}{\pi} - \frac{f(1)}{3} - \frac{2}{\pi}\sqrt{1 - \frac{\pi f(1)}{3}}$$

where t(2) is not directly measured during the experiment, and is less than t(1) (see Figure 3.8). $D(2)/a^2$ can also be defined as:

$$\frac{D(2)t(2)'}{a^2} = \frac{2}{\pi} - \frac{f(1)+f(2)}{3} - \frac{2}{\pi}\sqrt{1 - \frac{\pi[f(1)+f(2)]}{3}}$$

Upon subtraction of the two equations, $\frac{D(2)}{a^2}(t(2)' - t(2))$ can be calculated such that:

$$\frac{D(2)}{a^2} = \frac{-\frac{f(2)}{3} - \frac{2}{\pi}\left(\sqrt{1 - \frac{\pi[f(1)+f(2)]}{3}} + \sqrt{1 - \frac{\pi f(1)}{3}}\right)}{\Delta t(2)}$$

where $\Delta t(2) = t(2)'-t(2)$, and represents the measured duration of the second step. For an entire step-heating experiment, this calculation is repeated iteratively for each step, providing a series of D/a^2 values as a function of temperature that are based on the ^{39}Ar released. A plot of $\log(D/a^2)$ versus $1000/T$ (K^{-1}) yields a straight line on an Arrhenius plot (equation 8, section 3.1.2):

$$\text{i.e.,} \quad \log\left(\frac{D}{a^2}\right) = \frac{-0.4343E_a(1000)}{RT} + \log\left(\frac{D_o}{a^2}\right)$$

Where the y-intercept gives $\log(D_o/a^2)$ and the activation energy of the system (E_a) is derived from the slope of the line. It is this method (Berger and York, 1981) that has been applied to some of the K-feldspar data in this study.

Arrhenius plots for data from experiments on K-feldspars are commonly not linear for the entire temperature range of argon release. Rather, they may exhibit one or

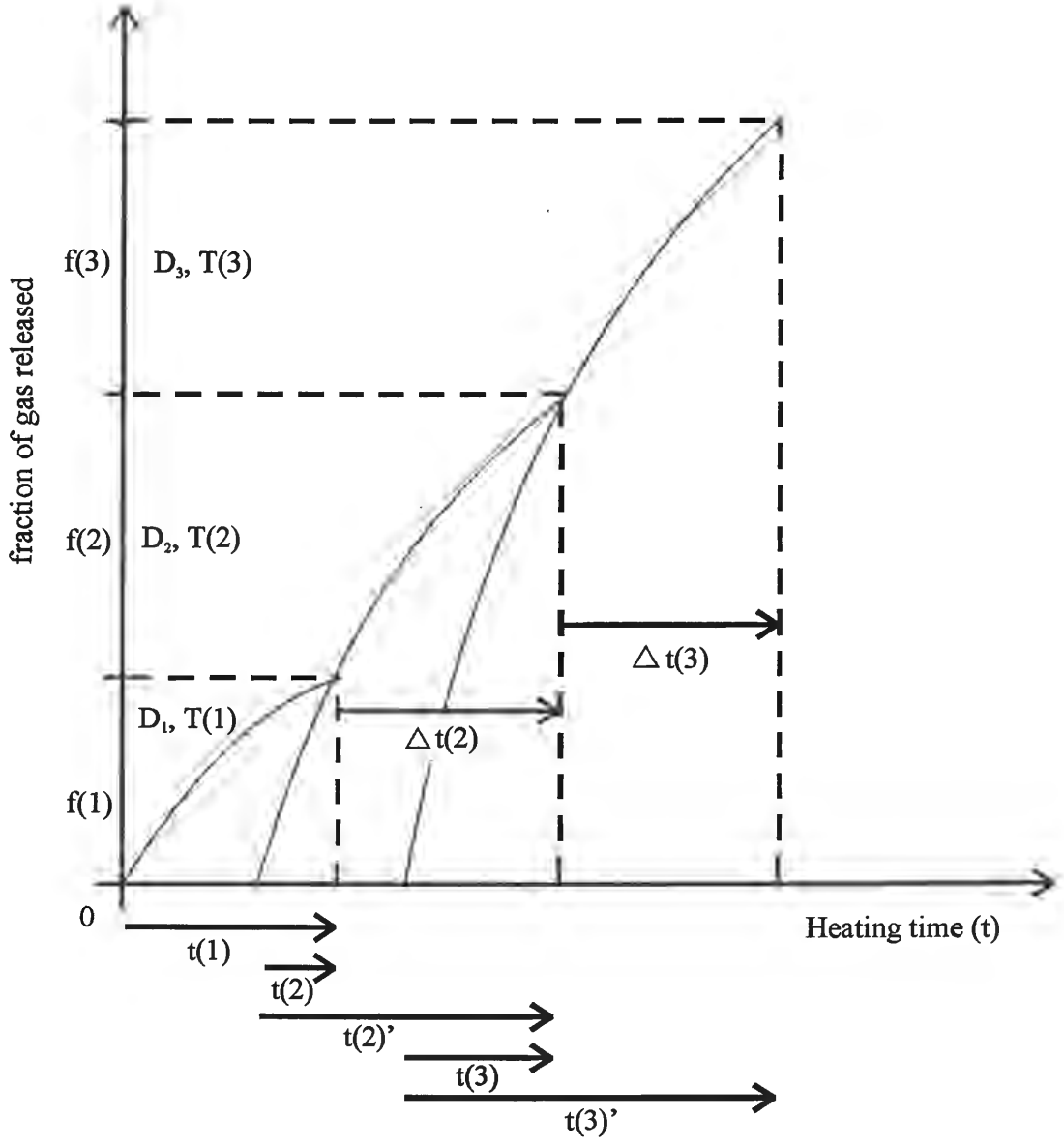

Figure 3.8: Schematic diagram of the Berger and York (1981) method of calculating diffusion parameters (D/a^2; see text for a more detailed discussion). The fractions of gas released during temperatures T(1), T(2) and T(3) are presented along the y-axis such that f(1) + f(2) + f(3) = 1. Times t(1), △t(2) and △t(3) are known heating times that are measured in the laboratory. Times t(2), t(2)', t(3) and t(3)' are theoretical times required for the diffusion of equivalent fractions of gas, assuming heating is done at elevated temperatures T(2) and T(3) respectively. At temperatures T(1), T(2) and T(3) the corresponding diffusion parameters are D_1, D_2 and D_3. (Reynolds, 1992)

more "kinks" at which the D/a^2 value drops abruptly below the initial trend, and then continues to rise (Figure 3.9). Harrison et al. (1986) and Heizler et al. (1988) suggested that these kink features might result from rehomogenization of mineral structures such as plagioclase exsolution lamellae, causing a change in the diffusion parameters of the sample. In this case, only the low temperature, linear portion of the curve would yield valid diffusion parameters to produce calculated closure temperatures of up to 315 ^{0}C for orthoclase and 125 – 185 ^{0}C for microcline (Harrison & McDougall, 1982; Heizler et al., 1988).

An alternative explanation for the presence of kinks in the Arrhenius plots for K-feldspars is to assume that, rather than being made up of a single "diffusion domain", a sample contains a number of domains (Multiple Diffusion Domain model (MDD) of Lovera et al., 1989). This model assumes that the domains are much smaller than the physical grain size and that they act independently of one another (Zeitler, 1988; Lovera et al., 1989). When out-gassed in the laboratory, each "diffusion domain" will release Ar over a characteristic temperature range, where the smallest ones dominate gas released at low temperatures, and larger ones dominate the gas released at high temperature increments. Kinks in the Arrhenius plot correspond to the transition between domains (Zeitler, 1987). Based on the experimentally determined Arrhenius plot, this method permits determination of the size and diffusion parameters of domains. Domain ages and cooling rates are determined by modelling the corresponding age spectra using assumed cooling rates. The closure temperature corresponding to the age of each domain is then calculated using a modified form of the Dodson (1973) equation. The result is a series of temperature-time (T-t) points which can be used to calculate corresponding cooling rates for each sample.

Before geological histories can be obtained using the MDD model, however, several stringent mathematical conditions must be met. Firstly, ^{39}Ar release in the experiment must be controlled by the same diffusion mechanism that controls the retention of ^{40}Ar in nature. Secondly, a diffusion "domain" must have formed at some temperature above its closure temperature. Thirdly, recoil effects must be of little importance, implying that domains must maintain their integrity during sample preparation and neutron irradiation. Similarly, during the step-heating experiment,

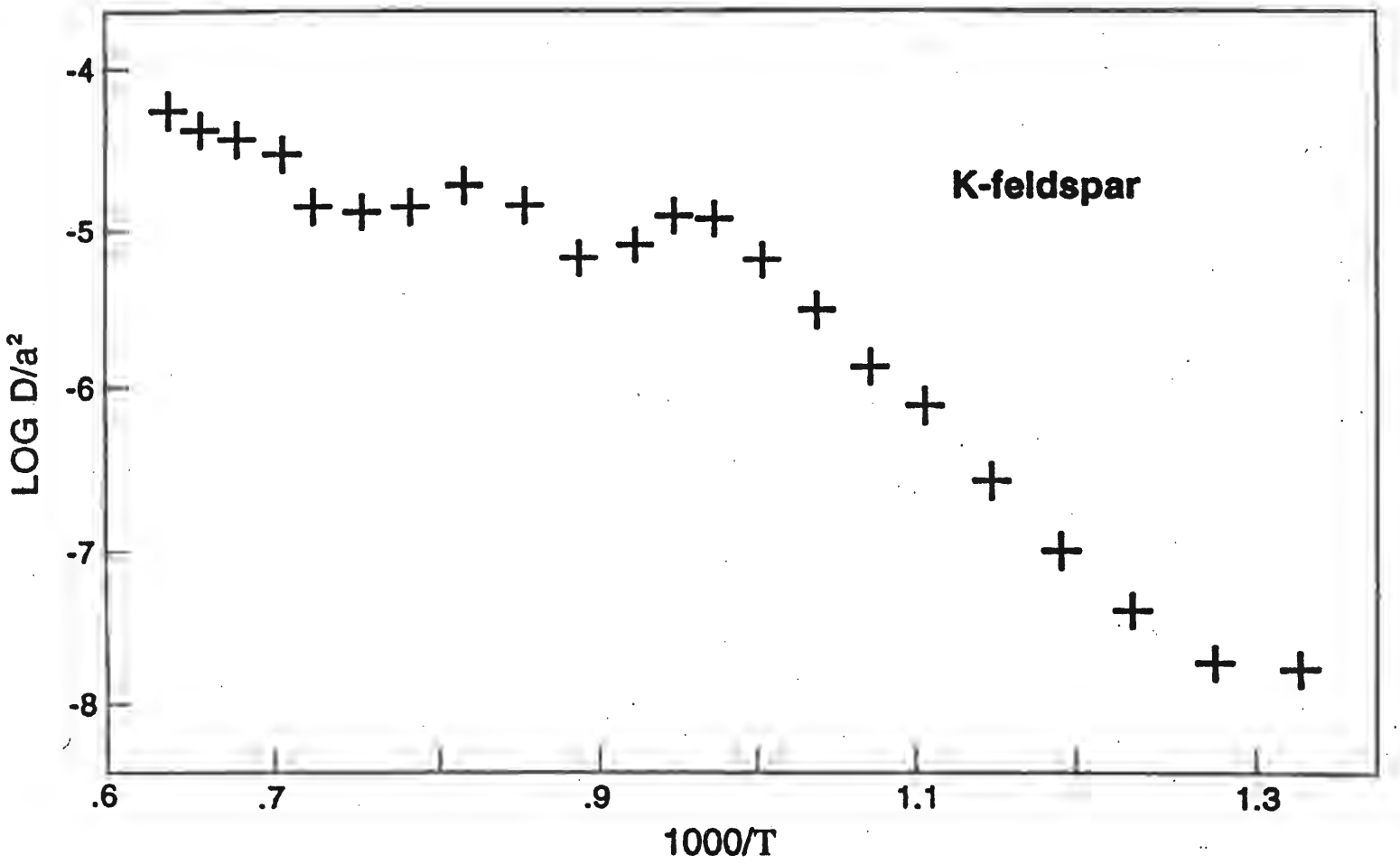

Figure 3.9: A representative Arrhenius plot for K-feldspar (as derived from the Ar abundance data). Note the linear segment obtained at low extraction temperatures and the kinked pattern that appears as more gas is released. (Reynolds, 1992)

domains must not change character before releasing all of their Ar. Fourthly, diffusion domains must fall within a finite number of size-ranges and must be approximated by a single, simple geometrical shape (Lovera et al., 1989; Parsons et al., 1999).

Recently, Parsons et al. (1999) provided several persuasive mineralogical arguments against the MDD model, demonstrating that several if not all of the assumptions on which the model is based are not obeyed. However, regardless of whether or not the model truly describes retention of radiogenic ^{40}Ar in naturally occurring K-feldspars, it has been applied to samples from a variety of geological settings, yielding temperature-time paths that appear to correspond to independent thermochronological constraints (Haggart et al., 1993; Reynolds et al., 1995; Heizler et al., 2000). In the present study, selected K-feldspars have been modeled using the MDD method, keeping in mind that modeled results must be consistent with higher temperature constraints provided by $^{40}Ar/^{39}Ar$ data presented in the previous sections.

A few points regarding K-feldspar domain modeling should be noted here. Based on the observation that experimentally calculated diffusion distances in microcline are on the order of the spacing between ubiquitous albite exsolution lamellae, microcline is commonly modeled using planar sheet geometry (Parsons et al., 1999). On the other hand, for orthoclase, which is typically not perthitic, a spherical geometry seems to work best for describing diffusion behaviour (Heizler et al., 1988; Lovera et al., 1989). However, Parsons et al. (1988, 1991, 1999), insist that micro-textures (lamellae) are largely coherent and not likely to behave as fast pathways for the escape of Ar. In other words, coherent micro-textures are morphologically controlled by the minimization of coherency strain energy and therefore, have a tendency to retain Ar, unlike incoherent microtextures in which unretentive micropores and subgrains are widely developed. Parsons et al. (1988, 1991, 1999) also noted that there is no evidence to suggest that the domains or reservoirs from which Ar diffuses have simple geometric shapes. For this study, in order to avoid unjustifiable bias between samples, samples were modeled using spherical geometry regardless of the presence of optically visible exsolution lamellae.

In some of the present cases the step-heating schedules were less than ideal for determining Arrhenius parameters because relatively low (i.e., less than 50%) of the total gas was released at temperatures $\leq 1100\ ^{0}C$, the approximate upper limit for diffusion

modeling. In other cases, there appeared to be a great deal of contamination by sericite and/or plagioclase. As a result, only two of the six K-feldspars were modeled.

3.5.2 K-Feldspar Results

Due to the lack of muscovite in the northern reaches of the current study area, K-feldspar was analysed in attempt to acquire low temperature (< 500 ^{0}C) data from this area. Data have been grouped according to the domain from which samples were collected, and are presented in order of their position along the transect, from south (La Ronge Domain) to north (Wathaman Batholith). Age spectra are presented below along with the Arrhenius plots for the modeled samples. For each of the latter cases, the best-fitting MDD modeled Arrhenius plot is shown along with the data-based one. In the age spectra, initial and final steps contributing less than 3% of the total ^{39}Ar gas released, which are likely due to minor irregularities and/or recoil effects, are not discussed in detail. Complete microprobe data and ^{40}Ar/^{39}Ar data summary sheets are found in Appendices B-3 and C-3.

La Ronge Domain

Fine-grained sample 97-D85, a muscovite-bearing psammite from the Milton Island metasedimentary assemblage (Map 1), contains homogeneous orthoclase grains that are 500 – 800 μm in size. In some cases, orthoclase grains are in contact with plagioclase grains that are partly altered to sericite. The spectrum is discordant (Figure 3.10a). Apparent ages within the first 34% of Ar released step up from 1620 ± 15 Ma to 1724 ± 18 Ma at 800 ^{0}C; this is followed by a series of discordant steps (825 - 1150 ^{0}C) that each contribute less than 3% of the total Ar released. The concave-down nature of the steps is matched by a concave-up pattern in the measured ^{37}Ar/^{39}Ar ratios, suggesting contamination by a low Ca, high K phase, possibly sericite. The concave-up nature of the high temperature part of these steps is matched by a concave-down pattern in measured ^{37}Ar/^{39}Ar values indicating possible contamination by plagioclase. This implies, therefore, that 20% of the total Ar gas released during this experiment was not derived from K-feldspar, but from sericite and plagioclase. Three steps following the discordant increments (1200 - 1350 ^{0}C), comprising 33% of the total gas released, define a mean age of 1740 ± 22 Ma.

$^{40}Ar/^{39}Ar$ K-feldspar results from the La Ronge Domain

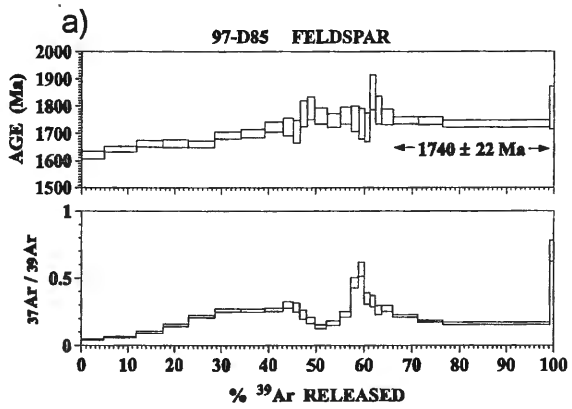

$^{40}Ar/^{39}Ar$ K-feldspar results from the Wathaman Batholith

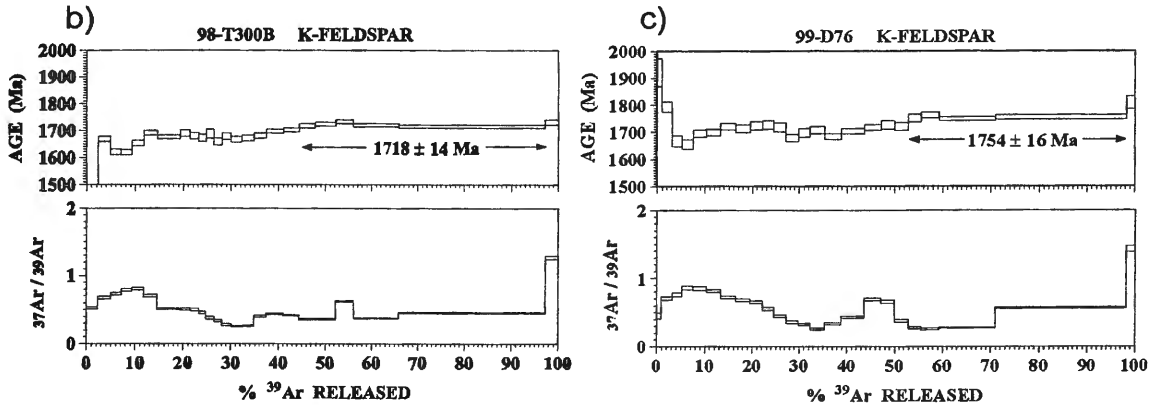

Figure 3.10: a) $^{40}Ar/^{39}Ar$ K-feldspar age spectra for fine grained sample 97-D85 from the Milton Island metasediments, La Ronge domain. b) $^{40}Ar/^{39}Ar$ K-feldspar age spectra for sample 98-T300B from the marginal zone of the Wathaman Batholith. c) $^{40}Ar/^{39}Ar$ K-feldspar age spectra for sample 99-D76 from the marginal zone of the Wathaman Batholith.

$^{40}Ar/^{39}Ar$ K-feldspar results from the Wathaman Batholith

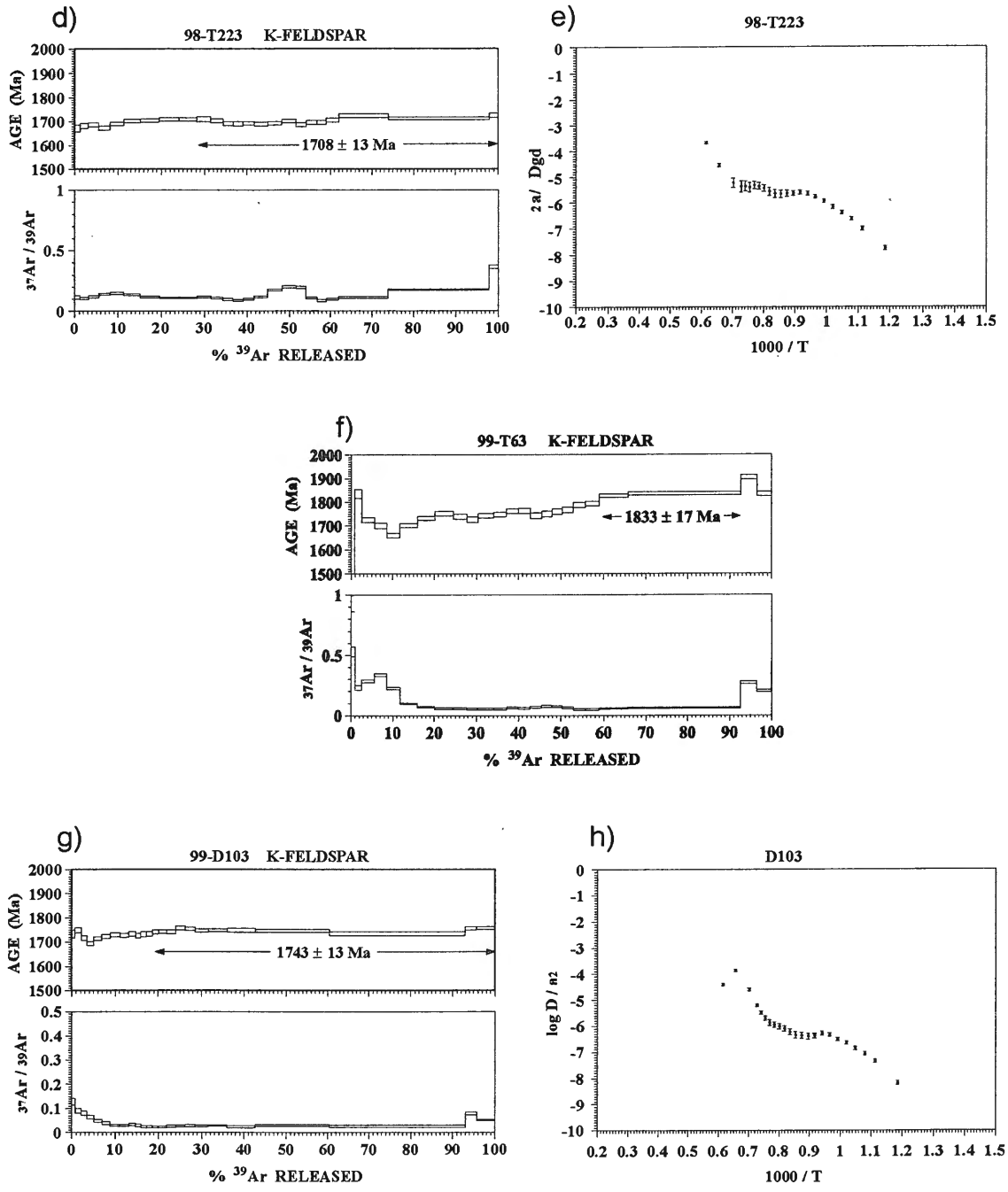

Figure 3.10 (cont'd): d) $^{40}Ar/^{39}Ar$ K-feldspar age spectra for sample 98-T223 from the main body of the Wathaman Batholith. e) Corresponding Arrhenius plot for sample 98-T223. f) $^{40}Ar/^{39}Ar$ K-feldspar age spectra for sample 99-T63 from the Wathaman Batholith. g) $^{40}Ar/^{39}Ar$ K-feldspar age spectra for sample 99-D103 from the Patterson Island megacrystic syenite. h) Corresponding Arrhenius plot for sample 99-D103.

Wathaman Batholith

Orthoclase in sample 98-T300B, a diorite - granodiorite from the marginal zone of the Wathaman Batholith (Map 1), is difficult to distinguish in thin-section as the matrix is equigranular and the concentration of the plagioclase is greater than that of K-feldspar. K-feldspar grains range in size from 0.5 – 0.8 mm. The spectrum is typical of K-feldspar (Figure 3.10b). The first part, though irregular, is characterized by apparent ages that step up from 1669 ± 10 Ma to 1702 ± 8 Ma at 1050 ^{0}C. The irregular part of the spectrum, comprising ~ 43% of the total gas released, is matched by an equally irregular $^{37}Ar/^{39}Ar$ spectrum that may be due to contamination by a high Ca phase, possibly plagioclase. Five concordant steps (1075 - 1350 ^{0}C), comprising 53% of the total ^{39}Ar released, define a mean apparent age of 1718 ± 13 Ma for this sample.

In sample 99-D76, from a foliated granodiorite from the marginal zone of the Wathaman Batholith (Map 1), orthoclase grains are up to 1 mm in size. Most grains are optically homogeneous, but a few have large (up to 200 μm) inclusions of plagioclase that has been altered to white mica. Mean apparent ages for this sample step up from 1700 ± 12 Ma at 750 ^{0}C to 1721 ± 14 Ma at 1075 ^{0}C (Figure 3.10c). The concave – down portion (775 – 975 ^{0}C) in this part of the spectrum corresponds to a decrease in the measured $^{37}Ar/^{39}Ar$ values, suggesting a decrease in Ca concentrations, or an increase in K concentrations, possibly due to outgassing of inclusions of sericitized plagioclase. Four concordant increments at the highest extraction temperature (1100 - 1350 ^{0}C), comprising 45% of the total ^{39}Ar released, define a mean apparent age of 1754 ± 16 Ma for this sample.

Orthoclase in sample 98-T223, from a granodiorite – quartz monzodiorite phase of the Wathaman Batholith (Map 1), is coarsely perthitic and 0.2 – 3 mm in size. The age spectrum is concordant with fifteen steps (850 - 1450 ^{0}C), contributing to 71% of the total ^{39}Ar released, defining a mean apparent age of 1708 ± 13 Ma (Figure 3.10d). The Arrhenius plot for this sample (Figure 3.10e), which is linear over the lowest temperature steps, has a characteristic kink beginning at ~ 800 ^{0}C. The imprecise data justify the calculation of only a two-domain model. The model-derived closure temperatures for the large domain is 260 ± 30 ^{0}C, at an assumed cooling rate of ~ 1 ^{0}C/ 10^6 years, 280 ± 30 ^{0}C at a cooling rate of 5 ^{0}C/My and 295 ± 30 ^{0}C at a cooling rate of 10 ^{0}C/My. The quoted

uncertainty value is defined by the range of Arrhenius model plots that fit the observed plot within error. From the age spectrum data, the large domain apparent age is 1708 ± 13 Ma.

In sample 99-T63, from a granite that intruded into a dioritic phase of the Wathaman Batholith (Map 1), orthoclase grains are recrystallized, equigranular and intergrown with plagioclase that has been altered to white mica. The spectrum is similar in shape to that obtained from sample 99-D76, gradually stepping up from 1661 ± 9 Ma at 700 ^{0}C to 1833 ± 10 Ma at 1250 ^{0}C. High ages in the initial 15% of the total gas released may be due to the presence of excess ^{39}Ar or a high Ca phase such as plagioclase. Two concordant high temperature increments (1150 - 1250 ^{0}C) comprising 34% of the total ^{39}Ar released define a mean apparent age of 1833 ± 17 Ma (Figure 3.10f).

Orthoclase grains in sample 99-D103, from the Patterson Island megacrystic syenite (Map 1), are 0.3 – 3 mm in size and coarsely perthitic. The spectrum is concordant at high temperature increments (925 - 1250 ^{0}C) and is matched by an equally concordant ^{37}Ar/^{39}Ar spectrum (Figure 3.10g), with the exception of the initial and final 7% total gas released. These portions of the spectrum are characterized by high measured ^{37}Ar/^{39}Ar values, which may be due to the presence of a high-Ca phase such as plagioclase. Seven increments (1000 - 1250 ^{0}C) contributing 67% of the total ^{39}Ar released define a total gas age of 1742 ± 14 Ma. The Arrhenius plot for this sample (Figure 3.10e), which is linear over the lowest temperature steps, has a characteristic kink beginning at ~ 800 ^{0}C. The relatively imprecise data justify the calculation of only a two-domain model. The model-derived closure temperature for the large domain is 240 ± 40 ^{0}C, at an assumed cooling rate of ~ 1 ^{0}C/My, 259 ± 40 ^{0}C at a cooling rate of 5 ^{0}C/My and 275 ± 40 ^{0}C at a cooling rate of 10 ^{0}C/ 10^6 years, where the quoted uncertainty value is defined by the range of Arrhenius model plots that fit the observed plot within error. From the age spectrum data, the large domain apparent age is 1743 ± 13 Ma.

3.6 Summary of ^{40}Ar/^{39}Ar Results

^{40}Ar/^{39}Ar hornblende and muscovite ages show slight variation from south to north. One hornblende age from the northern Glennie Domain suggests it cooled through 500 ^{0}C by ~ 1800 Ma. Hornblende ages within the Kisseynew Domain suggest cooling

through 500 ^{0}C by ~ 1770 Ma. Within the La Ronge Domain, young hornblende ages are observed in the south (average ~ 1750 Ma) and become progressively older to the north (average ~ 1770). Within error, hornblende ages from the southern margin of the Wathaman Batholith are concordant with those from the northern La Ronge Domain. The oldest hornblende ages are observed in the Peter Lake Domain (~1818 Ma). Muscovite ages from the Kisseynew and La Ronge Domains are also concordant within error, suggesting they passed through ~ 350 ^{0}C by ~ 1730 Ma. Assuming the K-feldspar model ages are reliable, at a cooling rate of 1^{0}C/My, the northern portion of the orogen passed through 260 ^{0}C at ~ 1708 Ma.

CHAPTER IV – Thermal History

Exposure of once deeply buried rocks at the Earth's surface requires that substantial exhumation has occurred. Depending on the system being studied – whether it be an ancient (> 1000 Ma) or recent (≤ 55 Ma) orogenic system, the rate at which exhumation occurs varies in time and space in three dimensions (England & Thompson, 1984; Ring et al., 1999). Processes that lead to exhumation are ductile thinning, normal faulting, syn-tectonic erosion, and post-tectonic erosion (Martignole, 1992; Ring et al., 1999). The processes of ductile thinning and post-tectonic erosion are characterized by slow exhumation and cooling rates (i.e. < 5 km/My; < 10 ^{0}C/My). Normal faulting and erosion, on the other hand, are characterized by faster exhumation and cooling rates, reaching upper limits of > 5-10 km/My and ≥ 10 ^{0}C/My respectively (Ring et al., 1999). A challenging, yet important task in studying orogenic belts of any age, therefore, is to determine the processes that led to exhumation. One way in which this is done is by using thermochronological techniques in which patterns of radiometric ages from metamorphic minerals with different closure temperatures are used to constrain the cooling rate and thus distinguish the different exhumation processes (Hanes, 1991; Ring et al., 1999).

4.1 Closure Temperatures of Radioactive Isotopic Systems

For the U-Pb and K-Ar decay schemes, the temperature at which the daughter product ceases to diffuse out of a specific mineral is termed the closure temperature (T_c). Before thermochronological data can be interpreted in the context of a thermal history, the T_c's of the decay scheme in question must be calculated, experimentally derived, estimated or assumed for each mineral being analyzed. T_c's may then be applied to samples that have simple cooling histories. Minerals in which the isotopic system has been reset by thermal overprinting following primary crystallization cannot be assigned a specific T_c as they may not have cooled through the same temperature at which daughter products "closed" following primary crystallization. Thus, when using T_c to construct cooling paths all ages must first be assessed with this in mind. Since T_c is a function of the effective diffusion distance, activation energy and cooling rate (Dodson, 1973), the T_c

of each mineral should be presented as a range of temperatures when constraints on these parameters are not available.

In this study, U-Pb ages obtained from monazite and titanite by David Corrigan at the Geological Survey of Canada have been compared with $^{40}Ar/^{39}Ar$ ages obtained from hornblende, muscovite, and K-feldspar. With the exception of K-feldspar, nominal T_c's of monazite, titanite, hornblende and muscovite have been assumed (Table 4.1).

T_c of the U-Pb System			**T_c of the $^{40}Ar/^{39}Ar$ System**	
Zircon (Heaman & Parrish, 1991)	**Monazite** (Parrish, 1990)	**Titanite** (Heaman & Parrish, 1991)	**Hornblende** (Hanes, 1991)	**Muscovite** (Purdy & Jager, 1976)
> 800 ^{0}C	725 ± 25 ^{0}C	600 ± 30 ^{0}C	500 ± 50 ^{0}C	350 ± 50 ^{0}C

Table 4.1: Closure temperatures (T_c) for the U-Pb system in zircon, monazite and titanite, and for the $^{40}Ar/^{39}Ar$ system in hornblende and muscovite.

4.2 Resetting Radioactive Isotopic Systems

The systematics of K-Ar in hornblende and muscovite and U-Pb in monazite and titanite during heating are poorly understood. As discussed by Zeitler (1989), for T_c to have any meaning it must be evaluated for a specific cooling rate in a system that has undergone simple cooling, not one that has experienced episodic reheating. Thus the concept of T_c is useful when describing the retention of daughter products in one mineral relative to another. However, differences in kinetic behaviour during heating versus cooling, or differences in heating rates versus cooling rates, lead to no direct correlation between the T_c of a system and the "opening" temperature (T_o) – the temperature at which a system is reset during a re-heating event (Cliff, 1985). Lack of correspondence between T_c and T_o is due to the fact that systems may be reset at temperatures remote from the typical T_c. As a rough rule of thumb, slow cooling (~ 10 ^{0}C/My) systems reheated to T_c for a duration of ~ 10 My will be nearly totally reset (~ 99%; Zeitler, 1989). Alternatively, to achieve the same degree of resetting in 1 My, the system must be heated to temperatures 50 – 100 ^{0}C above T_c. In increasingly ancient, cold systems, an even greater degree of overprinting is required for complete resetting.

In the case of the diffusive loss of Ar it is known, however, that the degree to which K-Ar isotopic ages are reset is mainly a function of temperature (McDougall and Harrison, 1988). Studies conducted by Desmons et al. (1982) and Berry and McDougall (1986) showed that a temperature increase accompanied by recrystallization may also facilitate resetting of the system due to the generation of smaller new grains that increase diffusive Ar loss (Dempster, 1986). The same is true of the U-Pb system in zircon and titanite.

In the case of monazite, recent interest in chemical dating of grains using X-ray maps of U, Th and Pb obtained from crystals as small as 10 μm (Williams et al., 1999), indicates that discordant monazite ages may not reflect diffusive loss of Pb. Rather, monazite ages may reflect distinct age domains within the crystal (which may or may not correlate with compositional domains, i.e. compositional zoning) that developed during different stages in a rock's tectonic history. Distinct U-Pb age domains may correlate with individual tectonic events.

4.3 Interpretation of Results

$^{40}Ar/^{39}Ar$ results obtained in this study have been interpreted by comparison with nearby samples and with U-Pb isotopic ages from zircon, monazite and titanite grains. Cooling versus crystallization ages have been interpreted by comparison with the metamorphic grade of the terrane from which the sample was taken. Monazite ages display a slight gradient across the Reindeer Lake transect (Figure 4.1; Map.1), ranging from 1817 ± 2 Ma in the south to 1822 ± 1 Ma in the north, suggesting the southern part (orogen core) of the Trans-Hudson Orogen was heated to temperatures ≥ 725 ^{0}C by 1815 – 1819 Ma. Similarly, titanite ages display a slight variation ranging from 1776 ± 4 in the south to 1790 ± 8 Ma in the north suggesting that part of the orogen cooled through 600 ^{0}C by 1790 Ma in the north, and 1776 Ma in the south. The gradient in ages also appears to correspond with metamorphic grade, where younger monazite and titanite ages in the south correspond to higher grade rocks of transitional granulite – upper amphibolite facies (Figure 4.8) and older ages in the north correspond to lower grade rocks of mid – low amphibolite facies. In the southern part of the transect, zircon ages are interpreted as crystallization ages whereas monazites are interpreted to represent peak metamorphic growth ages. Titanite ages from the southern part of the transect are

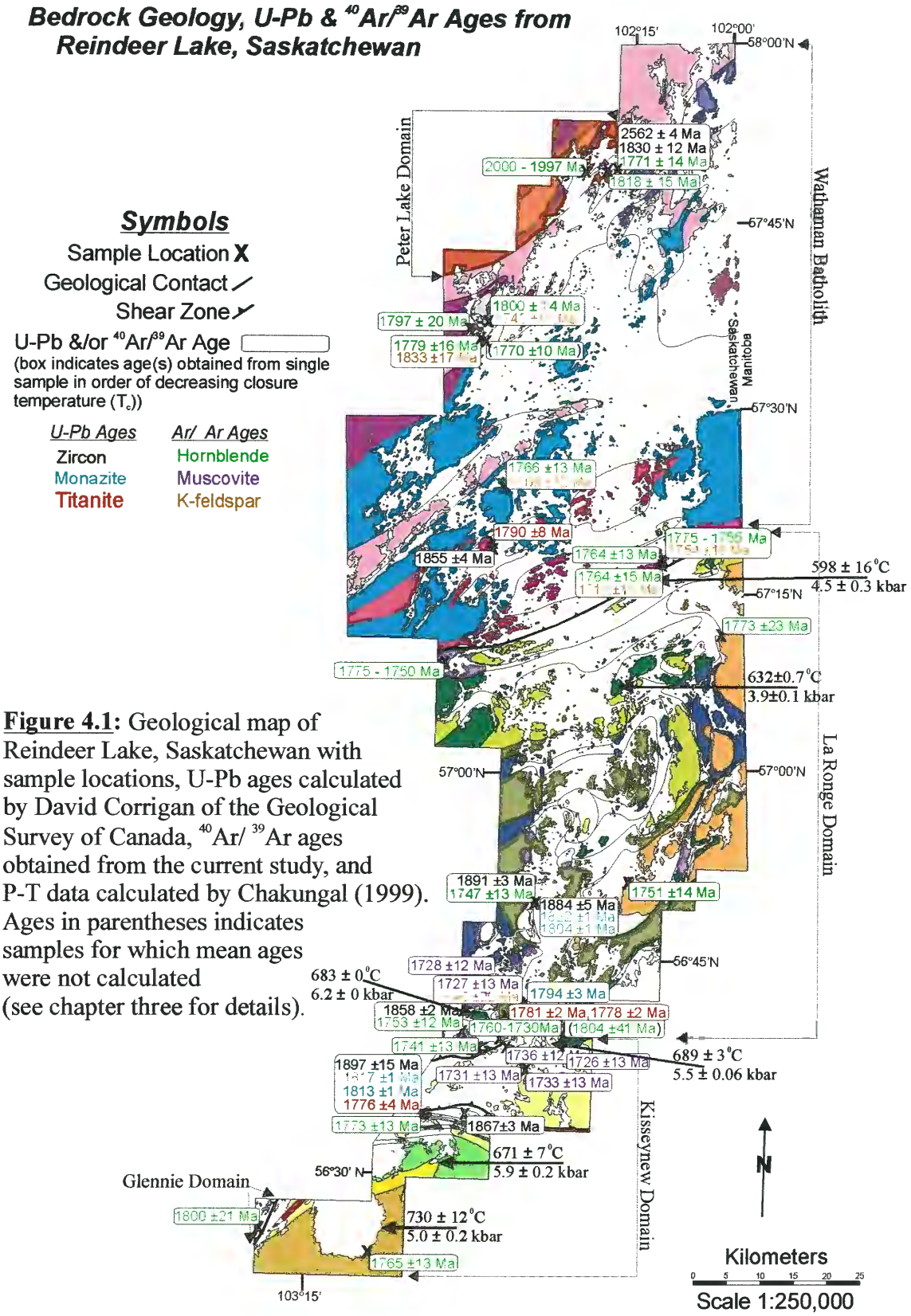

Figure 4.1: Geological map of Reindeer Lake, Saskatchewan with sample locations, U-Pb ages calculated by David Corrigan of the Geological Survey of Canada, $^{40}Ar/^{39}Ar$ ages obtained from the current study, and P-T data calculated by Chakungal (1999). Ages in parentheses indicates samples for which mean ages were not calculated (see chapter three for details).

interpreted as post-metamorphic cooling ages, as this part of the orogen was heated to temperatures above 700 ^{0}C. In the northern portion of the transect, U-Pb monazite ages are interpreted as crystallization ages, and titanite ages are interpreted as metamorphic growth ages, as this part of the orogen only reached temperatures approaching the T_c for titanite.

4.3.1 Glennie Domain

For the northernmost portion of the Glennie Domain studied in the current project, U-Pb zircon, monazite and titanite data are unavailable. Based on U-Pb zircon data from previous studies, however, plutonism within the Glennie Domain occurred during three pulses between ca. 1893 – 1831 Ma (Durocher et al., 2001 and references therein). An orogen-wide study done by Heizler et al. (1999, 2000) suggested that the average crystallization age of plutons within the Glennie Domain is ~ 1840 Ma. In the same study recrystallized titanite grains yielded U-Pb ages of 1838 Ma and 1804 ± 3 Ma, where the older age has been interpreted as a crystallization age, and younger ages are interpreted to represent the time of post-peak metamorphic cooling through 525 ± 25 ^{0}C (Heizler et al., 2000). $^{40}Ar/^{39}Ar$ hornblende, muscovite, biotite and K-feldspar ages also obtained by Heizler et al. (2000) and quoted in this study (Table 4.2), are averages of the time at which the orogen as a whole cooled through 500 ^{0}C, 350 ^{0}C, 300 ^{0}C and 200 ^{0}C respectively. As the exact location of samples is unknown, the U-Pb zircon and $^{40}Ar/^{39}Ar$ ages presented by Heizler et al. (2000) have not been used to calculate cooling rates.

In a study conducted by Durocher et al. (2001; Table 4.2), an average of $^{40}Ar/^{39}Ar$ hornblende ages suggests the Glennie Domain along Santoy Lake, Saskatchewan, south of the current study area, cooled through 500 ^{0}C by ~ 1724 Ma following peak metamorphism. However, $^{40}Ar/^{39}Ar$ biotite ages, also from the Santoy Lake area, are older than hornblende ages obtained in their study. For this reason, the data obtained by Durocher et al. (2001) was not used to calculate the cooling rate of the Glennie Domain. Rather, results obtained by Heizler et al. (2000) and Durocher et al. (2001) have been used here as a basis of comparing the single $^{40}Ar/^{39}Ar$ hornblende age obtained in this study with those obtained in previous studies.

In the current study, hornblende in a single diorite sample (98-D42) from the northern Glennie Domain yielded an isochron age of 1800 ± 21 Ma. According to U-Pb

and Pb-Pb zircon ages from plutonic rocks (Durocher et al., 2001), peak metamorphism in the Glennie Domain occurred after a thermal event at 1830 Ma. It is assumed here, therefore, that peak metamorphism in the Glennie Domain occurred during the same interval of peak metamorphism experienced by the Reindeer Zone along Reindeer Lake at ca. 1820 – 1790 Ma. Thus, the hornblende age from sample 98-D42 is interpreted to represent the time of post-peak metamorphic cooling through ~ 500 ^{0}C.

Sample	*Zircon*	*Monazite*	*Titanite*	*Hornblende*	*Muscovite*	*Biotite*	*K-feldspar*
98-D42	-----	--	-----	1800 ±21Ma	-----	-----	-----
Durocher et al. (2001) and references therein. Ages are for the Glennie Domain, Santoy Lake area.	1893 Ma 1831 Ma	--	-----	1716± 9 Ma 1741±19 Ma 1718±19 Ma 1716±11 Ma	-----	(1713 ± 9 Ma) (1758 ± 9 Ma) (1732 ± 6 Ma) (1733 ± 8 Ma)	-----
Heizler et al. (2000)	(1840 Ma)	--	1838 Ma 1804 ± 3 Ma	(1760 Ma)	(1740 Ma)	(1720 Ma)	(1700Ma)

Table 4.2: Samples from the Glennie Domain and their associated U-Pb and ^{40}Ar/^{39}Ar ages. The single hornblende age for sample 98-D42 was obtained in the current study. All other ages are from previous work. Parentheses indicate data for which the significance of the age is poorly understood.

A plot of U-Pb and ^{40}Ar/^{39}Ar ages versus their respective closure temperatures (Figure 4.2) indicates that following peak metamorphism, the Glennie Domain cooled quickly from ~ 550 ^{0}C (the T_c of titanite assumed by Heizler et al., 2000) to 500 ^{0}C over 4 My. Based on a titanite age of 1804 ± 3 Ma (Heizler et al., 2000) and a hornblende age of 1800 ± 21 Ma (from 98-D42), and calculating the difference between their respective closure temperatures, the Glennie Domain cooled from 550 ^{0}C through 500 ^{0}C at a rate of 12.5 ^{0}C/ My. Using a closure temperature of 600 ^{0}C for titanite, as is done for all titanite data presented in the following sections the calculated cooling rate is 25 ^{0}C/My. When the range of possible slopes is taken into consideration, the average rate at which the Glennie Domain cooled from 600 ^{0}C – 500 ^{0}C is 14.3 ± 11 ^{0}C/My. Considering the uncertainty associated with ages obtained from previous work, however, no significance has been attributed to the calculated cooling rate.

4.3.2 Kisseynew Domain

Zircons from a leucotonalite (97-D12) and tonalite (97-D297) that intruded into the volcanosedimentary assemblage of the Levesque Bay supracrustal assemblage (Map

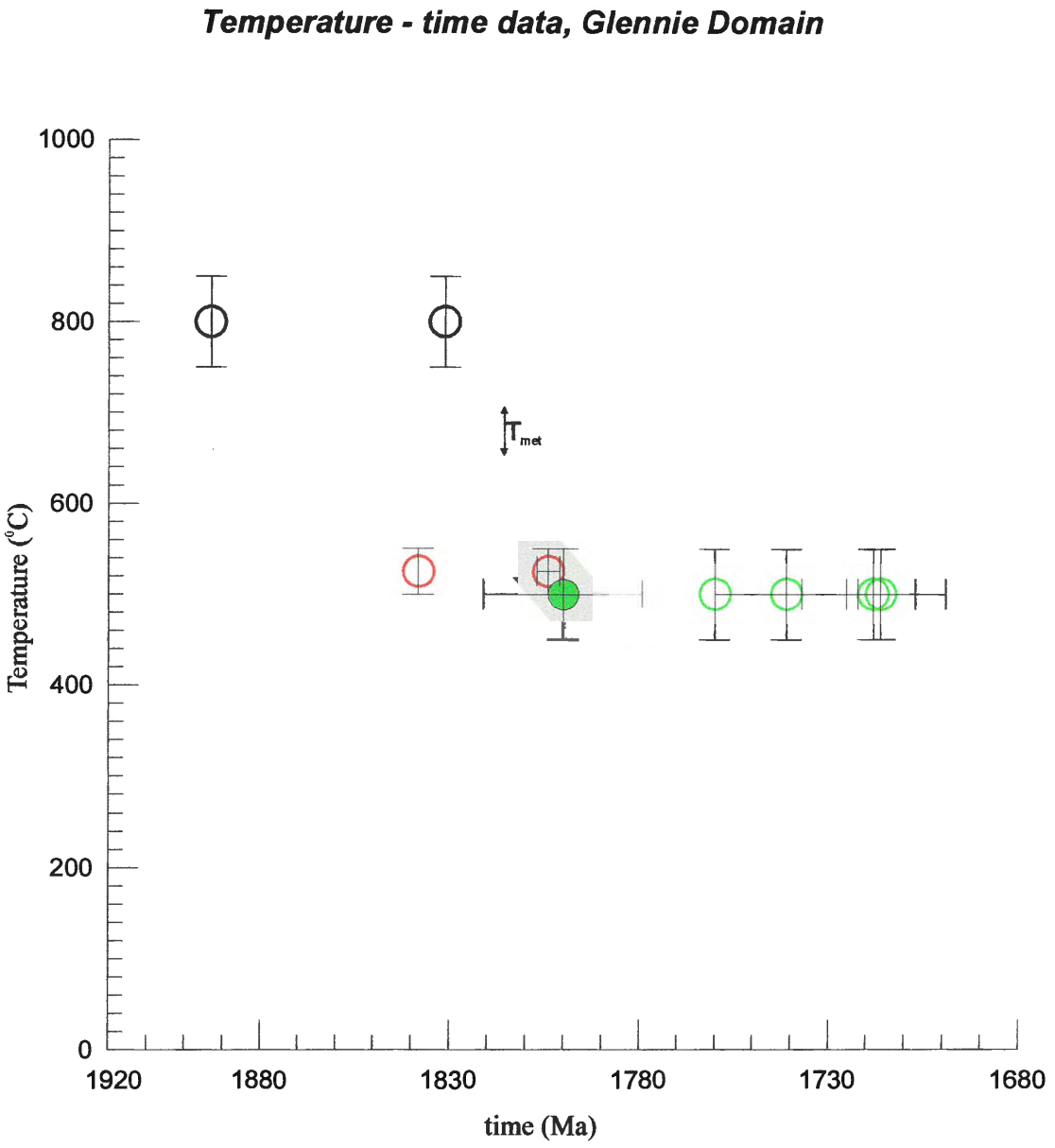

Figure 4.2: Temperature - time (T-t) data from the Glennie Domain. ***Legend:*** *solid circle,* date obtained in this study; *open circle,* ages from Durocher et al. (2001) and Heizler et al. 2000; *black,* U-Pb zircon; *red,* U-Pb titanite; *green,* $^{40}Ar/^{39}Ar$ hornblende; T_{met}, T range during peak metamorphism at ca. 1820-1790 Ma (Durocher et al., 2001; Chakungal, 1999); *grey arrow*, estimated T-t path of rocks in the Glennie domain. Note: T_c for titanite is that used by Heizler et al. (2000).

1) yielded U-Pb ages of 1897 ± 15 Ma and 1867 ± 3 Ma respectively (Table 4.3). Monazites from the same granodiorite yielded U-Pb ages of 1817 ± 1 Ma and 1813 ± 1 Ma, and titanite from the same sample yielded a U-Pb age of 1776 ± 4 Ma. P-T estimates obtained from an orthopyroxene-bearing gneiss just south of the sample locations suggest this part of the orogen reached temperatures of 730 ± 12 ^{0}C (Chakungal, 1999) during peak metamorphism at ca.1820 Ma. Zircons are therefore interpreted to represent crystallization ages, whereas monazites may represent metamorphic growth ages. Titanite U-Pb ages are interpreted as post-metamorphic cooling ages through 600 ^{0}C.

Sample #	*Zircon*	*Monazite*	*Titanite*	*Hornblende*	*Muscovite*
98-L48 (tonalite)	-----	-----	-----	1765 ± 13 Ma	-----
98-D12 (granodiorite)	1897 ± 15 Ma	1817 ± 1 Ma 1813 ± 1 Ma	1776 ± 4 Ma	-----	-----
98-D12 (metavolcanic)	-----	-----	-----	1773 ± 13 Ma	-----
97-D297 (tonalite)	1867 ± 3 Ma	-----	-----	-----	-----
97-D222 (metasediment)	-----	-----	-----	-----	1733 ± 13 Ma
97-D31 (metasediment)	-----	-----	-----	-----	1731 ± 13 Ma
97-D26A (metasediment)	-----	-----	-----	-----	1736 ± 12 Ma
97-D26B (s-type granite)	-----	-----	-----	-----	1726 ± 13 Ma

Table 4.3: Samples from the Kisseynew Domain and their associated U-Pb and ^{40}Ar/^{39}Ar ages. Samples are listed from south (98-L48) to north (97-D26B) with increasing proximity to the Duck Lake Shear Zone. Boxes with dashed lines indicate samples for which data are not available.

Hornblende from a tonalite (98-L48) that intruded the southern Burntwood Group yielded a ^{40}Ar/^{39}Ar age of 1765 ± 13 Ma, and hornblende from a metavolcanic rock located within the Levesque Bay supracrustal assemblage, where peak temperatures were 671 ± 7 ^{0}C, yielded a ^{40}Ar/^{39}Ar age of 1773 ± 13 Ma. ^{40}Ar/^{39}Ar ages from both samples are concordant within error and overlap with the U-Pb titanite age from the tonalite in the central portion of the domain. Hornblende ^{40}Ar/^{39}Ar ages are therefore interpreted to represent post-peak metamorphic cooling through 500 ^{0}C by 1765 Ma. Muscovites from four metasedimentary samples within the McLennan Group yielded ^{40}Ar/^{39}Ar ages of 1733 ± 13 Ma, 1731 ± 13 Ma, 1736 ± 12 Ma, and 1726 ± 13 Ma. As all muscovite ages

are concordant within error, an average of the ages suggests the McLennan Group arkoses cooled through 350 ^{0}C by 1732 ± 13 Ma.

A plot of U-Pb ages and ^{40}Ar/^{39}Ar ages versus their respective closure temperatures (Figure 4.3) indicates that following peak metamorphism, the Kisseynew Domain cooled from 600 ^{0}C to 350 ^{0}C over 50 My. Based on a titanite age of 1776 ± 4 Ma and a muscovite age of 1726 ± 13 Ma, and calculating the difference between their respective closure temperatures, the Kisseynew Domain cooled from 600 ^{0}C through 350 ^{0}C at a rate of 5.0 ± 3 ^{0}C/ My, where the uncertainty reflects the range of slope when the range error associated with the titanite and muscovite ages is taken into account.

4.3.3 La Ronge Domain

Within the La Ronge Domain, U-Pb zircon ages were obtained from plutonic bodies. The Butler Island diorite in the south yielded an age of 1858 ± 2 Ma and a tonalite (97-D373A) and granite (97-D373B) in the central region of the domain (possibly the plutonic root of the La Ronge arc) yielded ages of 1891 ± 3 Ma and 1884 ± 5 Ma respectively (Table 4.4). Monazites, also from the granitic body, yielded U-Pb ages of 1822 ± 1 Ma, 1810 ± 1 Ma and 1804 ± 1 Ma. Titanites from a metavolcanic rock yielded U-Pb ages of 1781 ± 2 Ma and 1778 ± 2 Ma. Based on work by Chakungal (1999), this part of the orogen was heated to temperatures of 689 ± 2 ^{0}C during peak metamorphism; therefore, U-Pb ages obtained from zircons are interpreted to represent pluton crystallization ages, whereas those obtained from monazites have been interpreted to represent metamorphic growth ages. Titanites are interpreted as metamorphic cooling ages.

Within the La Ronge suite of samples, hornblende from a metavolcanic rock situated 200 m from the leading edge of the Duck Lake Shear Zone, but situated within it, yielded the youngest ^{40}Ar/^{39}Ar age of 1741 ± 13 Ma. All other amphiboles were obtained from intrusive bodies and yielded mean ages that progressively increase to the north. Ages range from 1745 ± 12 Ma in the south, where the metamorphic grade is upper amphibolite facies (689 ± 2 ^{0}C – 683 ± 0 ^{0}C), to 1773 ± 23 Ma in the north, near the margin of the Wathaman Batholith, where rocks are of mid-amphibolite facies (632 ± 0.7 ^{0}C – 598 ± 16 ^{0}C; Chakungal, 1999). Thus, hornblende ages across the La Ronge

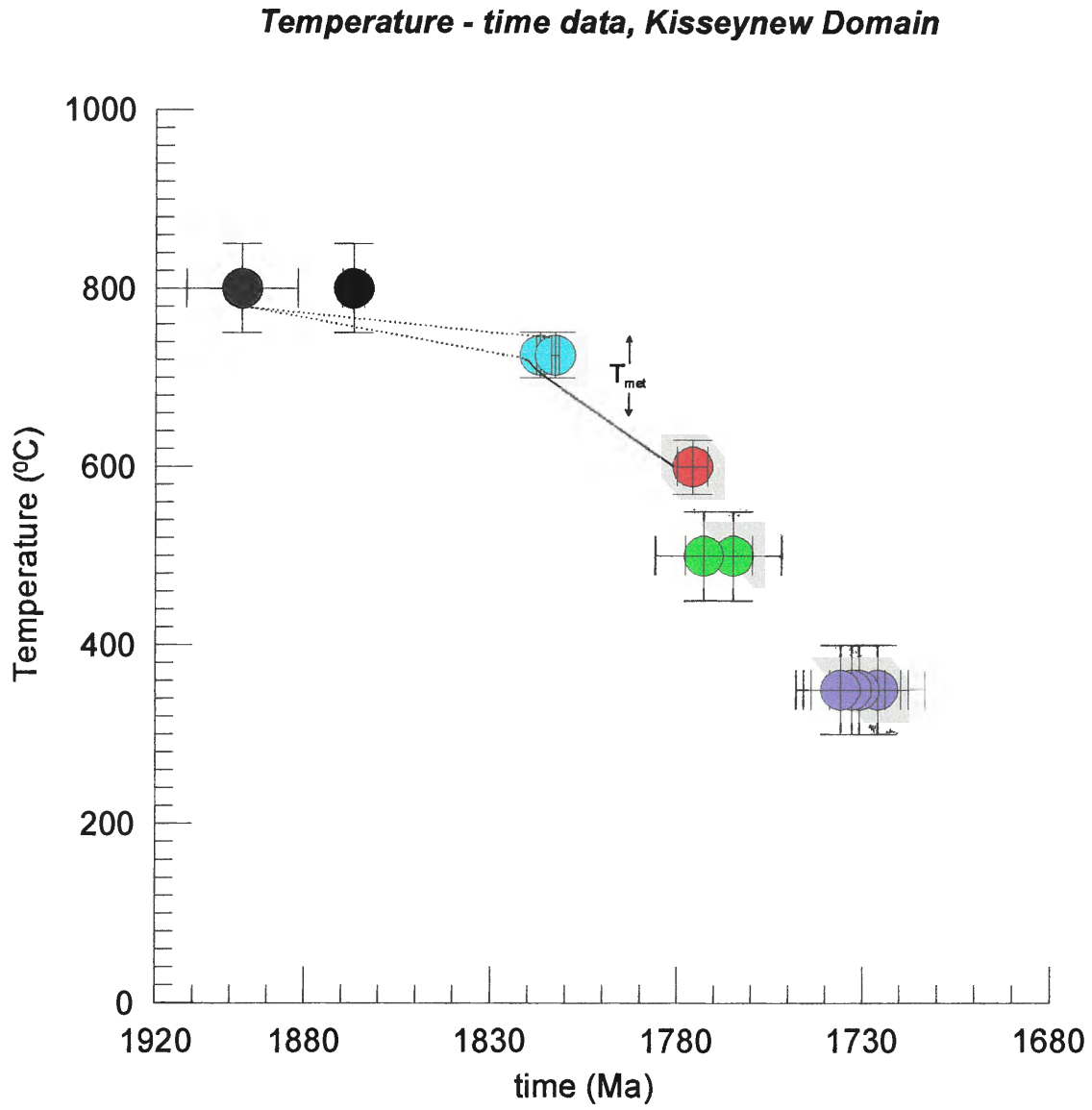

Figure 4.3: Temperature - time (T-t) data from the Kisseynew Domain. Lines connecting individual points indicate ages that were obtained from the same sample horizon. ***Legend:*** *black,* U-Pb zircon; *blue,* U-Pb monazite; *red,* U-Pb titanite; *green,* $^{40}Ar/^{39}Ar$ hornblende; *purple,* $^{40}Ar/^{39}Ar$ muscovite; T_{met}, T range during peak metamorphism at ca. 1820 - 1790 Ma (Chakungal,1999); *dotted line,* relationship between ages unclear; *solid line,* represents post-metamorphic cooling; *grey arrow*, estimated T-t path of rocks in the Kisseynew Domain..

Domain are interpreted to represent cooling through 500 ^{0}C following peak metamorphism.

Sample	*Zircon*	*Monazite*	*Titanite*	*Hornblende*	*Muscovite*	*K-feldspar*
97-D004 (metavolcanic)	-----	-----	-----	1741 ±13 Ma	-----	-----
97-A404A (metavolcanic)	-----	-----	-----	(1804 ±41 Ma)	-----	-----
97-D23 (diorite)	-----	-----	-----	1745 ±12 Ma	-----	-----
97-A001 (diorite)	1858 ± 2Ma	-----	-----	1753 ±12 Ma	-----	-----
97-D85 (c.gr metasediment)	-----	-----	-----	-----	1728 ±12Ma	-----
97-D85 (f.gr metasediment)	-----	-----	-----	-----	1727 ±13Ma	1740±22Ma
97-D84 (metasediment)	-----	1794 ± 3Ma	-----	-----	-----	-----
97-D127 (metavolcanic)	-----	-----	1781 ± 2Ma 1778 ± 2Ma	-----	-----	-----
97-D373B (granite)	1884 ± 5Ma	1822 ± 1Ma 1810 ± 1Ma 1804 ± 1Ma	-----	-----	-----	-----
97-D373A (tonalite)	1891 ± 3Ma	-----	-----	1747 ±13 Ma	-----	-----
98-D93 (monzogranite)	-----	-----	-----	1751 ±14 Ma	-----	-----
99-D53 (pegmatitic gabbro)	-----	-----	-----	1773 ±23 Ma	-----	-----
98-T201 (granite)	-----	-----	-----	1750-1775 Ma	-----	-----

Table 4.4: Samples from the La Ronge Domain and their associated U-Pb and $^{40}Ar/^{39}Ar$ ages. Samples are listed from south (97-D004) to north (99-D53) with increasing distance from the Duck Lake Shear Zone, and increasing proximity to the Wathaman Batholith. Ages enclosed in brackets are samples for which the calculated mean age was not used (see Chapter 3 for details). Dashed lines indicate samples for which data are not available.

Muscovites from within a single horizon of the Milton Island metasedimentary assemblage yielded concordant $^{40}Ar/^{39}Ar$ ages of 1728 ± 12 Ma and 1727 ± 13 Ma. K-feldspar from one of the muscovite samples yielded an age of 1740 ± 22 Ma. Ages from both minerals are concordant within error, suggesting similar closure temperatures (ca. 350 ^{0}C, the T_c of muscovite). If, however, the T_c of K-feldspar is the same as that modelled for the two K-feldspars from the Wathaman Batholith, the closure temperature of K-feldspar in the La Ronge Domain is ~ 250 ^{0}C. In this case, an older K-feldspar age relative to the youngest muscovite age may be attributed to excess argon. Due to the

uncertainty associated with the K-feldspar data, these have not been used to calculate the cooling rate for the La Ronge Domain. Rather, a plot of the ages versus their respective closure temperatures (Figure 4.4) indicates that following peak metamorphism, this part of the orogen cooled from 600 ^{0}C to 350 ^{0}C over 54 My at a rate of 4.6± 1 ^{0}C/My.

4.3.4 Wathaman Batholith

One sample collected from the Wathaman Batholith yielded a U-Pb zircon age of 1855 ± 1 Ma. For this portion of the transect U-Pb data from monazites are not available; however, titanite from one sample yielded a U-Pb age of 1790 ± 8 Ma (Table 4.5). Both samples were collected from the southern part of the batholith, north of the reworked intrusive contact with the La Ronge Domain, where metamorphic grade is upper green-schist – lower amphibolite facies (≤ 530 ^{0}C). Thus, the U-Pb zircon age is interpreted as a crystallization age, whereas the titanite age is likely a metamorphic growth age.

^{40}Ar/^{39}Ar hornblende ages at the southern margin of the batholith, within the reworked intrusive contact zone, are concordant within analytical error and yield ages of 1765 Ma and 1764 Ma. To the north, within the batholith, ages do not vary significantly from those obtained to the south (Table 4.5) with the exception of the two northernmost samples (99-D214 and 99-D103), which yielded ages of 1797 ± 20 Ma and 1800 ± 14 Ma respectively. Metamorphic grade throughout the batholith is upper greenschist – lower amphibolite facies; therefore, all but the two northern most hornblende ages are interpreted to represent post-metamorphic cooling. Ages from 99-D214 and 99-D103, on the otherhand, are interpreted as partially reset crystallization ages.

^{40}Ar/^{39}Ar ages of K-feldspars from the Wathaman Batholith range from ~ 1705 ± 12 Ma to 1833 ± 17 Ma. Ages show no correlation with distance from the reworked intrusive contact, or with proximity to the intrusive contact with the Archean Peter Lake Domain. MDD modeling of samples 98-T223 and 99-D103 yielded closure temperatures of 260 ± 30 ^{0}C and 240 ± 40 ^{0}C respectively for a cooling rate of 1 ^{0}C/My, and temperatures of 280 ± 30 ^{0}C and 259 ± 40 ^{0}C respectively for a cooling rate of 5 ^{0}C/My. Based on the consistency of the metamorphic grade and U-Pb and ^{40}Ar/^{39}Ar ages, it seems that this part of the orogen cooled slowly. For representation on a T–t graph (Figure 4.5), therefore, K-feldspar samples have been plotted at the closure temperature calculated for a cooling rate of 1 ^{0}C/My. For the remaining three samples on which

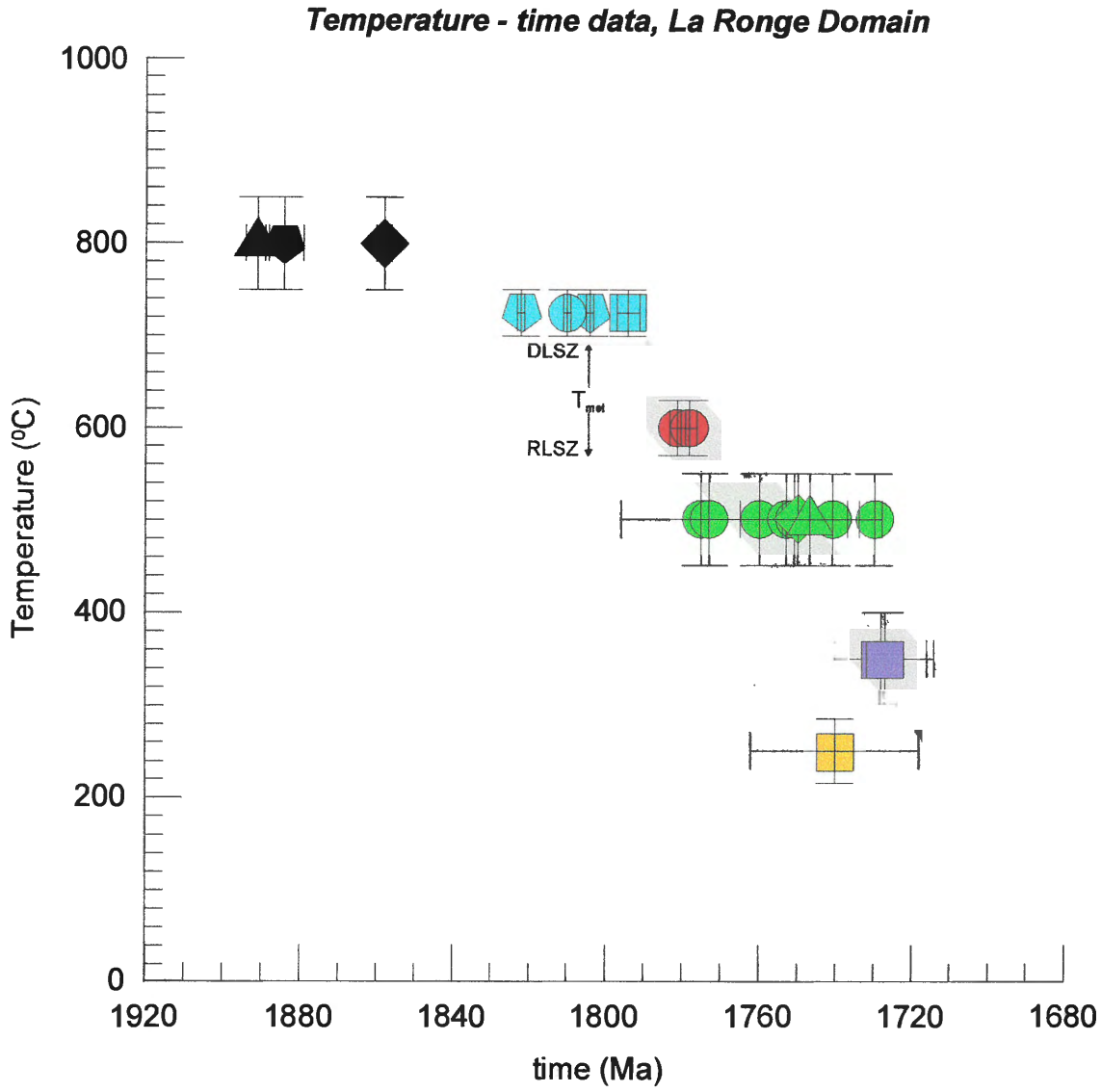

Figure 4.4: Temperature - time (T-t) data from the La Ronge Domain. Lines connecting individual points indicate ages that were obtained from the same sample horizon. ***Legend:*** ***black,*** U-Pb zircon; ***blue,*** U-Pb monazite; ***red,*** U-Pb titanite; ***green,*** $^{40}Ar/^{39}Ar$ hornblende; ***purple,*** $^{40}Ar/^{39}Ar$ muscovite; ***orange,*** $^{40}Ar/^{39}Ar$ K-feldspar, large domain age; T_{met}, T range during peak metamorphism at ca. 1820 - 1790 Ma, from Chakungal (1999); *DLSZ,* Duck Lake Shear Zone; *RLSZ,* Reilly Lake Shear Zone; *grey arrow,* T-t path of rocks in the La Ronge Domain. Points represented by a circular symbol represent data obtained from one sample. Triangle, octagon, square and diamond symbols indicate which data points were obtained from the same sample.

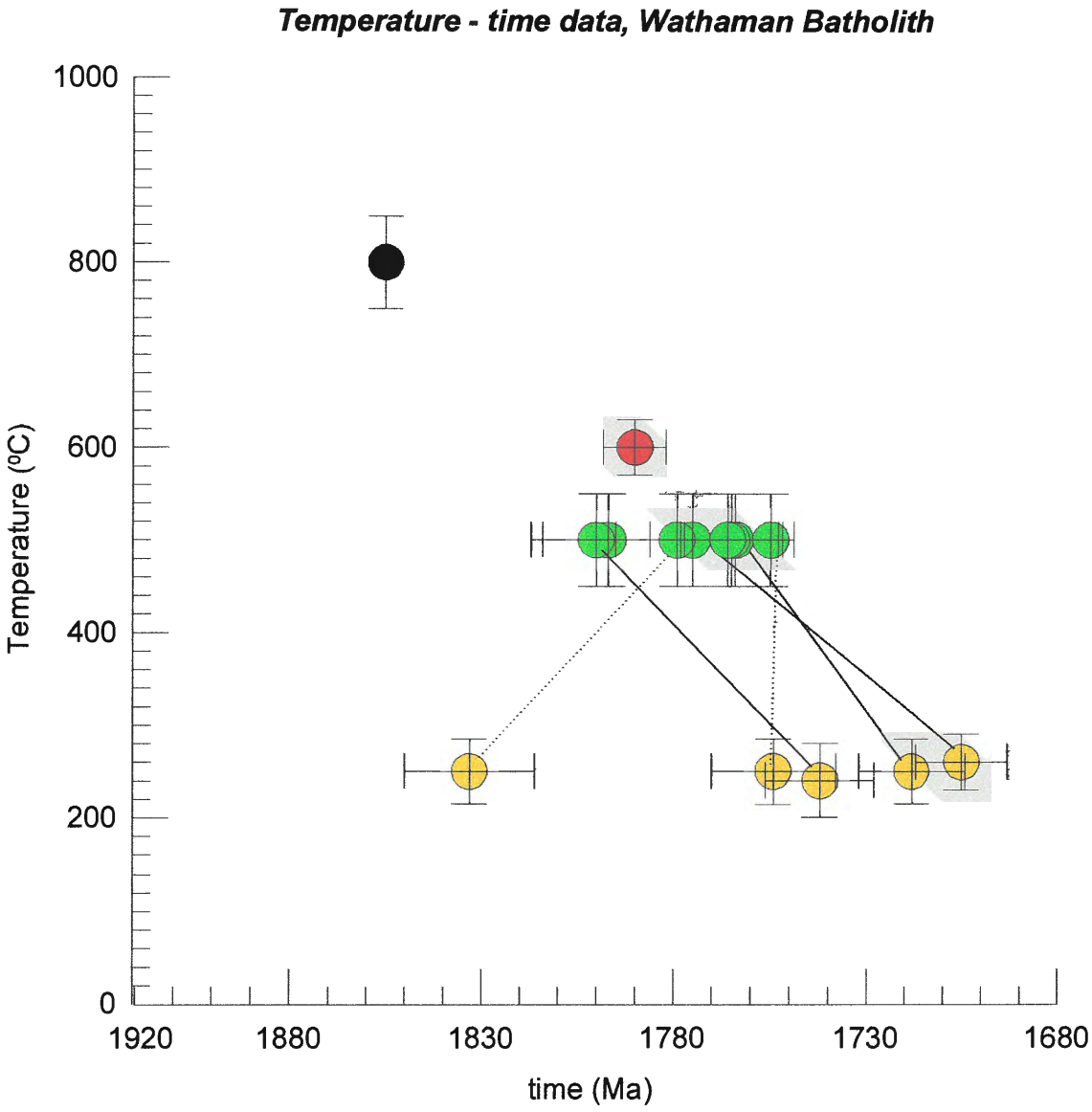

Figure 4.5: Temperature - time (T-t) data from the Wathaman Batholith. Lines connecting individual points indicate ages that were obtained from the same sample outcrop. ***Legend:*** *black,* U-Pb zircon; *red,* U-Pb titanite; *green,* $^{40}Ar/^{39}Ar$ hornblende; *orange,* $^{40}Ar/^{39}Ar$ K-feldspar; *dotted line,* relationship between ages uncertain; *solid line,* represents cooling.

MDD modeling was not conducted, a mean of the two temperatures was used. It is evident from the T-t graph that two of the three unmodelled K-feldspar ages are older than their respective hornblende ages, which may be attributed to excess argon or other analytical problems such as the presence of a high K phase like as sericite.

Based on calculation of the difference between the closure temperatures of hornblende and K-feldspar (for a cooling rate of 1 ^{0}C/My), and dividing the difference by the time between the hornblende age for sample 99-T63 and minimum K-feldspar age (sample 98-T223; in My), the Wathaman Batholith cooled to ~ 260 ^{0}C at a rate of 4.1 ± 2 ^{0}C/My.

Sample	*Zircon*	*Monazite*	*Titanite*	*Hornblende*	*Muscovite*	*K-feldspar*
98-T300A (diorite)	-----	-----	-----	1765 ± 13 Ma	-----	-----
98-T300B (granodiorite)	-----	-----	-----	1764 ± 15 Ma	-----	1718 ± 14 Ma
99-D76 (granodiorite)	-----	-----	-----	1755-1775 Ma	-----	1754 ± 16 Ma
98-D301 (granite)	-----	-----	1790 ± 8 Ma	-----	-----	-----
98-D300	1855 ± 1 Ma	-----	-----	-----	-----	-----
98-T223 (quartz – monzodiorite)	-----	-----	-----	1766 ± 13 Ma	-----	1708 ± 13 Ma
99-T62 (monzodiorite)	-----	-----	-----	(1770 ±10Ma)	-----	-----
99-T63 (granite)	-----	-----	-----	1779 ± 16 Ma	-----	1833 ± 17 Ma
99-D214 (metavolcanic)	-----	-----	-----	1797 ± 20 Ma	-----	-----
99-D103 (syenite)	-----	-----	-----	1800 ± 14 Ma	-----	1742 ± 13 Ma

Table 4.5: Samples from the Wathaman Batholith and their associated U-Pb and ^{40}Ar/^{39}Ar ages. Samples are listed from south (98-T300A) to north (98-D103) with increasing distance from the reworked intrusive contact with the La Ronge Domain. Ages enclosed in brackets are samples for which the calculated mean age was not used (see Chapter 3 for justification). Boxes with dashed lines indicate samples for which data are not available.

4.3.5 Peter Lake Domain

Zircon from sample 99-D89A, a gabbro from the Swan River complex of the Peter Lake Domain, yielded a discordia with an upper intercept age of 2562 ± 4 Ma and a lower intercept age of 1830 ± 12 Ma. The upper limit is interpreted to represent the

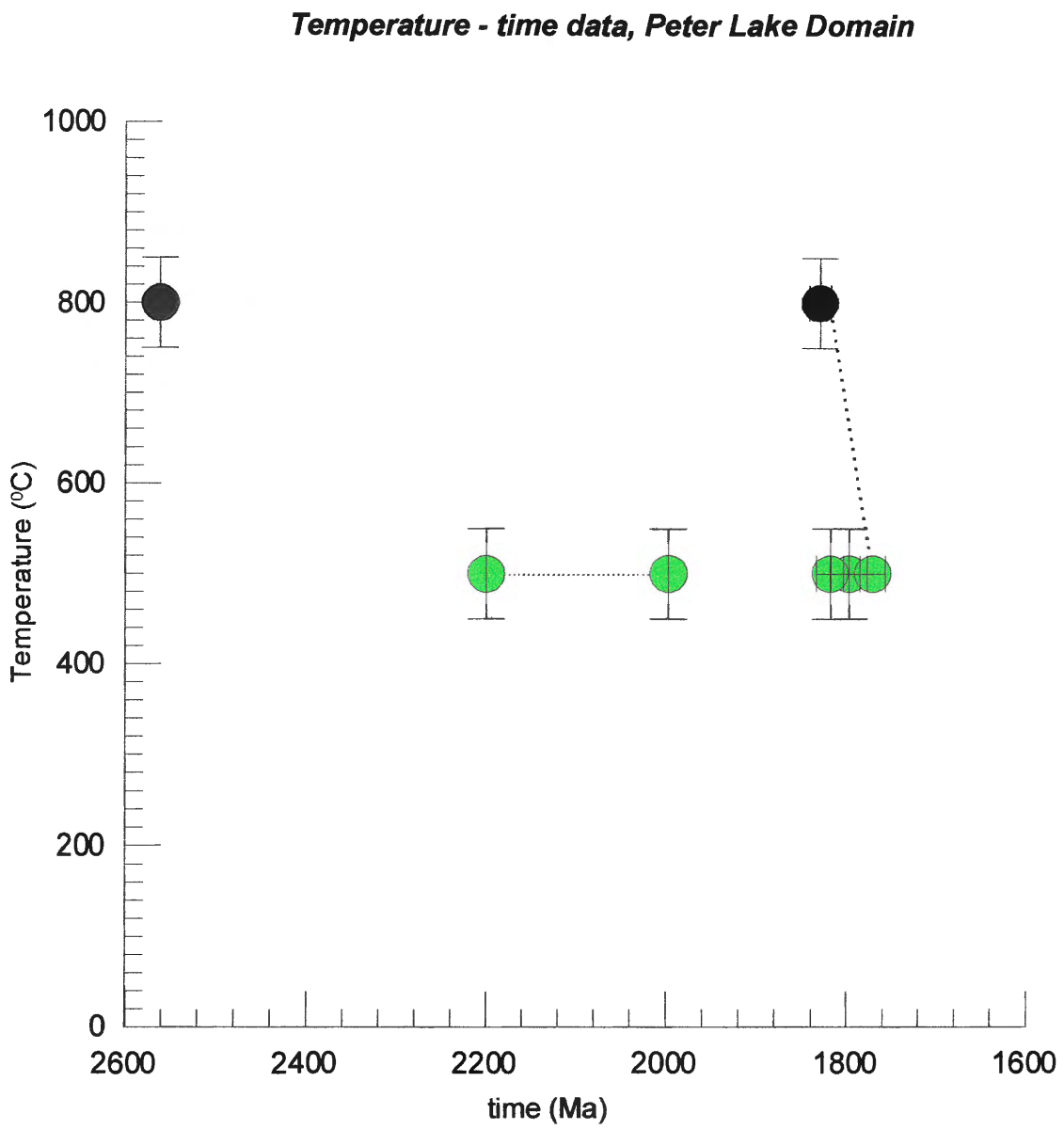

Figure 4.6: Temperature - time (T-t) data from the Archean Peter Lake Domain. Dotted line connecting individual points indicate ages that were obtained from the same sample. ***Legend:*** *black,* U-Pb zircon; *green,* $^{40}Ar/^{39}Ar$ hornblende. *Note*: due to the Archean zircon age, the horizontal scale here differs from those presented in previous sections of this chapter.

crystallization age, whereas the lower limit may represent a metamorphic growth age or Pb-loss during metamorphism (Table 4.6).

$^{40}Ar/^{39}Ar$ hornblende ages become progressively older from south to north, where the youngest ages were obtained from gabbroic samples from the Swan River Complex, which was metamorphosed at upper-mid amphibolite facies conditions. The oldest ages, ranging from 1997 – 2200 Ma, come from sample 99-D162, a migmatitic orthogneiss, and are interpreted as partially reset crystallization ages. Younger ages of 1818 ± 15 Ma and 1771 ± 14 Ma from the Swan River Complex are interpreted as post-peak metamorphic cooling ages. Due to the lack of thermochronological data for temperatures below 500 ^{0}C from the area, a cooling rate cannot be determined for the Peter Lake Domain. It is concluded, therefore, that the Swan River gabbros cooled through 500 ^{0}C at roughly the same time as the central and northern parts of the Wathaman Batholith.

Sample	*Zircon*	*Monazite*	*Titanite*	*Hornblende*	*Muscovite*	*K-feldspar*
99-D89A	1830±12 Ma 2562 ± 4 Ma	-----	-----	1771 ± 14 Ma	-----	-----
99-D87B	-----	-----	-----	1818 ± 15 Ma	-----	-----
99-D162 (migmatitic orthogneiss)	-----	-----	-----	1997-2200 Ma	-----	-----

Table 4.6: Samples from the Archean Peter Lake Domain and their associated U-Pb and $^{40}Ar/^{39}Ar$ ages. Samples are listed from south (99-D89A) to north (99-D162). Boxes with dashed lines indicate samples for which data are not available.

4.4 Discussion

Comparison of the ages in a distance vs. time graph (Figure 4.7) reveals a slight variation between monazite ages and hornblende ages, with noticeably young and old ages concentrated immediately above the Duck Lake Shear Zone (DLSZ) and in the Peter Lake Domain respectively. The distribution of $^{40}Ar/^{39}Ar$ hornblende data suggests, therefore, that cooling was heterogeneous both spatially and temporally across the Reindeer Zone following peak metamorphism at ca. 1820 – 1790 Ma.

The youngest U-Pb monazite and $^{40}Ar/^{39}Ar$ hornblende ages were obtained from samples taken from the La Ronge Domain just north of the Duck Lake Shear Zone. Monazite ages north of the shear zone are 13-23 My younger than those from the Levesque Bay supracrustal assemblage in the Kisseynew Domain (Figure 4.1).

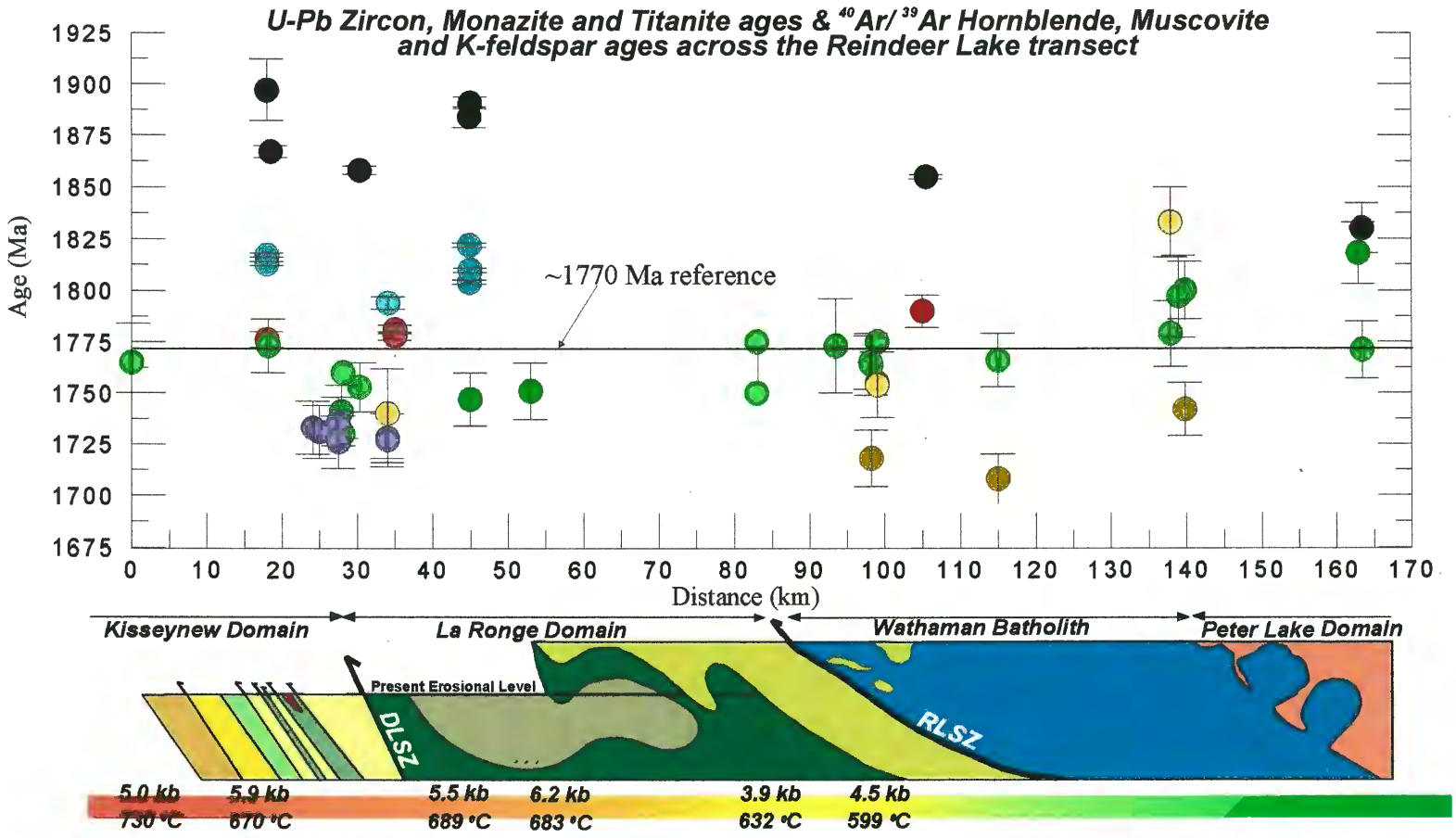

Figure 4.7: Comparison of the distribution of U-Pb and $^{40}Ar/^{39}Ar$ ages across the Reindeer Lake transect. U-Pb ages were obtained by Dr. David Corrigan at the GSC. Argon ages are those obtained in the current study. Line at ~ 1770 Ma represents time at which most hornblende grains across the zone cooled through 500 ^{0}C. ***Legend***: *black,* U-Pb zircon; *blue,* U-Pb monazite; *red,* U-Pb titanite; *green,* $^{40}Ar/^{39}Ar$ hornblende; *purple,* $^{40}Ar/^{39}Ar$ muscovite; *orange,* $^{40}Ar/^{39}Ar$ K-feldspar; *DLSZ*, Duck Lake Shear Zone; *RLSZ*, Reilly Lake Shear Zone.

Hornblende ages are, on average, 20 My younger than those from the northern La Ronge Domain proximal to the Wathaman Batholith and the Kisseynew Domain. The youngest ages correlate with the highest pressures and temperatures (5.5 kb – 689 ^{0}C and 6.2 kb - 683 ^{0}C; Chakungal, 1999) calculated for the La Ronge Domain, from samples proximal to the DLSZ. The correlation between the highest pressures and young U-Pb and $^{40}Ar/^{39}Ar$ ages in the southern La Ronge Domain suggests that rocks immediately north of the Duck Lake Shear Zone remained at ~ 700 ^{0}C for ~ 20 My longer than rocks in the north and in the Kisseynew Domain. Contemporaneous movement along the Reilly Lake Shear Zone may have been negligible, or may have taken place at temperatures too low to be recorded in the $^{40}Ar/^{39}Ar$ system, although data allows for a small thermal perturbation.

Preservation of early Paleoproterozoic ages in low-grade rocks to the north implies that intrusion of the batholith and subsequent peak metamorphism had little thermal effect on the Peter Lake Domain, possibly because it was not buried to depths comparable to those achieved by rocks in the south. Based on the pattern of radiometric ages on either side of the DLSZ, therefore, the structural level of the Reindeer Zone now exposed along Reindeer Lake appears to have been exhumed by a period of denudation that was dominated by erosion.

A comparison of the temperature – time curves (Figure 4.8) for the domains discussed above reveals that with the exception of the Glennie Domain, the Reindeer Zone as a whole cooled slowly (i.e. ≤ 10 ^{0}C/My). A calculated cooling rate of 14.3 ± 11 ^{0}C/My for the Glennie Domain suggests it cooled rapidly relative to domains in the north. However, due to the uncertainty associated with data from other studies, the cooling rate calculated for the Glennie Domain is questionable. On the other hand, based on the data acquired in this study, the Kisseynew and La Ronge Domains, and Wathaman Batholith cooled slowly at rates of 5.0 ± 3 ^{0}C/My, 4.6 ± 1 ^{0}C/My and 4.1 ± 2 ^{0}C/My respectively.

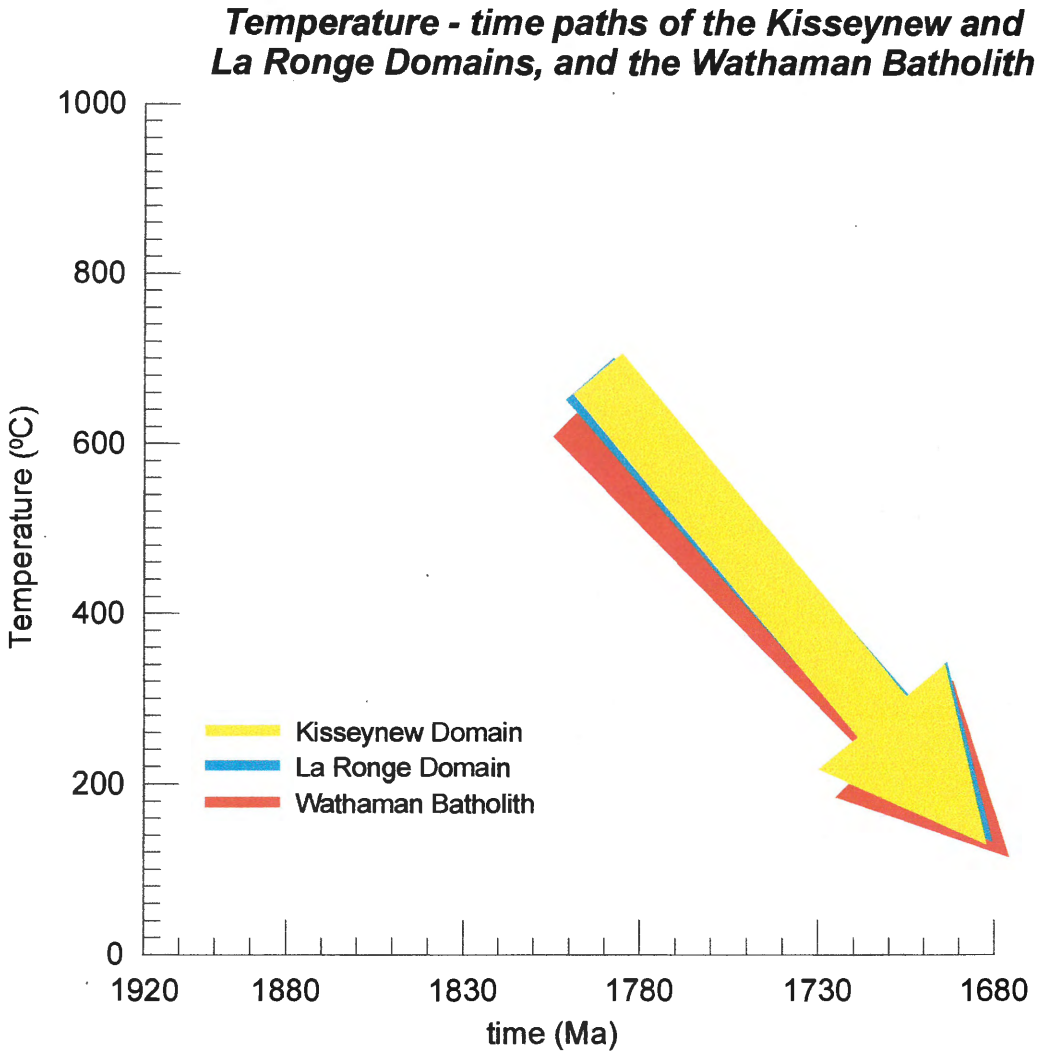

Figure 4.8: A comparison of the T-t paths of all the domains across the Reindeer Lake transect, for which cooling rates were calculated.

Chapter V - Discussion & Conclusions

A number of studies conducted over the last 25 years have provided geological, geochemical, geochronological and geophysical data to constrain the depositional, metamorphic and exhumation history of the Reindeer Zone. The following is an attempt to summarize all available data in the context of a tectonic model for the Trans-Hudson Orogen – Reindeer Zone. Data obtained from this study are combined with data obtained by Yang (1999), Heizler et al. (2000) and Durocher et al. (2001).

5.1 Tectonic Evolution of the THO – Reindeer Zone: A Summary

The THO – Reindeer Zone comprises a collage of deformed and metamorphosed juvenile terranes (Stauffer, 1984; Hoffman, 1988; Lewry et al., 1994; Lucas et al., 1996) that were trapped between the Archean Superior, Sask and Rae-Hearne cratons during continent – continent collision at ca. 1830 – 1800 Ma (Gordon et al., 1990; Machado, 1990). The Reindeer Zone in northern Manitoba and Saskatchewan comprises a complex collage of mantle-derived arc-related volcanic and plutonic rocks, coeval or derived volcanogenic clastic rocks and younger arkosic molasse assemblages. From south to north, the different lithotectonic blocks include the Flin Flon, Glennie, Kisseynew and La Ronge Domains that are bounded by the Churchill-Superior boundary zone in the southeast (Figure 5.1), and the Wollaston Domain in the north-northwest. Underlying the Flin Flon and Glennie Domains, and separated from them by a ductile mylonite zone, is the Archean Sask craton (e.g. Chiarenzelli et al., 1996).

Nd, Pb and Sr isotopic data from a variety of rock types, and major and trace element data from volcanic and plutonic rocks, suggest that much of the Reindeer Zone is allochthonous, having formed in an oceanic, subduction-related arc setting prior to collision of the Archean cratons (Lewry, 1981; Hoffman, 1988).

Formation of Mantle-Derived Crust (2100 Ma (?) – 1830 Ma)

Observations of rift-related mafic rocks along the margins of the Superior and Rae-Hearne cratons suggest that at ~ 2100 Ma, the cratons likely experienced continental rifting (Heaman & Corkery, 1996; Halls & Heaman, 1997), giving rise to the Manikewan ocean (Stauffer, 1984). Most of the Manikewan ocean floor was destroyed as a result of subduction during later arc development, though ca. 1900 Ma mid-ocean ridge basalts (MORB) and ocean island basalts (OIB), interpreted as remnants of the ocean floor, are

Major geological subdivisions of the THO - Reindeer Zone

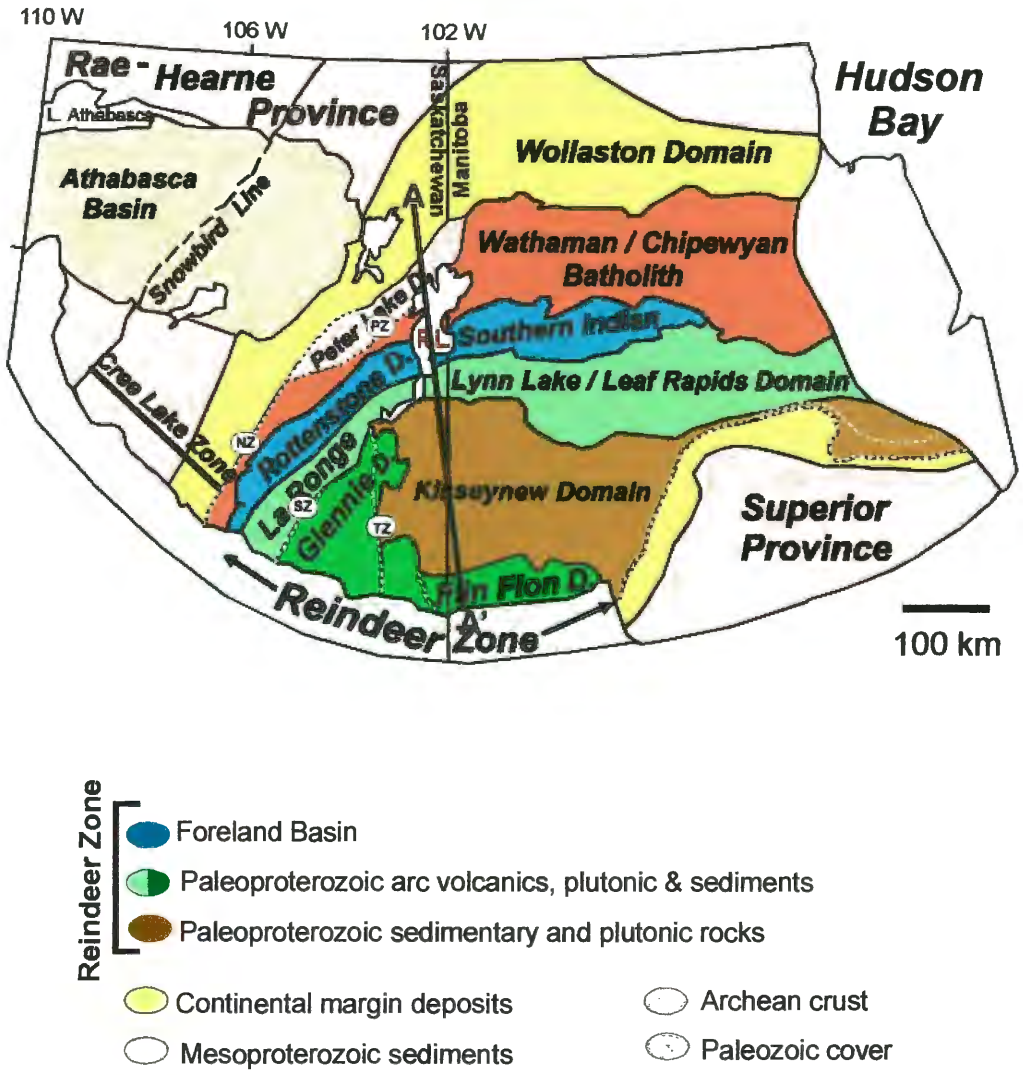

Figure 5.1: Generalized map of the Trans-Hudson Orogen as was presented in chapter 1. Heavy dashed lines indicate major ductile shear zones or brittle-ductile faults. **Legend:** *TZ*, Tabbernor Fault Zone; *SZ*, Stanley Fault Zone; *NZ & PZ*, Needle Falls and Parker Lake Shear Zones; *RL*, Reindeer Lake; *A-A'*, Geology depicted in the cross-sections presented in Figure 5.2 are representative of geology observed along this line. (Lewry et al., 1990)

Figure 5.2: Schematic cross-sections and plan view diagrams of the evolution of the Trans-Hudson orogen along line A-A' outlined in Figure 5.1. Cross-sections are modified from Lewry et al. (1981) incorporating information from Lucas et al. (1997), Corrigan et al. (1999, 2000) and Yang (1999). In panel H (1800-1780 Ma), during which time the orogen was undergoing post-orogenic erosion, the topography is exaggerated as a consequence of the difficulty in illustrating details of the geology of the orogen. An estimate of the present day erosional surface is outlined in panel H with a thick, solid black line. For a detailed explanation of individual panels, refer to text.

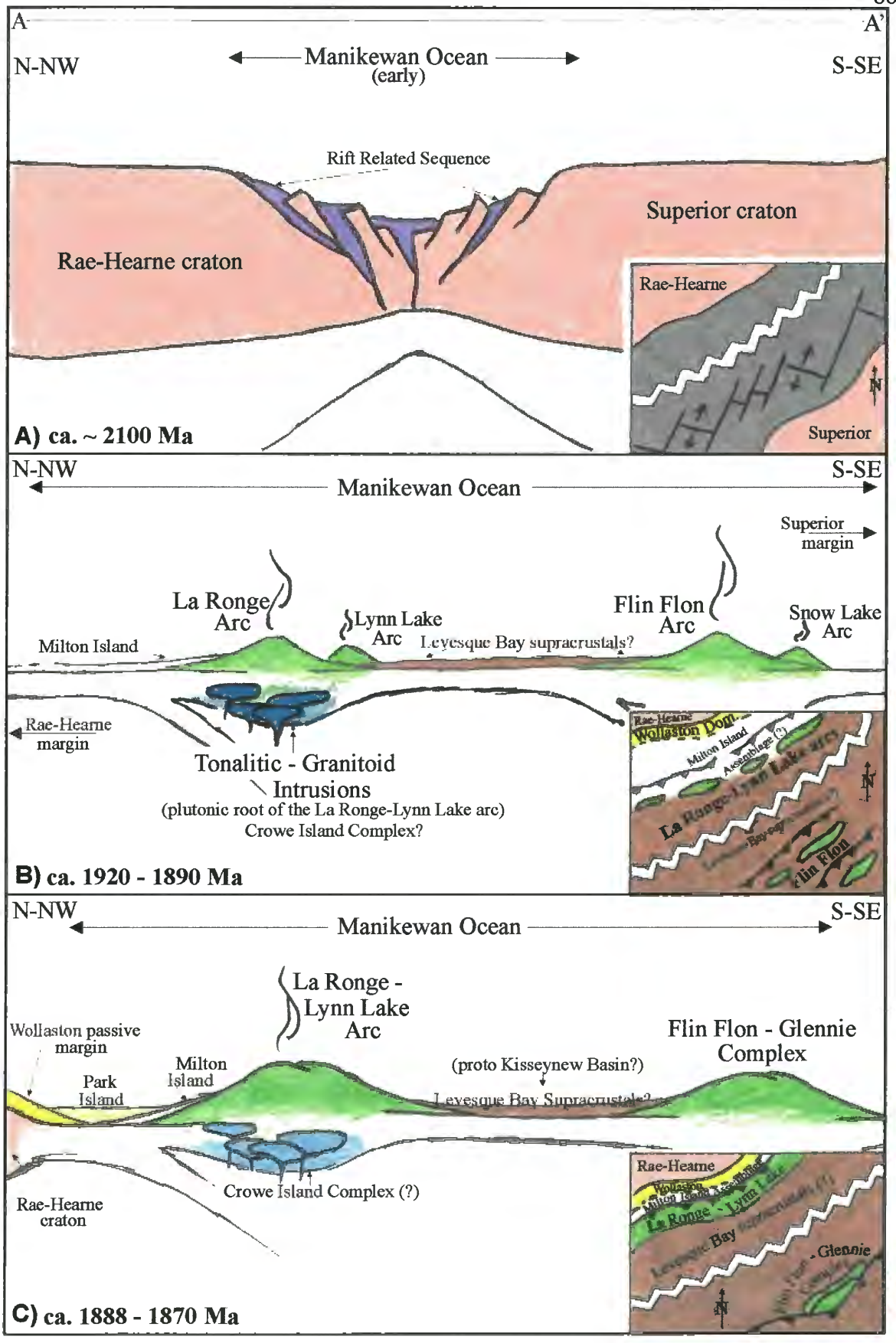
A
A'
N-NW
Manikewan Ocean
(early)
S-SE
Rift Related Sequence
Superior craton
Rae-Hearne craton
Rae-Hearne
Superior
A) ca. ~ 2100 Ma
N-NW
Manikewan Ocean
S-SE
Superior
margin
La Ronge
Arc
Lynn Lake
Arc
Flin Flon
Arc
Snow Lake
Arc
Milton Island
Levesque Bay supracrustals?
Rae-Hearne
margin
Tonalitic - Granitoid
Intrusions
(plutonic root of the La Ronge-Lynn Lake arc)
Crowe Island Complex?
Rae-Hearne
Wollaston Dom.
Milton Island
Assemblage (?)
La Ronge-Lynn Lake arc
Bayoo
Flin Flon
B) ca. 1920 - 1890 Ma
N-NW
Manikewan Ocean
S-SE
La Ronge -
Lynn Lake
Arc
Wollaston passive
margin
Park
Island
Milton
Island
(proto Kisseynew Basin?)
Levesque Bay Supracrustals?
Flin Flon - Glennie
Complex
Crowe Island Complex (?)
Rae-Hearne
craton
Rae-Hearne
La Ronge - Lynn Lake
Levesque Bay supracrustals (?)
Glennie
C) ca. 1888 - 1870 Ma

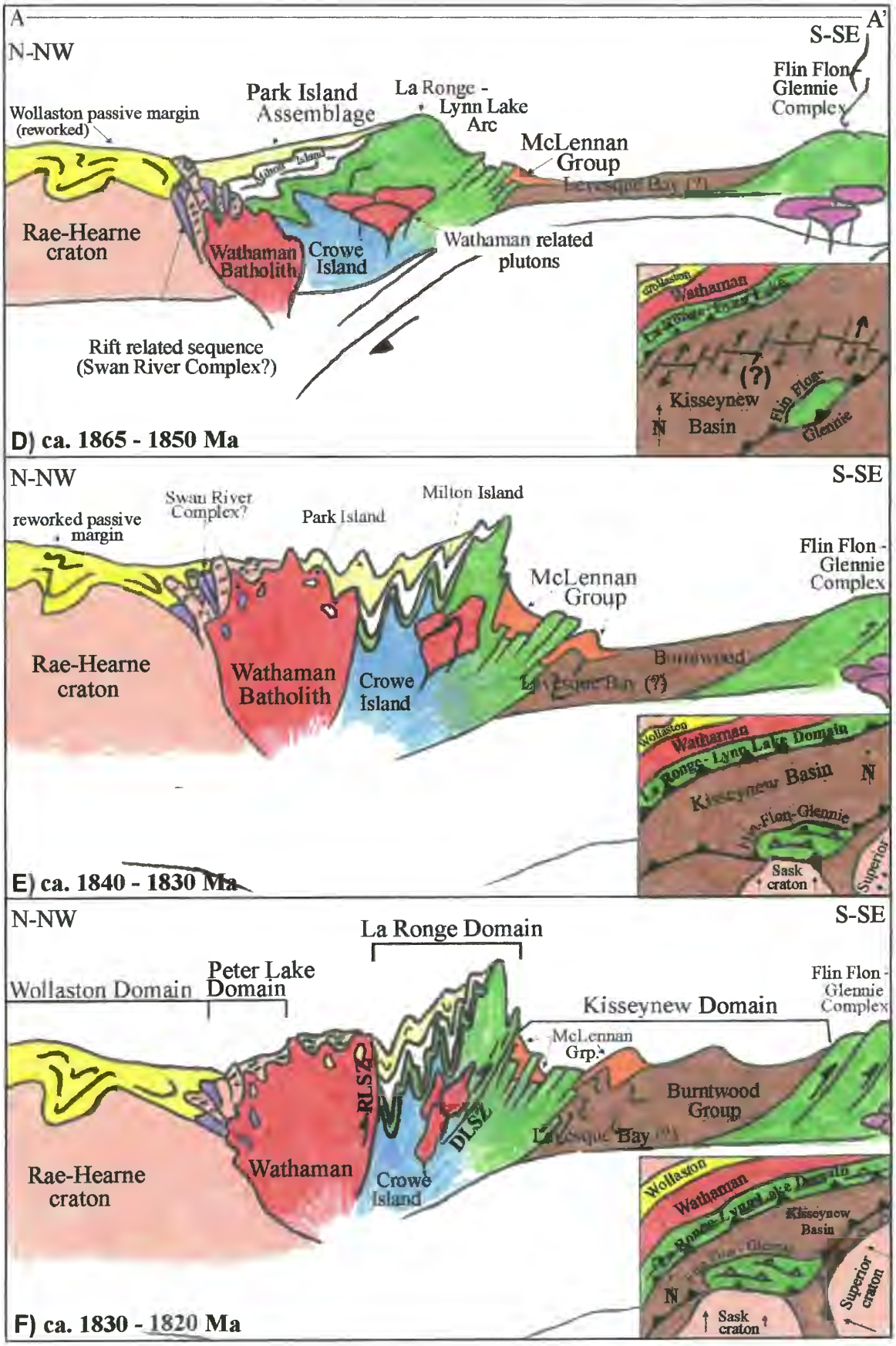
A
A'
N-NW
S-SE
Wollaston passive margin (reworked)
Park Island Assemblage
La Ronge - Lynn Lake Arc
McLennan Group
Flin Flon - Glennie Complex
Rae-Hearne craton
Wathaman Batholith
Crowe Island
Wathaman related plutons
Rift related sequence (Swan River Complex?)
Kisseynew Basin
D) ca. 1865 - 1850 Ma
reworked passive margin
Swan River Complex?
Park Island
Milton Island
McLennan Group
Flin Flon - Glennie Complex
Rae-Hearne craton
Wathaman Batholith
Crowe Island
Kisseynew Basin
Sask craton
Superior
E) ca. 1840 - 1830 Ma
La Ronge Domain
Wollaston Domain
Peter Lake Domain
Kisseynew Domain
Flin Flon - Glennie Complex
McLennan Grp.
Burntwood Group
RLSZ
DLSZ
Rae-Hearne craton
Wathaman
Crowe Island
Kisseynew Basin
Sask craton
Superior craton
F) ca. 1830 - 1820 Ma

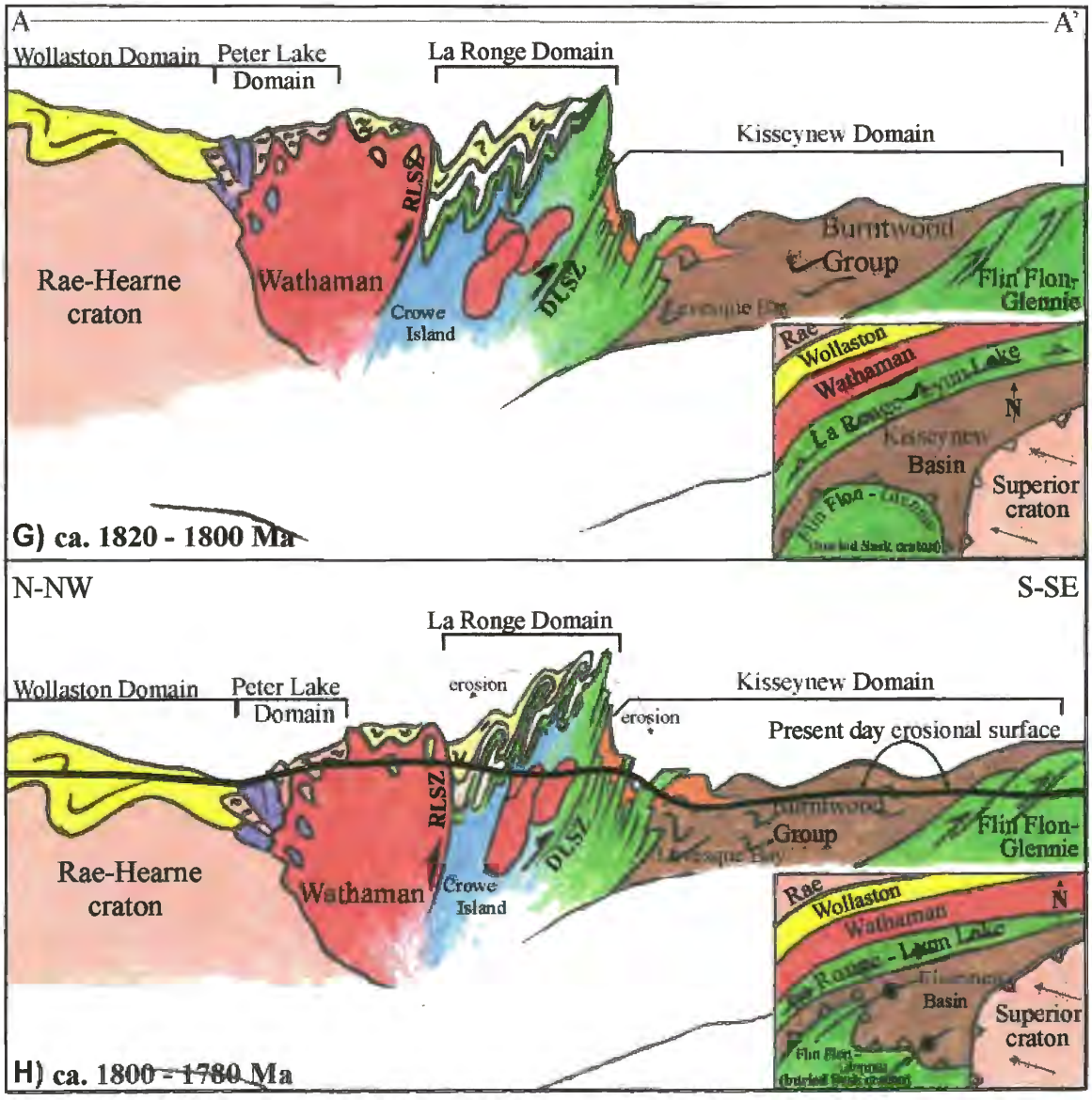
A
A'
Wollaston Domain
Peter Lake Domain
La Ronge Domain
Kisseynew Domain
RLSZ
DLSZ
Rae-Hearne craton
Wathaman
Crowe Island
Burntwood Group
Flin Flon-Glennie
Rae
Wollaston
Wathaman
La Ronge - Lynn Lake
N
Kisseynew Basin
Superior craton
G) ca. 1820 - 1800 Ma
N-NW
S-SE
La Ronge Domain
Wollaston Domain
Peter Lake Domain
erosion
erosion
Kisseynew Domain
Present day erosional surface
RLSZ
DLSZ
Rae-Hearne craton
Wathaman
Crowe Island
Burntwood Group
Flin Flon-Glennie
Rae
Wollaston
Wathaman
N
Basin
Superior craton
H) ca. 1800 - 1780 Ma

preserved in the Flin Flon Domain (Stern et al., 1995). A gabbro from the Swan River complex yielded a U-Pb zircon age of 2562 ± 4 Ma (Corrigan et al., in prep), suggesting that some or all of this complex may be related to a rift sequence of mafic rocks along the Hearne margin. If so, the crystallization age suggests that it may be part of a failed intra-continental rift sequence that formed some 400 My before opening of the Manikewan ocean.

Between ~ 1920 – 1890 Ma, subduction of early-formed Manikewanian oceanic crust commenced. The Flin Flon and La Ronge - Lynn Lake oceanic arcs developed outboard of the Superior and Rae-Hearne cratons respectively, within the ocean where related volcaniclastic assemblages were deposited (Figure 5.2b; Bickford et al., 1990; Gordon et al., 1990; Syme, 1990; Lucas et al., 1997). From 1890 – 1870 Ma the La Ronge - Lynn Lake arc segment in the north was accreted to the Rae-Hearne margin and was intruded by numerous tonalitic – granitoid plutons (Baldwin et al., 1987). Geochemical data for arc-related metavolcanic rocks of the La Ronge Domain indicate that they are enriched in the incompatible elements (Watters & Pearce, 1987), although Nd isotope signatures indicate that there was only a minor component of continental material involved in their formation (Syme et al., 1990; Thom et al., 1990). The basement of the La Ronge – Lynn Lake arc is, therefore, believed to have developed on early-formed juvenile arc segments. U-Pb zircon ages of 1892 ± 2 Ma and 1886 ± 4 Ma (Corrigan et al., 1999) from the Crowe Island complex, a compositionally heterogeneous, predominantly felsic, banded orthogneiss unit that is interpreted to represent the plutonic root of the La Ronge Domain, substantiates the interpretation based on the geochemical data. Deposition of the Levesque Bay supracrustal assemblage, and psammites and semipelites of the Milton Island assemblage were contemporaneous with volcanism in the La Ronge arc (Corrigan et al., 2001). Also occurring at this time was the formation of the Glennie, and Flin-Flon arcs to form the Flin Flon – Glennie complex (Figure 5.2c; Ansdell et al., 1996; Lucas et al., 1997).

On the basis of structural and geophysical asymmetries of major lithotectonic elements of the Reindeer Zone and the locations of the Wathaman continental margin magmatic arc and intrusive Rottenstone tonalite-migmatite complex (Lewry et al., 1981; Lewry et al., 1994; Stauffer, 1984), the subduction polarity beneath the La Ronge - Lynn

Lake arc at ca. 1888 - 1875 Ma was believed to have been towards the northwest, beneath the Rae-Hearne craton. The Wathaman Batholith is known to have intruded the Rae-Hearne margin and was initially interpreted to have been emplaced concomitantly with magmatism in the La Ronge arc (Lewry et al., 1981). U-Pb zircon data, however, suggest it was emplaced at ca. 1865 – 1850 Ma (Ray & Wanless, 1980; Weber et al., 1975), some 10 – 20 My after magmatism in the La Ronge arc, suggesting that the two were not coeval.

Recent mapping by Corrigan et al. (1998, 1999) has shown that along the Reindeer Lake transect, the "intrusive" Rottenstone Domain is not an intrusive complex, but rather, comprises a large component of supracrustal rocks, and volcanic rocks that appear similar in age and composition to the Central Metavolcanic Belt (CMB) of the La Ronge Domain. Spatially related to the volcanic rocks are penecontemporaneous, compositionally heterogeneous orthogneisses that are interpreted as the plutonic root of the La Ronge arc. The supracrustal rocks that comprise much of the Rottenstone Domain were deposited contemporaneously with arc magmatism and were later migmatized during emplacement of the Wathaman Batholith and exhumed during post-collisional convergence (Figure 5.2d, e).

Yang (1999) noted that the protoliths of the amphibolitic gneisses in the MacLean Lake belt south of the La Ronge Domain (analogous to the Levesque Bay supracrustal assemblage of Corrigan et al. (1998, 1999)) are chemically more primitive than magmas of the CMB, possibly indicating sea-floor spreading. Since the amphibolite gneisses bear similarities to metavolcanic rocks within the Burntwood Group of the Kisseynew Domain, which is interpreted to have formed in a back-arc basin, Yang (1999) suggested that the MacLean Lake belt may also represent a back-arc basin behind the CMB of the La Ronge Domain. The present structural configuration of the Reindeer Zone, therefore, may reflect later complex accretion and collision (Lucas et al., 1997). Yang (1999) suggested that over time, earlier southeast-directed subduction "dragged" continental rocks of the Rae-Hearne towards the subduction front. It seems more likely, however, that subduction of sialic crust would have been driven by the pull of cold, subducting oceanic lithosphere. If so, attempted subduction of buoyant sialic crust might have clogged the subduction zone and resulted in a subduction polarity reversal to the

northwest. The 10 My gap between La Ronge volcanism (≥ 1875 Ma) and continental arc plutonism (≤ 1865 Ma) may represent the period of re-establishment of the subduction zone with a northwest-directed polarity.

From 1870 – 1840 Ma, plutonism, minor volcanism, and sedimentation occurred in successor arcs that developed on the Flin Flon-Glennie complex (Figure 5.2e; Ansdell et al., 1995; Lucas et al., 1997). By 1865 Ma the La Ronge-Lynn Lake arc was accreted to the Rae-Hearne margin and the Park Island assemblage was deposited on its northern flank. To the south, detritus from the La Ronge-Lynn Lake arc and surrounding arc complexes was deposited as turbidites in the Kisseynew back-arc basin (Ansdell et al., 1995; Zwanzig, 1990).

During the interval 1865 – 1850 Ma, the Wathaman Batholith was emplaced along the suture between the Rae-Hearne craton and the La Ronge Domain (Figure 5.2d; Lewry et al., 1981; Lewry, 1981). In the main body of the La Ronge Domain, satellite plutons were emplaced at ~ ca. 1855 Ma. Based on geochemical data, the Wathaman Batholith and its satellite plutons were derived from the mixing of three end members. In the La Ronge Domain, magmas were derived from depleted, subduction zone affected mantle, whereas the main body of the Wathaman Batholith was derived from predominantly enriched mantle material (Chauvel et al., 1987; Hagner et al., 1989; MacHattie et al., 2001). Geochemical evidence for continental contamination is seen only in the north, proximal to the Rae-Hearne margin (MacHattie et al., 2001).

Since evidence for a substantial Archean component is lacking in the geochemical data for the plutons that intruded the CMB of the La Ronge Domain, Yang (1999) suggested that at ~ 1865 – 1855 Ma, the La Ronge arc might have been tectonically and/or geographically separated from the Archean Saskatchewan and Rae-Hearne cratons. If this was the case, then the Wathaman Batholith should not contain enclaves of the La Ronge Domain. Based on field mapping done by Corrigan et al. (1999, 2000), however, the southern margin of the batholith contains enclaves of metasediments and migmatitic orthogneisses that are interpreted to be from the Park Island assemblage and Crowe Island complex respectively. Hence, field observations suggest the La Ronge arc was accreted to the Rae-Hearne margin prior to 1865 Ma, when the Wathaman Batholith was emplaced.

Syn-Collisional History of the Reindeer Zone (1840 – 1780 Ma)

The present day configuration of the Reindeer Zone is probably the result of a complex post-collisional history during the interval ca. 1840 – 1780 Ma (Lucas et al., 1997). At this time, continued convergence throughout the zone was characterized by large-scale thrust imbrication (Bickford et al., 1990; Lewry et al., 1994). In the southeast, collision of the Archean Sask craton with the Flin Flon-Glennie complex resulted in thrusting of the Flin Flon-Glennie complex onto the now buried Sask craton that was approaching from the southwest (inset in Figure 5.2f). In the north-western Reindeer Zone, contemporaneous with collision and southwest-directed thrusting of the Flin Flon-Glennie complex, the Reilly Lake and Duck Lake Shear Zones developed at the structural base of the Wathaman Batholith and CMB respectively, thrusting rocks in the northwest onto rocks in the southeast (Figure 5.2f; Lewry et al., 1990; Yang, 1999). Regional deformation and shearing led to the development of a series of fault-controlled basins into which detritus from the elevated La Ronge Domain was deposited to form the McLennan Group arkoses. As post-collisional convergence continued, rocks of the Reindeer Zone were buried, reaching peak metamorphic conditions of ~ 730 ± 12 ^{0}C and 5.0 ± 0.2 kbar in the Kisseynew Domain (Chakungal, 1999) by ca. 1820 – 1790 Ma (Figure 5.2g; Gordon, 1989; Kyser & Stauffer, 1995).

Following peak metamorphism, continued migration of the Superior craton to the north-northwest was characterized by the development of high angle faults in the southwestern Reindeer Zone, along which deformation was mainly brittle (Figure 5.2h). These include the northeast-trending dextral Needle Falls Shear Zone, which separates the reworked marginal marine sediments of the Rae-Hearne craton from the Wathaman Batholith, and the north-south trending sinistral Tabbernor Fault. In the transect exposed along Reindeer Lake, however, post-collisional deformation entailed the development of large wavelength upright folds with axial traces trending north - northwest. Within this segment of the zone, there is no evidence of late brittle faults.

5.2 Post-Collisional History Based on the Thermochronological Data Set

The current thermochronological data set suggests that following peak metamorphism at ca. 1820 – 1790 Ma, exhumation was spatially and temporally heterogeneous across the Reindeer Zone. With the exception of data collected

immediately north of the DLSZ and in the Peter Lake Domain, $^{40}Ar/^{39}Ar$ hornblende ages suggest that as a whole, the Reindeer Zone along Reindeer Lake cooled through 500 ^{0}C by ~ 1770 Ma (Figure 5.3b; i.e. during the time frame depicted in Figure 5.2g). Based on the distribution of hornblende ages on either side of the DLSZ, at ~ 1770 Ma it appears that erosion was the main mechanism by which the Reindeer Zone exposed along Reindeer Lake was exhumed.

Preservation of the youngest hornblende ages within the DLSZ (~ 1740 Ma) indicates that rocks within it cooled through 500 ^{0}C approximately 30 My later than surrounding rocks (Figure 5.3b). The presence of syn-peak metamorphic textures along the DLSZ implies movement along the shear zone occurred during peak metamorphism, not after. Therefore, young $^{40}Ar/^{39}Ar$ ages in the DLSZ may be attributed to i) the diffusive loss of argon by the presence of hydrothermal fluids in the structure; ii) to cooling of the crust by fluid flow along the shear zone; or iii) elevated temperatures across the DLSZ during and immediately following peak metamorphism (Figure 5.3).

Models of the thermal evolution of thickened orogenic crust (see section 1.2; Jamieson et al., 1998; 2002) illustrate deflected crustal isotherms in the vicinity of crustal-scale thrust zones. Figure 5.3 illustrates an interpretation for data collected along the Reindeer Lake transect, in which a region of elevated temperature is associated with the DLSZ at the time of peak metamorphism (Figure 5.3a). Following peak metamorphism, rocks in the hangingwall of the shear zone probably cooled through 500 ^{0}C later than rocks to the north and south of it (Figure 5.3b,c). The data obtained in this study are consistent with this interpretation, suggesting hornblende grains in the hanging wall of the DLSZ cooled through 500 ^{0}C by ~ 1740 Ma, 30 My later than rocks to the north and south of it. Furthermore, muscovite-bearing rocks at the same structural level as hornblende bearing rocks would be expected to preserve $^{40}Ar/^{39}Ar$ ages younger than hornblende ages. In the current study, preservation of muscovite ages averaging ~ 1730 Ma concurs with this interpretation.

Preservation of the oldest ages in the Archean Peter Lake Domain, and their correlation with the lowest metamorphic grade observed across the transect, suggests the Peter Lake Domain escaped high-grade metamorphism, thus retaining evidence of Archean ages.

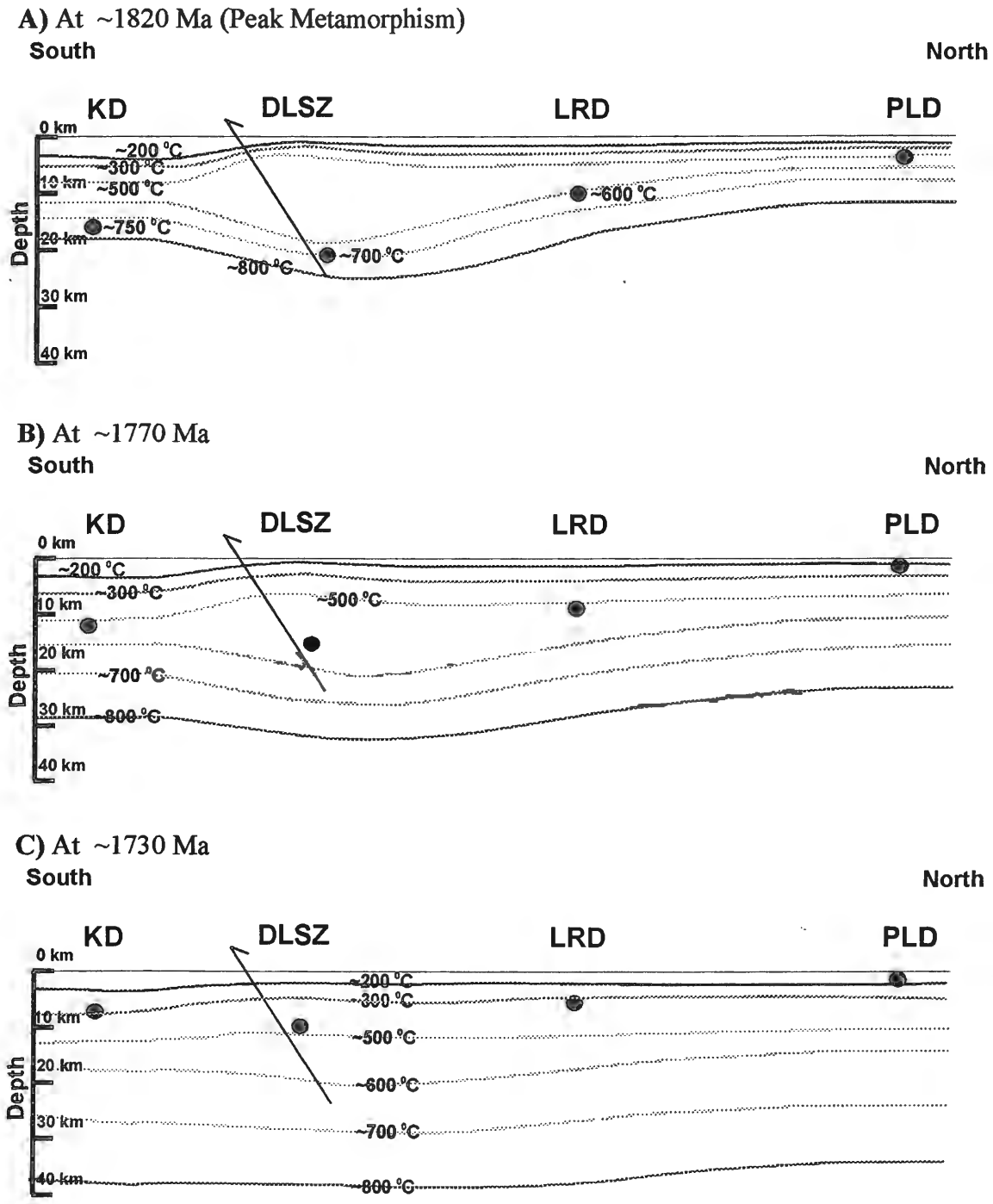

Figure 5.3: A schematic diagram illustrating the thermal evolution of the Trans-Hudson Orogen - Reindeer Zone along the Reindeer Lake transect. Isotherms about the shear zone have been drawn based on the thermal model of Jamieson et al. 2002 a) Thermal structure of the orogen during peak metamorphism. Points have been plotted based on P-T data calculated by Chakungal (1999); b) Thermal structure of the orogen at 1770 Ma, when most hornblende grains across the orogen passed through ~ 500 °C; c) Thermal structure of the orogen at 1730 Ma, when the orogen cooled through ~ 350 °C, the closure temperature of muscovite.

Cooling rates calculated from the $^{40}Ar/^{39}Ar$ data suggest the Reindeer Zone along the Reindeer Lake transect cooled slowly at an average rate of $\leq 5.0\ ^{0}C/My$ (Figure 4.8). Cooling rates calculated by Heizler et al. (2000), however, differ from the findings of this project. In their orogen-wide study, south of the current study area, muscovites from the eastern Reindeer Zone produced ages that were concordant with hornblende ages (Figure 5.4) implying the southern part of the orogen cooled rapidly at a rate of $\sim 20\ ^{0}C/My$. They noted that the break between differential cooling rates in the orogen occurs west of the Tabbernor fault where muscovite ages are consistently 40 My younger than hornblende ages thus implying slower cooling rates. This difference is similar to the differences observed between muscovite and hornblende ages in the current study, which is situated east of the Tabbernor fault zone.

Hornblende and muscovite cooling ages obtained in this study are older than those obtained west of the Tabbernor fault zone in the La Ronge and Glennie Domains (Figure 5.4; Yang, 1999; Durocher et al., 2001). Preservation of young ages within the La Ronge, Kisseynew and Glennie Domains west of the Tabbernor fault zone suggests that rocks west of it were buried and maintained at elevated temperatures longer than rocks exposed along the Reindeer Lake transect. Mapping done by Corrigan et al. (1999) across the northern tip of the fault in the southwest part of Reindeer Lake, however, indicate lithologies of the La Ronge and Kisseynew Domains are traceable across the fault with no noticeable variations in metamorphic grade. Thus, the contrast between cooling ages obtained in the current study and previous work may be attributed to the location of the Yang (1999) and Durocher et al. (2001) studies, which are situated proximal to the Stanley (SZ) and Tabbernor fault zones (TZ) respectively (Figure 5.4). Further investigation into the thermal history of the interior of the domains may provide some insights as to whether the interior of the La Ronge and Glennie Domains west of the TZ and SZ cooled later than in the Reindeer Lake transect.

5.3 Conclusions

Based on P-T data, U-Pb monazite and titanite ages, and $^{40}Ar/^{39}Ar$ hornblende, muscovite and K-feldspar ages, the northwestern Reindeer Zone exposed along the shores and islands of Reindeer Lake, Saskatchewan, experienced spatially heterogeneous post-peak metamorphic cooling about the Duck Lake shear zone. Based on the distribution of

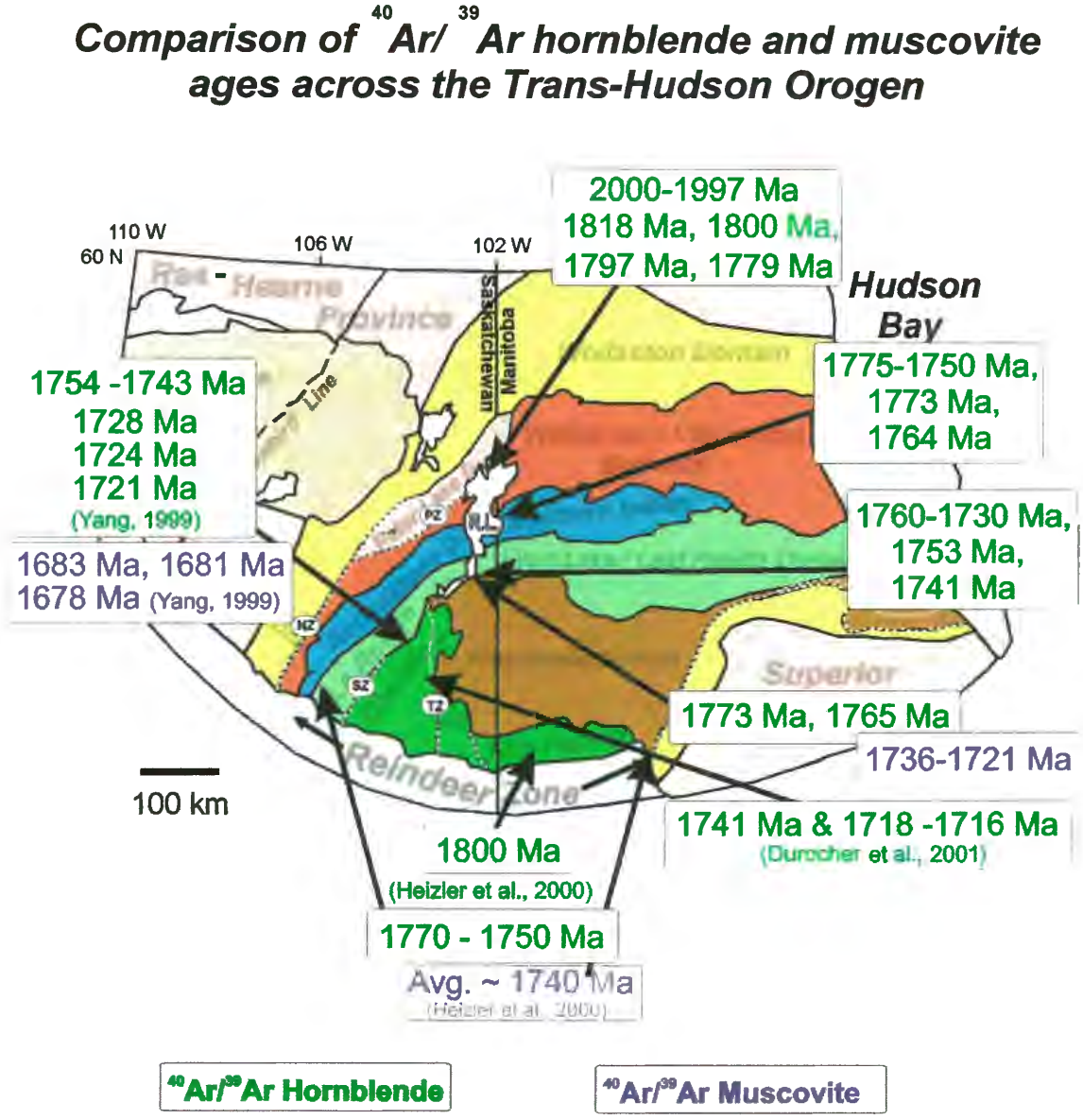

Figure 5.4: Distribution of $^{40}Ar/^{39}Ar$ hornblende and muscovite ages across the Trans-Hudson Orogen. Ages without reference to source are ages that were obtained in the current study. Muscovite ages from Yang (1999) are from the western extent of the McLennan group arkoses, on the west side of the Tabbernor fault zone (TZ).

comparatively uniform ages on either side of the shear zone, and calculation of slow cooling rates across the zone, it is estimated that exhumation of the Reindeer Zone was predominantly controlled by post-tectonic erosion. Preservation of young ages immediately above the shear zone suggest that during and immediately following peak metamorphism, rocks in the footwall of the DLSZ were maintained at temperatures $\geq 500\ ^{0}C$ as a consequence of the configuration of isotherms during orogenesis, until ~ 1740 Ma.

1) One $^{40}Ar/^{39}Ar$ hornblende age obtained from the northern reaches of the Glennie Domain in the current study suggests it cooled through 500 ^{0}C by ~ 1775 Ma. Due to the lack of radiometric data fore the area, however, the T-t path followed by Glennie Domain rocks along the Reindeer Lake transect remains poorly constrained.
2) In the Kisseynew Domain, where metamorphic grade across the transect is highest (transitional granulite facies), two $^{40}Ar/^{39}Ar$ hornblende ages indicate the domain cooled through 500 ^{0}C by ~ 1765Ma. Four muscovite ages indicate the northern Kisseynew Domain cooled through 350 ^{0}C by ~ 1726 Ma. Cooling rates calculated from the data suggest the Kisseynew Domain cooled at a rate of 5.0 ± 3 $^{0}C/My$.
3) $^{40}Ar/^{39}Ar$ hornblende ages from the La Ronge Domain vary from south to north (Figure 4.7). Hornblende grains in the south, above (north of) the Duck Lake shear zone where metamorphic grade in the domain is highest (upper amphibolite facies), preserve an average mean age of ~ 1745 Ma. In the north, proximal to the Wathaman Batholith where metamorphic grade is upper greenschist facies, hornblende ages are ~ 20 My older suggesting the northern La Ronge Domain cooled through 500 ^{0}C by ~ 1760 Ma. Muscovite ages indicate the domain cooled through 350 ^{0}C by ~ 1727 Ma. Cooling rates calculated from the data suggest that as a whole, the La Ronge Domain cooled at a rate of 4.6 ± 1 $^{0}C/My$.
4) Within the Wathaman Batholith, hornblende grains preserve an average mean $^{40}Ar/^{39}Ar$ age of ~ 1765 Ma. K-feldspar data suggest the batholith cooled through 260 ^{0}C by 1695 Ma (Figure 4.7). Available U-Pb and $^{40}Ar/^{39}Ar$ data suggest the batholith cooled at a rate of ~ 4.1 ± 2 $^{0}C/My$.

5) Much of the Reindeer Zone along Reindeer Lake, Saskatchewan cooled through 500 ^{0}C by ~ 1770 Ma. Rocks within the footwall of the DLSZ preserve the youngest ages as a consequence of differential cooling through 500 ^{0}C, as they were maintained at temperatures $\geq$ 500 ^{0}C until ~ 1740 Ma. The oldest ages are preserved in the Peter Lake Domain because it was not buried to the same depths as rocks in the south.
6) Slow cooling rates averaging 5.0 ^{0}C/My across the Reindeer Lake transect suggest the main mechanism by which much of the Reindeer Zone was exhumed was by the process of erosion.

5.4 Recommendations for Further Work

The current project has brought to light new data concerning the thermal evolution of the Trans-Hudson Orogen – Reindeer Zone. It has also brought to light one question concerning the evolution of the orogen.

1) Thermochronological studies of the Reindeer Zone have been conducted in the Glennie and La Ronge Domains west of the Tabbernor fault. A detailed thermochronological study of rocks along a southeast – northwest transect across domain boundaries, including the Glennie, La Ronge and Rottenstone domains, would provide constraints on the exhumation and cooling rates of rocks bounded by the Needle Falls shear zone and Tabbernor fault.
2) Based on the current thermochronological data set, the eastern part of the THO cooled rapidly. However, findings of this study and several other workers suggest that much of the THO cooled slowly (i.e. < 5 ^{0}C), just as many other well characterized Proterozoic orogens. A detailed thermochronological study of the eastern segment of the THO may provide the clues needed to resolve why it cooled faster.

APPENDIX A

Sample Descriptions
(Includes outcrop and thin-section descriptions)

Sample Descriptions

The following sample descriptions are presented in order of their position along the study transect, from south (core of the orogen) to north (margin of the orogen).

CXA98 – D42:

Domain: Glennie Domain.
Outcrop: I did not study this outcrop. Diorite sample was obtained from David Corrigan of the Geological Survey of Canada in Ottawa.
Thin – Section: Deformed, recrystallized amphibole + biotite + plagioclase + quartz ± minor K-feldspar (?) + titanite diorite - monzodiorite. Grain boundaries of quartz and plagioclase subgrains are highly sutured. In cross nichols, individual grains are characterized by an undulose or "sweeping" extinction. Sericitic patches characterize plagioclase grains. Amphibole grains define a fabric and are intensely intergrown with brown biotite. Grain margins appear to have been recrystallized to a fine grained aggregate.
Dated Phase(s): amphibole (150 – 250 μ)

Photo A-1:

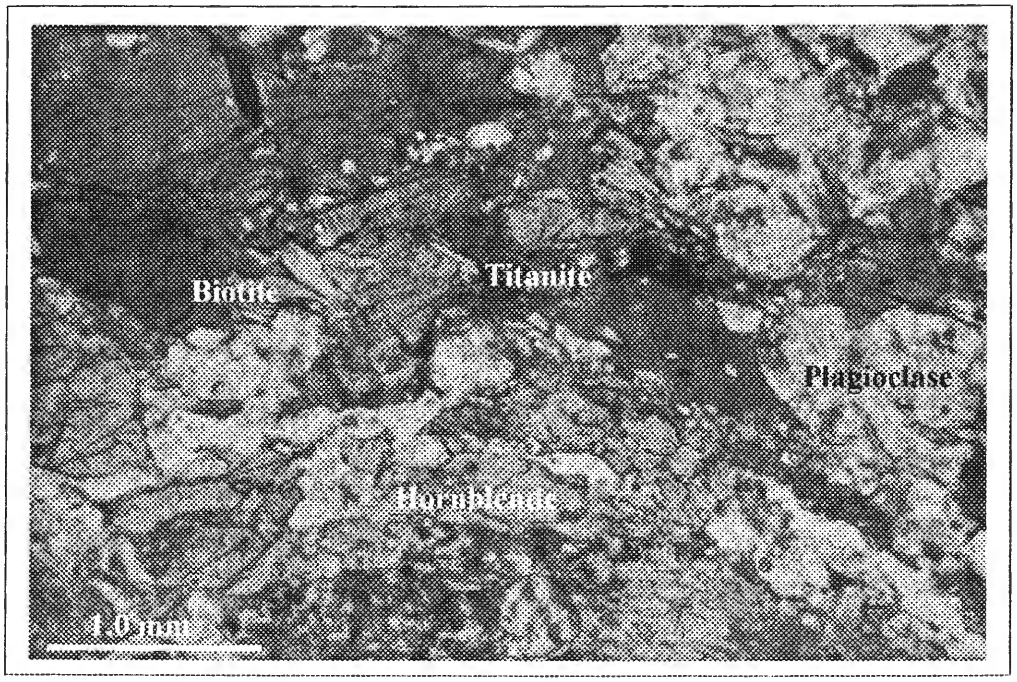

PPL (plane polarized light)

CXA98 – L48:

Domain: Kisseynew Domain – Burntwood Group.
Outcrop: I did not study this outcrop. Granodiorite was obtained from David Corrigan of the Geological Survey of Canada in Ottawa.
Thin – Section: Rock has experienced some cataclasis and minor recrystallization (?). Quartz, plagioclase and K-feldspar grains are variable in size, where quartz is commonly characterized by undulose extinction in cross nichols, and K-feldspars are finely perthitic. Plagioclase grains have been altered to sericite predominantly along grain margins. Amphibole grains are anhedral and intergrown with biotite. Amphiboles also vary in size, where larger grains often contain inclusions of quartz + feldspar + biotite.
Dated Phase(s): amphibole (200 μ – 3 mm)

Photo A-2:

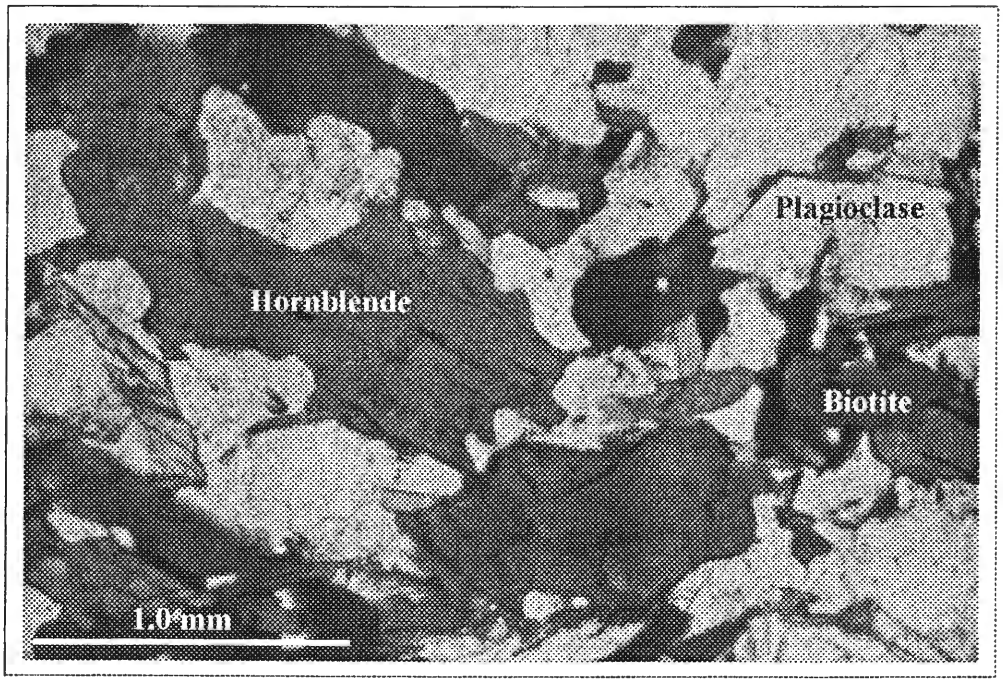

PPL (plane polarized light)

CXA98 – D12:

Domain: Kisseynew Domain – Levesque Bay Supracrustal Assemblage.
Outcrop: Garnet amphibolite with plagioclase porphyroblasts, where some plagioclase porphyroblasts are cored by garnets. Intruded by, and foliated with a 1896 Ma leucotonalite. Locally, mafic layers contain layers rich in graphite and appear rusty in outcrop. Mafic rocks have been interpreted to represent the Levesque Bay volcanics.
Thin – Section: Granoblastic and altered intensely. Beige-brown amphibole grains are subhedral – euhedral. Margins of amphibole grains appear to be replaced by green biotite and chlorite, but for the most part, grains are free of inclusions. Minute fragments of garnet grains are present, where the original grain has since been replaced by plagioclase and biotite. Both quartz and plagioclase grains display undulose extinction in cross nichols where grain boundaries are characterized by a fine-grained aggregate (sericite?).
Dated Phase(s): amphibole (200 μ - 1 mm)

Photo A-3:

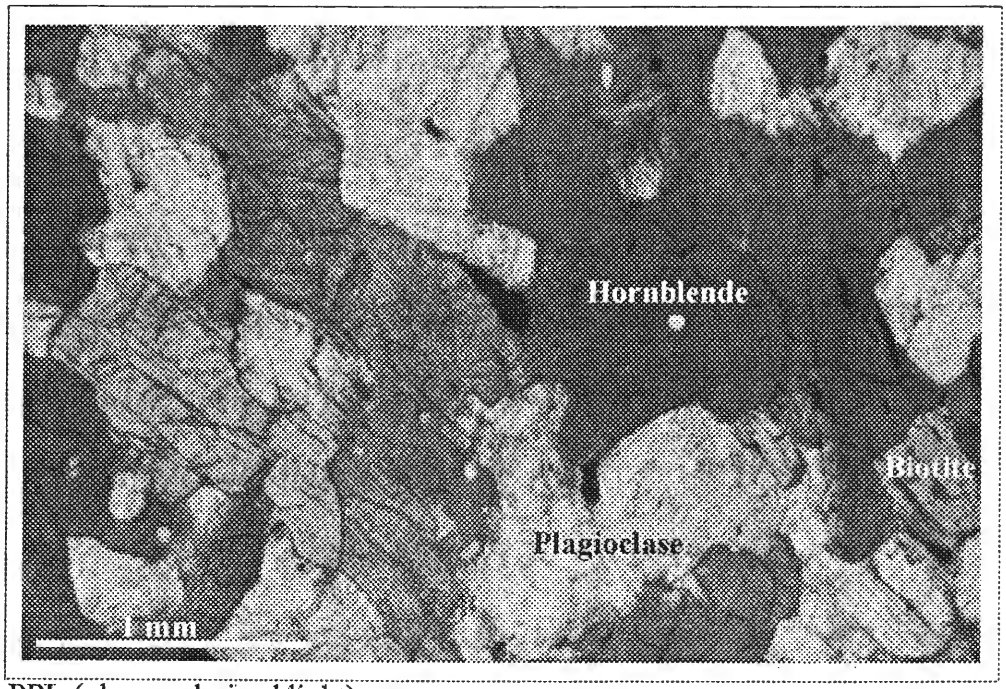

PPL (plane polarized light)

CXA97 – D222:

Domain: Kisseynew Domain – McLennan Group arkoses
Outcrop: Medium grained, pink weathering biotite + magnetite + fibrolite + muscovite psammite locally containing calc-silicate pods. The outcrop is located just south of the Duck Lake shear zone and is variably foliated. Locally outcrop is cross cut by amphibolite dykes that have been transposed to the foliation.
Thin – Section: Coarse grained and recrystallized. Large K-feldspar, plagioclase and quartz grains are separated by a zone of subgrains. Minor myrmekite is present and locally grain boundaries of quartz are moderately sutured. K-feldspar grains are locally intergrown with intensely sericitized plagioclase. Biotite grains are subhedral – euhedral and intergrown with muscovite. Muscovite grain boundaries are poorly defined, variable in size (0.5 – 4.0 mm), anhedral and rich with inclusions of K-feldspar and quartz. Quartz grains proximal to muscovite grain margins, and those that occur as inclusions contain sillimanite inclusions.
Dated Phase(s): muscovite (200 μ - 4 mm)

Photo A-4:

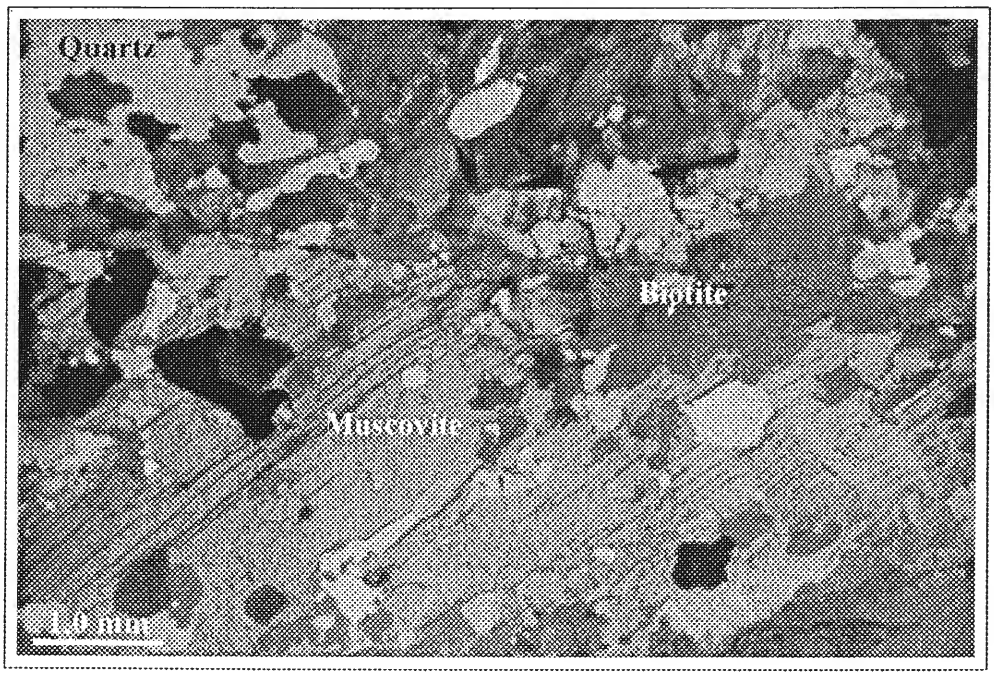

Crossed Nichols

CXA97 – D31:

Domain: Kisseynew Domain – McLennan Group arkoses
Outcrop: Pink weathering, homogeneous, medium grained biotite + muscovite ± magnetite granite with enclaves of McLennan Group arkoses.
Thin – Section: Plagioclase grains are intensely sericitized. Distribution of both plagioclase and K-feldspar grains is bimodal. Large K-feldspar grains are perthitic and myrmekitic textures locally characterize the grain boundaries of adjacent plagioclase and quartz grains. Individual quartz and plagioclase grains have highly sutured grain boundaries and are often separated by a fine-grained aggregate. Muscovite grains are poorly developed and vary in size. Grain margins have also been altered to a fine-grained aggregate. Inclusions of quartz and K-feldspar are observed in larger muscovite grains
Dated Phase(s): muscovite (250 μm - 1 mm)

Photo A-5:

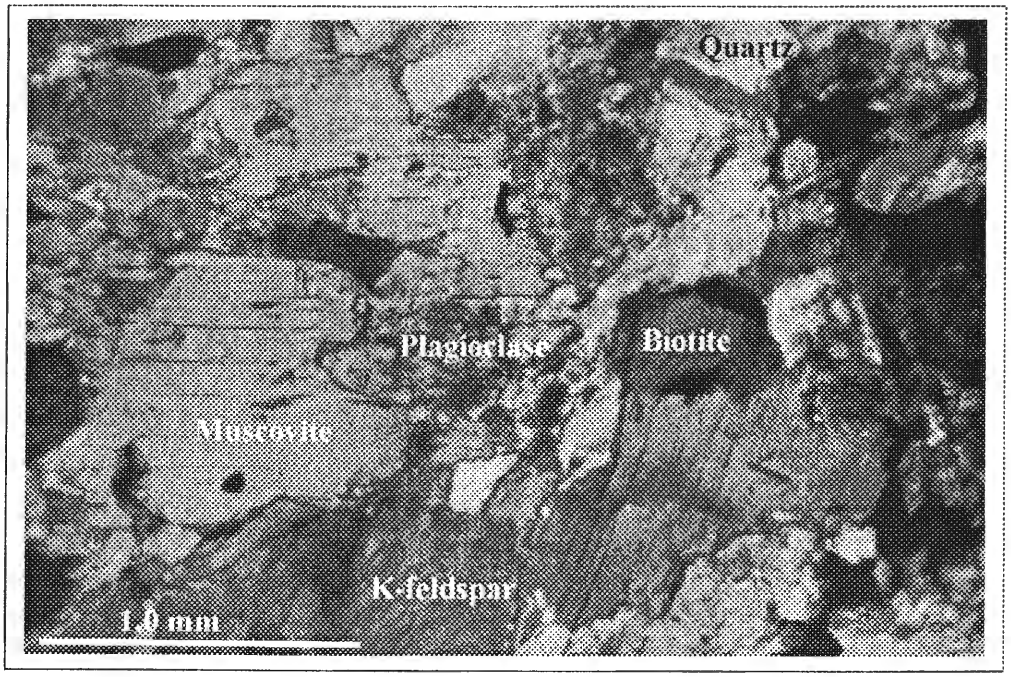

Crossed Nichols

CXA97 – D26A:

Domain: Kisseynew Domain – McLennan Group arkoses
Outcrop: Located just south of the Duck Lake Shear zone, the outcrop is medium grained, grey weathering, very well foliated biotite + muscovite psammite. Two phase muscovite growth was observed, where S_1 muscovite is parallel to bedding (S_0) and has been crenulated by subsequent deformation during which S_2 muscovite developed parallel to the F_3 fold axis. Note: S_1 muscovite in the McLennan Group developed during regional F_2 deformation.
Thin Section: Muscovite and biotite grains are prismatic, subhedral – euhedral and intergrown with each other. Mica intergrowths resemble ribbons with a preferred orientation, where muscovite ribbons are kinked. There are also subhedral grains of muscovite that have developed perpendicular to the fabric defined by mica ribbons (second generation of muscovite growth?). Quartz and plagioclase grain boundaries are sutured. Locally, patches of intensely sericitized plagioclase are also present.
Dated Phase(s): muscovite (250 μm –1 mm)

Photo A-6:

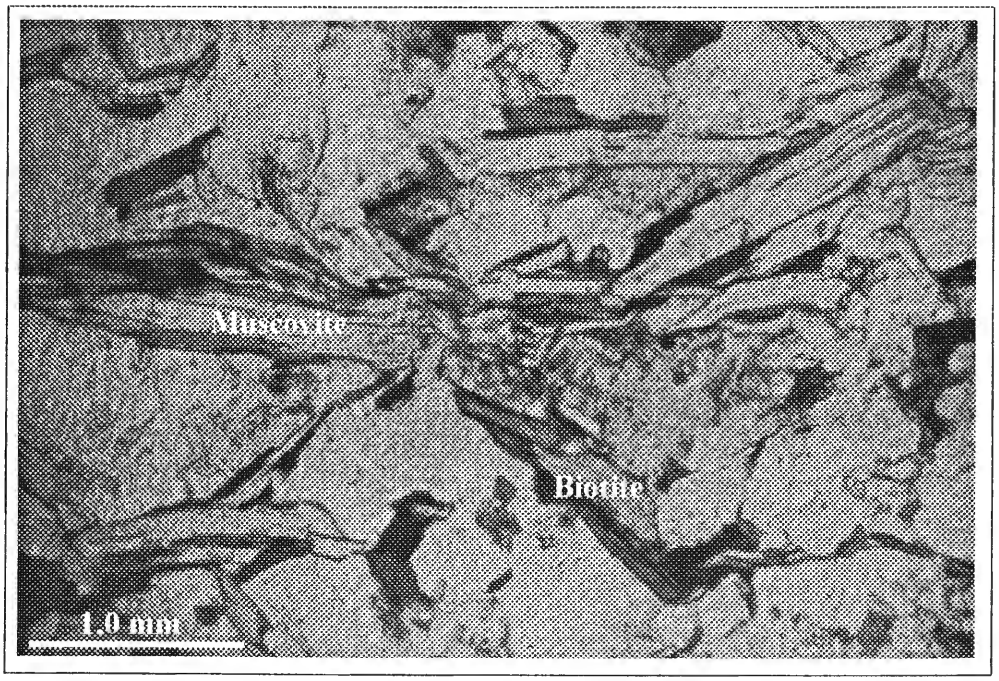

PPL (plane polarized light)

CXA97 – D26B:

Domain: Kisseynew Domain – McLennan Group arkoses
Outcrop: Late-phase muscovite bearing pegmatite intruding outcrop from which sample CXA97 – D26B was collected.
Thin – Section: Coarse grained (2 - 3mm). Quartz, plagioclase and K-feldspar grain boundaries are moderately – highly sutured. Locally large grains are separated by subgrains (10-20 μ), or are otherwise separated by a fine-grained aggregate. K-feldspars are coarsely perthitic. Most quartz and feldspar grains display an undulose or "sweeping" extinction in cross nicols. Muscovite grains are large and have locally experienced hematite alteration. Margins of most muscovite grains have been altered to a fine-grained aggregate.
Dated Phase(s): muscovite (1-3 mm)

Photo A-7:

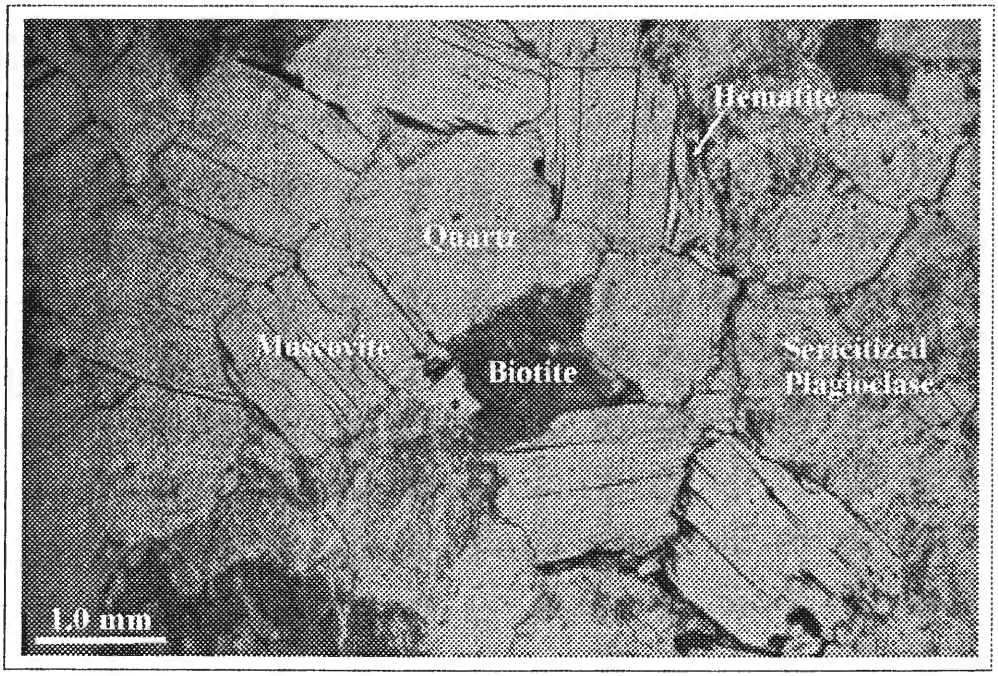

PPL (plane polarized light)

CXA97 – A404A:

Domain: La Ronge Domain – Central Metavolcanic Belt (CMB)
Outcrop: Fine grained, highly sheared mafic rocks of the CMB in contact with an equally sheared polymictic conglomerate (basal unit of the McLennan Group Arkoses). The contact itself is believed to be the Duck Lake Shear Zone (DLSZ). Sample was taken 0.5 m above (north of) the contact. Rotated quartz porphyroclasts within the polymictic conglomerate suggests top to the north movement along the DLSZ. This implies movement along the DLSZ was extensional?
Thin – Section: Fine grained and layered where millimeter scale layering is defined by varying concentrations of biotite, and amphibole and tourmaline. Some layers comprise ~ 95 % amphibole and others ~ 75% biotite. In both shape and colour, amphibole looks to be actinolitic hornblende that appears to be overgrowing brown biotite, but locally appears to be intergrown with it. Both biotite and amphibole are randomly oriented and zoned. Matrix quartz and plagioclase appear "blebby". No textural equilibrium in this rock.
Dated Phase(s): amphibole (200 – 500 μm)

Photo A-8:

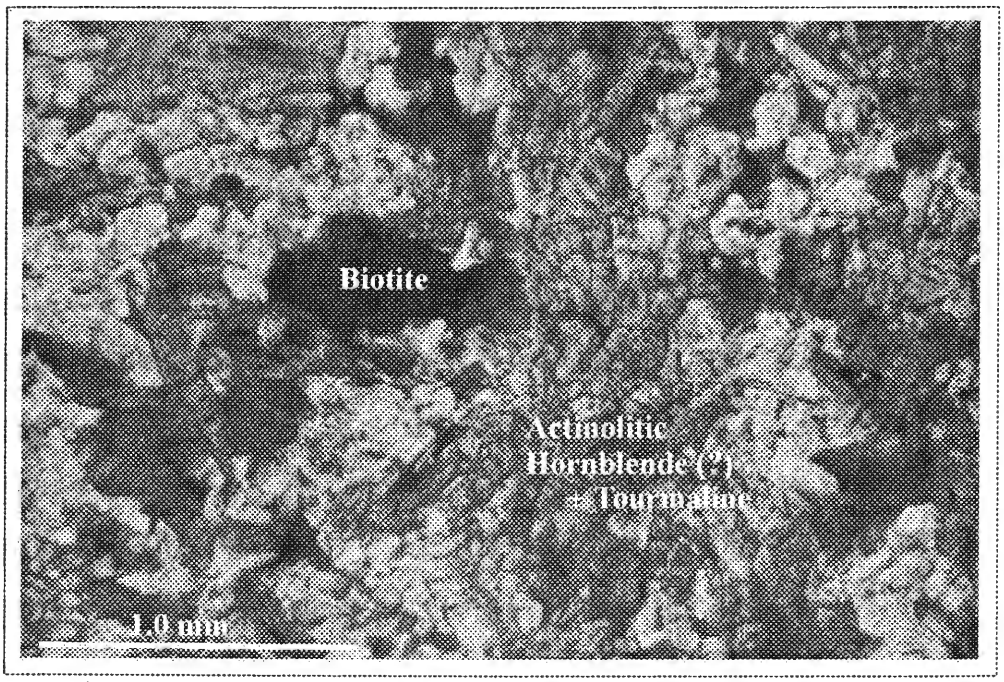

PPL (plane polarized light)

CXA97 – D004:

Domain: La Ronge Domain – Central Metavolcanic Belt (CMB)
Outcrop: Fine grained, highly sheared mafic rocks of the CMB with both boudinaged and coherent calc-silicate layers. Outcrop is located some 200 m north of the DLSZ.
Thin – Section: Extremely fine grained (100 - 500 μm) and granoblastic. Plagioclase grains have been intensely altered to sericite. Amphibole grains are euhedral – subhedral, free of inclusions and define a weak fabric. Grain boundaries of some amphiboles appear diffuse – evidence for recrystallization?
Dated Phase(s): amphibole (200 -300 μm)

Photo A-9:

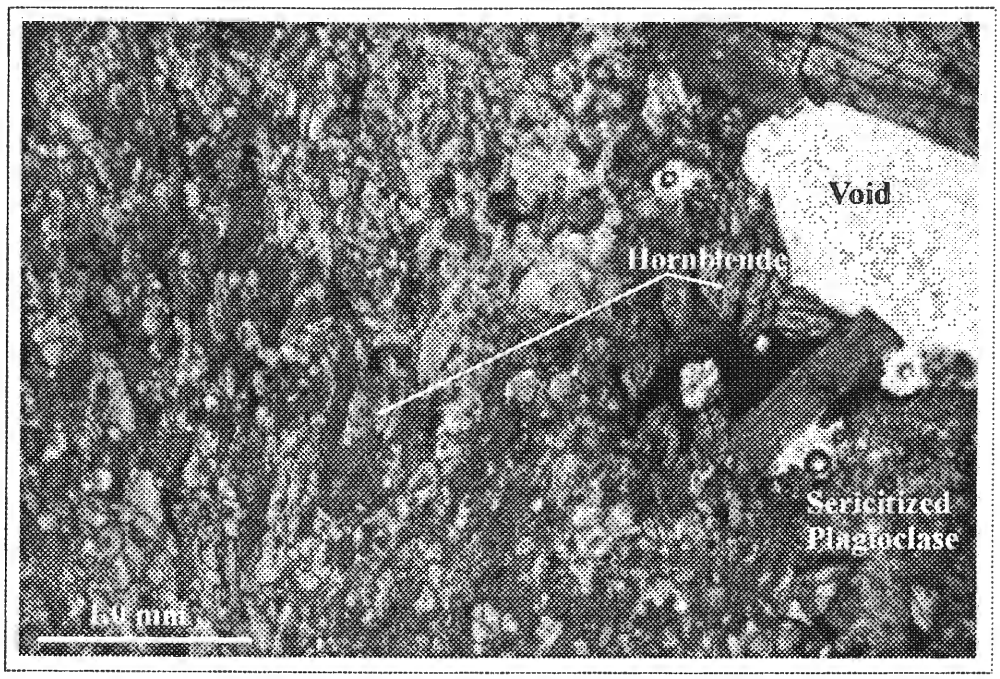

PPL (plane polarized light)

CXA97 – D23:

Domain: Butler Island Diorite (proximal to CMB; intrudes into La Ronge Domain)
Outcrop: Medium grained, highly sheared hornblend + biotite + titanite ± epidote "border phase" Butler Island Diorite. Sample is referred to as "border phase" because the outcrop is located at the margin of the pluton, close to the sheared (?) contact with the CMB. Here, igneous hornblende is preserved and appears "knobby". Recrystallized hornblende is also preserved as elongate grains that define the lineation.
Thin – Section: The first type of amphibole is characterized by subhedral grains with well defined but irregular grain boundaries. These grains are large (1-4 mm), rich with inclusions of quartz, plagioclase and titanite and are discordant to the foliation. Finer grained laths (0.3-1 mm) have a preferred orientation and are generally lacking an abundance of inclusions. Both types of amphibole are intergrown with brown biotite along grain boundaries. The matrix comprises granoblastic quartz, plagioclase and possibly minor amounts of K-feldspar. Grains have well defined grain boundaries and locally display undulose extinction.
Dated Phase(s): amphibole (0.3 –1 mm)

Photo A-10:

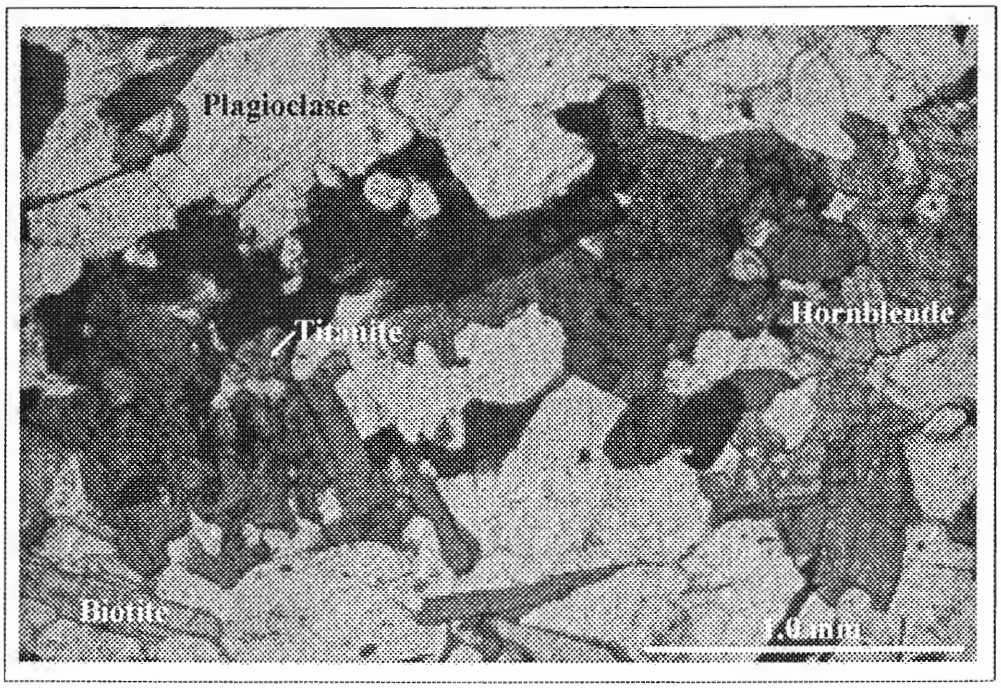

PPL (plane polarized light)

CXA97 – A001:

Domain: Butler Island Diorite (intrudes into La Ronge Domain)
Outcrop: White – grey weathering, medium to coarse grained, homogeneous, weakly foliated biotite + hornblende + quartz + plagioclase diorite.
Thin – Section: Quartz and plagioclase grains vary in size, where large grains are separated by a zone of subgrains. Grain boundaries are moderately sutured and plagioclase has been sericitized. Amphibole grains are subhedral – euhedral and contain inclusions of quartz, plagioclase, titanite ± K-feldspar. Grain boundaries are irregular and appear to be intergrown with, and/or replaced by euhedral, prismatic brown biotite
Dated Phase(s): amphibole (0.4 - 2 mm)

Photo A-11:

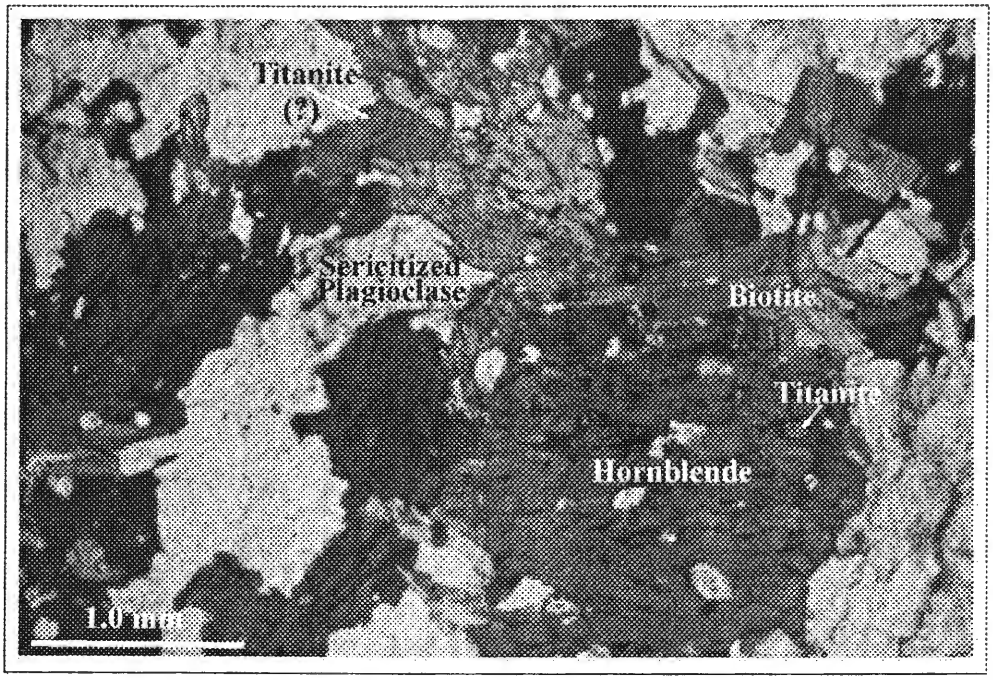

PPL (plane polarized light)

CXA97 – D85:

Domain: La Ronge Domain – Milton Island metasedimentary assemblage
Outcrop: Migmatic, coarse grained, well-foliated biotite + muscovite psammite. Leucosomes are generally rimmed by biotite. In outcrop there may be two phases of muscovite growth visible. One is parallel to bedding and the second that is parallel to the crenulation cleavage. Locally this assemblage contains both boudinaged and coherent calc-silicate layers. Apatite may also be found locally.
Thin – Section: Matrix is granoblastic and comprises quartz, plagioclase and K-feldspar. Plagioclase grains have been moderately altered to sericite. Myrmekitic intergrowth of plagioclase and quartz characterizes grain boundaries between the two. Prismatic brown biotite has developed along grain boundaries of quartz and is intergrown with fine muscovite (0.5-1 mm). Together, micas define a foliation that has been crenulated. Muscovite looks like it is replacing biotite that is being replaced by an opaque mineral. Locally margins of muscovite grains are characterized by symplectic intergrowth with quartz.
Dated Phase(s): muscovite (300 -700 μm)

Photo A-12:

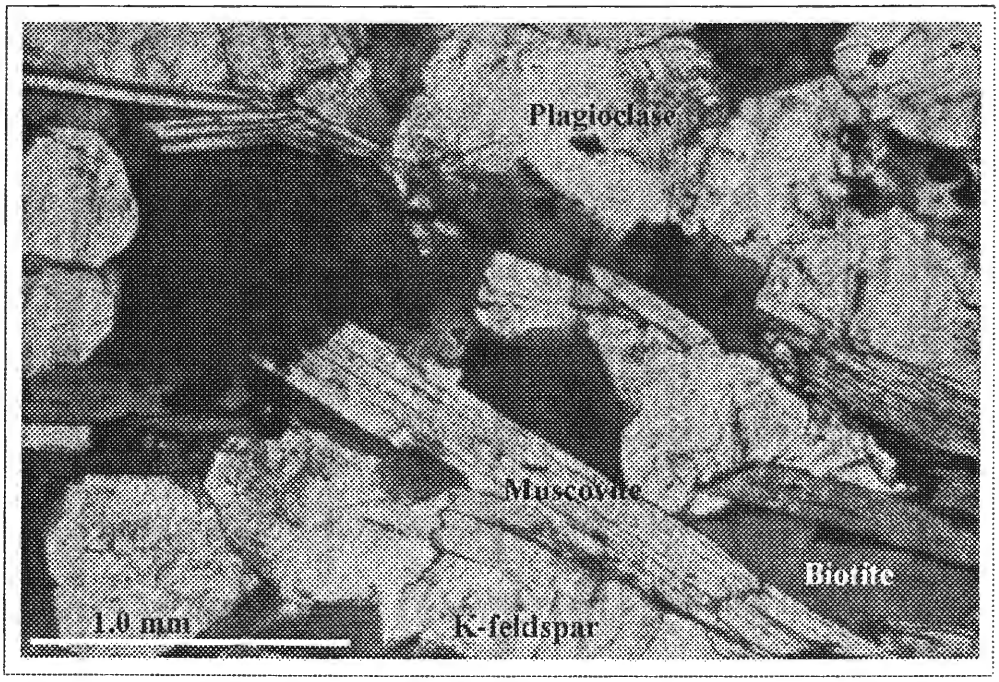

PPL (plane polarized light)

CXA97 – D85:

Domain: La Ronge Domain – Milton Island Metasedimentary Assemblage
Outcrop: Fine grained and well foliated biotite + muscovite psammite. This sample was collected from the same outcrop as the previous sample, but from a finer grained bed some tens of metres
Thin – Section: Fine grained and granoblastic (15-40 μ). Biotite laths define a fabric and are locally intergrown with fine, prismatic muscovite (5-10 μ). Large muscovite grains (> 3 mm) are poorly developed with ill defined grain boundaries characterized by symplectic intergrowth of muscovite and quartz. Plagioclase grains slightly altered.
Dated Phase(s): muscovite (100-500 μm); K-feldspar (150-250 μm).

Photo A-13:

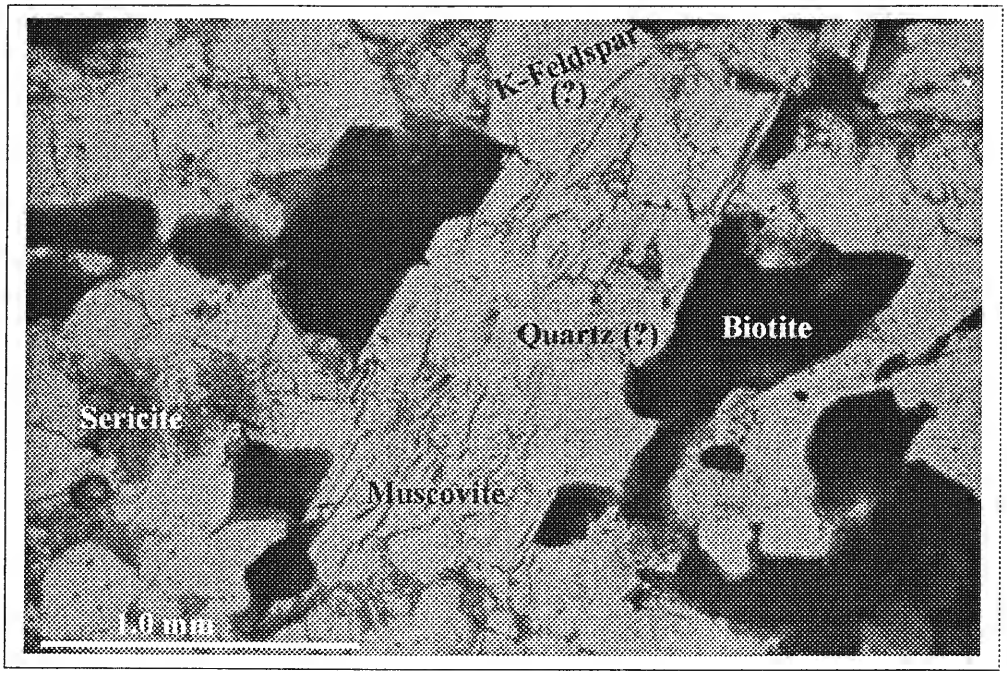

PPL (plane polarized light)

CXA97 – D373A:

Domain: Tonalite intruding into La Ronge Domain
Outcrop: I did not study this outcrop. Sample obtained from David Corrigan of the Geological Survey of Canada.
Thin – Section: Plagioclase grains have been altered slightly. Amphibole grains are subhedral – euhedral and intergrown with brown biotite along grain margins, though locally some grains also contain inclusions of biotite.
Dated Phase(s): amphibole (200-850 μm).

Photo A-14:

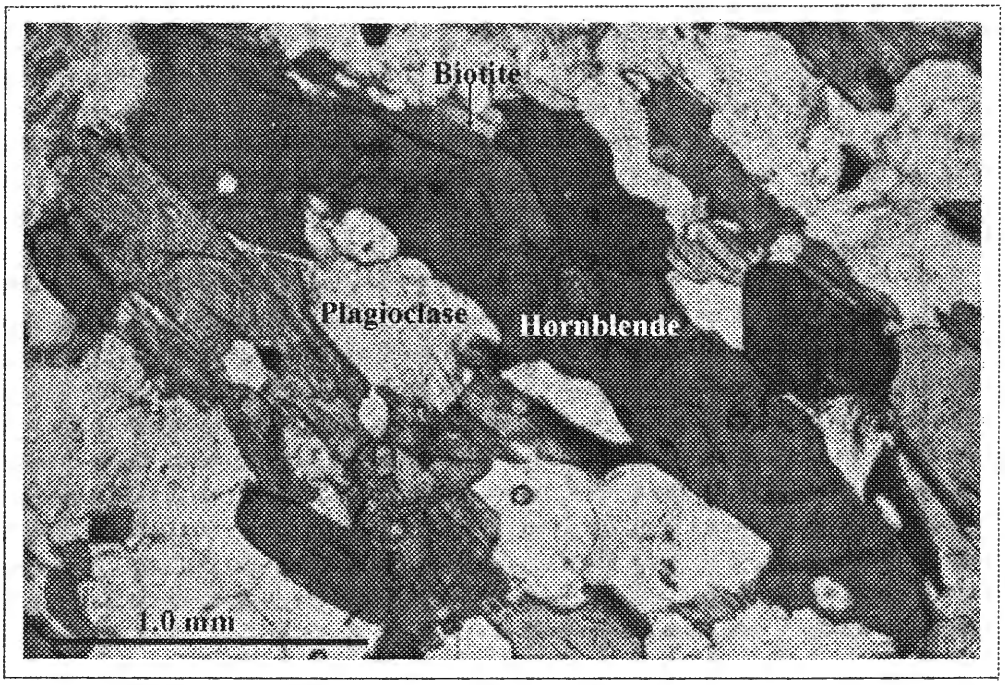

PPL (plane polarized light)

CXA98 – D93:

Domain: MacMillian Lake monzogranite intruding into La Ronge Domain
Outcrop: I did not study this outcrop. Sample obtained from David Corrigan of the Geological Survey of Canada.
Thin – Section: Recrystallized. Boundaries between quartz and plagioclase grains are characterized by a myrmekitic texture. Plagioclase grains are altered slightly and large quartz grains contain inclusions of biotite and altered plagioclase. Amphibole grains are anhedral, vary in size (0.8 - 1 mm), contain inclusions of quartz ± feldspar ± allanite ± titanite, and are intergrown with brown biotite.
Dated Phase(s): amphibole (0.8 – 1 mm)

Photo A-15:

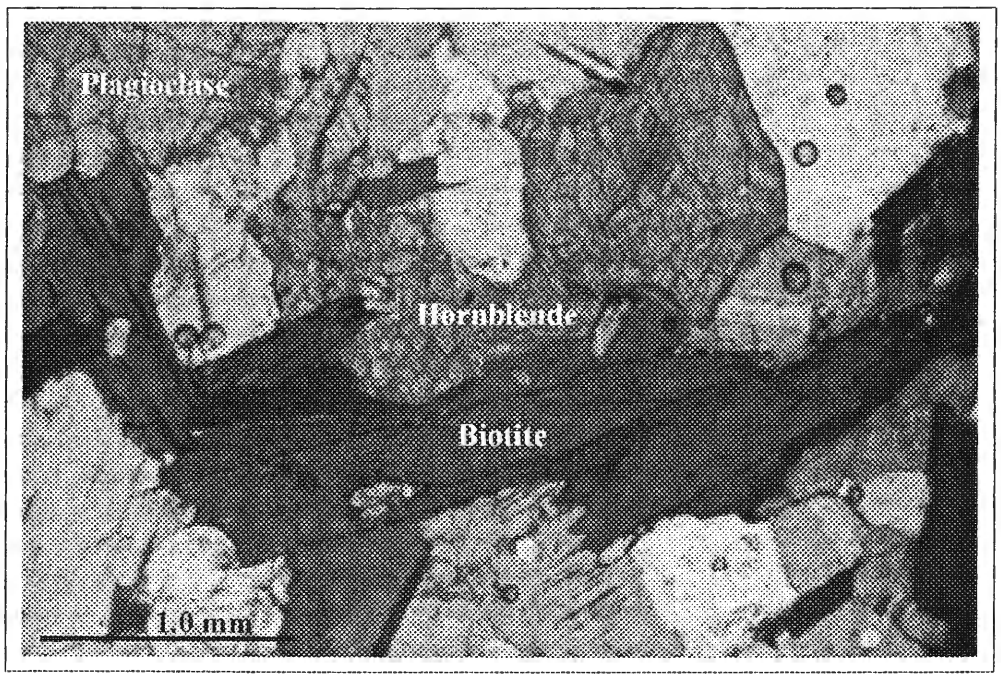

PPL (plane polarized light)

CXA99 – D53: (located in Paskwatchi Bay area) *A-3*

Domain: La Ronge Domain – pegmatitic gabbro intruding into McMillian Lake monzogranite?
Outcrop: A layered ultramafic intrusion with alternating layers of dark green, almost black, gabbroic material; apple green actinolite-anthophyllite layers; and white felsic layers. Could this be a boudinaged section of the Lawernce Bay ultramafics?
Thin – Section: Coarse grained. Amphiboles vary in size (0.1 – 4 mm). Small amphibole grains generally occur as euhedral, elongate inclusions in plagioclase grains that have almost entirely been altered. Inclusions are oriented parallel to albite twins. Large amphibole grains contain inclusions of titanite ± quartz. Large grains are also fractured and altered to a dark, fine grained aggregate.
Dated Phase(s): amphibole (0.5 – 2 mm)

Photo A-16:

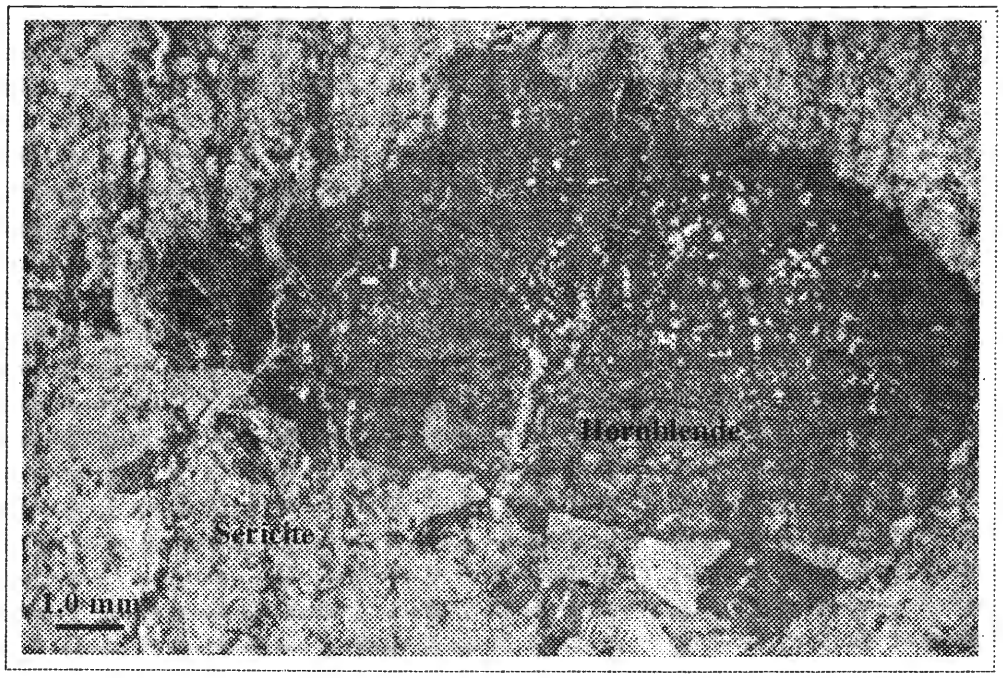

Crossed Nichols

CXA98 – T201:

Domain: La Ronge Domain – Crowe Island Complex
Outcrop: I did not study this outcrop. Sample obtained from David Corrigan of the Geological Survey of Canada.
Thin – Section: Amphibole grains intensely intergrown with biotite and titanite. Matrix comprises quartz and feldspar grains of variable size. Individual grains are often separated by a zone of subgrains and/or a fine grained aggregate. Quartz and feldpsar grain boundaries are irregular but well defined. K-feldspar grains are finely perthitic.
Dated Phase(s): amphibole (100 -250 μm); K-feldspar (100 - 850 μm)

Photo A-17:

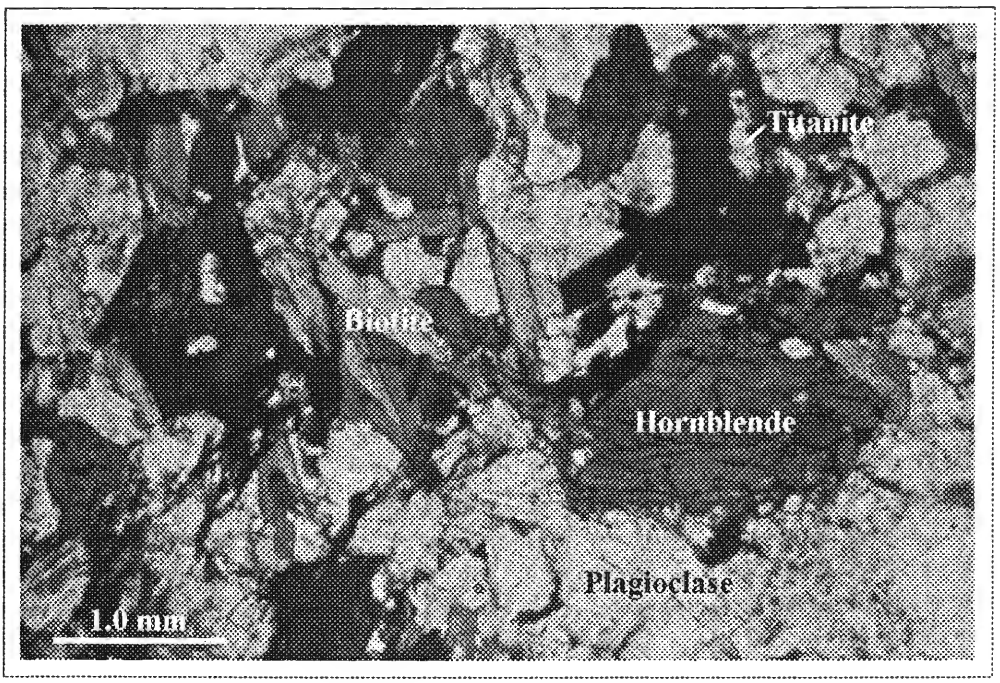

PPL (plane polarized light)

CXA98 – T300A: (sample taken just east of station T300) *A-4*

Domain: Wathaman Batholith – marginal zone (diorite).
Outcrop: A chaotic outcrop with enclaves of metasediments and two different phases of Wathaman intrusions. This sample has been interpreted to represent the earliest phase (?) of the batholith. It is a medium – coarse-grained, foliated hornblende + biotite + plagioclase + titanite diorite-granodiorite with ~ 65% mafics and appears to have been subsequently intruded by a medium – coarse grained, foliated hornblende + biotite + titanite + magnetite granodiorite with only 25% mafics (second phase?). The entire outcrop has been cross-cut by a pink, foliated apalitic magnetite + biotite + allanite granite.
Thin – Section: Amphiboles vary in size (~5-400 μ). Small grains are subhedral and contain less than 1% inclusions. Most amphibole grains, however, contain an abundance of titanite ± allanite ± quartz inclusions, and are intergrown with brown biotite that has been retrograded to chlorite along grain margins. Plagioclase grains are variably altered to sericite.
Dated Phase(s): amphibole (0.5 –1 mm)

Photo A-18:

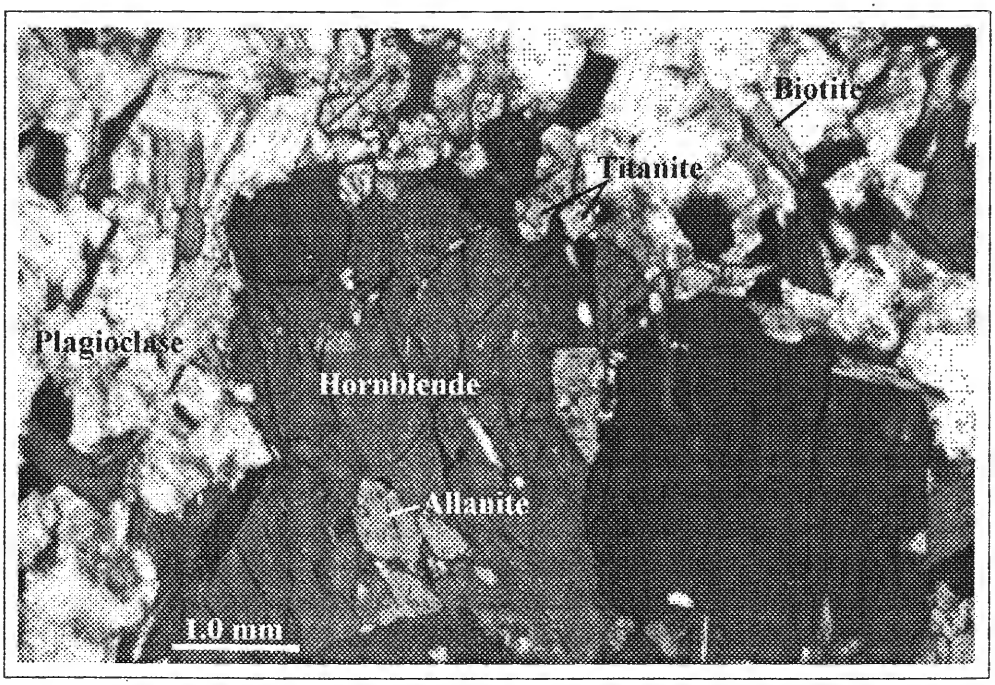

PPL (plane polarized light)

CXA98 – T300B: (sample taken just east of station T300)

Domain: Wathaman Batholith – marginal zone (granodiorite).
Outcrop: Medium – coarse grained, foliated hornblende + biotite +titanite + magnetite granodiorite with ~ 25% mafics. In outcrop, this rock type appears to be the second phase of the Wathaman Batholith that intruded in to CXA98 – T300A.
Thin – Section: Variably recrystallized. Locally margins of matrix quartz and plagioclase grains are characterized by myrmekitic texture. Also, K-feldspar, plagioclase and quartz grain boundaries are highly sutured. Plagioclase grains are variably altered. It is difficult to distinguish K-feldspar from plagioclase in this sample due to granoblastic nature of matrix material. Amphibole grains are subhedral and vary in size (8-100 μ). Along grain margins amphiboles have been retrograded to chlorite and/or intergrown with brown biotite. Individual grains contain inclusions of quartz ± titanite.
Dated Phase(s): amphibole (0.8 - 1 mm); K-feldspar (150 - 500 μm)

Photo A-19:

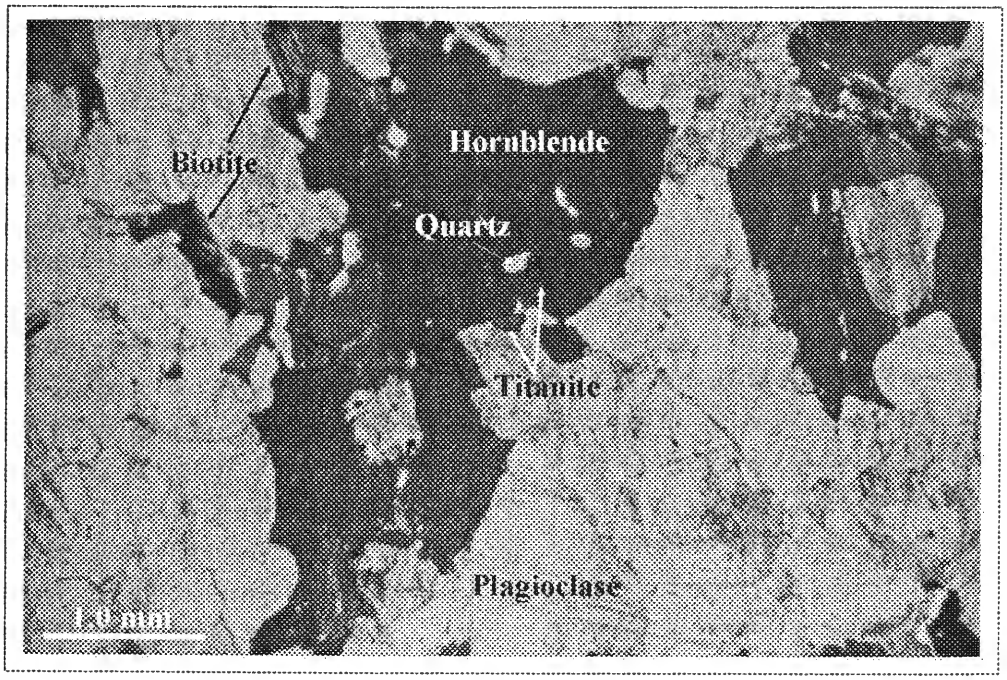

PPL (plane polarized light)

CXA99 – D76:

Domain: Wathaman Batholith – marginal zone
Outcrop: Foliated, medium to coarse-grained, recrystallized megacrystic K-feldspar + hornblende + biotite + magnetite + titanite granodiorite. Locally, veins of apalitic granite cross cut the outcrop (as seen at CXA98 - T300).
Thin – Section: Feldspar and quartz grain boundaries are highly sutured and locally characterized by a myrmekitic texture. Zones of subgrains separate large feldspar and quartz grains. Plagioclase grains are altered and K-feldspars contain inclusions of sericitized plagioclase. Amphibole grains are anhedral – subhedral and vary in size (0.25 –2 mm), where grains larger than ~ 0.3 mm contain inclusion of quartz + titanite ± allanite ± plagioclase. Amphibole grains of all sizes are intergrown with brown biotite.
Dated Phase(s): amphibole (250 -950 μm); K-feldspar (250 - 850 μm)

Photo A-20:

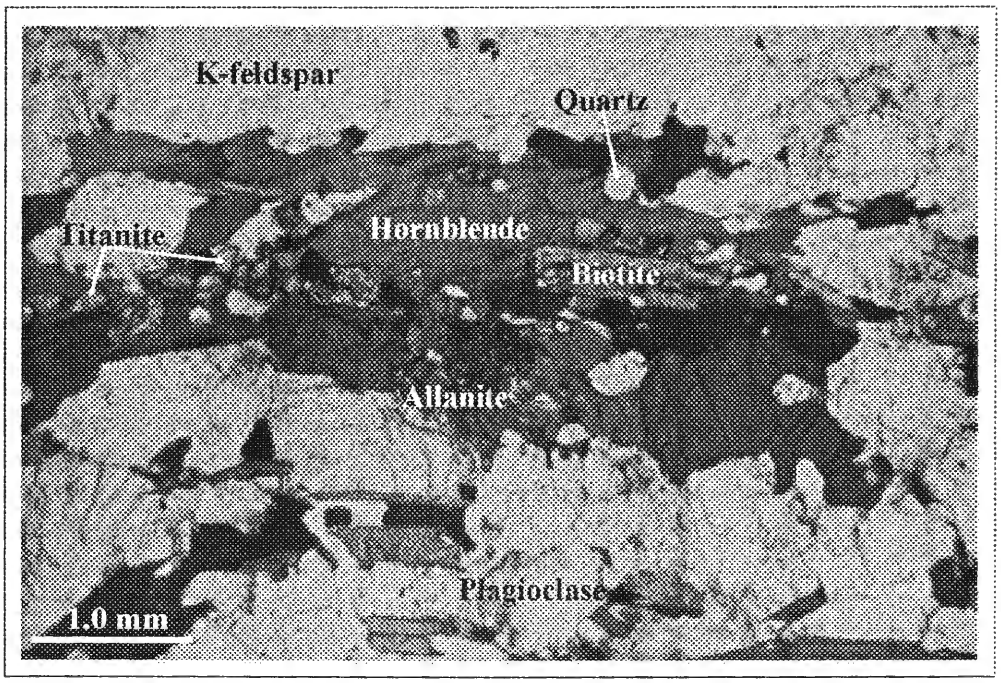

PPL (plane polarized light)

CXA98 – T223:

Domain: Wathaman Batholith - granodiorite-quartz monzodiorite
Outcrop: I did not study this outcrop. Sample obtained from David Corrigan of the Geological Survey of Canada.
Thin – Section: Coarse grained, where amphibole, biotite, epidote and titanite occur together in clots. Amphibole grains are subhedral and intergrown with brown biotite along grain margins. Locally amphibole appears to be replaced by chlorite and green biotite. Plagioclase grains are intensely altered. K-feldspars are coarsely perthitic. Feldspar grains greater than 3 mm are often surrounded by a fine grained aggregate, or subgrains – some of which look myrmekitic.
Dated Phase(s): amphibole (450 - 850 μm); K-feldspar (0.5 -1 mm)

Photo A-21:

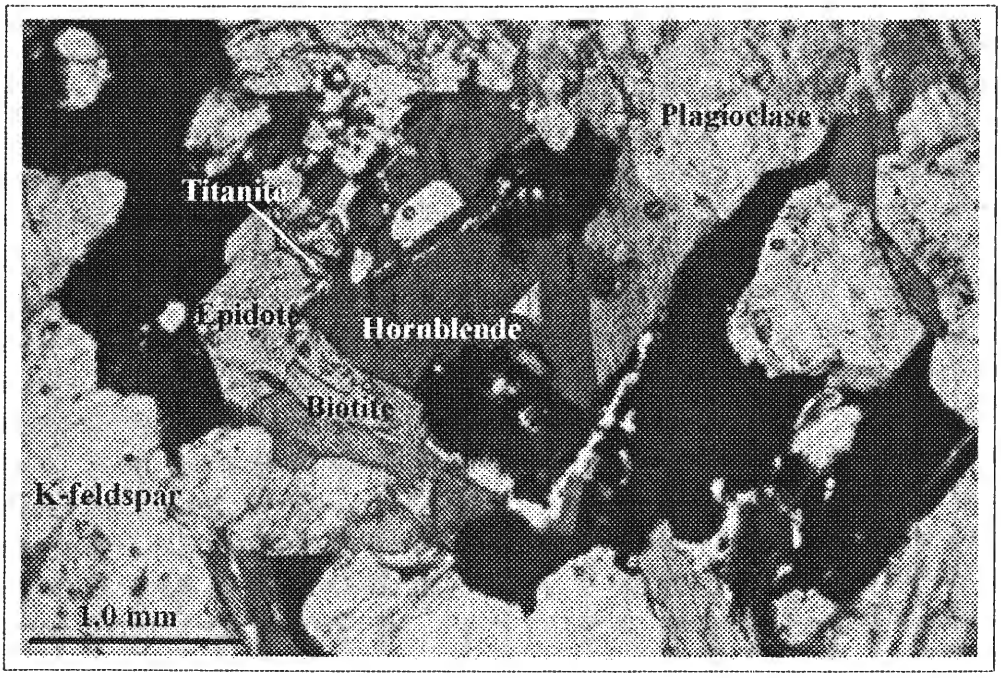

PPL (plane polarized light)

CXA99 – T62B:

Domain: Wathaman Batholith
Outcrop: Coarse-grained hornblende + biotite + magnetite + titanite + epidote quartz monzodiorite locally containing 2 – 5 cm K-feldspar megacrysts. Within outcrop there are enclaves of fine-grained diorite - quartz diorite.
Thin – Section: Rock has experienced some cataclasis and minor recrystallization. Matrix of quartz, plagioclase and K-feldspar are variable in size. Grains larger then 3 mm are characterized by well defined by irregular grain boundaries and are surrounded by subgrains (8-90 μ). Locally myrmekite textures are observed between plagioclase and quartz. Amphibole grains are anhedral, small (≤ 1 mm) and intergrown with biotite, epidote and titanite. Some amphibole grains may contain inclusions of quartz.
Dated Phase(s): amphibole (0.25 – 0.75 mm)

Photo A-22:

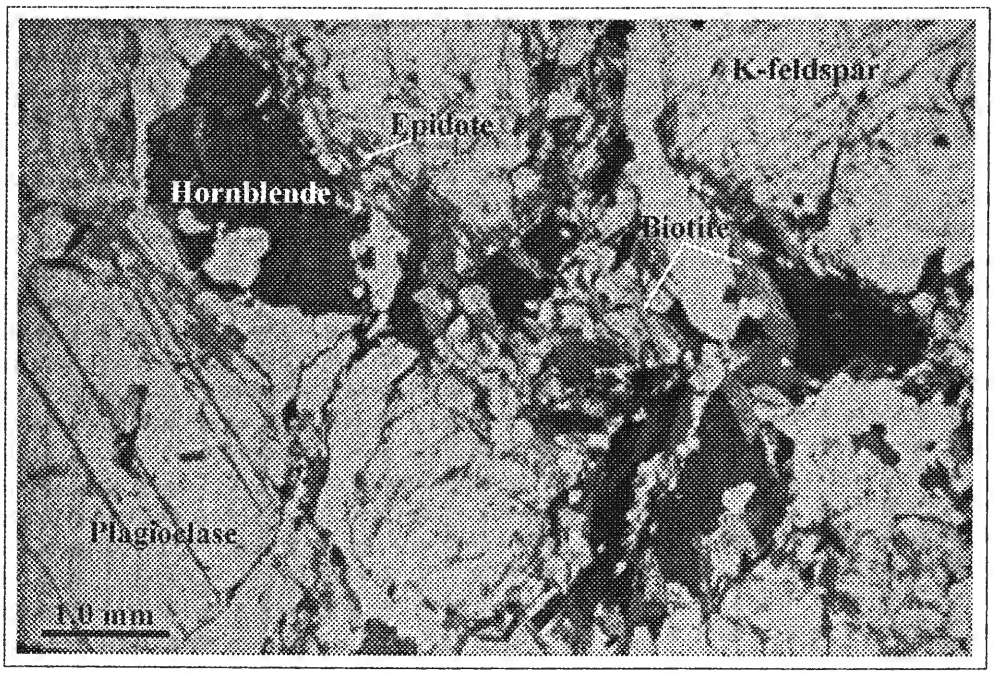

PPL (plane polarized light)

CXA99 – T63:

Domain: Wathaman Batholith
Outcrop: Recrystallized, well foliated hornblende + magnetite granite that cross cuts dioritic – quartz dioritic material of the Wathaman batholith.
Thin – Section: Recrystallized such that quartz and feldspar grains of the matrix are granoblastic. Plagioclase and K-feldspar are closely associated, and intergrown such that the intergrowth appears almost graphitic. Grain boundaries are irregular, where locally they appear to be highly sutured. Plagioclase grains are variably altered. Amphibole grains are small (50 -700 μ), euhedral grains that occur in clots and are intergrown with brown biotite, allanite and titanite. Could amphiboles be replacing clinopyroxene? Grains less than ~ 300 μ are free of inclusions, where larger grains may contain biotite ± titanite ± allanite ± quartz.
Dated Phase(s): amphibole (50 – 700 μ); K-feldspar (0.25 – 0.85 mm)

Photo A-23:

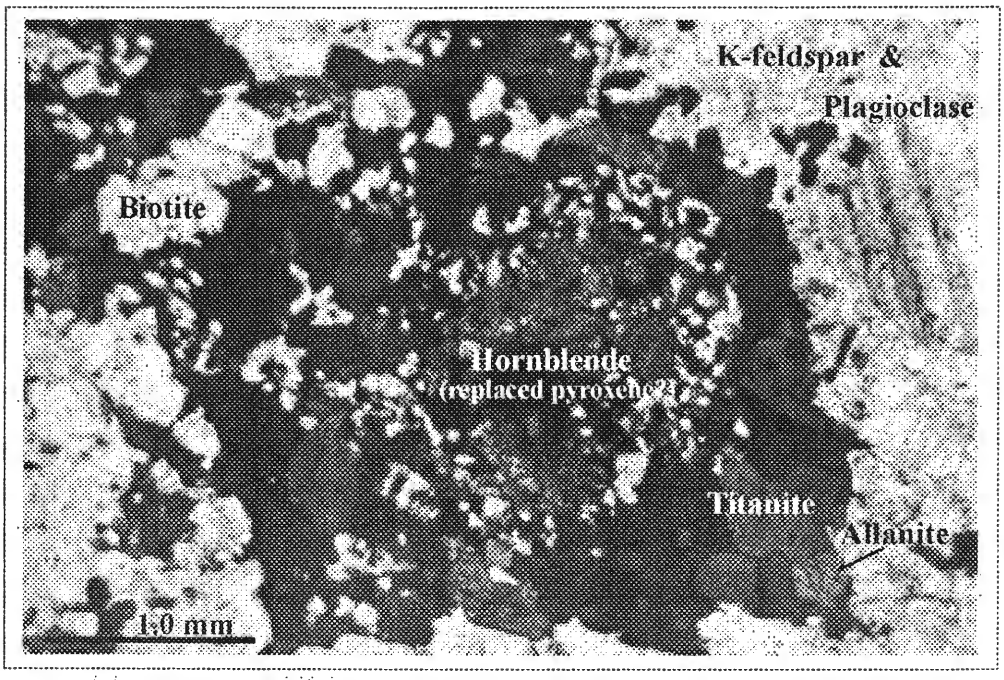

PPL (plane polarized light)

CXA99 – D214: (actual outcrop is ~ 200 m north of station D214)

Domain: Peter Lake Domain (?)
Outcrop: Dark green, fine-grained hornblende ± biotite mafic metavolcanic rock that has been intruded by gabbroic material. If in fact these rocks are volcanic what is their age? Is this an enclave of Archean volcanic material in the batholith? Or does it belong to the CMB of the La Ronge Domain?
Thin – Section: Rock is layered, with millimeter scale layers defined by varying concentrations of biotite and amphibole. Dark layers have a high concentration of amphibole, where lighter layers have very little amphibole, lots of biotite and an extremely fine grained aggregate (sericitized plagioclase?). Amphibole grains are subhedral – euhedral, free of inclusions and locally intergrown with brown biotite.
Dated Phase(s): amphibole (100 - 500 μm)

Photo A-24:

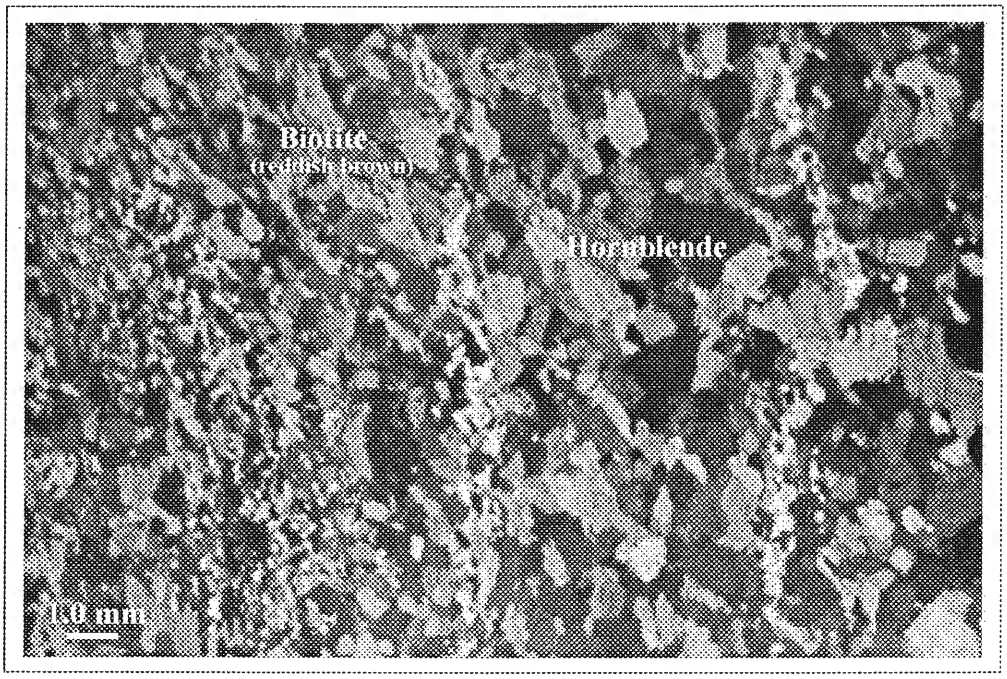

PPL (plane polarized light)

CXA99 – D103:

Domain: Wathaman Batholith – Patterson Island megacrystic syenite
Outcrop: Undeformed, hornblende + biotite + minor plagioclase + minor quartz + titanite syenite with 1 – 6 cm K-feldspar megacrysts and ~ 50% mafics. Also in outcrop are enclaves of more mafic material.
Thin – Section: Coarse grained and moderately recrystallized. K-feldspar grains are generally greater than 3 mm, coarsely perthitic and contain euhedral – subhedral inclusions of plagioclase that often occur in clots. Patches of coarse plagilcase grains have been altered to sericite. Amphibole grains are replacing clinopyroxene, where aggregates of amphibole are cored by and intergrown with clinopyroxene. Amphibole grains themselves are intergrown with brown biotite and contain inclusions of titanite ± quartz ± feldspars.
Dated Phase(s): amphibole (150 - 450 μm); K-feldspar (150 - 500 μm)

Photo A-25:

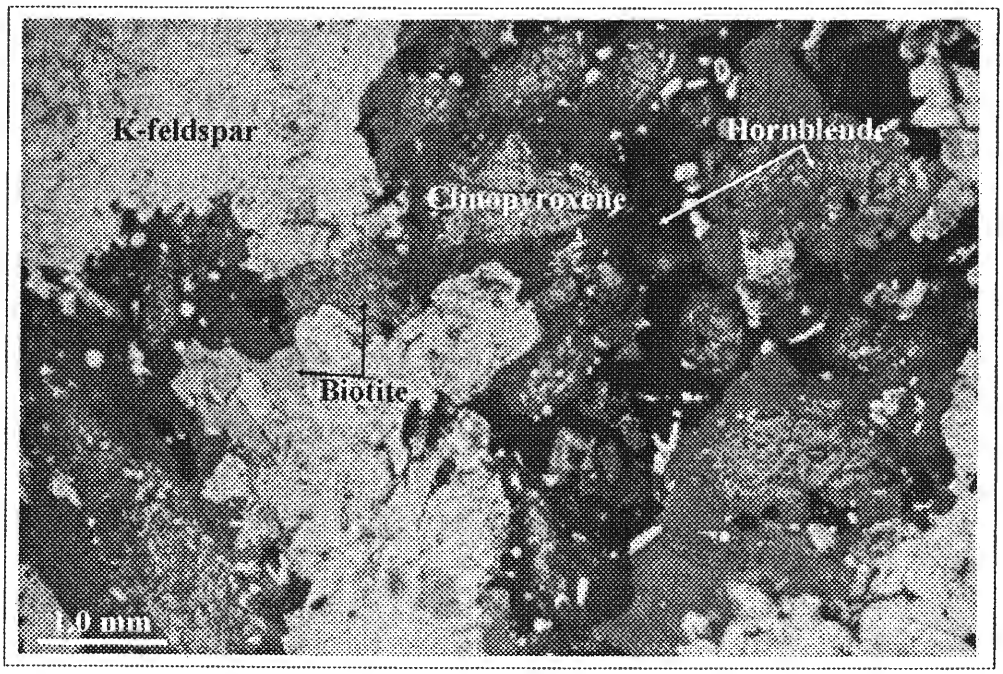

PPL (plane polarized light)

CXA99 – D162:

Domain: Peter Lake Domain
Outcrop: Medium grained, highly migmatized orthogneiss ranging in composition from granite to diorite.
Thin – Section: Recrystallized matrix of granoblastic quartz and plagioclase. Quartz and plagioclase grain boundaries are characterized by a myrmekitic texture. Most plagioclase grains are altered. Amphibole grains are intergrown with, and "bearded" by brown biotite along grain margins. Some amphibole grains contain inclusions of biotite ± titanite + quartz, and have been retrograded to chlorite along grain margins.
Dated Phase(s): amphibole (100 - 500 μm)

Photo A-26:

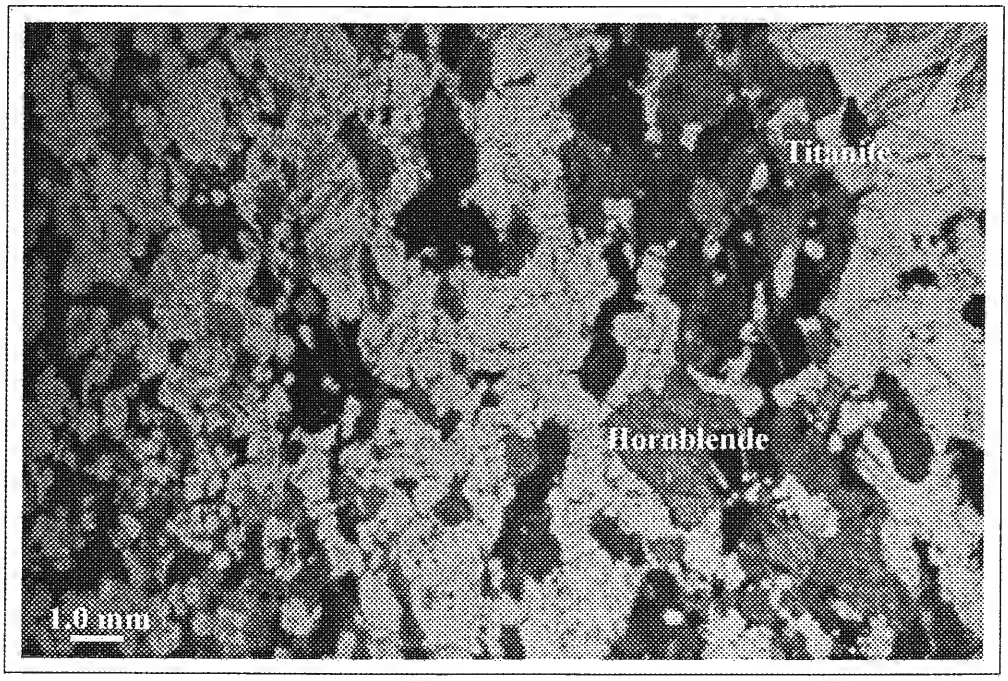

PPL (plane polarized light)

CXA99 – D87B:

Domain: Peter Lake Domain – Swan River Complex
Outcrop: Pristine gabbro with porphyroblasts of orthopyroxene surrounded by pargasitic hornblende.
Thin – Section: Moderately recrystallized. In cross nichols, large plagioclase grains (≥ 4 mm) display "sweeping" extinction, and are surrounded by subgrains. Some plagioclase grains appear to be kinked. Amphibole occurs as clots in which it is intensely intergrown with and replacing clinopyroxene. In aggregates that have completely replace clinopyroxene, there appears to be two phases of amphibole growth – one that is prismatic-acicular and colourless (actinolitic?), the one that is a subhedral – euhedral and dark green-brown in colour (hornblende?). The outer margins of aggregates/clots that have completely replaced clinopyroxene are characterized by a symplectic intergrowth of amphibole with quartz ± plagioclase. Amphibole grains are free of inclusions.
Dated Phase(s): amphibole (100 - 700 μm)

Photo A-27:

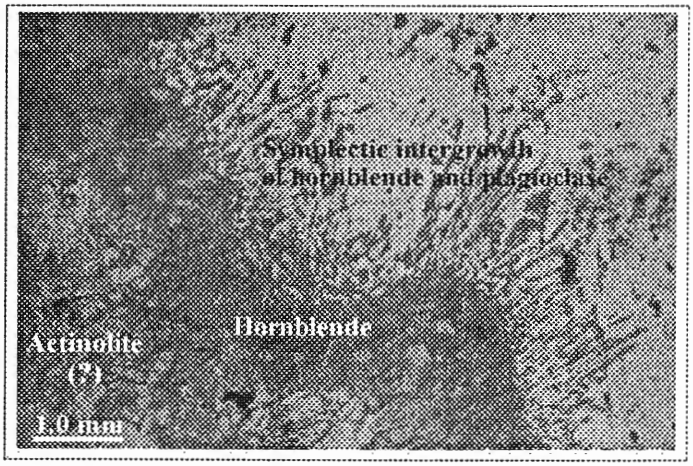

PPL (plane polarized light)

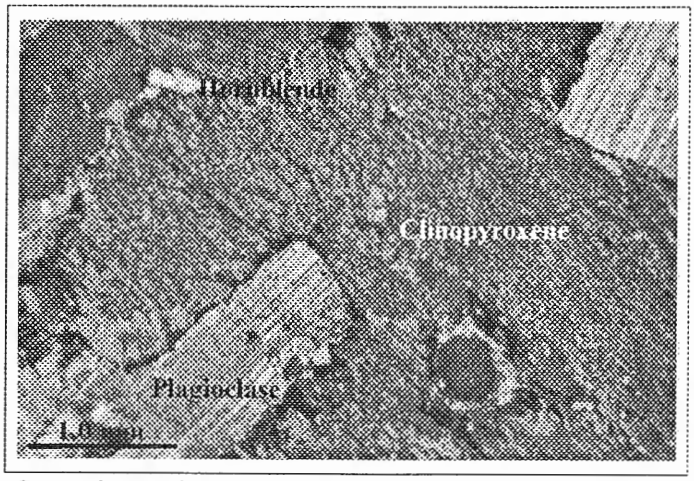

Crossed Nichols

CXA99 – D89A:

Domain: Peter Lake Domain – Swan River Complex
Outcrop: I did not study this outcrop. Sample obtained from David Corrigan of the Geological Survey of Canada.
Thin – Section: Plagioclase grains are varied in size and intensely altered, some beyond recognition. Amphibole grains are subhedral – euhedral and vary in size (0. 5 -1 mm). Locally, amphiboles are altered to a dark, fine grained aggregate and/or contain inclusions of altered plagioclase.
Dated Phase(s): amphibole (100 - 750 μm)

Photo A-28:

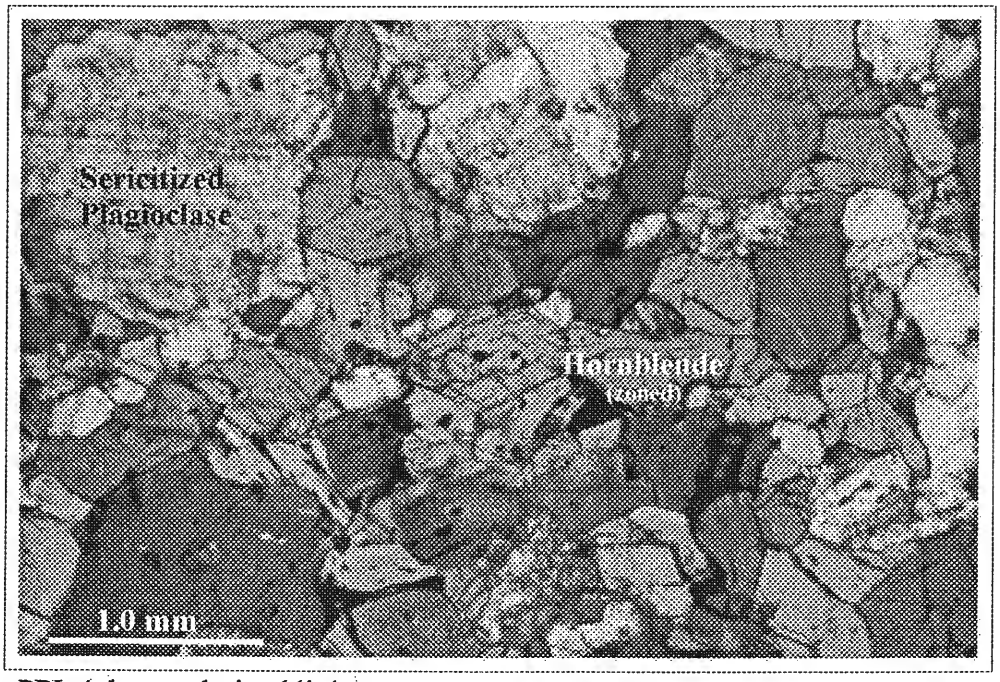

PPL (plane polarized light)

APPENDIX B

Mineral Chemistry

(Of mineral phases analyzed by the $^{40}Ar/^{39}Ar$ method. Mineral chemistry was obtained by electron probe X-ray microanalysis conducted at Dalhousie University. The fully automated JOEL 733 microanalyzer is equipped with four wavelength spectrometers and an Oxford Link eXL 131eV energy dispersive detector. Detection limits are on the order of 0.01 weight percent. Instrument precision is +/- 0.5 weight percent on cobalt metal (x=10), at one standard deviation. Accuracy for major elements is +/- 1.5 – 2.0 weight percent.)

Amphibole (Basis of 23 oxygen)

	98-D42-2	98-D42-3	98-D42-6	98-D42-8	98-D42-10	98-L48-1	98-L48-2	98-L48-3	98-L48-4
SiO_2	47.561	45.261	46.256	48.178	48.306	42.254	41.955	42.107	42.194
TiO_2	0.829	0.938	0.996	0.804	0.698	1.099	1.076	1.287	1.193
Al_2O_3	7.733	8.974	8.370	6.952	6.938	11.115	11.529	10.697	10.660
FeO	13.749	14.133	14.147	13.411	13.678	21.116	20.214	20.326	20.603
MnO	0.000	0.302	0.317	0.000	0.000	0.407	0.455	0.509	0.478
MgO	13.472	12.625	12.816	13.806	13.838	8.451	8.450	8.651	8.693
CaO	12.547	12.353	12.418	12.467	12.607	11.666	12.018	11.646	11.888
Na_2O	0.975	1.189	1.043	1.027	1.016	1.224	1.305	1.417	1.444
K_2O	0.732	0.893	0.840	0.654	0.607	1.174	1.283	1.261	1.288
Cl	0.000	0.000	0.000	0.000	0.000	0.096	0.096	0.000	0.097
Cr_2O_3	0.000	0.000	0.000	0.000	0.000	0.000	0.000	0.000	0.000
Total	97.597	96.668	97.203	97.298	97.688	98.381	98.381	97.902	98.537
Si	6.992	6.785	6.877	7.084	7.084	6.440	6.394	6.463	6.440
Ti	0.092	0.115	0.115	0.092	0.069	0.115	0.115	0.138	0.138
Al^{iv}	1.334	1.587	1.472	1.196	1.196	2.001	2.070	1.932	1.909
Fe^{2+}	1.675	1.771	1.748	1.656	1.679	2.691	2.576	2.599	2.622
Mn	0.000	0.046	0.046	0.000	0.000	0.046	0.069	0.069	0.069
Mg	2.944	2.806	2.829	3.036	3.013	1.932	1.932	1.978	1.978
Ca	1.976	1.978	1.978	1.955	1.978	1.909	1.955	1.909	1.955
Na	0.276	0.345	0.299	0.299	0.299	0.368	0.391	0.414	0.437
K	0.138	0.161	0.161	0.115	0.115	0.230	0.253	0.253	0.253
Cl	0.000	0.000	0.000	0.000	0.000	0.023	0.023	0.000	0.023
Cr^{3+}	0.000	0.000	0.000	0.000	0.000	0.000	0.000	0.000	0.000
Total	15.427	15.594	15.525	15.433	15.433	15.755	15.778	15.755	15.824

Amphibole (Basis of 23 oxygen)

	98-D12-8	98-D12- 9	98-D12-10	98-D12-12	98-D12-13	98-D12-15	98-D12-16	97-A404A-1	97-A404A-4
SiO_2	45.652	45.079	44.666	45.906	46.111	45.190	44.629	49.177	49.965
TiO_2	1.268	1.693	1.608	1.237	1.327	1.738	1.482	0.000	0.000
Al_2O_3	9.361	10.388	9.733	9.274	8.855	9.206	9.665	7.563	7.492
FeO	15.989	16.321	16.623	16.268	15.912	16.271	16.428	10.813	11.561
MnO	0.306	0.296	0.267	0.301	0.000	0.000	0.000	0.304	0.000
MgO	11.178	10.813	10.563	11.335	11.506	11.101	10.641	15.107	15.593
CaO	11.662	11.537	10.852	11.596	11.545	11.447	11.323	11.790	12.294
Na_2O	1.411	1.507	1.487	1.125	1.256	1.468	1.340	0.740	0.771
K_2O	0.271	0.421	0.478	0.308	0.278	0.453	0.425	0.000	0.174
Cl	0.000	0.000	0.250	0.000	0.000	0.000	0.000	0.000	0.000
Cr_2O_3	0.000	0.000	0.000	0.000	0.000	0.000	0.000	0.000	0.000
Total	97.099	98.056	96.527	97.350	96.790	96.874	95.933	95.495	97.850
Si	6.808	6.670	6.739	6.831	6.877	6.785	6.762	7.199	7.176
Ti	0.138	0.184	0.184	0.138	0.138	0.207	0.161	0.000	0.000
Al^{iv}	1.656	1.817	1.725	1.633	1.564	1.633	1.725	1.311	1.265
Fe^{2+}	2.001	2.024	2.093	2.024	1.978	2.047	2.070	1.334	1.380
Mn	0.046	0.046	0.023	0.046	0.000	0.000	0.000	0.046	0.000
Mg	2.484	2.392	2.369	2.507	2.553	2.484	2.392	3.312	3.335
Ca	1.863	1.840	1.748	1.840	1.840	1.840	1.840	1.863	1.886
Na	0.414	0.437	0.437	0.322	0.368	0.437	0.391	0.207	0.207
K	0.046	0.069	0.092	0.069	0.046	0.092	0.092	0.000	0.023
Cl	0.000	0.000	0.069	0.000	0.000	0.000	0.000	0.000	0.000
Cr^{3+}	0.000	0.000	0.000	0.000	0.000	0.000	0.000	0.000	0.000
Total	15.456	15.479	15.479	15.410	15.364	15.525	15.433	15.272	15.272

Amphibole (Basis of 23 oxygen)

	97-A404A-8	97-A404A-11	97-A404A-12	97-A404A-14	97-A404A-15	97-D004-1	97-D004-2	97-D004-3	97-D004-4
SiO_2	50.370	49.291	47.798	50.335	50.796	46.231	46.668	46.450	47.202
TiO_2	0.000	0.441	0.411	0.285	0.000	1.053	0.956	1.108	0.855
Al_2O_3	6.467	7.556	9.071	6.991	6.366	9.463	8.984	9.320	8.752
FeO	11.670	11.674	12.299	11.351	10.810	16.161	16.070	16.452	15.823
MnO	0.321	0.292	0.334	0.283	0.387	0.000	0.294	0.365	0.264
MgO	16.029	15.514	14.465	15.913	15.995	11.664	12.013	11.795	12.199
CaO	11.607	11.856	11.970	12.348	12.059	12.240	11.781	12.102	12.152
Na_2O	0.758	0.828	1.196	0.860	0.799	1.185	1.114	1.392	1.137
K_2O	0.149	0.186	0.244	0.183	0.158	0.156	0.137	0.141	0.000
Cl	0.000	0.000	0.000	0.000	0.088	0.000	0.000	0.000	0.000
Cr_2O_3	0.000	0.000	0.244	0.275	0.282	0.000	0.000	0.000	0.000
Total	97.371	97.639	98.031	98.823	97.739	98.153	98.018	99.126	98.385
Si	7.268	7.107	6.923	7.176	7.291	6.808	6.877	6.808	6.923
Ti	0.000	0.046	0.046	0.023	0.000	0.115	0.115	0.115	0.092
Al^{iv}	1.104	1.288	1.541	1.173	1.081	1.633	1.564	1.610	1.518
Fe^{2+}	1.403	1.403	1.495	1.357	1.288	2.001	1.978	2.024	1.932
Mn	0.046	0.046	0.046	0.023	0.046	0.000	0.046	0.046	0.023
Mg	3.450	3.335	3.128	3.381	3.427	2.553	2.645	2.576	2.668
Ca	1.794	1.840	1.863	1.886	1.863	1.932	1.863	1.909	1.909
Na	0.207	0.230	0.345	0.230	0.230	0.345	0.322	0.391	0.322
K	0.023	0.023	0.046	0.023	0.023	0.023	0.023	0.023	0.000
Cl	0.000	0.000	0.000	0.000	0.023	0.000	0.000	0.000	0.000
Cr^{3+}	0.000	0.000	0.023	0.023	0.023	0.000	0.000	0.000	0.000
Total	15.295	15.318	15.456	15.295	15.295	15.410	15.433	15.502	15.387

Amphibole (Basis of 23 oxygen)

	97-D004-6	97-D004-8	97-D23-1	97-D23-2	97-D23-3	97-D23-4	97-D23-5	97-D23-6	97-D23-8
SiO_2	46.569	46.118	43.129	43.257	43.122	42.659	43.308	42.931	43.009
TiO_2	0.889	1.063	0.935	0.716	0.976	1.013	1.017	0.934	0.855
Al_2O_3	9.764	9.291	10.621	10.229	10.490	10.732	10.630	10.346	10.376
FeO	16.482	16.304	17.956	17.820	17.901	18.444	17.998	17.961	18.211
MnO	0.000	0.000	0.000	0.000	0.444	0.000	0.446	0.372	0.442
MgO	11.660	11.585	10.358	10.156	10.211	10.179	10.161	10.044	9.927
CaO	12.341	12.174	12.250	12.299	12.253	12.200	12.420	12.059	12.100
Na_2O	1.182	1.353	1.494	1.330	1.491	1.502	1.240	1.210	1.386
K_2O	0.131	0.140	0.885	0.829	0.832	0.867	0.929	0.913	0.774
Cl	0.000	0.000	0.000	0.000	0.000	0.000	0.000	0.000	0.000
Cr_2O_3	0.000	0.000	0.000	0.000	0.000	0.000	0.000	0.000	0.000
Total	99.018	98.028	97.629	96.636	97.718	97.597	98.381	97.071	97.081
Si	6.808	6.808	6.532	6.601	6.532	6.486	6.532	6.555	6.555
Ti	0.092	0.115	0.115	0.092	0.115	0.115	0.115	0.115	0.092
Al^{iv}	1.679	1.610	1.886	1.840	1.863	1.909	1.886	1.863	1.863
Fe^{2+}	2.024	2.024	2.277	2.277	2.277	2.346	2.277	2.300	2.323
Mn	0.000	0.000	0.000	0.000	0.046	0.000	0.046	0.046	0.046
Mg	2.530	2.553	2.346	2.300	2.300	2.300	2.277	2.277	2.254
Ca	1.932	1.932	1.978	2.001	1.978	1.978	2.001	1.978	1.978
Na	0.345	0.391	0.437	0.391	0.437	0.437	0.368	0.437	0.414
K	0.023	0.023	0.161	0.161	0.161	0.161	0.184	0.184	0.161
Cl	0.000	0.000	0.000	0.000	0.000	0.000	0.000	0.000	0.000
Cr^{3+}	0.000	0.000	0.000	0.000	0.000	0.000	0.000	0.000	0.000
Total	15.433	15.456	15.732	15.663	15.709	15.732	15.686	15.755	15.686

Amphibole (Basis of 23 oxygen)

	97-D23-9	97-D23-12	97-A001-1	97-A001-3	97-A001-7	97-D373A-3	97-D373A-5	97-D373A-7	97-D373A-8
SiO_2	42.715	43.113	44.094	43.869	44.681	41.156	40.802	41.151	40.787
TiO_2	0.996	0.911	0.922	0.872	0.833	1.334	1.644	1.517	1.609
Al_2O_3	10.590	10.378	9.377	9.534	8.461	11.208	11.329	11.337	11.362
FeO	18.288	17.922	16.865	17.155	16.202	21.181	21.080	21.523	21.181
MnO	0.000	0.356	0.452	0.370	0.330	0.462	0.343	0.395	0.483
MgO	10.133	10.016	11.205	11.028	11.600	7.334	7.304	7.406	7.421
CaO	11.883	12.347	12.261	12.075	12.038	11.868	11.988	11.975	11.697
Na_2O	1.485	1.410	1.254	1.431	1.324	1.241	1.406	1.364	1.432
K_2O	1.005	0.857	0.781	0.823	0.639	1.365	1.437	1.438	1.422
Cl	0.130	0.000	0.000	0.000	0.000	0.000	0.000	0.000	0.000
Cr_2O_3	0.000	0.000	0.000	0.000	0.000	0.000	0.000	0.000	0.000
Total	97.225	97.311	97.212	97.157	96.109	97.149	97.334	98.105	97.395
Si	6.509	6.555	6.670	6.647	6.785	6.394	6.348	6.348	6.325
Ti	0.115	0.115	0.115	0.092	0.092	0.161	0.184	0.184	0.184
Al^{iv}	1.909	1.863	1.679	1.702	1.518	2.047	2.070	2.070	2.070
Fe^{2+}	2.323	2.277	2.139	2.162	2.070	2.760	2.737	2.783	2.760
Mn	0.000	0.046	0.069	0.046	0.046	0.069	0.046	0.046	0.069
Mg	2.300	2.277	2.530	2.484	2.622	1.702	1.702	1.702	1.725
Ca	1.932	2.001	1.978	1.955	1.955	1.978	2.001	1.978	1.955
Na	0.437	0.414	0.368	0.414	0.391	0.368	0.414	0.414	0.437
K	0.184	0.161	0.161	0.161	0.115	0.276	0.276	0.276	0.276
Cl	0.023	0.000	0.000	0.000	0.000	0.000	0.000	0.000	0.000
Cr^{3+}	0.000	0.000	0.000	0.000	0.000	0.000	0.000	0.000	0.000
Total	15.732	15.709	15.709	15.663	15.594	15.755	15.778	15.801	15.801

Amphibole (Basis of 23 oxygen)

	97-D373A-11	97-D373A-12	97-D373A-13	98-D93-47	98-D93-48	98-D93-49	98-D93-50	98-D93-51	98-D93-52
SiO_2	40.845	40.965	41.776	42.384	41.695	42.818	41.814	41.785	42.461
TiO_2	1.640	1.738	1.222	0.957	1.087	1.182	1.101	1.107	0.665
Al_2O_3	11.165	11.361	11.015	10.051	10.390	10.190	10.407	10.296	10.236
FeO	21.261	21.262	21.559	19.801	19.577	19.198	19.587	19.895	20.058
MnO	0.360	0.446	0.384	0.385	0.406	0.384	0.442	0.454	0.467
MgO	7.332	7.393	7.781	9.083	9.120	9.437	9.242	8.778	9.075
CaO	11.883	11.985	11.274	11.975	12.097	12.086	11.920	11.827	12.027
Na_2O	1.527	1.376	1.255	1.249	1.227	1.288	1.511	1.544	1.163
K_2O	1.417	1.500	1.350	1.241	1.425	1.261	1.404	1.408	1.244
Cl	0.000	0.000	0.000	0.000	0.000	0.000	0.000	0.000	0.000
Cr_2O_3	0.000	0.000	0.000	0.000	0.000	0.000	0.000	0.000	0.000
Total	97.430	98.026	97.615	97.127	97.024	97.844	97.429	97.095	97.396
Si	6.348	6.325	6.440	6.532	6.440	6.532	6.440	6.463	6.532
Ti	0.184	0.207	0.138	0.115	0.115	0.138	0.138	0.138	0.069
Al^{iv}	2.047	2.070	2.001	1.817	1.886	1.840	1.886	1.886	1.863
Fe^{2+}	2.760	2.737	2.783	2.553	2.530	2.438	2.530	2.576	2.578
Mn	0.046	0.069	0.046	0.046	0.046	0.046	0.069	0.069	0.069
Mg	1.702	1.702	1.794	2.093	2.093	2.139	2.116	2.024	2.070
Ca	1.978	1.978	1.863	1.978	2.001	1.978	1.978	1.955	1.978
Na	0.460	0.414	0.368	0.368	0.368	0.391	0.460	0.460	0.345
K	0.276	0.299	0.276	0.253	0.276	0.253	0.276	0.276	0.253
Cl	0.000	0.000	0.000	0.000	0.000	0.000	0.000	0.000	0.000
Cr^{3+}	0.000	0.000	0.000	0.000	0.000	0.000	0.000	0.000	0.000
Total	15.801	15.801	15.709	15.755	15.755	15.755	15.893	15.847	15.757

Amphibole (Basis of 23 oxygen)

	98-D93-54	98-D93-55	99-D53-1	99-D53-2	99-D53-3	99-D53-4	99-D53-5	99-D53-6	98-T201-2
SiO_2	41.978	42.231	51.161	49.183	49.953	49.832	49.400	49.889	42.861
TiO_2	1.151	1.094	0.861	0.933	0.690	0.878	0.948	0.988	1.274
Al_2O_3	10.526	10.104	5.954	7.144	7.240	7.167	7.191	7.186	10.802
FeO	19.822	19.456	11.532	11.418	11.794	11.764	11.378	11.635	19.210
MnO	0.511	0.387	0.286	0.000	0.000	0.288	0.000	0.000	0.413
MgO	8.973	9.206	15.447	15.084	15.382	15.117	15.184	15.164	8.332
CaO	11.822	12.001	12.683	12.585	12.366	12.487	12.541	12.702	11.984
Na_2O	1.437	1.346	0.642	0.942	1.132	0.953	0.848	0.775	1.229
K_2O	1.348	1.281	0.276	0.315	0.195	0.309	0.376	0.425	1.092
Cl	0.130	0.000	0.000	0.000	0.000	0.000	0.000	0.000	0.091
Cr_2O_3	0.000	0.000	0.000	0.000	0.000	0.000	0.000	0.000	0.000
Total	97.568	97.106	98.842	97.603	98.754	98.795	97.866	97.763	97.288
Si	6.463	6.509	7.291	7.107	7.130	7.130	7.130	7.130	6.555
Ti	0.138	0.138	0.092	0.092	0.069	0.092	0.092	0.115	0.138
Al^{iv}	1.909	1.840	0.989	1.219	1.219	1.219	1.219	1.219	1.955
Fe^{2+}	2.553	2.507	1.380	1.380	1.403	1.403	1.380	1.380	2.461
Mn	0.069	0.046	0.023	0.000	0.000	0.046	0.000	0.000	0.046
Mg	2.047	2.116	3.289	3.243	3.266	3.220	3.266	3.220	1.909
Ca	1.955	1.978	1.932	1.955	1.886	1.909	1.932	1.955	1.955
Na	0.437	0.391	0.184	0.253	0.322	0.253	0.230	0.207	0.368
K	0.253	0.253	0.046	0.069	0.046	0.046	0.069	0.069	0.207
Cl	0.000	0.000	0.000	0.000	0.000	0.000	0.000	0.000	0.023
Cr^{3+}	0.000	0.000	0.000	0.000	0.000	0.000	0.000	0.000	0.000
Total	15.824	15.778	15.226	15.318	15.341	15.318	15.318	15.295	15.617

Amphibole (Basis of 23 oxygen)

	98-T201-3	98-T201-5	98-T201-6	98-T201-8	98-T201-9	98-T201-10	98-T201-11	98-T201-14	98-T300A-1
SiO_2	42.495	42.376	42.540	42.812	42.330	42.184	42.610	42.883	40.095
TiO_2	1.248	1.311	1.311	1.079	1.155	1.247	1.379	1.198	1.167
Al_2O_3	10.644	10.640	10.670	10.887	10.744	11.143	10.700	10.769	12.140
FeO	19.366	19.704	19.285	20.071	19.695	20.257	20.169	19.475	20.474
MnO	0.351	0.464	0.280	0.000	0.292	0.411	0.462	0.385	0.403
MgO	8.379	8.564	8.552	8.425	8.264	8.233	8.289	8.770	8.382
CaO	11.827	12.096	12.144	11.952	12.036	12.121	12.160	12.331	11.794
Na_2O	1.359	1.235	1.176	1.279	1.206	1.389	1.179	1.200	1.543
K_2O	1.076	1.097	1.063	1.175	1.089	1.241	1.134	1.047	1.706
Cl	0.000	0.099	0.000	0.000	0.000	0.000	0.000	0.000	0.097
Cr_2O_3	0.000	0.000	0.000	0.000	0.000	0.000	0.000	0.000	0.000
Total	97.568	97.586	97.085	97.679	96.811	98.226	98.081	98.058	97.801
Si	6.555	6.486	6.532	6.532	6.532	6.440	6.509	6.509	6.210
Ti	0.138	0.161	0.161	0.115	0.138	0.138	0.161	0.138	0.138
Al^{iv}	1.932	1.932	1.932	1.955	1.955	2.001	1.932	1.932	2.208
Fe^{2+}	2.484	2.530	2.484	2.553	2.530	2.576	2.576	2.484	2.645
Mn	0.046	0.069	0.046	0.000	0.046	0.046	0.069	0.046	0.046
Mg	1.932	1.955	1.955	1.909	1.909	1.863	1.886	1.978	1.932
Ca	1.955	1.978	2.001	1.955	1.978	1.978	1.978	2.001	1.955
Na	0.414	0.368	0.345	0.368	0.368	0.414	0.345	0.345	0.460
K	0.207	0.207	0.207	0.230	0.207	0.253	0.230	0.207	0.345
Cl	0.000	0.023	0.000	0.000	0.000	0.000	0.000	0.000	0.023
Cr^{3+}	0.000	0.000	0.000	0.000	0.000	0.000	0.000	0.000	0.000
Total	15.663	15.709	15.663	15.617	15.663	15.709	15.686	15.640	15.962

Amphibole (Basis of 23 oxygen)

	98-T300A-2	98-T300A-3	98-T300A-4	98-T300A-5	98-T300A-6	98-T300A-7	99-D76-1	99-D76-2	99-D76-3
SiO_2	41.117	40.706	40.351	40.238	40.339	40.166	41.371	41.099	41.107
TiO_2	0.617	1.279	1.156	1.311	1.216	1.311	1.423	1.487	1.420
Al_2O_3	12.293	12.041	11.979	12.133	12.051	12.179	10.339	10.559	10.355
FeO	20.706	20.285	20.341	20.280	20.488	20.518	19.695	19.549	19.462
MnO	0.000	0.342	0.439	0.000	0.299	0.376	0.562	0.608	0.553
MgO	8.095	8.531	8.386	8.345	8.440	8.468	8.863	9.206	9.016
CaO	12.098	11.930	11.835	11.894	11.794	11.795	11.608	11.647	11.368
Na_2O	1.395	1.410	1.514	1.446	1.315	1.641	1.643	1.685	1.553
K_2O	1.508	1.754	1.662	1.644	1.707	1.704	1.397	1.576	1.418
Cl	0.124	0.000	0.092	0.000	0.000	0.091	0.000	0.086	0.096
Cr_2O_3	0.000	0.000	0.000	0.000	0.000	0.000	0.000	0.000	0.000
Total	97.953	98.277	97.756	97.291	97.650	98.248	97.003	97.503	96.349
Si	6.325	6.256	6.233	6.233	6.233	6.187	6.417	6.348	6.417
Ti	0.069	0.138	0.138	0.161	0.138	0.161	0.161	0.184	0.161
Al^{iv}	2.231	2.185	2.185	2.208	2.185	2.208	1.886	1.932	1.909
Fe^{2+}	2.668	2.599	2.622	2.622	2.645	2.645	2.553	2.530	2.530
Mn	0.000	0.046	0.069	0.000	0.046	0.046	0.069	0.069	0.069
Mg	1.863	1.955	1.932	1.932	1.955	1.955	2.047	2.116	2.093
Ca	2.001	1.955	1.955	1.978	1.955	1.955	1.932	1.932	1.909
Na	0.414	0.414	0.460	0.437	0.395	0.483	0.483	0.506	0.460
K	0.299	0.345	0.322	0.322	0.345	0.345	0.276	0.322	0.276
Cl	0.023	0.000	0.023	0.000	0.000	0.023	0.023	0.023	0.023
Cr^{3+}	0.000	0.000	0.000	0.000	0.000	0.000	0.000	0.000	0.000
Total	15.893	15.893	15.939	15.893	15.897	16.008	15.847	15.962	15.847

Amphibole (Basis of 23 oxygen)

	99-D76-4	99-D76-5	99-D76-6	99-D76-10	99-D76-11	99-D76-12	99-D76-13	99-D76-14	98-T223-1
SiO_2	41.460	41.470	41.395	41.489	41.130	41.070	41.360	41.125	40.664
TiO_2	1.490	1.242	1.136	1.378	1.204	1.400	1.190	1.274	1.036
Al_2O_3	10.600	10.591	10.369	10.208	10.185	10.210	10.310	10.182	11.176
FeO	19.100	19.709	19.034	19.249	19.359	19.580	19.870	19.835	20.781
MnO	0.620	0.516	0.557	0.507	0.550	0.710	0.630	0.592	0.503
MgO	9.230	9.113	9.076	9.231	8.997	8.930	8.930	8.787	8.035
CaO	11.760	11.654	11.721	11.693	11.747	11.430	11.660	11.649	11.850
Na_2O	1.700	1.374	1.566	1.552	1.446	1.630	1.480	1.434	1.618
K_2O	1.440	1.347	1.289	1.312	1.381	1.470	1.360	1.381	1.554
Cl	0.050	0.118	0.000	0.000	0.000	0.080	0.090	0.119	0.108
Cr_2O_3	0.020	0.000	0.000	0.000	0.000	0.000	0.000	0.000	0.000
Total	00.000	97.134	96.143	96.620	95.998	96.750	97.130	96.378	97.324
Si	0.000	6.417	6.440	6.440	6.440	0.000	0.000	6.440	6.325
Ti	0.000	0.138	0.138	0.161	0.138	0.000	0.000	0.161	0.115
Al^{iv}	0.000	1.932	1.909	1.863	1.886	0.000	0.000	1.886	2.047
Fe^{2+}	0.000	2.553	2.484	2.507	2.530	0.000	0.000	2.599	2.714
Mn	0.000	0.069	0.069	0.069	0.069	0.000	0.000	0.069	0.069
Mg	0.000	2.093	2.116	2.139	2.093	0.000	0.000	2.047	1.863
Ca	0.003	1.932	1.955	1.955	1.978	0.000	0.000	1.955	1.978
Na	0.000	0.414	0.483	0.460	0.437	0.000	0.000	0.437	0.483
K	0.000	0.276	0.253	0.253	0.276	0.000	0.000	0.276	0.299
Cl	0.000	0.023	0.000	0.000	0.000	0.000	0.000	0.023	0.023
Cr^{3+}	0.000	0.000	0.000	0.000	0.000	0.000	0.000	0.000	0.000
Total	00.000	15.847	15.847	15.847	15.847	00.000	00.000	15.893	15.916

Amphibole (Basis of 23 oxygen)

	98-T223-2	98-T223-3	98-T223-4	98-T223-5	98-T223-6	99-T62B-1	99-T62B-2	99-T62B-7	99-T62B-8
SiO_2	41.168	41.210	41.168	40.232	40.884	43.455	43.264	43.072	44.683
TiO_2	1.605	1.381	1.128	1.128	1.138	0.973	0.702	1.358	0.779
Al_2O_3	10.810	10.713	10.929	11.375	11.340	10.076	9.901	9.810	9.818
FeO	20.881	20.725	20.705	21.272	21.011	19.472	18.594	19.191	18.598
MnO	0.381	0.500	0.411	0.419	0.421	0.387	0.440	0.376	0.411
MgO	8.561	8.189	8.251	8.232	8.416	9.999	10.012	9.810	10.454
CaO	11.961	11.750	11.931	11.890	12.090	11.933	11.899	11.860	11.564
Na_2O	1.608	1.512	1.523	1.507	1.591	1.310	1.277	1.401	1.464
K_2O	1.483	1.442	1.504	1.620	1.560	1.153	1.099	1.261	1.109
Cl	0.099	0.117	0.113	0.103	0.102	0.110	0.000	0.144	0.109
Cr_2O_3	0.000	0.000	0.000	0.000	0.000	0.000	0.000	0.000	0.000
Total	98.556	97.539	97.663	97.778	98.554	98.868	97.189	98.284	98.988
Si	6.325	6.394	6.371	6.256	6.279	6.555	6.601	6.532	6.670
Ti	0.184	0.161	0.138	0.138	0.138	0.115	0.092	0.161	0.092
Al^{iv}	1.955	1.955	2.001	2.098	2.047	1.794	1.771	1.748	1.725
Fe^{2+}	2.691	2.691	2.691	2.760	2.714	2.461	2.369	2.438	2.323
Mn	0.046	0.069	0.046	0.046	0.046	0.046	0.046	0.046	0.046
Mg	1.955	1.886	1.909	1.909	1.932	2.254	2.277	2.231	2.323
Ca	1.978	1.955	1.978	1.978	2.001	1.932	1.955	1.932	1.863
Na	0.483	0.460	0.460	0.460	0.483	0.391	0.368	0.414	0.414
K	0.299	0.276	0.299	0.322	0.299	0.230	0.207	0.253	0.207
Cl	0.023	0.023	0.023	0.023	0.023	0.023	0.000	0.046	0.023
Cr^{3+}	0.000	0.000	0.000	0.000	0.000	0.000	0.000	0.000	0.000
Total	15.939	15.870	15.916	15.990	15.962	15.801	15.686	15.801	15.686

Amphibole (Basis of 23 oxygen)

	99-T62B-12	99-T62B-13	99-T62B-16	99-T62B-17	99-T63-2	99-T63-7	99-T63-8	99-T63-9	99-T63-12
SiO_2	43.714	43.576	44.195	42.127	40.265	40.621	39.910	40.752	41.207
TiO_2	1.293	1.006	1.268	0.594	0.657	1.323	1.479	1.251	0.871
Al_2O_3	9.233	10.031	9.199	10.735	10.558	9.800	9.991	9.253	9.287
FeO	18.425	18.855	18.559	19.289	27.044	27.709	27.683	28.149	26.621
MnO	0.448	0.354	0.473	0.434	1.135	1.280	1.138	1.249	1.088
MgO	10.377	9.981	10.526	9.499	4.262	3.866	3.842	3.827	4.281
CaO	11.835	11.789	11.783	11.765	11.507	10.858	10.900	10.995	11.252
Na_2O	1.346	1.490	1.479	1.471	1.594	1.680	1.746	1.566	1.743
K_2O	1.235	1.199	1.075	1.330	1.473	1.518	1.469	1.398	1.410
Cl	0.127	0.111	0.000	0.133	0.000	0.165	0.184	0.158	0.127
Cr_2O_3	0.000	0.000	0.000	0.000	0.000	0.000	0.000	0.000	0.000
Total	98.032	98.391	98.556	97.377	98.495	98.821	98.340	98.598	97.887
Si	6.624	6.578	6.647	6.463	6.394	6.463	6.371	6.509	6.550
Ti	0.138	0.115	0.138	0.069	0.069	0.161	0.184	0.161	0.115
Al^{iv}	1.656	1.794	1.633	1.955	1.978	1.840	1.886	1.748	1.748
Fe^{2+}	2.346	2.392	2.323	2.484	3.588	3.680	3.703	3.749	3.542
Mn	0.046	0.046	0.069	0.046	0.161	0.161	0.161	0.161	0.138
Mg	2.346	2.254	2.369	2.185	1.012	0.920	0.920	0.920	1.012
Ca	1.932	1.909	1.909	1.932	1.955	1.840	1.863	1.886	1.932
Na	0.391	0.437	0.437	0.437	0.483	0.506	0.552	0.483	0.529
K	0.230	0.230	0.207	0.253	0.299	0.299	0.299	0.276	0.276
Cl	0.023	0.023	0.000	0.046	0.000	0.046	0.046	0.046	0.023
Cr^{3+}	0.000	0.000	0.000	0.000	0.000	0.000	0.000	0.000	0.000
Total	15.732	15.778	15.732	15.870	15.939	15.916	15.985	15.939	15.865

Amphibole (Basis of 23 oxygen)

	99-T63-13	99-D214-1	99-D214-5	99-D214-7	99-D214-8	99-D214-9	99-D214-10	99-D214-11	99-D162-1
SiO_2	40.306	42.558	43.508	42.076	41.470	42.917	41.649	43.238	44.609
TiO_2	1.273	0.648	0.729	0.803	0.670	0.627	0.553	0.648	1.162
Al_2O_3	9.642	11.282	10.697	11.544	13.063	11.193	12.386	10.408	8.846
FeO	27.880	19.334	18.590	18.161	18.080	18.160	19.430	19.148	17.190
MnO	1.204	0.838	0.851	0.848	0.719	0.768	0.951	0.765	0.411
MgO	4.006	9.094	9.552	8.991	8.729	9.359	8.274	9.121	11.482
CaO	11.003	11.889	11.723	11.766	11.983	11.754	11.877	11.903	12.108
Na_2O	1.621	1.221	1.324	1.316	1.423	1.206	1.299	1.171	1.248
K_2O	1.556	0.823	0.619	0.826	0.839	0.597	0.787	0.691	1.032
Cl	0.176	0.201	0.150	0.184	0.191	0.131	0.209	0.155	0.000
Cr_2O_3	0.000	0.000	0.000	0.272	0.403	0.289	0.000	0.270	0.000
Total	98.667	97.889	97.744	97.778	98.554	97.001	97.414	97.518	98.118
Si	6.417	6.486	6.601	6.463	6.325	6.555	6.394	6.601	6.693
Ti	0.161	0.069	0.092	0.092	0.069	0.069	0.069	0.069	0.138
Al^{iv}	1.817	2.024	1.909	2.093	2.346	2.001	2.231	1.863	1.564
Fe^{2+}	3.726	2.461	2.346	2.323	2.300	2.323	2.484	2.438	2.162
Mn	0.161	0.115	0.115	0.115	0.092	0.092	0.115	0.092	0.046
Mg	0.943	2.070	2.162	2.047	1.978	2.116	1.886	2.070	2.576
Ca	1.886	1.932	1.909	1.932	1.955	1.909	1.955	1.955	1.932
Na	0.506	0.368	0.391	0.391	0.414	0.368	0.391	0.345	0.368
K	0.322	0.161	0.115	0.161	0.161	0.115	0.161	0.138	0.207
Cl	0.046	0.046	0.046	0.046	0.046	0.023	0.046	0.046	0.000
Cr^{3+}	0.000	0.000	0.000	0.023	0.046	0.046	0.000	0.023	0.000
Total	15.985	15.732	15.686	15.686	15.732	15.617	15.732	15.640	15.686

Amphibole (Basis of 23 oxygen)

	99-D162-2	99-D162-4	99-D162-5	99-D162-6	99-D162-9	99-D162-10	99-D162-11	99-D162-12	99-D87B-2
SiO_2	45.984	44.399	45.190	45.904	45.654	46.694	45.097	45.709	45.337
TiO_2	1.093	1.421	1.212	0.678	1.036	0.661	1.045	1.135	0.000
Al_2O_3	8.121	9.199	8.624	7.960	8.674	7.883	8.750	8.192	11.902
FeO	16.353	17.623	17.031	17.027	16.513	15.753	16.628	16.312	11.355
MnO	0.398	0.407	0.462	0.418	0.455	0.378	0.394	0.399	0.305
MgO	11.975	11.145	11.442	11.825	12.004	12.729	11.736	11.756	15.004
CaO	12.155	11.981	12.059	12.242	12.089	12.209	11.994	12.112	11.622
Na_2O	1.359	1.395	1.424	1.243	1.317	1.156	1.383	1.294	2.130
K_2O	0.885	1.047	0.911	0.707	0.896	0.767	1.001	0.928	0.278
Cl	0.000	0.000	0.000	0.000	0.000	0.000	0.000	0.000	0.000
Cr_2O_3	0.000	0.000	0.000	0.000	0.000	0.000	0.000	0.000	0.000
					SO_4 0.330				
Total	98.322	98.617	98.356	98.004	98.968	98.230	98.027	97.836	97.932
Si	6.831	6.647	6.739	6.854	6.739	6.900	6.739	6.831	6.578
Ti	0.115	0.161	0.138	0.069	0.115	0.069	0.115	0.138	0.000
Al^{iv}	1.426	1.633	1.518	1.403	1.518	1.380	1.541	1.449	2.024
Fe^{2+}	2.024	2.208	2.116	2.139	2.047	1.955	2.070	2.047	1.380
Mn	0.046	0.046	0.069	0.046	0.046	0.046	0.046	0.046	0.046
Mg	2.645	2.484	2.553	2.645	2.645	2.806	2.622	2.622	3.243
Ca	1.932	1.909	1.932	1.955	1.909	1.932	1.932	1.932	1.817
Na	0.391	0.414	0.414	0.368	0.368	0.322	0.391	0.368	0.598
K	0.161	0.207	0.184	0.138	0.161	0.138	0.184	0.184	0.046
Cl	0.000	0.000	0.000	0.000	0.000	0.000	0.000	0.000	0.000
Cr^{3+}	0.000	0.000	0.000	0.000	0.000	0.000	0.000	0.000	0.000
					S 0.023				
Total	15.571	15.709	15.663	15.617	15.571	15.548	15.640	15.617	15.732

Amphibole (Basis of 23 oxygen)

	99-D87B-7	99-D87B-8	99-D87B-9	99-D87B-10	99-D87B-11	99-D87B-12	99-D87B-14	99-D87B-15	99-D87B-16
SiO_2	45.753	49.215	47.318	46.988	46.443	46.735	46.143	47.998	45.153
TiO_2	0.000	0.000	0.000	0.000	0.000	0.000	0.000	0.000	0.000
Al_2O_3	11.930	8.929	11.030	11.030	11.732	11.229	11.148	9.285	11.464
FeO	11.139	9.738	10.917	10.917	11.451	18.126	11.279	10.378	11.178
MnO	0.000	0.000	0.000	0.000	0.000	0.000	0.000	0.000	0.000
MgO	15.148	16.693	15.416	15.416	15.049	15.167	14.902	15.972	14.711
CaO	11.751	12.143	11.692	11.692	11.515	11.824	11.172	11.944	11.237
Na_2O	2.195	1.330	1.982	1.982	2.070	1.839	1.968	1.580	2.691
K_2O	0.303	0.189	0.217	0.217	0.217	0.302	0.275	0.206	0.503
Cl	0.000	0.000	0.000	0.000	0.000	0.000	0.000	0.000	0.226
Cr_2O_3	0.000	0.000	0.000	0.000	0.000	0.000	0.000	0.000	0.000
Total	98.219	98.237	98.724	98.242	98.533	98.223	96.888	97.363	97.163
Si	6.601	6.992	6.762	6.739	6.670	6.716	6.739	6.923	6.624
Ti	0.000	0.000	0.000	0.000	0.000	0.000	0.000	0.000	0.000
Al^{iv}	2.024	1.495	1.886	1.863	1.978	1.909	1.909	1.587	1.978
Fe^{2+}	1.344	1.150	1.288	1.311	1.380	1.334	1.380	1.242	1.380
Mn	0.000	0.000	0.000	0.000	0.000	0.000	0.000	0.000	0.000
Mg	3.266	3.542	3.312	3.289	3.220	3.243	3.243	3.427	3.220
Ca	1.817	1.840	1.794	1.794	1.771	1.817	1.748	1.840	1.771
Na	0.621	0.368	0.529	0.552	0.575	0.506	0.552	0.437	0.759
K	0.046	0.023	0.046	0.046	0.046	0.046	0.046	0.046	0.092
Cl	0.000	0.000	0.000	0.000	0.000	0.000	0.000	0.000	0.046
Cr^{3+}	0.000	0.000	0.000	0.000	0.000	0.000	0.000	0.000	0.000
Total	15.709	15.410	15.617	15.594	15.640	15.571	15.617	15.502	15.870

Amphibole (Basis of 23 oxygen)

	99-D87B-17	99-D87B-18	99-D87B-19	99-D87B-20	99-D87B-21	99-D87B-22	99-D87B-23	99-D87B-24	99-D87B-25
SiO_2	45.130	44.822	44.283	43.561	43.639	44.112	44.312	43.683	44.030
TiO_2	0.000	0.000	0.000	0.000	0.000	0.000	0.000	0.000	0.000
Al_2O_3	12.441	12.742	14.049	13.992	14.401	13.870	13.769	14.833	14.490
FeO	11.061	11.237	11.850	11.823	12.029	11.390	11.940	11.516	11.737
MnO	0.000	0.000	0.000	0.000	0.000	0.255	0.000	0.000	0.000
MgO	14.532	14.299	13.641	13.107	13.063	13.253	13.174	13.009	12.882
CaO	11.644	11.665	11.585	11.702	11.674	11.636	11.662	11.822	11.803
Na_2O	2.175	2.111	2.220	2.341	2.248	2.119	2.073	2.036	2.075
K_2O	0.353	0.340	0.342	0.406	0.413	0.340	0.398	0.318	0.257
Cl	0.000	0.000	0.000	0.000	0.000	0.000	0.000	0.000	0.000
Cr_2O_3	0.000	0.000	0.000	0.000	0.000	0.000	0.000	0.000	0.000
Total	97.336	97.217	97.969	96.933	97.467	96.976	97.329	97.216	97.274
Si	6.578	6.532	6.440	6.417	6.394	6.463	6.486	6.371	6.440
Ti	0.000	0.000	0.000	0.000	0.000	0.000	0.000	0.000	0.000
Al^{iv}	2.139	2.185	2.415	2.415	2.484	2.392	2.369	2.553	2.484
Fe^{2+}	1.357	1.380	1.449	1.449	1.472	1.403	1.449	1.403	1.426
Mn	0.000	0.000	0.000	0.000	0.000	0.023	0.000	0.000	0.000
Mg	3.151	3.105	2.944	2.875	2.852	2.898	2.875	2.829	2.806
Ca	1.817	1.817	1.794	1.840	1.840	1.817	1.817	1.840	1.840
Na	0.621	0.598	0.621	0.667	0.644	0.598	0.598	0.575	0.598
K	0.069	0.069	0.069	0.069	0.069	0.069	0.069	0.069	0.046
Cl	0.000	0.000	0.000	0.000	0.000	0.000	0.000	0.000	0.000
Cr^{3+}	0.000	0.000	0.000	0.000	0.000	0.000	0.000	0.000	0.000
Total	15.732	15.686	15.732	15.732	15.755	15.663	15.663	15.640	15.640

Amphibole (Basis of 23 oxygen)

	99-D87B-26	99-D87B-27	99-D89A-28	99-D89A-29	99-D89A-30	99-D89A-31	99-D89A-32	99-D89A-33	99-D89A-34
SiO_2	43.713	44.332	50.168	50.129	51.082	51.748	49.047	51.204	49.290
TiO_2	0.000	0.000	0.000	0.298	0.305	0.000	0.000	0.323	0.000
Al_2O_3	14.607	13.516	6.768	7.137	6.206	5.626	7.548	6.139	7.422
FeO	11.841	11.701	12.135	11.936	11.517	11.553	12.276	11.423	12.174
MnO	0.000	0.000	0.435	0.323	0.000	0.330	0.000	0.000	0.000
MgO	12.901	13.001	15.071	15.050	15.488	16.031	14.533	15.675	14.634
CaO	11.627	11.864	12.644	12.720	12.576	12.984	12.691	12.672	12.593
Na_2O	2.330	2.040	0.762	0.805	0.627	0.684	0.911	0.695	0.777
K_2O	0.340	0.308	0.439	0.363	0.385	0.281	0.541	0.316	0.509
Cl	0.000	0.000	0.000	0.000	0.000	0.000	0.000	0.000	0.000
Cr_2O_3	0.000	0.000	0.000	0.000	0.000	0.000	0.000	0.000	0.000
Total	97.359	96.763	98.421	98.761	98.186	99.238	97.548	98.447	97.397
Si	6.394	6.509	7.222	7.176	7.314	7.337	7.130	7.314	7.153
Ti	0.000	0.000	0.000	0.023	0.023	0.000	0.000	0.046	0.000
Al^{iv}	2.507	2.346	1.150	1.196	1.058	0.943	1.288	1.035	1.265
Fe^{2+}	1.449	1.426	1.449	1.426	1.380	1.380	1.495	1.357	1.472
Mn	0.000	0.000	0.046	0.046	0.000	0.046	0.000	0.000	0.000
Mg	2.806	2.852	3.243	3.220	3.312	3.381	3.151	3.335	3.174
Ca	1.817	1.863	1.955	1.955	1.932	1.978	1.978	1.932	1.955
Na	0.667	0.575	0.207	0.230	0.184	0.184	0.253	0.184	0.230
K	0.069	0.069	0.092	0.069	0.069	0.046	0.092	0.069	0.092
Cl	0.000	0.000	0.000	0.000	0.000	0.000	0.000	0.000	0.000
Cr^{3+}	0.000	0.000	0.000	0.000	0.000	0.000	0.000	0.000	0.000
Total	15.709	15.640	15.364	15.341	15.272	15.295	15.387	15.272	15.341

Amphibole (Basis of 23 oxygen)

	99-D89A-35	99-D89A-36	99-D89A-37	99-D89A-38	99-D89A-39	99-D89A-41	98-T300B-1	98-T300B-3	98-T300B-4
SiO_2	49.433	50.550	50.754	49.155	50.520	50.390	40.888	41.162	41.469
TiO_2	0.385	0.000	0.000	0.000	0.286	0.000	1.355	1.493	1.414
Al_2O_3	7.358	6.690	6.460	7.606	6.866	6.738	10.466	10.501	10.268
FeO	12.193	11.928	11.981	12.420	12.374	12.288	19.818	20.214	19.992
MnO	0.000	0.277	0.000	0.278	0.334	0.000	0.506	0.315	0.455
MgO	14.775	15.262	15.477	14.637	15.111	15.260	8.309	8.781	8.499
CaO	12.470	12.742	12.800	12.613	12.719	12.461	11.774	11.866	11.821
Na_2O	0.740	0.952	0.979	0.957	0.854	0.650	1.382	1.389	1.159
K_2O	0.515	0.408	0.414	0.620	0.415	0.522	1.441	1.513	1.497
Cl	0.000	0.000	0.000	0.000	0.000	0.000	0.099	0.109	0.095
Cr_2O_3	0.000	0.000	0.000	0.000	0.000	0.000	0.000	0.000	0.000
Total	97.870	98.809	98.866	98.285	99.478	98.309	96.037	97.345	96.670
Si	7.153	7.245	7.245	7.107	7.199	7.245	6.417	6.371	6.463
Ti	0.046	0.000	0.000	0.000	0.023	0.000	0.161	0.184	0.161
Al^{iv}	1.265	1.127	1.081	1.288	1.150	1.150	1.932	1.909	1.886
Fe^{2+}	1.472	1.426	1.426	1.495	1.472	1.472	2.599	2.622	2.599
Mn	0.000	0.023	0.000	0.023	0.046	0.000	0.069	0.046	0.069
Mg	3.174	3.266	3.289	3.151	3.197	3.266	1.932	2.024	1.978
Ca	1.932	1.955	1.955	1.955	1.932	1.909	1.978	1.978	1.978
Na	0.207	0.253	0.276	0.276	0.230	0.184	0.414	0.414	0.345
K	0.092	0.069	0.069	0.115	0.069	0.092	0.299	0.299	0.299
Cl	0.000	0.000	0.000	0.000	0.000	0.000	0.023	0.023	0.023
Cr^{3+}	0.000	0.000	0.000	0.000	0.000	0.000	0.000	0.000	0.000
Total	15.341	15.364	15.341	15.410	15.318	15.318	15.824	15.870	15.801

Amphibole (Basis of 23 oxygen)

	98-T300B-8	98-T300B-11	98-T300B-14	98-T300B-15	98-T300B-16	98-T300B-18	98-T300B-20	98-T300B-21	99-D103-26
SiO_2	41.022	40.424	41.312	41.022	40.459	40.729	41.006	40.278	43.986
TiO_2	1.065	1.275	1.284	1.294	1.538	1.361	1.156	1.386	0.969
Al_2O_3	10.695	10.269	10.858	10.948	10.715	10.711	10.549	10.125	8.535
FeO	19.738	18.767	20.239	20.073	20.314	20.015	20.727	18.926	19.507
MnO	0.514	0.544	0.605	0.539	0.464	0.519	0.463	0.507	0.788
MgO	8.295	8.571	8.525	8.170	8.180	8.589	8.519	8.372	9.974
CaO	11.583	11.332	11.632	11.682	11.574	11.937	11.739	11.368	11.999
Na_2O	1.407	1.343	1.354	1.524	1.632	1.405	1.550	1.356	1.451
K_2O	1.377	1.423	1.563	1.511	1.491	1.454	1.483	1.436	1.111
Cl	0.088	0.103	0.096	0.156	0.096	0.091	0.000	0.103	0.000
Cr_2O_3	0.000	0.000	0.000	0.000	0.000	0.000	0.000	0.000	0.000
Total	95.783	94.049	97.468	96.919	96.464	96.811	97.192	93.856	98.320
Si	6.440	6.440	6.394	6.394	6.348	6.348	6.371	6.440	6.693
Ti	0.115	0.161	0.138	0.161	0.184	0.161	0.138	0.161	0.115
Al^{iv}	1.978	1.932	1.978	2.001	1.978	1.978	1.932	1.909	1.518
Fe^{2+}	2.599	2.507	2.622	2.622	2.668	2.599	2.691	2.530	2.484
Mn	0.069	0.069	0.069	0.069	0.069	0.069	0.069	0.069	0.092
Mg	1.932	2.047	1.955	1.886	1.909	2.001	1.978	2.001	2.254
Ca	1.955	1.932	1.932	1.955	1.955	2.001	1.955	1.955	1.955
Na	0.437	0.414	0.414	0.460	0.506	0.414	0.460	0.414	0.437
K	0.276	0.299	0.299	0.299	0.299	0.299	0.299	0.299	0.207
Cl	0.023	0.023	0.023	0.046	0.023	0.023	0.000	0.023	0.000
Cr^{3+}	0.000	0.000	0.000	0.000	0.000	0.000	0.000	0.000	0.000
Total	15.824	15.824	15.824	15.893	15.939	15.893	15.893	15.801	15.755

Amphibole (Basis of 23 oxygen)

	99-D103-29	99-D103-35	99-D103-37	99-D103-38	99-D103-39	99-D103-40	99-D103-45	99-D103-46	99-D103-48
SiO_2	43.468	42.263	45.578	45.002	42.604	42.823	43.346	42.276	42.742
TiO_2	0.627	0.864	0.888	0.979	0.951	0.996	1.124	0.689	0.838
Al_2O_3	8.294	10.511	7.172	7.592	9.794	9.581	9.124	10.246	9.516
FeO	18.896	20.934	18.281	18.937	20.309	20.398	20.179	20.535	20.090
MnO	0.898	1.032	0.942	0.843	0.976	0.898	0.766	0.824	0.744
MgO	10.940	8.820	10.536	10.250	9.026	9.223	9.383	9.185	8.956
CaO	10.792	12.077	12.385	12.159	11.964	11.874	11.765	12.066	11.980
Na_2O	1.342	1.777	1.381	1.345	1.718	1.768	1.774	1.522	1.547
K_2O	0.983	1.442	0.760	0.965	1.398	1.312	1.246	1.371	1.291
Cl	0.000	0.104	0.092	0.000	0.117	0.139	0.121	0.160	0.120
Cr_2O_3	0.000	0.000	0.000	0.000	0.000	0.000	0.000	0.000	0.000
Total	96.241	99.824	98.015	98.072	98.858	99.014	98.828	98.874	97.823
Si	6.716	6.417	6.900	6.831	6.509	6.532	6.601	6.463	6.578
Ti	0.069	0.092	0.092	0.115	0.115	0.115	0.138	0.069	0.092
Al^{iv}	1.518	1.886	1.288	1.357	1.771	1.725	1.633	1.840	1.725
Fe^{2+}	2.438	2.668	2.323	2.392	2.599	2.599	2.576	2.622	2.576
Mn	0.115	0.138	0.115	0.115	0.115	0.115	0.092	0.115	0.092
Mg	2.530	2.001	2.369	2.323	2.047	2.093	2.139	2.093	2.047
Ca	1.794	1.955	2.001	1.978	1.955	1.932	1.909	1.978	1.978
Na	0.391	0.529	0.414	0.391	0.506	0.529	0.529	0.460	0.460
K	0.184	0.276	0.138	0.184	0.276	0.253	0.253	0.276	0.253
Cl	0.000	0.023	0.023	0.000	0.023	0.046	0.023	0.046	0.023
Cr^{3+}	0.000	0.000	0.000	0.000	0.000	0.000	0.000	0.000	0.000
Total	15.755	15.985	15.663	15.686	15.916	15.939	15.893	15.962	15.824

Amphibole (Basis of 23 oxygen)

	99-D103-49	99-D103-50	99-D103-51	99-D103-52	99-D103-53	99-D103-55
SiO_2	42.167	44.459	43.008	42.967	43.700	43.594
TiO_2	1.199	0.991	0.971	0.879	0.832	0.852
Al_2O_3	9.634	8.063	8.932	8.868	8.629	9.060
FeO	19.663	19.167	19.655	21.783	19.854	19.756
MnO	0.827	0.790	0.821	0.818	0.825	0.829
MgO	9.013	10.354	9.565	7.948	9.822	9.679
CaO	11.780	11.932	11.884	11.748	12.058	11.887
Na_2O	1.756	1.506	1.703	1.604	1.546	1.722
K_2O	1.368	0.991	1.208	1.205	1.102	1.220
Cl	0.108	0.000	0.116	0.115	0.000	0.000
Cr_2O_3	0.000	0.000	0.000	0.000	0.000	0.000
Total	97.514	98.253	97.862	97.937	98.368	98.601
Si	6.509	6.739	6.601	6.647	6.647	6.624
Ti	0.138	0.115	0.115	0.092	0.092	0.092
Al^{iv}	1.748	1.449	1.610	1.610	1.541	1.633
Fe^{2+}	2.530	2.438	2.530	2.829	2.530	2.507
Mn	0.115	0.092	0.115	0.115	0.115	0.115
Mg	2.070	2.346	2.185	1.840	2.231	2.185
Ca	1.955	1.932	1.955	1.955	1.978	1.932
Na	0.529	0.437	0.506	0.483	0.460	0.506
K	0.276	0.184	0.230	0.230	0.207	0.230
Cl	0.023	0.000	0.023	0.023	0.000	0.000
Cr^{3+}	0.000	0.000	0.000	0.000	0.000	0.000
Total	15.893	15.732	15.870	15.824	15.801	15.824

Muscovite

	97-D222-3B	97-D222-4B	97-D222-5B	97-D222-6B	97-D222-11B	97-D222-12B	97-D31-1	97-D31-2	97-D31-3
SiO_2	46.111	45.839	45.762	45.678	45.815	45.565	47.488	49.332	48.344
TiO_2	1.002	0.857	0.870	0.801	0.896	0.876	1.540	0.874	0.843
Al_2O_3	33.137	33.083	33.033	32.886	32.895	32.719	30.948	32.752	32.075
FeO	4.069	4.440	4.342	4.306	4.378	4.193	4.704	4.607	4.863
MgO	0.867	0.871	0.858	0.847	0.984	0.927	1.247	1.356	1.368
Na_2O	0.394	0.493	0.439	0.419	0.501	0.445	0.285	0.000	0.238
K_2O	11.045	11.072	11.207	10.835	10.938	11.065	7.562	8.187	8.446
BaO	0.000	0.000	0.000	0.000	0.000	0.000	0.000	0.000	0.000
Total	96.625	96.656	96.511	95.771	96.407	95.790	93.774	97.109	96.176

	97-D31-5	97-D31-6	97-D26A-3B	97-D26A-5B	97-D26A-6B	97-D26A-7B	97-D26A-9B	97-D26A-12B	97-D26A-13B
SiO_2	46.314	46.628	45.463	45.654	45.603	45.467	45.163	45.022	45.500
TiO_2	0.921	1.106	0.588	0.608	0.648	0.651	0.513	0.578	0.415
Al_2O_3	30.480	31.927	33.514	33.549	33.467	32.865	33.181	32.853	34.096
FeO	5.013	3.892	3.470	3.564	3.559	3.572	4.223	3.567	3.830
MgO	1.264	1.205	0.789	0.790	1.046	0.992	0.870	1.002	0.838
Na_2O	0.301	0.277	0.482	0.523	0.512	0.337	0.441	0.473	0.522
K_2O	10.907	11.119	10.726	11.717	10.722	10.485	10.615	10.801	10.844
BaO	0.000	0.000	0.886	0.000	0.000	0.000	0.000	0.000	0.749
Total	95.201	96.155	95.919	95.405	95.556	94.368	95.005	94.296	96.795

Muscovite

	97-D26B-1B	97-D26B-2B	97-D26B-3B	97-D26B-4B	97-D26B-12C	97-D26B-13B	97-D26B-14B	97-D85f-1B	97-D85f-2B
SiO_2	45.728	45.752	46.745	45.865	46.297	46.215	46.563	45.361	46.266
TiO_2	0.748	0.557	0.554	0.719	0.554	0.586	0.699	1.375	0.564
Al_2O_3	32.913	32.925	32.788	33.204	33.470	33.779	33.730	32.931	35.574
FeO	3.904	3.914	3.794	3.887	4.071	3.983	4.118	1.820	1.132
MgO	0.815	0.769	1.132	0.887	0.976	0.994	0.969	1.038	0.813
Na_2O	0.590	0.362	0.466	0.439	0.487	0.612	0.556	0.470	0.442
K_2O	10.639	10.583	11.169	10.876	10.988	10.929	10.914	10.723	10.961
BaO	0.000	0.000	0.000	0.000	0.000	0.000	0.000	0.000	0.000
Total	95.337	94.862	96.649	95.877	96.842	97.097	97.549	93.719	95.752

	97-D85f-3B	97-D85f-5B	97-D85f-6A	97-D85f-7B	97-D85f-10B	97-D85c-4	97-D85c-5	97-D85c-6
SiO_2	45.870	46.510	46.106	45.664	46.432	45.860	45.613	45.861
TiO_2	0.369	0.666	0.655	0.688	0.548	0.743	0.662	0.553
Al_2O_3	35.048	34.949	35.564	35.002	34.692	35.381	35.006	35.508
FeO	1.335	1.204	1.250	1.248	1.184	1.307	1.378	1.084
MgO	0.766	0.902	0.795	0.888	0.834	0.850	0.879	0.727
Na_2O	0.463	0.339	0.555	0.526	0.410	0.355	0.238	0.287
K_2O	10.434	11.099	10.676	11.048	11.114	8.452	8.533	7.965
BaO	0.000	0.000	0.000	0.000	0.000	0.000	0.000	0.000
Total	94.285	95.670	95.601	95.066	95.213	92.948	92.309	91.986

K-feldspar

	97-D85f-11	97-D85f-13	97-D85f-14	98-T300B-6	98-T300B-7	98-T300B-9	98-T300B-10	98-T300B-13
SiO_2	64.705	65.253	64.560	63.359	64.064	63.449	63.472	63.856
Al_2O_3	19.284	19.236	19.249	18.262	18.540	18.485	18.374	18.423
Na_2O	1.072	1.172	1.010	1.258	1.307	1.183	1.151	1.198
K_2O	13.669	14.525	14.577	14.947	15.039	14.775	14.951	15.018
BaO	0.748	0.887	0.790	1.137	0.990	1.398	1.170	1.092
Total	99.478	101.073	100.186	98.964	99.940	99.290	99.118	99.587

	98-T300B-17	98-T300B-19	98-T300B-22	99-D76-5	99-D76-7	99-D76-8	99-D76-9	99-D76-10
SiO_2	64.063	63.027	63.106	63.481	63.530	63.430	63.468	63.396
Al_2O_3	18.402	17.988	18.177	18.548	18.650	18.440	18.477	18.913
Na_2O	1.044	1.068	1.241	1.069	1.090	1.120	1.331	1.165
K_2O	15.234	15.306	15.042	14.643	15.020	14.970	14.448	15.039
BaO	1.121	0.898	1.007	1.130	1.010	0.980	1.221	1.191
Total	99.864	98.288	98.574	98.870	99.440	99.310	98.946	99.704

	98-T223-15	98-T223-17	98-T223-19	98-T63-4	98-T63-5	98-T63-6	98-T63-10	98-T63-11
SiO_2	63.782	63.988	63.707	64.516	64.684	64.419	64.617	64.923
Al_2O_3	19.110	19.111	18.892	18.881	18.775	18.533	18.781	18.639
Na_2O	1.091	0.493	0.874	0.785	0.765	1.024	0.837	0.822
K_2O	13.930	14.774	14.143	15.150	15.610	15.130	15.458	15.684
BaO	1.809	1.930	2.033	0.872	0.791	0.870	0.876	0.779
Total	99.723	100.297	99.649	100.204	100.625	99.976	100.568	100.847

	99-D103-23	99-D103-24	99-D103-25	99-D103-31	99-D103-32	99-D103-33	99-D103-34
SiO_2	64.342	64.384	64.655	64.399	64.463	64.580	65.610
Al_2O_3	18.188	18.227	18.367	18.286	18.429	18.354	18.680
Na_2O	1.249	0.921	1.148	1.194	1.093	1.098	1.017
K_2O	15.136	15.628	15.317	15.543	15.570	15.724	15.623
BaO	0.000	0.573	0.576	0.000	0.000	0.000	0.000
Total	98.914	99.733	100.064	99.421	99.555	99.756	100.931

APPENDIX C

Argon Summary Sheets
(Includes description of method followed for sample analysis)

Sample Analysis

All samples analyzed in this study were irradiated for ten hours in position 5C within the nuclear reactor at McMaster University, Hamilton, Ontario. The neutron flux of site 5C was known to be ~ (35 to 40) x 10^{12} Neutrons cm^{-2}/sec.

Upon irradiation, samples were analyzed with a VG3600 mass spectrometer that is coupled to a double-vacuum tantalum resistance furnace at any one time. To permit successive automated analyses, 12 samples were loaded into a circular loading port inside the vacuum system. Samples were admitted in turn to the extraction furnace. After each analysis, the furnace was thoroughly out-gassed to a maximum temperature of ~ 1500 ^{0}C in order to achieve a sufficiently low blank.

Temperatures within the sample chamber were measured by a platinum-rhodium thermocouple that was calibrated using a second, external thermocouple inserted directly into the hot zone. There was no temperature offset between the inner and outer thermocouples, but rather a longer time to set-point delay for the inner thermocouple which sits in the center of the sample crucible. As the sample crucible, made with highly conductive tantalum and contained within the outer controlling thermocouple, is heated by conduction the center (where the sample sits) reaches the desired temperature some time after the outer controlling thermocouple, and does so within error. The time it takes for the entire system to reach isothermal conditions is inversely proportional to the temperature, where the delay is longer at low temperatures and shorter at higher temperatures. To accommodate for this time delay, hornblende, muscovite and K-feldspar samples were maintained at each temperature step for 20 minutes. During analysis, the inner thermocouple cannot be in with the sample (K. Taylor, pers. com., 2001).

98-D42 HORNBLENDE ARGON SUMMARY

T°C	mV 39	39%	AGE (Ma)±1σ	% ATM	37/39	36/40	39/40	% IIC
650	10.8	2	1516.4 ± 29.6	6.1	4.12	0.000208	0.00183	0.32
750	10.3	2	1646.6 ± 25.3	7	1.82	0.000239	0.001601	0.14
850	10.6	2	1842.9 ± 27.5	1.2	1.69	0.000044	0.001427	0.12
950	29.3	5.6	1849.9 ± 10.9	0.9	6.83	0.000034	0.001422	0.51
975	29.7	5.7	1840.7 ± 11.2	0.3	8.4	0.000012	0.001443	0.63
1000	55.4	10.7	1808.3 ± 8.2	0.3	7.57	0.000012	0.001484	0.57
1025	111.3	21.5	1774.7 ± 6.2	0.2	6.77	0.00001	0.001529	0.51
1050	36.2	6.9	1782 ± 9.9	2.3	6.29	0.000079	0.001488	0.48
1075	42	8.1	1776.5 ± 8.7	0.2	6.18	0.000008	0.001528	0.47
1100	17	3.2	1789.5 ± 18.6	0.1	7.11	0.000007	0.001511	0.54
1125	24.9	4.8	1800.5 ± 13	0.1	7.02	0.000005	0.001497	0.53
1150	15.8	3	1819.2 ± 19.2	0	7.45	0.000003	0.001474	0.56
1175	14.8	2.8	1817.9 ± 18.5	0.3	7.33	0.000012	0.001472	0.55
1200	25.6	4.9	1831.8 ± 12.9	0.1	6.68	0.000008	0.001456	0.5
1250	57.8	11.1	1795.2 ± 7.7	0.3	7.13	0.000012	0.001501	0.54
1300	9.6	1.8	1829.4 ± 28.7	2.5	7.97	0.000086	0.001426	0.6
1350	5.4	1	1818.1 ± 54.6	9.1	7.2	0.00031	0.001342	0.54
1450	10.2	1.9	1874.6 ± 33	17.4	7.3	0.00059	0.001161	0.55

TOTAL GAS AGE = 1794.1 ± 8.2 Ma

J = .00257 ± 1.285E-05 (.5 %)

37/39, 36/40 and 39/40 Ar ratios are corrected for mass spectrometer discrimination, interfering isotopes and system blanks.

% IIC - INTERFERING ISOTOPES CORRECTION

98-L48 HORNBLENDE ARGON SUMMARY

T°C	mV 39	39%	AGE (Ma)±1σ	% ATM	37/39	36/40	39/40	% IIC
650	2.5	0.2	1764.4 ± 75.8	5.4	3.21	0.000183	0.001396	0.24
750	6	0.4	1515 ± 35.9	12.6	2.01	0.000427	0.001627	0.15
850	6.1	0.4	1674.3 ± 34.3	2.1	2.51	0.000073	0.001567	0.19
950	118.5	9.5	1774.9 ± 9.7	0.2	4.07	0.000007	0.00146	0.31
975	145.4	11.7	1769.9 ± 8.9	0	4.18	0.000001	0.001469	0.31
1000	213.6	17.1	1766.4 ± 7	0	4.22	0.000003	0.001473	0.32
1025	268.2	21.5	1761.9 ± 6.6	0	4.22	0.000002	0.001479	0.32
1050	239.5	19.2	1757.3 ± 6.9	0	4.24	0.000002	0.001485	0.32
1075	28.8	2.3	1770.6 ± 9.3	0	4.24	0.000002	0.001468	0.32
1100	19.6	1.5	1776.4 ± 13.7	0	4.27	0.000002	0.00146	0.32
1125	24.7	1.9	1769.2 ± 10	0	4.4	0.000003	0.001469	0.33
1150	28.4	2.2	1772.2 ± 9.7	0.1	4.39	0.000007	0.001464	0.33
1175	6	0.4	1720.7 ± 33.8	1.1	4.06	0.000039	0.001518	0.31
1200	10.3	0.8	1761.7 ± 22.3	0.9	4.3	0.000033	0.001466	0.32
1250	57.1	4.5	1765.7 ± 6.8	0.4	4.36	0.000017	0.001468	0.33
1350	27.7	2.2	1770.5 ± 9.8	3	4.45	0.000102	0.001424	0.33
1450	39.6	3.1	1764.6 ± 9	3.5	4.31	0.000121	0.001423	0.32

MEAN AGE (950*°C-1350°C) = 1765.1 ± 12.8 Ma (2σ uncertainty, including error in J)

J = .002452 ± .000025 (1 %)

37/39,36/40 and 39/40 Ar ratios are corrected for mass spectrometer discrimination, interfering isotopes and system blanks.

% IIC - INTERFERING ISOTOPES CORRECTION

98-D12 HORNBLENDE ARGON SUMMARY

T°C	mV 39	39%	AGE (Ma)±1σ	% ATM	37/39	36/40	39/40	% IIC
650	3.3	0.8	1300.4 ± 84.6	13.9	18.06	0.000474	0.002095	1.5
750	3.4	0.9	1518.2 ± 95.1	29.4	9.58	0.000998	0.001373	0.76
850	2.9	0.7	1671.4 ± 101	14.8	9.76	0.000503	0.001435	0.75
950	10	2.6	1709.9 ± 24.3	3.4	13.4	0.000117	0.001569	1.03
975	14.4	3.8	1797.1 ± 19.9	0.4	12.94	0.000019	0.001495	0.98
1000	85.5	22.5	1768.6 ± 6.3	0.4	12.55	0.000016	0.001534	0.96
1025	83.3	22	1767.6 ± 6.4	0.2	11.77	0.00001	0.001538	0.9
1050	10.6	2.8	1725.8 ± 22.1	0.1	11.55	0.000008	0.001598	0.89
1075	6.3	1.6	1814.7 ± 35.6	0.6	11.93	0.000024	0.00147	0.9
1100	21.6	5.7	1776.5 ± 12.1	0.3	12.58	0.000016	0.001523	0.96
1125	26.2	6.9	1787.6 ± 11.5	0.4	12.68	0.000017	0.001508	0.96
1150	45.6	12	1780.3 ± 8	0.3	12.17	0.000013	0.001519	0.93
1175	27.7	7.3	1778.5 ± 10.5	0.5	12.69	0.000019	0.001519	0.97
1200	5.1	1.3	1706 ± 38.4	1.1	12.07	0.000042	0.001612	0.93
1250	24.9	6.5	1775 ± 11.8	0.6	12.57	0.000024	0.001522	0.96
1300	2	0.5	2126.1 ± 128	6.8	11.1	0.000232	0.001065	0.81
1350	2.4	0.6	1899.2 ± 92.7	14.3	11.99	0.000487	0.00118	0.9
1450	2.4	0.6	2025.8 ± 134	41.9	11.49	0.001421	0.000719	0.85

MEAN AGE (975°C-1250°C) = 1772.9 ± 13 Ma (2σ uncertainty, including error in J)

J = .002568 ± .0000257 (1 %)

37/39,36/40 and 39/40 Ar ratios are corrected for mass spectrometer discrimination, interfering isotopes and system blanks.

% IIC - interfering isotopes correction

97-A404A HORNBLENDE ARGON SUMMARY

T°C	mV 39	39%	AGE (Ma)±1σ	% ATM	37/39	36/40	39/40	% IIC
650	7.4	7.1	1153.9 ± 33.4	5.7	2.29	0.000196	0.002698	0.19
750	6	5.8	1539.9 ± 36.9	12.3	2.82	0.000419	0.001667	0.22
850	6.3	6.1	1616.7 ± 43.1	6.1	2.77	0.00021	0.001659	0.21
950	16.8	16.3	1739.6 ± 13.2	1.8	13.83	0.000065	0.001549	1.06
990	16.5	16	1756.1 ± 13	1.4	17.35	0.000052	0.001533	1.33
1030	18.4	17.9	1768.8 ± 14.4	0.9	18.58	0.000034	0.001524	1.42
1070	6.7	6.5	1695.4 ± 32.7	1.3	19.51	0.00005	0.001621	1.51
1110	4.2	4.1	1725.4 ± 50.9	1.8	21.67	0.000069	0.001569	1.67
1150	5.2	5	1819.3 ± 38.7	2.7	23.15	0.000098	0.001431	1.76
1200	7.9	7.6	1779.4 ± 25.8	3.4	23.86	0.000118	0.001472	1.82
1300	4.4	4.2	1902.3 ± 50.2	5.7	23.28	0.000199	0.001292	1.75
1350	1.3	1.3	1901.2 ± 168	20.9	15.54	0.000709	0.001087	1.17
1450	1.3	1.3	1848.4 ± 246	50.5	13.91	0.001713	0.00071	1.05

MEAN AGE (1110°C-1300°C) = 1804.1 ± 40.6 Ma (2σ uncertainty, including error in J)

J = .002565 ± .000026 (1 %)

37/39,36/40 and 39/40 Ar ratios are corrected for mass spectrometer discrimination, interfering isotopes and system blanks.

% IIC - interfering isotopes correction

97-D004 HORNBLENDE ARGON SUMMARY

T°C	mV 39	39%	AGE (Ma)±1σ	% ATM	37/39	36/40	39/40	% IIC
650	6.5	1.6	975.4 ± 29.2	21.5	5.48	0.000729	0.00282	0.5
750	4.1	1	3486.9 ± 289	6.5	11.42	0.000222	0.000407	0.78
800	2.4	0.6	1508.7 ± 85.8	16.3	14.78	0.000555	0.001649	1.18
850	3.3	0.8	1585.7 ± 48.9	11.5	17.43	0.000392	0.001619	1.37
900	5.5	1.3	1488.4 ± 31.3	7.4	20.05	0.000254	0.00186	1.6
950	17.5	4.3	1714.8 ± 9.6	2.9	22.88	0.000102	0.001574	1.76
975	54.6	13.5	1734.3 ± 6.3	1.2	20.91	0.000043	0.001574	1.61
1000	97.8	24.2	1741.7 ± 5.8	0.8	19.85	0.000029	0.00157	1.52
1025	52.7	13	1742 ± 7	0.9	19.07	0.000033	0.001568	1.46
1050	15.6	3.8	1735.3 ± 10.9	2	19.83	0.000072	0.00156	1.52
1075	10.3	2.5	1725.5 ± 16.7	2.9	20.45	0.000103	0.001559	1.57
1100	16.1	4	1729.7 ± 10.9	2.6	20.02	0.000089	0.001559	1.54
1125	31.9	7.9	1742 ± 9.7	2	19.34	0.000071	0.00155	1.48
1150	24.9	6.1	1735.9 ± 8.6	2.4	18.83	0.000083	0.001553	1.45
1175	11.1	2.7	1754.1 ± 16.9	4	19.1	0.000137	0.001504	1.46
1200	9	2.2	1791.6 ± 20	4.7	18.82	0.000163	0.001443	1.43
1250	7	1.7	1723.3 ± 25.2	8.1	18.53	0.000278	0.001479	1.43
1300	16.1	4	1753.3 ± 11	5.8	19.04	0.000197	0.001477	1.46
1350	9.3	2.3	1765.6 ± 18.9	13.6	18.27	0.000463	0.001339	1.4
1450	6.8	1.7	1743.4 ± 36.1	38.4	8.67	0.001302	0.000973	0.66

MEAN AGE (950°C-1450°C) = 1740.2 ± 12.3 Ma (2σ uncertainty, including error in J)

J = .002577 ± .0000257 (.9 %)

37/39,36/40 and 39/40 Ar ratios are corrected for mass spectrometer discrimination, interfering isotopes and system blanks.

% IIC - interfering isotopes correction

97-D23 HORNBLENDE ARGON SUMMARY

T°C	mV 39	39%	AGE (Ma)±1σ	% ATM	37/39	36/40	39/40	% IIC
650	19.5	2.4	833.8 ± 14.8	14.9	0.7	0.000504	0.003726	0.06
750	18.5	2.3	1658.3 ± 14.5	6.9	1.37	0.000235	0.001587	0.1
800	17	2.1	1700.8 ± 18.1	2.3	1.32	0.000078	0.001603	0.1
850	18.8	2.3	1713.5 ± 13.9	1.6	1.54	0.000057	0.001595	0.11
900	28.5	3.5	1690.3 ± 9.5	0.6	1.41	0.000021	0.001646	0.1
950	43.9	5.4	1734 ± 8.3	0.2	2.21	0.00001	0.001587	0.17
975	55	6.8	1731.1 ± 6.9	0.2	3.48	0.000009	0.001592	0.26
1000	104.9	13	1730.7 ± 5.9	0.3	5.09	0.000013	0.00159	0.39
1025	149.6	18.5	1739.7 ± 5.9	0.3	6.24	0.000011	0.001578	0.48
1050	92.4	11.4	1742.5 ± 6.1	0.1	5.07	0.000007	0.001576	0.39
1075	24.1	2.9	1737.2 ± 10.9	0.2	4.62	0.00001	0.001583	0.35
1100	27.9	3.4	1740.8 ± 10.1	0.3	5.11	0.000012	0.001577	0.39
1125	52.1	6.4	1754.3 ± 7.4	0.2	5.12	0.00001	0.001558	0.39
1150	42.7	5.3	1761.7 ± 7.9	0.4	5.56	0.000015	0.001546	0.42
1175	14.5	1.8	1756.6 ± 16.6	1.2	7.58	0.000045	0.00154	0.58
1200	12.3	1.5	1773.7 ± 19	1.8	7.16	0.000064	0.001508	0.54
1250	43.2	5.3	1764 ± 7.9	1.1	7.66	0.00004	0.001531	0.58
1300	23.4	2.9	1768.1 ± 11.8	2.9	9.52	0.000099	0.001499	0.73
1350	8.4	1	1795.6 ± 30.3	11.1	8.37	0.000376	0.00134	0.63
1450	7.9	0.9	1774.6 ± 39.5	28.2	7.81	0.000958	0.001101	0.59

MEAN AGE (1000°C-1250°C) = 1744.5 ± 12.4 Ma (2σ uncertainty, including error in J)

J = .002572 ± .000026 (1 %)

37/39,36/40 and 39/40 Ar ratios are corrected for mass spectrometer discrimination, interfering isotopes and system blanks.

% IIC - interfering isotopes correction

97-A001 HORNBLENDE ARGON SUMMARY

T°C	mV 39	39%	AGE (Ma)±1σ	% ATM	37/39	36/40	39/40	% IIC
650	2.6	0.2	1189 ± 76.7	1.7	0.32	0.000059	0.002718	0.02
750	11.2	1.1	1764.3 ± 19.7	0.4	0.45	0.000016	0.001545	0.03
800	10.4	1	1736.7 ± 19.5	0.5	0.91	0.000018	0.001583	0.07
850	8.2	0.8	1718.7 ± 23.5	0.9	2.17	0.000032	0.001602	0.16
900	9.3	0.9	1783.7 ± 32.2	1	4.18	0.000034	0.001511	0.32
950	31.7	3.1	1741 ± 8.7	0.8	7.21	0.00003	0.001571	0.55
975	58.4	5.7	1749.5 ± 6.9	0.5	8.23	0.000018	0.001565	0.63
1000	122.1	12	1744.8 ± 5.9	0.3	8.51	0.000013	0.001573	0.65
1025	256.8	25.3	1746.4 ± 6.7	0.2	8.39	0.000008	0.001573	0.64
1050	148.4	14.6	1751.3 ± 5.8	0.1	7.9	0.000006	0.001567	0.6
1075	21.4	2.1	1763.6 ± 11.2	0.5	8.29	0.000019	0.001545	0.63
1100	38	3.7	1754.8 ± 8.1	0.4	9	0.000016	0.001558	0.69
1125	56.2	5.5	1763.2 ± 6.9	0.4	9.27	0.000015	0.001547	0.71
1150	32.4	3.2	1764.2 ± 9.1	0.7	9.59	0.000025	0.001541	0.73
1175	17.2	1.7	1775.2 ± 13.4	1.5	9.5	0.000052	0.001514	0.72
1200	16.6	1.6	1752.9 ± 14.5	1.8	9.91	0.000064	0.001539	0.76
1250	118.6	11.7	1762.4 ± 6.1	0.6	9	0.000021	0.001545	0.69
1300	24.4	2.4	1765.5 ± 10.7	2.9	9.88	0.000099	0.001505	0.75
1350	12.3	1.2	1771.3 ± 20.5	9.4	9.72	0.000319	0.001398	0.74
1450	15.5	1.5	1754.9 ± 21.1	25.2	4.51	0.000856	0.00117	0.34

MEAN AGE (950°C-1450°C) = 1752.8 ± 12.2 Ma (2σ uncertainty, including error in J)

J = .002577 ± .0000257 (.9 %)

37/39,36/40 and 39/40 Ar ratios are corrected for mass spectrometer discrimination, interfering isotopes and system blanks.

% IIC - interfering isotopes correction

97-D373A HORNBLENDE ARGON SUMMARY

T°C	mV 39	39%	AGE (Ma)±1σ	% ATM	37/39	36/40	39/40	% IIC
650	4.4	0.5	1420.5 ± 40.5	4.2	2.18	0.000144	0.002063	0.17
750	6.4	0.8	1360.2 ± 30.2	7.9	1.87	0.00027	0.002111	0.15
850	5.8	0.7	1954.7 ± 40.8	2.9	1.78	0.000099	0.001282	0.13
950	83	10.4	1751.3 ± 6	0.5	3.5	0.000017	0.001567	0.26
980	127.8	16.1	1738.2 ± 7.7	0	3.61	0.000003	0.001592	0.27
1010	192.1	24.2	1742.2 ± 6.7	0	3.66	0.000002	0.001587	0.28
1040	190.9	24	1739.3 ± 6.4	0	3.68	0.000002	0.001591	0.28
1070	80.4	10.1	1751.1 ± 6	0	3.68	0.000001	0.001575	0.28
1100	24.3	3	1756.8 ± 8.6	0	3.7	0.000002	0.001567	0.28
1130	20.8	2.6	1753.9 ± 9.6	0	4.08	0.000003	0.00157	0.31
1160	12.2	1.5	1794.4 ± 15.6	0.1	3.91	0.000005	0.001513	0.29
1190	8.1	1	1763.5 ± 22.4	0.6	3.81	0.000021	0.001548	0.29
1240	11.3	1.4	1767.6 ± 17.1	0.7	4.08	0.000024	0.001541	0.31
1300	5.8	0.7	1815 ± 28	2.7	3.75	0.000094	0.001447	0.28
1350	7.5	0.9	1812.8 ± 25.6	3.1	3.45	0.000106	0.001444	0.26
1450	11	1.3	1788.4 ± 19.8	5.9	3.63	0.000202	0.001433	0.27

MEAN AGE (950°C-1450°C) = 1746.9 ± 12.5 Ma (2σ uncertainty, including error in J)

J = .002585 ± .0000257 (.9 %)

37/39,36/40 and 39/40 Ar ratios are corrected for mass spectrometer discrimination, interfering isotopes and system blanks.

% IIC - interfering isotopes correction

98-D93 HORNBLENDE ARGON SUMMARY

T°C	mV 39	39%	AGE (Ma)±1σ	% ATM	37/39	36/40	39/40	% IIC
650	9.7	1.2	1508 ± 20.7	3.7	0.51	0.000125	0.001899	0.04
750	57.6	7.1	1704.9 ± 7	0.5	0.12	0.000017	0.00163	0
850	67	8.3	1733.6 ± 6.4	0.1	0.12	0.000003	0.001595	0
950	74	9.1	1749.1 ± 6.3	0.1	1.12	0.000004	0.001573	0.08
975	52.5	6.5	1740.8 ± 6.9	0	2.05	0.000001	0.001586	0.15
1000	69.1	8.5	1740.1 ± 6.4	0	2.76	0.000002	0.001586	0.21
1025	141.3	17.5	1748.1 ± 7.9	0	3.46	0.000003	0.001575	0.26
1050	128.5	15.9	1751.5 ± 8.8	0	3.52	0.000002	0.00157	0.27
1075	102.7	12.7	1748.4 ± 5.9	0	3.51	0.000001	0.001575	0.27
1100	19.7	2.4	1746.7 ± 12.3	0	3.06	0.000003	0.001576	0.23
1150	29.2	3.6	1760 ± 8.7	0.1	4.02	0.000005	0.001557	0.3
1200	14.7	1.8	1763.4 ± 17.1	0.3	4.16	0.000014	0.001548	0.31
1250	20.8	2.5	1762.3 ± 12.6	0.4	4.23	0.000016	0.001549	0.32
1350	12.9	1.6	1763.7 ± 18.9	1.7	4.1	0.000059	0.001527	0.31
1450	6.6	0.8	1755.8 ± 34.1	8.5	3.48	0.000288	0.001431	0.26

MEAN AGE (1025*°C-1450°C) = 1751.4 ± 13.6 Ma (2σ uncertainty, including error in J)

J = .002579 ± .000026 (1 %)

37/39,36/40 and 39/40 Ar ratios are corrected for mass spectrometer discrimination, interfering isotopes and system blanks.

% IIC - interfering isotopes correction

98-T201 HORNBLENDE ARGON SUMMARY

T°C	mV 39	39%	AGE (Ma)±1σ	% ATM	37/39	36/40	39/40	% IIC
650	22.2	2	1553.6 ± 14.3	3.4	0.78	0.000117	0.001811	0.06
750	63	5.6	1691.4 ± 7.7	2	0.32	0.000069	0.001615	0.02
850	60.1	5.4	1730.4 ± 7.5	2	0.44	0.00007	0.001559	0.03
900	39.8	3.5	1743.9 ± 9.3	0.7	1.06	0.000024	0.001562	0.08
950	86	7.7	1750.5 ± 6.8	0.1	2.87	0.000007	0.00156	0.22
975	116.7	10.4	1754.9 ± 6	0.1	3.94	0.000006	0.001554	0.3
1000	192.4	17.2	1760.9 ± 7.9	0	4.46	0.000001	0.001549	0.34
1025	232.2	20.8	1753.2 ± 7.7	0	4.62	0.000002	0.001559	0.35
1050	48	4.3	1748.5 ± 8.3	0	3.52	0.000003	0.001565	0.27
1075	35.9	3.2	1759.2 ± 10.1	0.2	4.08	0.000008	0.001548	0.31
1100	42	3.7	1764.5 ± 9.1	0.2	4.91	0.00001	0.00154	0.37
1125	73	6.5	1774.3 ± 7.1	0.3	5.11	0.000011	0.001526	0.39
1150	28.5	2.5	1778.2 ± 12.5	0.3	5.41	0.000013	0.00152	0.41
1175	14.1	1.2	1807 ± 18.6	0.5	5.49	0.00002	0.001479	0.41
1200	27.4	2.4	1773.2 ± 11.7	0.5	5.26	0.000018	0.001524	0.4
1250	17	1.5	1787.3 ± 17.3	1	5.53	0.000038	0.001497	0.42
1350	8.7	0.7	1810.6 ± 30.4	4.7	5.77	0.00016	0.001413	0.44
1450	5.6	0.5	1834.3 ± 64.8	20.8	5.2	0.000704	0.001151	0.39

MEAN AGE (1000*°C-1450°C) = 1763 ± 13.4 Ma (2σ uncertainty, including error in J)

J = .002564 ± .000026 (1 %)

37/39,36/40 and 39/40 Ar ratios are corrected for mass spectrometer discrimination, interfering isotopes and system blanks.

% IIC - interfering isotopes correction

99-D53 HORNBLENDE ARGON SUMMARY

T°C	mV 39	39%	AGE (Ma)±1σ	% ATM	37/39	36/40	39/40	% IIC
650	5.5	1.8	3050.3 ± 115	17.9	3.89	0.000608	0.000475	0.27
750	4	1.4	1985.3 ± 118	43.6	28.14	0.001476	0.000723	2.1
850	3.3	1.1	1779.9 ± 99	24.2	31.14	0.000821	0.001159	2.38
950	24.8	8.5	1984.7 ± 14.5	11.5	27.71	0.000391	0.001132	2.07
975	23.5	8	1818 ± 13	2.4	22.83	0.000086	0.001438	1.73
1000	45.2	15.5	1783.2 ± 8.2	1.6	21.76	0.000058	0.001495	1.66
1025	37.5	12.8	1776.6 ± 9.5	0.7	20.47	0.000028	0.001517	1.56
1050	9.2	3.1	1802.8 ± 30.4	1.2	20.65	0.000046	0.001476	1.57
1075	8.5	2.9	1796 ± 33.8	1.6	21.14	0.000058	0.001479	1.61
1100	7.7	2.6	1792.1 ± 37.5	1.4	20.98	0.000054	0.001486	1.6
1125	8.9	3	1836.6 ± 30.6	1.2	21.77	0.000047	0.001433	1.65
1150	9.2	3.1	1880.6 ± 28.7	1.8	22.4	0.000067	0.001371	1.69
1175	13.2	4.5	1848.7 ± 23.4	2.2	22.46	0.000079	0.001404	1.7
1200	12.9	4.4	1827.9 ± 22.9	2.5	22.5	0.000088	0.001425	1.71
1250	49	16.8	1812.3 ± 8.9	2.2	22.05	0.000076	0.001449	1.68
1300	19.1	6.5	1826.1 ± 17.6	3.2	22.41	0.000111	0.001417	1.7
1350	4.5	1.5	1821.1 ± 61	12.6	20.88	0.000429	0.001287	1.59
1450	4.9	1.6	1935.5 ± 70.9	25.3	20.05	0.000859	0.000997	1.5

MEAN AGE (950°C-1450°C) = 1826.9 ± 14.7 Ma (2σ uncertainty, including error in J)

J = .002567 ± .000026 (1 %)

37/39,36/40 and 39/40 Ar ratios are corrected for mass spectrometer discrimination, interfering isotopes and system blanks.

% IIC - interfering isotopes correction.

□

98-T300A HORNBLENDE ARGON SUMMARY

T°C	mV 39	39%	AGE (Ma)±1σ	% ATM	37/39	36/40	39/40	% IIC
650	5.4	0.2	2133.5 ± 79	8.4	1.93	0.000286	0.000996	0.14
750	8.5	0.3	1841.4 ± 50.5	12.3	1.46	0.000417	0.001216	0.11
850	9.1	0.4	1815.1 ± 46	6	1.3	0.000206	0.001333	0.09
950	222.1	10.2	1770.3 ± 9.4	0.4	3.22	0.000015	0.00147	0.24
975	180.5	8.3	1763.2 ± 10.4	0	3.22	0.000001	0.001486	0.24
1000	246.7	11.4	1765.7 ± 8.7	0	3.22	0.000002	0.001482	0.24
1025	305.3	14.1	1763.7 ± 7.9	0	3.22	0.000002	0.001485	0.24
1050	431.3	19.9	1766 ± 6.9	0	3.2	0.000003	0.001481	0.24
1075	408.6	18.9	1759.9 ± 7	0	3.19	0.000002	0.00149	0.24
1100	40.3	1.8	1765.2 ± 11.3	0	3.52	0.000003	0.001482	0.26
1125	72.1	3.3	1765.4 ± 8	0.1	3.86	0.000004	0.001481	0.29
1150	150.1	6.9	1776.8 ± 11.5	0	3.83	0.000001	0.001468	0.29
1175	42.3	1.9	1770.9 ± 10.5	0.3	4.05	0.000013	0.00147	0.3
1200	9.6	0.4	1788.6 ± 40.7	0.9	4.64	0.000032	0.001439	0.35
1250	13.2	0.6	1785.6 ± 29.8	0.9	4.44	0.000034	0.001443	0.33
1350	7.4	0.3	1823.9 ± 51.9	4	4.46	0.000136	0.001352	0.33
1450	4.5	0.2	1931.7 ± 91	10.5	4.08	0.000356	0.001149	0.3

MEAN AGE (950*°C-1100°C) = 1764.5 ± 13.1 Ma (2σ uncertainty, including error in J)

J = .002465 ± .000025 (1 %)

37/39,36/40 and 39/40 Ar ratios are corrected for mass spectrometer discrimination, interfering isotopes and system blanks.

% IIC - interfering isotopes correction.

98-T300B HORNBLENDE ARGON SUMMARY

T°C	mV 39	39%	AGE (Ma)±1σ	% ATM	37/39	36/40	39/40	% IIC
650	9.4	0.9	1207.3 ± 48.9	5	0.91	0.000172	0.002446	0.07
750	9.4	0.9	1413.7 ± 51	4.3	0.86	0.000145	0.001975	0.06
850	8.8	0.8	1716.9 ± 56	1.2	1.28	0.000041	0.001525	0.09
950	106.7	10.5	1782.1 ± 7.7	0.2	3.39	0.000008	0.001453	0.25
975	126.2	12.4	1760.5 ± 18.1	0	3.39	0.000003	0.001484	0.25
1000	176.1	17.4	1759.3 ± 13.1	0	3.48	0.000002	0.001486	0.26
1025	141.1	13.9	1750.1 ± 15.5	0	3.53	0.000002	0.001498	0.27
1050	150.6	14.8	1750.3 ± 14.7	0	3.52	0.000002	0.001498	0.26
1075	72.2	7.1	1768.8 ± 8.8	0	3.54	0.000002	0.001473	0.27
1100	44.3	4.3	1771.9 ± 12.8	0	3.61	0.000003	0.001469	0.27
1125	39.3	3.8	1762.6 ± 14.5	0.1	3.66	0.000005	0.00148	0.27
1150	63.4	6.2	1772.7 ± 10.2	0.1	3.71	0.000004	0.001467	0.28
1175	9.7	0.9	1777.9 ± 53.8	0.9	4.03	0.000031	0.001449	0.3
1200	5.9	0.5	1803 ± 76	1.5	4.16	0.000051	0.001409	0.31
1250	31.8	3.1	1788.3 ± 16.4	0.4	4.06	0.000016	0.001442	0.3
1350	9.6	0.9	1830.5 ± 51.8	3.1	4.06	0.000105	0.001353	0.3
1450	6	0.5	1794.2 ± 86.2	9.3	3.92	0.000317	0.001306	0.29

MEAN AGE (950°C-1450°C) = 1763.8 ± 14.7 Ma (2σ uncertainty, including error in J)

J = .002457 ± .000024 (.9 %)

37/39,36/40 and 39/40 Ar ratios are corrected for mass spectrometer discrimination, interfering isotopes and system blanks.

% IIC - interfering isotopes correction.

99-D76 HORNBLENDE ARGON SUMMARY

T°C	mV 39	39%	AGE (Ma)±1σ	% ATM	37/39	36/40	39/40	% IIC
650	19.4	0.9	1524.4 ± 9.8	3.2	0.31	0.000108	0.001802	0.02
750	108.6	5	1714 ± 5.8	0.8	0.1	0.000027	0.001546	0
850	138.2	6.4	1740 ± 6.9	0.1	0.07	0.000004	0.001521	0
950	313.4	14.5	1758.2 ± 6.2	0.2	1.47	0.000008	0.001495	0.11
1000	273	12.6	1759.5 ± 6.1	0	2.64	0.000003	0.001495	0.2
1025	285.1	13.2	1760.2 ± 6	0	2.97	0.000003	0.001494	0.22
1050	294.2	13.6	1761.3 ± 6	0	3.02	0.000002	0.001493	0.23
1075	340.8	15.7	1759.8 ± 6	0	2.91	0.000002	0.001495	0.22
1100	95.7	4.4	1753.2 ± 5.8	0.1	1.73	0.000004	0.001503	0.13
1125	64.4	2.9	1764.7 ± 6	0.2	3.24	0.000007	0.001486	0.24
1150	107.9	5	1773.8 ± 5.9	0.1	4	0.000006	0.001475	0.3
1175	51.6	2.3	1771.3 ± 6.6	0.3	4.12	0.000013	0.001475	0.31
1200	12.4	0.5	1745.7 ± 12.7	2.1	4	0.000073	0.001482	0.3
1250	28.9	1.3	1779.5 ± 7.5	1.4	4.34	0.00005	0.001448	0.33
1300	10.9	0.5	1802 ± 14.9	3.9	3.7	0.000132	0.001385	0.28
1350	7.2	0.3	1783.1 ± 23.6	8.1	4.28	0.000276	0.001346	0.32
1450	5.3	0.2	1811.7 ± 35.9	20.8	3.4	0.000704	0.001132	0.25

MEAN AGE (1025*°C-1450°C) = 1762.6 ± 12.4 Ma (2σ uncertainty, including error in J)

J = .002474 ± .000025 (1 %)

37/39,36/40 and 39/40 Ar ratios are corrected for mass spectrometer discrimination, interfering isotopes and system blanks.

% IIC - interfering isotopes correction.

98-T223 HORNBLENDE ARGON SUMMARY

T°C	mV 39	39%	AGE (Ma)±1σ	% ATM	37/39	36/40	39/40	% IIC
650	15.1	0.7	1671.3 ± 16.1	2	0.13	0.000069	0.001657	0.01
750	77.6	3.7	1706.1 ± 6.2	0.8	0.04	0.000027	0.001625	0
850	68.9	3.2	1729.8 ± 6.5	0.2	0.05	0.00001	0.001599	0
900	36.5	1.7	1748.9 ± 8.4	0.3	0.14	0.000011	0.001572	0.01
950	211.8	10	1765.2 ± 6.9	0.3	0.73	0.000011	0.001549	0.05
975	214.8	10.2	1762 ± 7.4	0.3	0.79	0.000011	0.001553	0.06
1000	270.7	12.9	1757.4 ± 6.6	0.2	0.84	0.000006	0.001562	0.06
1025	324.4	15.4	1760.6 ± 6.2	0.1	0.86	0.000004	0.001558	0.06
1050	375.6	17.9	1766.4 ± 6.1	0	0.87	0.000003	0.001551	0.06
1075	253.4	12	1772.7 ± 6.9	0	0.84	0.000002	0.001543	0.06
1100	35.6	1.6	1771.2 ± 9	0.1	0.7	0.000004	0.001544	0.05
1125	41	1.9	1785.8 ± 7.3	0.2	0.91	0.000007	0.001523	0.06
1150	121.5	5.7	1772.5 ± 9.6	0.1	0.94	0.000004	0.001542	0.07
1175	35.4	1.6	1773.9 ± 8.2	0.5	0.93	0.000019	0.001533	0.07
1200	2	0	1532.8 ± 93.6	11.7	0.63	0.000396	0.001702	0.05
1250	5.7	0.2	1681 ± 39.1	5.3	0.87	0.000179	0.001588	0.06
1300	2.1	0.1	1703.9 ± 97.3	14.9	0.79	0.000504	0.001397	0.06
———	4.6	0.2	1780.2 ± 62.9	24.2	1.95	0.000822	0.001161	0.14

MEAN AGE (1000*°C-1175°C) = 1765.9 ± 12.5 Ma (2σ uncertainty, including error in J)

J = .002582 ± .0000257 (.9 %)

37/39,36/40 and 39/40 Ar ratios are corrected for mass spectrometer discrimination, interfering isotopes and system blanks.

% IIC - interfering isotopes correction.

99-T62B HORNBLENDE ARGON SUMMARY

T°C	mV 39	39%	AGE (Ma)±1σ	% ATM	37/39	36/40	39/40	% IIC
650	84.7	3	1619.4 ± 8	0.7	0.06	0.000025	0.001684	0
750	384.4	13.8	1737.7 ± 7.9	0.1	0.02	0.000004	0.00152	0
850	310	11.1	1767.9 ± 8.6	0	0.03	0.000001	0.001481	0
950	517	18.5	1758.5 ± 17.1	0	0.66	0.000002	0.001493	0.05
975	303	10.8	1773 ± 8.6	0	1.52	0.000002	0.001474	0.11
1000	323.7	11.6	1785.4 ± 8.7	0	2.48	0.000002	0.001458	0.18
1025	357.6	12.8	1791.4 ± 8.2	0	3.3	0.000002	0.001451	0.25
1050	294.6	10.5	1802.2 ± 9.2	0	3.35	0.000001	0.001437	0.25
1075	87.6	3.1	1789.8 ± 8.4	0	1.75	0.000001	0.001453	0.13
1100	37.9	1.3	1808.6 ± 14	0	3.05	0.000003	0.001428	0.23
1125	22.4	0.8	1816.9 ± 21.2	0	3.75	0.000003	0.001418	0.28
1150	13.1	0.4	1828.2 ± 36.1	0.2	3.61	0.000008	0.001402	0.27
1175	7.8	0.2	1836.3 ± 62.6	0.7	3.72	0.000026	0.001385	0.28
1200	3.4	0.1	1804 ± 135	3.3	3.57	0.000114	0.001387	0.27
1250	18.4	0.6	1846.8 ± 28.2	1.1	4.77	0.000038	0.001367	0.36
1350	11.9	0.4	1845 ± 42.1	4	4.55	0.000136	0.001329	0.34
1450	4.2	0.1	2003.2 ± 120	12.8	3.93	0.000433	0.001056	0.29

MEAN AGE (1250°C-1350°C) = 1846.1 ± 49 Ma (2σ uncertainty, including error in J)

J = .002468 ± .000025 (1 %)

37/39,36/40 and 39/40 Ar ratios are corrected for mass spectrometer discrimination, interfering isotopes and system blanks.

% IIC - interfering isotopes correction.

98-T63 HORNBLENDE ARGON SUMMARY

T°C	mV 39	39%	AGE (Ma)±1σ	% ATM	37/39	36/40	39/40	% IIC
650	14.9	1.2	1636.2 ± 17.7	4.9	1.36	0.000166	0.001579	0.1
750	11.8	0.9	1442.6 ± 21.9	6.8	0.9	0.00023	0.001867	0.07
850	17	1.4	1828.8 ± 15	2.5	1.8	0.000085	0.001362	0.13
950	529.5	44.2	1781.9 ± 9.8	0.1	3.26	0.000005	0.001454	0.24
975	401.6	33.5	1779.1 ± 6.3	0	3.46	0.000002	0.001459	0.26
1000	117.2	9.8	1763.2 ± 9.4	0	3.39	0.000002	0.001479	0.25
1025	18.4	1.5	1775 ± 13.2	0.1	3.14	0.000005	0.001463	0.23
1050	11.7	0.9	1706.3 ± 20.1	0.2	3.1	0.00001	0.001553	0.23
1075	14.1	1.1	1810.5 ± 19.4	0	3.33	0.000003	0.001418	0.25
1100	24.6	2	1792.2 ± 10.2	0.1	3.3	0.000005	0.001441	0.25
1125	20.2	1.6	1803.8 ± 11.8	0.1	3.39	0.000007	0.001425	0.25
1150	3.7	0.3	1666.6 ± 54.2	1.9	2.25	0.000066	0.001583	0.17
1175	2.5	0.2	1503.7 ± 70.5	3.9	2	0.000132	0.001811	0.15
1200	1.8	0.1	1410.8 ± 95.6	7.1	2.07	0.00024	0.00192	0.16
1250	1.8	0.1	1763.7 ± 111	8.2	3.15	0.000278	0.001357	0.24
1350	2.4	0.2	2056 ± 92.3	12.4	3.6	0.000419	0.001011	0.26
1450	2.3	0.1	1914.8 ± 122	23.2	3.71	0.000786	0.000996	0.27

MEAN AGE (950°C-1125°C)** = 1779.1 ± 15.5 Ma (2σ uncertainty, including error in J)

J = .002455 ± .000025 (1 %)

37/39,36/40 and 39/40 Ar ratios are corrected for mass spectrometer discrimination, interfering isotopes and system blanks.

% IIC - interfering isotopes correction.

99-D214 HORNBLENDE ARGON SUMMARY

T°C	mV 39	39%	AGE (Ma)±1σ	% ATM	37/39	36/40	39/40	% IIC
650	1.5	0.2	5989.6 ± 350	1.2	1.86	0.000041	0.000091	0.12
750	2.7	0.3	4188.3 ± 226	4.6	3.96	0.000157	0.000255	0.26
850	2.5	0.3	2741.1 ± 204	2	5.5	0.000069	0.000674	0.38
950	112.7	14.7	1831.7 ± 19.6	0.3	6.7	0.000011	0.001392	0.5
975	113.8	14.9	1808.8 ± 18.7	0	6.8	0.000003	0.001423	0.51
1000	335.7	43.9	1784.6 ± 8.4	0	6.75	0.000002	0.001454	0.51
1025	39.4	5.1	1793.8 ± 14.2	0	6.68	0.000003	0.001442	0.5
1050	14.1	1.8	1796.8 ± 34.8	0	6.72	0.000005	0.001437	0.51
1075	24.2	3.1	1797.8 ± 21.2	0	6.64	0.000003	0.001437	0.5
1100	30.9	4	1808.6 ± 17.7	0.1	6.73	0.000005	0.001422	0.51
1125	20.1	2.6	1802.7 ± 27.6	0.2	6.75	0.00001	0.001428	0.51
1150	13.4	1.7	1826.6 ± 36.6	0.5	6.67	0.00002	0.001394	0.5
1175	6.1	0.7	1891.9 ± 76.5	1.6	6.02	0.000056	0.001304	0.45
1200	9.3	1.2	1763.4 ± 53	1.6	6.45	0.000055	0.001458	0.49
1250	7.2	0.9	1793.8 ± 69.5	3.1	6.13	0.000106	0.001398	0.46
1350	18.7	2.4	1832.5 ± 28.9	2.2	6.67	0.000076	0.001364	0.5
1450	10.5	1.3	1820.8 ± 52.4	6.6	6.35	0.000226	0.001315	0.48

TOTAL GAS AGE = 1856.7 ± 20.3 Ma

J = .002459 ± 1.2295E-05 (.5 %)

37/39,36/40 and 39/40 Ar ratios are corrected for mass spectrometer discrimination, interfering isotopes and system blanks.

% IIC - interfering isotopes correction.

BEDROCK GEOLOGY, U-Pb & $^{40}Ar/^{89}Ar$ AGES FROM REINDEER LAKE, SASKATCHEWAN

Legend

Kisseynew Domain

Burntwood Group
(meta-turbidites and derived migmatites)

McLennan Group
(arkose, polymictic conglomerate, calcareous arkose)

Levesque Bay Supracrustal Assemblage

Opx-bearing gneiss & calc-silicate gneiss

Calc-silicate gneiss

Volcano-sedimentary assemblages

LaRonge Domain

Volcano-sedimentary assemblages

Milton Island Metasediments
(psammite, pelite)

Park Island metasediments
(arkose, polymictic conglomerate, calcareous arkose, psammite)

Intrusive Rocks

Granodiorite - Monzogranite

Tonalite - Granodiorite

Tonalite

Diorite - Quartz-diorite

Crowe Island Compex
(dioritic - granitic banded orthogneiss)

Wathaman Batholith

Granodiorite - Quartz-monzodiorite
(K-feldspar megacrysts + hornblende + biotite)

Granodiorite - Monzogranite
(Hornblende + biotite ± K-feldspar megacrysts)

Granodiorite - Monzogranite
(fine - coarse grained + biotite)

Diorite - Granite
(mixed intrusives of the marginal zone)

Monzodiorite - Monzonites
(with K-feldspar megacrysts)

Patterson Island Monzogranite
(with K-feldspar megacrysts)

Tonalite - Granodiorite
(fine - medium grained)

Peter Lake Domain

Swan River Intrusives
(Gabbro - Diorite)

Dioritic - Granitic Orthogneiss

Psammitic paragneiss

Symbols

Sample Location X

Geological Contact

Shear Zone

U-Pb &/or $^{40}Ar/^{39}Ar$ Age
(box indicates age(s) obtained from single sample in order of decreasing closure temperature (T_c))

U-Pb Ages	*$^{40}Ar/^{39}Ar$ Ages*
Zircon	Hornblende
Monazite	Muscovite
Titanite	K-feldspar

Kilometers
0 5 10 15 20 25

102°15’ 102°00’ 58°00’N 57°45’N 57°30’N 57°15’N 57°00’N 56°45’N 56°30’ N 103°15’

Saskatchewan Manitoba

2562 ± 4 Ma
1830 ± 12 Ma
1771 ± 14 Ma
CXA99-D89A

2000 - 1997 Ma
CXA99-D162

1818 ± 15 Ma
CXA99-D87B

1800 ± 14 Ma
1742 ±13 Ma
CXA99-D103

1797 ± 20 Ma
CXA99-D214

1779 ±16 Ma
1833 ± 17 Ma
CXA99-T63

(1770 ±10 Ma)
CXA99-T62

1766 ±13 Ma
1708 ±12 Ma
CXA98-T223

1790 ±8 Ma
CXA98-D301

1855 ±4 Ma
CXA98-D300

1764 ±13 Ma
CXA98-T300A

1775 - 1755 Ma
1754 ±16 Ma
CXA99-D76

1764 ±15 Ma
1718 ±14 Ma
CXA98-T300B

598 ± 16 °C
4.5 ± 0.3 kbar

1773 ±23 Ma
CXA99-D53

1775 - 1750 Ma
CXA98-T201

632±0.7 °C
3.9±0.1 kbar

1751 ±14 Ma
CXA98-D93

1891 ±3 Ma
1747 ±13 Ma
CXA97-D373A

1884 ±5 Ma
1822 ±1 Ma
1804 ±1 Ma
CXA97-D373B

683 ± 0 °C
6.2 ± 0 kbar

1728 ±12 Ma
CXA97-D85 (c.gr.)

1727 ±13 Ma
1740 ±22 Ma
CXA97-D85 (f.gr.)

1794 ±3 Ma
CXA97-D84

1781 ±2 Ma
1778 ±2 Ma
CXA97-D127

1858 ±2 Ma
1753 ±12 Ma
CXA97-A001

1745 ±12 Ma
CXA97-D23

(1804 ±41 Ma)
CXA97-A404A

1741 ±13 Ma
CXA97-D004

1736 ±12 Ma
CXA97-D26A

1726 ±13 Ma
CXA97-D26B

689 ± 3 °C
5.5 ± 0.06 kbar

1731 ±13 Ma
CXA97-D31

1733 ±13 Ma
CXA97-D222

1897 ±15 Ma
1817 ±1 Ma
1813 ±1 Ma
1776 ±4 Ma
CXA98-D12 (gdr)

1867±3 Ma
CXA97-D297

1773 ±13 Ma
CXA98-D12 (vlc)

671 ± 7 °C
5.9 ± 0.2 kbar

1800 ±21 Ma
CXA98-D42

730 ± 12 °C
5.0 ± 0.2 kbar

1765 ±13 Ma
CXA98-L48

Map 1: Generalized bedrock geology map of Reindeer Lake, Saskatchewan based on field mapping conducted by Corrigan et al. (1997, 1998, 1999, 2000). Map area covers map sheets 64D/06, 07, 09, 10, 15, 16 and 64E/01, 02, 07, 08, 09, 10, 15, 16. For clarity, geological contacts have been projected onto Reindeer Lake. Locations of samples collected for the current study are marked with an “X” and labeled with the sample number and corresponding U-Pb ages calculated by David Corrigan of the Geological Survey of Canada, and $^{40}Ar/^{39}Ar$ ages obtained in the current study. P-T data presented here are those obtained by Chakungal (1999). $^{40}Ar/^{39}Ar$ ages in parentheses indicate samples for which the age was considered insignificant (see chapter three for details).